Hydrodynamics and Geomorphology of Netley-Libau Marsh and the Lower Red River

by

Eric Schillberg

A thesis submitted to the Faculty of Graduate and Postdoctoral Studies of
the University of Manitoba
in partial fulfillment of the requirements for the degree of

MASTER OF SCIENCE

Department of Civil Engineering
Price Faculty of Engineering
University of Manitoba

Abstract

This thesis examined the hydrodynamics and geomorphology of Netley–Libau Marsh and the lower Red River as part of ongoing restoration and monitoring initiatives, including the Netley–Libau Marsh Restoration Project (NLMRP). The work was motivated by concerns about marsh degradation, altered sediment supply, and changing water level regimes, and addressed the lack of an integrated, field based description of how water and sediment were routed through Netley Cut, Netley Delta, Netley Lake, and the lower Red River within Netley-Libau Marsh. A multipronged approach was adopted, combining repeated bathymetric surveys, discharge and water level monitoring, and turbidity measurements to characterise some of the physical responses of the system and to provide a reference framework for future restoration planning and research.

Bathymetric analyses in this thesis indicate that morphological change across the marsh is variable but strongly structured in space. At Netley Cut, alternating erosion and deposition nearly balance over the 12-year record. The cumulative balance from 2010 to 2022 is a net depositional gain of 2,978 m^3, equivalent to an average rise of 0.083 m across the Cut. Netley Delta shows significant deposition along the newly formed islands, with an average increase in bed elevation from 2010 to 2022 of 0.417 to 0.484 m. The mean bed elevations in the west and north entrance channels increased by approximately 0.18 and 0.14 m (respectively) from 2010 to 2022, equivalent to 1.2–1.5 cm per year. Channels remained well organized across the study period, but the north entrance evolved into a continuous channel while the west entrance remained the dominant pathway into Netley Lake. Netley Lake experienced a rise in bed elevation on average by 0.247 m between 2010 and 2022, corresponding to a deposition rate of about 2.1 cm per year. At the Red River outlet and navigation corridor, cross-sectional comparisons show substantial

shoaling between 2010 and 2021, with minimum bed elevations within the maintained channel rising by 0.811 m, alongside complete infilling of the previous navigation channel through and adjacent to the former breakwaters. It was further found that the Red River, between 2010 and 2018, had significant evidence of erosion along the east channel and deposition through the center (main) channel. On average, 0.44 m of bed elevation was lost from the trifurcation to the east channel outlet and 0.144 m of bed elevation was gained along the center channel. Lastly, within the Netley–Libau Marsh Restoration Project footprint, bathymetric differencing quantifies net excavation of 7,740 m^3 at the Red River dredge site from pre- to post-dredging, including 3,588 m^3 removed within the defined dredge footprints, followed by partial recovery of approximately 940 m^3 within one year, which is about 26 percent of the excavated footprint volume. At the Netley Lake deposition site, placement within the bounded cell accounts for approximately 2,416 m^3 of added material, indicating retention on the order of two-thirds of the excavated material within the cell, with the remaining fraction redistributed within the cell, exported through open boundaries, or lost to consolidation at magnitudes that cannot be separated from erosion with the available datasets.

Discharge and water level results demonstrate that Netley Cut is a consistently important pathway for routing Red River water into the marsh and that flow partitioning responds to the combined influence of river discharge and Lake Winnipeg water levels. Under typical open-water conditions when the Red River provides the sole inflow, Netley Cut diverts 39.27% of the Red River discharge on average into Netley Lake, and is capable of reaching up to 56.6%. Flow was also recorded for the first time in a reversed state, whereby flow from Netley Lake was flowing into the Red River. At the Red River trifurcation, mean flow splits indicate that the east and centre channels convey nearly all flow (approximately 47.6% and 50.9%, respectively),

while the west channel carries a small residual (about 2.4%). Analysis of water level lag-time responses associated with seiche-driven fluctuations indicates that the marsh behaves as a hydraulically connected system. Propagation of water level changes from upstream of Netley Cut to the Red River outlet typically occurs over a period of approximately 1.05 to 1.07 hours.

Finally, turbidity monitoring indicates that dredging and sediment placement produced intense but highly localized plumes. Absorptometric field measurements recorded turbidity consistently exceeding 1,000 FAU within 5 m of the dredge head, but decreasing to below 100 FAU by 10 to 20 m downstream, with perimeter locations varying on the order of 100 FAU. Turbid water leaving the deposition zone dissipated within approximately 50 to 75 m of the containment barriers and converged on background lake conditions, with the maximum average turbidity at the furthest sampling locations reaching 157 FAU across comprehensive testing dates. Continuous nephelometric monitoring in Netley Lake ranged from 1 to 986 NTU during the deployment period, with episodic peaks approaching 1,000 NTU, and no sustained project-induced exceedances beyond containment were detected above naturally occurring background levels within the marsh. Collectively, these results indicate that project-induced turbidity generated by in-water works is unlikely to exceed turbidity levels naturally experienced within Netley Lake and that elevated concentrations decay rapidly with distance from the source.

Acknowledgments

I would like to thank my advisor, Dr. Shawn Clark, for his guidance, support, and sincerely admirable patience throughout this thesis. Your willingness to keep working with me as my "reasonable" timeline gradually turned into a much longer one is something I am especially grateful for.

Furthermore, Dr. Gordon Goldsborough and Dr. James Blatz for devoting their time and support throughout this project, and for being more than willing to provide guidance whenever it was needed during my studies.

This work relied heavily on field efforts, and I owe sincere thanks to the many people who contributed their time and expertise. Alex Wall, for his work as field technician and for his practical problem-solving on and off the water. Christopher Adams, for his assistance during field campaigns and for the many helpful discussions on UAV deployment and processing. Peguis First Nation, for their on-site support particularly in providing transportation and an extra set of hands during field monitoring. I am further grateful to the Red River Basin Commission for their guidance and collaboration throughout the field monitoring program. Special thanks are also due to Bryan Page and Dale Wrubleski for their generosity in lending field equipment and helping to make the turbidity monitoring component of this project feasible.

I am further grateful for the support provided through the University of Manitoba Graduate Fellowship, the Red River Basin Commission, and the collaboration with Manitoba Hydro.

Finally, to my friends and family, who never stopped asking when I would finally be finished this thesis, thank you for the never ending reminders about all the things I was consistently missing out on.

Navigating this Thesis

The work presented herein is multi-faceted in structure, reflecting investigations into several aspects of the Netley-Libau Marsh system rather than a single, continuous line of inquiry. Each component addresses a distinct parameter of the marsh environment (bathymetry, water levels and discharge, and turbidity) while maintaining a common geographical focus on the lower Red River within the marsh and the area surrounding the Netley Cut. The analyses collectively contribute to an improved understanding of marsh processes, but they are not bound by one overarching methodology beyond their shared study area.

The research spans both technical, research-based investigations and community-driven initiatives. In particular, the publicly funded Netley–Libau Marsh Restoration Pilot Program, initiated by the Red River Basin Commission, represents a phased, multi-year intervention aimed at evaluating restoration strategies within the marsh. The dredging activities conducted in the Netley–Libau Marsh constituted only the initial phase of this program and were focused on testing the feasibility of augmented sediment isles. Subsequent phases have shifted emphasis toward modifications at the Netley Cut, reflecting an evolving restoration approach that is perceived to carry fewer adverse environmental impacts than dredging. While the program provided important contextual background and field access for this thesis, it does not form the sole basis of any individual parameter investigated.

Accordingly, this thesis is organized to present a general overview of existing literature on the Netley-Libau Marsh, followed by focused studies of three primary research areas. Chapter 3 addresses bathymetry, emphasizing geomorphic change at the Red River outlet, Netley Cut, and associated depositional areas. Chapter 4 examines water levels and discharge, with specific focus

on flow distribution at Netley Cut. Chapter 5 evaluates turbidity, considering both background variability and project-influenced conditions in relation to environmental licensing requirements. Each chapter is self-contained, structured with an introduction and background, methodology, results and discussion, and conclusion.

Table of Contents

List of Tables

List of Figures

List of Symbols

α	Significance threshold used in hypothesis testing
a_{x}	Across-track footprint length on the seafloor
a_{γ}	Along-track footprint length on the seafloor
b	Number of permuted statistics more extreme than the observed value
B_{ij}	Absolute elevation difference between soundings i and j
$\bar{B}$	Mean absolute elevation difference within a cell
β	Receiving beam angle relative to vertical
C	Speed of sound in water
$C(z)$	Sound speed as a function of depth
C_{i}	Sound speed at the top of layer i
$C_{\mathrm{i-1}}$	Sound speed at the top of the overlying layer
d_{ij}	Euclidean distance between soundings i and j
$\bar{D}$	Mean pairwise Euclidean distance within a cell
ΔN	Geoid separation difference between vertical datums
Δt	Total two-way acoustic travel time
Δt_{i}	Acoustic travel time increment within layer i
g_{i}	Vertical sound-speed gradient within layer i (dC/dz)
H_{2013}	Orthometric height referenced to CGVD2013
H_{28}	Orthometric height referenced to CGVD28
i, j	Index variables identifying soundings, grid cells, or layers
I	Moran's spatial autocorrelation statistic
I_{obs}	Observed Moran's *I* value
I_p	Moran's *I* value from a permuted realization
$\bar{\mathrm{I}}_{perm}$	Mean Moran's *I* from all permutations

k	Ray parameter (Snell's constant), $\sin(\theta) / C$
N	Total number of soundings within a grid cell
p	Distance-decay exponent or permutation-based p-value (context dependent)
r	Number of random permutations used in significance testing
R	Mantel correlation statistic
s_B	Norm of centered pairwise elevation-difference deviations
s_D	Norm of centered pairwise distance deviations
S^0	Sum of all spatial weights
S_w	Total multibeam swath width
t	One-way acoustic travel time
T	Two-way acoustic travel time
w_{ij}	Spatial weight between soundings i and j
w_{ii}	Self-weight (set to zero)
x	Horizontal (across-track) offset from nadir
$x_{\mathrm{i}}, y_{\mathrm{i}}$	Planar coordinates of sounding i
y	Along-track direction aligned with vessel motion
z	Vertical coordinate (positive downward)
$z_{\mathrm{i}}, z_{\mathrm{j}}$	Measured bed elevations at soundings i and j
$\bar{z}$	Mean bed elevation within a cell
Z	True water depth
ζ	Local seafloor slope
θ	Acoustic beam angle relative to vertical
θ^1, θ^2	Beam incidence angles in adjacent layers
φ_r	Angle of receiving beamwidth
φ_t	Angle of transmitting beamwidth

1. Introduction

An investigation of hydrodynamic and geomorphologic characteristics within wetlands provides vital information for understanding complex environmental responses and interactions. Hydraulic parameters such as water level and discharge, along with bathymetric mapping of rivers and lakes, provide baseline data necessary for developing connections with environmental drivers such as wind, precipitation, and temperature. Discerning how wind-induced wave action and water level rise affect shoreline stability and internal flow regimes within a wetland illustrates two such connections. These relationships, which vary in magnitude depending on wetland size, configuration, and type, represent one of several properties used by researchers, consultants, and government entities to evaluate wetland function and relative condition. Fundamentally, wetlands are defined by three core characteristics: the presence of persistent or recurrent water, the development of anaerobic soil conditions resulting from restricted oxygen diffusion under sustained inundation, and the establishment of plant communities adapted to these hydrologic and biogeochemical conditions.

Within this broader classification, a marsh represents a specific wetland form rather than a separate category. Wetlands comprise a range of environments characterized by persistent or recurrent inundation and vegetation adapted to saturated conditions, while marshes represent a subset distinguished by shallow water depths and a blend of emergent and submergent vegetation. Other wetland types include swamps, which are characterized by woody vegetation, and peat-forming systems such as bogs and fens. In this context, the term wetland is used in a general sense, whereas marsh refers to a particular wetland form with structural and hydrologic characteristics relevant to the processes examined in this thesis.

Carbon, nitrogen, and phosphorus absorption, variability in water levels, wildlife abundance and diversity, and the composition of submergent and emergent vegetation are also commonly used indicators of wetland health. The plethoric contribution of numerous variables in evaluating wetland health makes proposing solutions for restoration and revitalization a multidisciplinary and scientifically intensive research undertaking. Civil engineers play an important role in simplifying complex hydraulic relationships within wetlands that assist proponents in advocacy, research, and project management tasks. For example, a historic review of water level trends provides advocates for wetland conservation a means to relate ecological damages to low and high-water periods. Field observations of channel geometry and flow splits can assist researchers in modelling the effects of hydrologic projects, analyzing the ability of waterbodies to handle flood events, or estimating sediment transport rates in rivers. Bathymetric maps provide contractors with the required information to undertake dredging activities and select suitable locations for material removal and deposition.

However, the size and complexity of connecting channels within a wetland and the impact of surrounding waterbodies can confound research efforts to establish relationships that connect the health of a wetland to long-term observations in hydrodynamic and geomorphologic characteristics. A significant undertaking of time, effort, and equipment is required to monitor and record hydraulic responses within a wetland.

The work presented in this thesis provides baseline information concerning the hydrodynamics and geomorphology of important features within Netley-Libau Marsh, with specific focus on areas around Netley Cut and the Red River Outlet to assist in these undertakings. The scope of this research is centred on three primary parameters: discharge, bathymetry, and turbidity, with bathymetric analysis forming the bulk of the findings. The

detailed bathymetric mapping and associated analyses are intended to establish a reference framework against which future changes can be measured, and to provide context for understanding hydraulic connectivity, sediment transport pathways, and channel morphology within the marsh. It is anticipated that these results will support future researchers or contractors (e.g., environmental consultants assessing habitat conditions, engineers planning restoration works, government agencies monitoring wetland health and function, etc.) by offering a reliable baseline dataset from which to plan, evaluate, and carry out research, restoration, or conservation initiatives within the marsh.

1.1 Motivation

Research concerning the geomorphology and hydrodynamics of the lower Red River and Netley-Libau Marsh remains limited, despite the ecological importance of this system. Since the cessation of dredging at the Red River Outlet in 1999, few investigations have been conducted to document changes in channel form and bed conditions at this location. While dredging history is relevant to understanding outlet morphology, it does not extend as a controlling factor across the wider marsh. More broadly, there is limited knowledge of how erosion, deposition, and sedimentation rates have influenced the geomorphic development of both the Outlet and Netley Cut over time. The scarcity of published work leaves considerable uncertainty in evaluating these processes and their implications for marsh stability, connectivity, and long-term function.

A further knowledge gap exists with respect to discharge and water level dynamics through both the Netley Cut and the Red River trifurcation. The enlargement of the Cut has been recognized as a significant driver of flow redistribution into Netley Lake, yet no published datasets quantify the proportion of flow entering this distributary or its potential influence on higher water levels within the marsh. At the same time, the Red River trifurcation downstream

remains poorly documented, with no published measurements of flow splits, velocity distribution, or water surface elevation changes across its branches. Without such information, it is difficult to evaluate the role of the Netley Cut in controlling connectivity and sediment delivery, and the role of the trifurcation in governing how flow is divided among the Red River's distributary channels.

In addition, although extensive research has examined suspended sediment transport, nutrient fluxes, and contaminant pathways from the Red River into Lake Winnipeg, relatively little attention has been directed toward turbidity conditions within Netley-Libau Marsh itself. Existing studies primarily emphasize nutrient enrichment and pollutant dynamics rather than the natural variability of turbidity levels or their modification by construction and restoration projects. No published research has documented project-induced turbidity changes, despite the fact that turbidity is a regulatory parameter in environmental licensing for in-water works. Understanding background turbidity variability and the degree to which project activities may elevate turbidity is critical for both compliance and impact assessment. The absence of such work presents a challenge for consultants, engineers, and regulators seeking to evaluate project performance or fulfill licensing requirements.

Addressing these knowledge gaps provides the principal motivation for this thesis. This research aims to establish a more comprehensive baseline against which future changes may be assessed by generating new bathymetric, hydrodynamic, and turbidity datasets for Netley Cut, the Red River outlet, and adjacent marsh environments. The findings will contribute not only to scientific understanding of geomorphic and hydraulic processes in the marsh, but also to practical applications in restoration design, environmental licensing, and long-term monitoring of one of Manitoba's most important wetland systems.

1.2 Study Site

The study area is situated within the Netley-Libau Marsh (NLM) at the southern end of Lake Winnipeg, where the Red River bifurcates before entering the lake. The marsh represents one of the largest freshwater coastal wetlands in North America and plays an essential role in hydrological connectivity, sediment transport, and ecological function in the Red River–Lake Winnipeg system. The study site has been divided into key areas of interest (A, B, and C) that reflect both geomorphic importance and data availability as shown in Figure 1-1. The background imagery used in this figure is derived from Sentinel-2 and corresponds to an acquisition date of 22 September 2021. This image was selected to clearly delineate shoreline features and the spatial extent of open water and vegetated areas, while also highlighting pronounced sediment plumes indicative of elevated turbidity within channels and basins. The imagery was developed specifically for this thesis through band combination and composite raster processing in ArcGIS Pro, using the visible and near-infrared Sentinel-2 bands (Bands 3, 4, and 8). The resulting composite has a spatial resolution of 10 m and is used consistently as background imagery for most figures presented throughout the thesis.

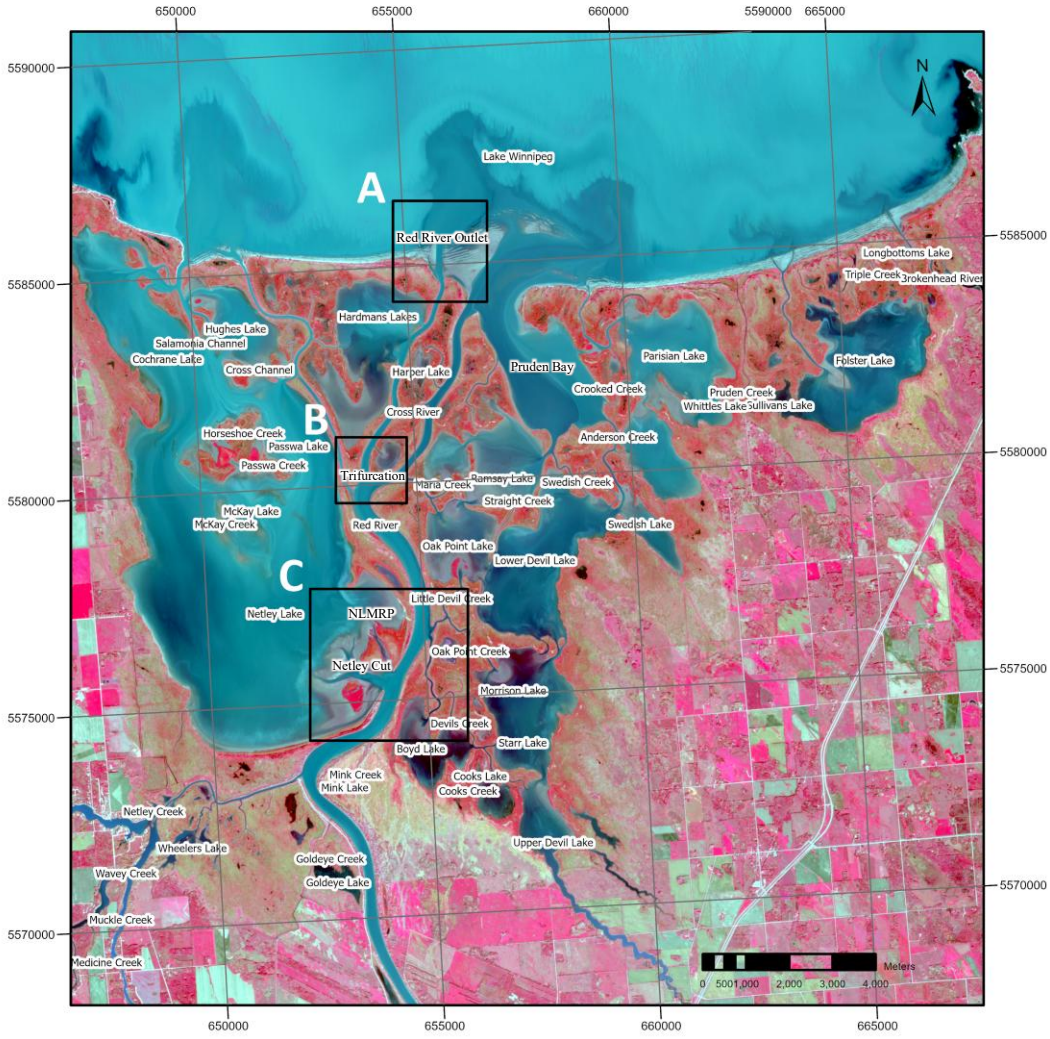

Figure 1-1 Spatial extents of the Netley-Libau Marsh study site with key areas of interest denoted by boxes A, B, and C

These three areas are:

A. The Red River Outlet – the terminus of the Red River where historic dredging activities were concentrated and where shoaling and sediment deposition are ongoing.

B. The Red River Trifurcation – the division of the Red River into distributary branches, which controls hydraulic connectivity and sediment routing through the marsh.

C. The Netley Cut Region – encompassing the Netley Cut, Netley Delta, and Netley Lake, as well as associated tributaries such as Little Devil's Creek and Devil's Creek. This

region also includes the Netley-Libau Marsh Restoration Project (NLMRP) dredge and deposition sites.

Within the Netley Cut Region, the NLMRP represents a multi-year restoration effort undertaken in several phases. Early phases of the project focused on dredging and sediment placement to evaluate sediment augmentation as a restoration strategy. More recent and ongoing work has shifted toward the Netley Cut itself, where the area is being used as a staging and testing environment for sediment retention structures and for future evaluation of plant establishment and root uptake in historically wind- and seiche-dominated zones. These interventions are intended to reduce local turbulence, limit sediment resuspension, and promote sediment deposition by protecting shallow areas from wave- and wind-driven disturbance.

Enlargements of the primary areas of interest are provided in Figure 1-2, which highlight sub-areas within Boxes B and C, including the trifurcation, Netley Cut, and restoration project site.

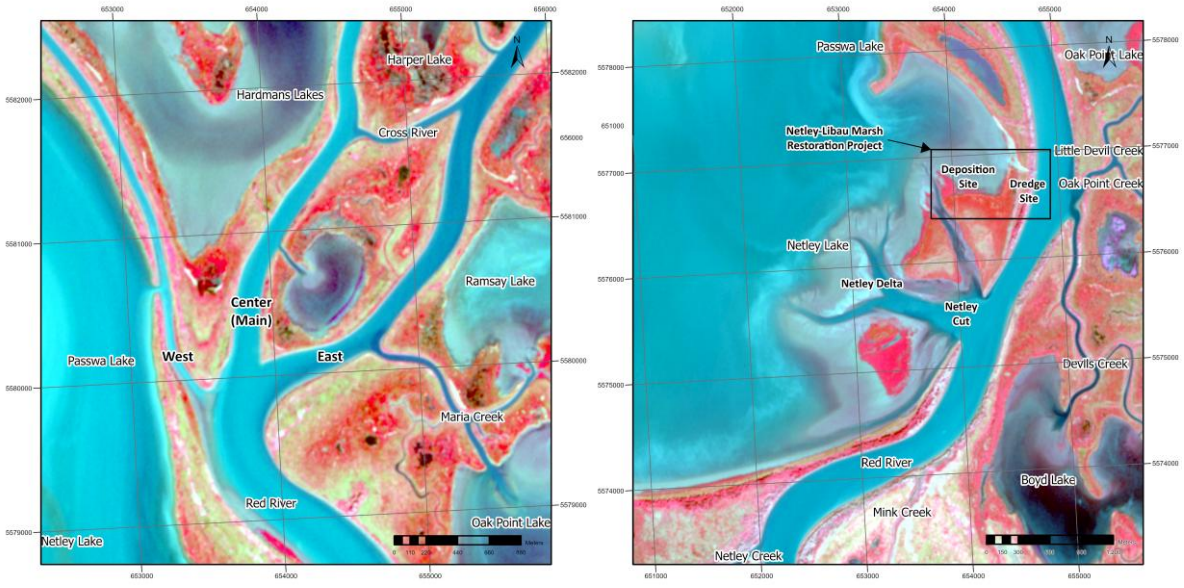

Figure 1-2 Spatial extents of key areas of interest B (left) and C (right)

Sentinel-2 Imagery – ArcGIS Developed False Colour Infrared, September 22, 2021. 10 m Resolution.

1.3 Site Description

NLM is a freshwater coastal wetland at the southern end of Lake Winnipeg where the lower Red River transitions from a confined river corridor into a broad, low-relief marsh and delta complex. The site includes shallow open-water areas, vegetated basins, and a network of channels that provide multiple pathways for exchange between the river, the marsh interior, and Lake Winnipeg. A chain of barrier beaches separates much of the marsh from the open lake, while natural openings and channel connections allow lake water to enter the marsh and marsh water to discharge to the lake under a wide range of conditions.

Hydrodynamics within NLM is governed by the interaction of Red River inflow, lake water levels at the lake–marsh boundary, and wind-driven forcing on Lake Winnipeg. Large water level fluctuations can occur in NLM over short time scales, but water-surface slopes remain small because the marsh is shallow and has minimal topographic relief. Under typical conditions, the predominant hydraulic gradient is northward from the lower Red River toward Lake Winnipeg, which supports lakeward conveyance through the connected channels in the marsh. Northern winds on Lake Winnipeg produce the largest departures from this condition by raising water levels at the south basin and pushing water into the marsh through the barrier beach openings, which can suppress or reverse the usual marsh -to-lake flow pattern. Wind setup and seiche activity on Lake Winnipeg imposes short-term water level variability that can weaken, offset, or reverse local gradients.

The geomorphic setting of the marsh is deltaic and dynamic. Sediment supply from the Red River, combined with frequent resuspension in shallow open-water areas and redistribution of Lake Winnipeg sediments during seiche events, produces spatially variable bed conditions and turbidity. Channel geometry and connectivity influence where sediment is stored, where it is

mobilized, and how suspended material is routed between the river, marsh interior, and lake. The study site represents a coupled hydrodynamic and sedimentary environment in which boundary forcing from both the Red River and Lake Winnipeg, together with shallow depths and complex connectivity, drives strong spatial gradients and event-scale variability that impact bathymetry, flow patterns, and water quality conditions.

1.4 Research Objectives

The aim of this research is to establish baseline data and analyses that characterize the geomorphology and hydrodynamics of the lower Red River and Netley-Libau Marsh, with particular focus on the Netley Region and Red River Outlet. This aim is pursued through three primary objectives:

I. Bathymetry
   - To compile, process, and analyze bathymetric datasets of the Red River outlet, the lower Red River from Breezy Point to the outlet, the Netley Cut, and the Netley-Libau Marsh Restoration Project area.
   - To evaluate changes in channel geometry and bed elevation at the Red River outlet through comparison of new and historical surveys.
   - To quantify erosion, deposition, and volumetric changes across multiple temporal windows to assess the geomorphic evolution of critical channels and key areas.

II. Water Levels and Discharge
   - To measure and analyze flow at two key locations: (i) the proportion of Red River discharge through Netley Cut, and (ii) the flow split at the Red River trifurcation.
   - To document variations in water surface elevations throughout the marsh and identify their influence on connectivity and flow exchange.

III. Turbidity

- To characterize naturally occurring turbidity levels within Netley Lake.
- To assess project-influenced turbidity generated during restoration activities under the Netley-Libau Marsh Restoration Pilot Program, with comparison to natural background conditions.
- To evaluate turbidity levels in the context of environmental licensing requirements for in-water works, thereby providing practical data to support consultants and regulators in assessing compliance.

2. Literature Review

NLM is a large coastal wetland at the south end of Lake Winnipeg, where the Red River forms a delta before entering the lake. Covering roughly 222 km^2, it is one of the largest freshwater coastal wetlands in North America (Grosshans et al., 2004). A 25-km chain of sand-barrier beaches separates the marsh from Lake Winnipeg, with multiple natural openings allowing water exchange (Wrubleski et al., 2018). The Red River flows northward through the middle of the marsh, dividing it into the Netley Marsh on the west side and Libau Marsh on the east. Historically, NLM supported extensive emergent vegetation, rich wildlife habitat, and provided valuable ecosystem services – including nutrient filtration, sediment trapping, and viable aquatic habitat that benefitted Lake Winnipeg's water quality and fisheries (Wrubleski et al., 2018). In recent decades, however, NLM's ecological integrity has severely declined, marked by dramatic loss of plant cover, eutrophication, invasive species, erosion of islands and shorelines, and expansion of open-water areas (Lake Winnipeg Foundation, 2014). Multiple stressors including hydrologic modifications, sediment/nutrient loading, fluctuating water levels, and invasive species have contributed to this degradation (Grosshans et al., 2004; Wrubleski et al., 2018). Understanding the marsh's hydrodynamics and geomorphology is essential for supporting and guiding future restoration efforts. Below, key physical and environmental aspects of Netley-Libau Marsh are presented, drawing on scientific literature and reports to provide a broad overview of hydrologic influences, seiching impacts, water quality, and geomorphic history. Additionally, this review highlights similar restoration efforts in comparable wetland systems, providing context for potential management strategies and ecological rehabilitation within NLM.

2.1 Hydrodynamics

NLM's hydrology is shaped by the interaction of river inflows, Lake Winnipeg water levels, and wind-driven exchanges (seiching). The Red River contributes the primary inflow, spreading through interconnected channels and shallow lakes in the marsh before reaching Lake Winnipeg. Flowing northward, the river bisects the middle of the marsh, dividing it into the Netley Marsh on the west side and Libau Marsh on the east. The Red River has three distributary channels: the West Channel, the East Channel, and the Centre (Main) Channel (also known as the Mouth of the Red River or the Red River Outlet). All three channels flow through the marsh before reaching Lake Winnipeg. Previous flow estimates reported by KGS (2002) during a verification of a previous *1998 LaSalle Engineering Report* details the flow split between these three branches as 43%, 41%, and 16% for the East, Main and West channels, respectively. Correspondingly, water exchange between NLM and Lake Winnipeg occurs primarily through the Salamonia channel to the west and the East, West, and Main channels of the Red River. Additional exchange occurs where the barrier beach has eroded at Pruden Bay, allowing greater connectivity between the marsh and lake. Other connections include Prudens Creek, which links the eastern marsh to Parisian Lake, and other narrow tributaries such as between Lake Winnipeg and Folster Lake. Lake Winnipeg historically received the main Red River outflow, whereas Libau Marsh was more isolated by natural levees and uplands (Grosshans et al., 2004; E. Nielsen, 1998; Wrubleski et al., 2018). Today, however, flow patterns have shifted (see 2.3 Netley Cut below), and a substantial portion of flow is diverted through the Cut at the southeastern edge of Netley Lake.

NLM is extremely flat and low-lying, so even modest river discharges or lake level changes can inundate large areas and cause significant water level fluctuations, similar to what has been

observed in the Great Lakes region (Keough et al., 1999). During spring snowmelt floods, Red River inflows can exceed the marsh's volume, flushing through the system and flowing north into Lake Winnipeg (McCullough, 2014). Conversely, when the water level at the south end of Lake Winnipeg rises (from seasonal peaks or wind setup), lake water flows south and pushes into the marsh via the Red River channels and the barrier beach openings, redistributing water across the NLM basins (Wrubleski et al., 2018). Wind-driven seiches on Lake Winnipeg are especially important: strong northerly or southerly winds cause rapid water level fluctuations in NLM on sub-daily timescales, sometimes > 1 m in magnitude (Einarsson & Lowe, 1968). These oscillations induce frequent reversals in flow direction (e.g. winds can force lake water into the marsh, followed by a seiche rebound that draws marsh water back out into Lake Winnipeg) driving intensive mixing of lake and marsh waters. Field monitoring with moored and boat-driven instruments (acoustic Doppler current profilers and sonar) have historically been used to measure bed elevation and water velocity in and around Netley Cut, showcasing that water levels and currents in the vicinity are susceptible to environmental factors (Haresign, 2012).

It is the subject of debate whether Lake Winnipeg's regulation (LWR) for hydropower has also impacted current and historical hydrodynamics in the NLM region. Since 1976, outflows into Lake Winnipeg have been partially managed by Manitoba Hydro to regulate hydroelectric generation capacity and protect communities from flooding. As part of this effort, Manitoba Hydro has been granted a license to hold lake levels between 216.7–217.9 m above sea level (asl) (Final Licence to Lake Winnipeg Regulation, 2021). Over the period of regulation, both mean inflow to and mean water level on Lake Winnipeg have increased. The monthly mean water level and inflow between the epochs of 1977 to 1998 and 2008 to 2016 saw an increase of 0.32 m and 766 m^3/s (44%), respectively (Environment and Climate Change Canada & Manitoba

Agriculture and Resource Development, 2020). Regulating lake levels has dampened the seasonal cycles and increased the mean water level, ultimately lowering peak levels and preventing very low levels, which are fundamental for healthy emergent-vegetation (Grosshans et al., 2004). While regulation did *not* significantly raise the long-term average level, it eliminated the prolonged drawdowns that historically allowed marsh sediments to dry and plants to regenerate. In NLM, the lack of extended low-water periods post-1970s has impeded emergent vegetation recovery and left shorelines more vulnerable to erosion, as plant root systems can no longer stabilize sediments during multiyear lows (Grosshans et al., 2004). On the other hand, short-term fluctuations from wind setup still occur and can expose mudflats briefly, but these events are erratic and too short-lived for widespread plant establishment. The net effect is a hydrologic regime that features less inter- and intra-annual variability with higher average water levels, punctuated by fluctuations due to wind-driven surges (Einarsson & Lowe, 1968; Lindgren & Netley Marsh Waterfowl Foundation, 2010).

2.2 Geomorphology

Geomorphology and sediment dynamics in NLM can be traced back to the geological events that shaped Glacial Lake Agassiz. The lake covered substantial portions of present-day Manitoba and significantly influenced regional topography through extensive sediment deposition across its basin (Michalek, 2013). Tyrrell (1896) describes how the retreat of the Laurentide ice sheet led to the formation of Glacial Lake Agassiz. As meltwater was impounded between retreating ice margins, large volumes of fine sediment were deposited across the Lake Winnipeg Basin. This formed a broad low-relief landscape of stratified sands and clays. The deposition of these sediments contributed to the formation of extensive deltaic and wetland environments as post-glacial rivers established new flow patterns. As the Red River became a conduit into Lake

Winnipeg, its sediment-laden floodwaters interacted with the retreating glacial terrain, creating conditions suitable for the formation of deltaic wetlands like NLM.

Today, the marsh is characterized by a barrier beach that has developed along the south shore of Lake Winnipeg, where Red River deltaic sediments are deposited in sheltered areas. Isostatic rebound in the northern portion of the Lake Winnipeg basin is progressively tilting the basin southward, producing a relative rise in water levels at the southern end of the lake on the order of 20 cm per century (E. Nielsen, 1998). This long-term rise in relative water level promotes sustained inundation at the south end of Netley-Libau Marsh, contributing to submergence and erosion of the barrier beach and altering marsh surface elevations. A hemi-marsh is a wetland condition characterized by approximately equal areas of emergent vegetation and open water, maintained by periodic exposure and inundation of marsh surfaces. Marsh vegetation within NLM includes both emergent and submergent classes that occupy narrow elevation ranges relative to typical water levels, such that prolonged inundation shortens exposure periods required for emergent vegetation to persist. Sustained elevation of water levels further limits light penetration to submerged vegetation, hindering photosynthesis and disrupting nutrient cycling that depends on alternating periods of exposure and submergence. Over time, these processes reduce the hydrologic variability required to maintain a hemi-marsh structure and favour conversion toward more persistent open-water conditions.

Correspondingly, the aforementioned barrier beach formation has been breached in many locations: historical air photos show about 7 inlet openings in 1946 versus 11 by 2001 (Watchorn, 2015). These additional channels enhance water and sediment exchange with Lake Winnipeg, especially during storm events. Inside the marsh, what was formerly a mosaic of smaller vegetated ponds and alluvial levees has transformed into large open bays (e.g. Netley

Lake) due to erosion of shorelines, loss of root-systems, and flooding of islands. Wave action on these open-water expanses further erodes shorelines and redistributes sediments, reinforcing the expansion of open water areas at the expense of hemi-marsh terrain (Wrubleski et al., 2018).

Sediment transport and deposition in NLM are primarily driven by interactions between the marsh, the Red River, and Lake Winnipeg. The Red River transports significant suspended sediment loads, mainly fine silts and clays originating from its expansive drainage basin, resulting in high turbidity levels relative to adjacent river systems such as the Winnipeg River (Brunskill & Graham, 1979; Erik Nielsen & Conley, 1994). Bottom sediment samples from channels near NLM—including the Main, East, West, and Salamonia Channels—consist mainly of sand (5–58%), silt (16–64%), and clay (15–35%), highlighting the dominance of fine-grained material in the marsh's sediment dynamics (Erik Nielsen & Conley, 1994). Sediment is delivered both through river transport and by coastal erosion processes. It is estimated that the Red River collectively supplies 2.65 million tonnes of sediment to Lake Winnipeg annually (Brunskill & Graham, 1979). Using paired total suspended solids measurements at Selkirk and near the mouth of the Red River, Goharrokhi (2022) showed that concentrations near the mouth are on average 32% lower than at Selkirk, implying that roughly one third of the lower Red River sediment load is diverted into the Netley–Libau marsh complex before reaching Lake Winnipeg. On this basis, approximately 0.9 million tonnes per year of suspended sediment are estimated to be trapped within the marshes, while about 1.9 million tonnes per year are delivered directly to the lake. Additional fine grained inputs from shore erosion along the south and north shores of Lake Winnipeg, on the order of 1–3 million tonnes per year, further augment the supply of mobile sediment that can be redistributed into NLM during storm driven exchange events (Brunskill & Graham, 1979; Goharrokhi, 2022). These sediments are then redistributed inland via breaches in

the barrier beach system during storm events. Deltaic fans and sediment plumes illustrate active sediment transport inland, with aerial photography showing that sediment-laden waters frequently enter the marsh interior, creating extensive flood deltas and reinforcing sediment deposition inland rather than toward the lake (Nielsen & Conley, 1994).

Historically, sediment dynamics have been partially influenced by dredging activities intended to maintain navigable channels from the Red River into Lake Winnipeg. As reported by Goldsborough and Grover (2021), dredging began in 1884 with the West Channel of the Red River serving as the primary navigation route for ships traveling to Lake Winnipeg. However, by spring 1893, sediment accumulation had severely obstructed this channel, making it too shallow for navigation. Consequently, from 1893 until approximately 1903, the East Channel served as the main navigation route until sediment infilling similarly prompted a shift to the Main Channel. The Main Channel then became (and has remained) the primary navigational route on the Red River. Between the years of 1960 to 1998, routine annual dredging of the mouth of the Red River was undertaken (KGS, 2002). However, dredging operations halted in 1999. Over the past century, changes in flow routing, particularly the creation and subsequent enlargement of Netley Cut, are postulated to have reduced the proportion of Red River discharge flowing directly into Lake Winnipeg via the main channel and increased the proportion routed through Netley Lake via the Cut, thereby increasing both flow and sediment delivery into Netley Lake (Clean Environment Commission, 2015).

2.3 Netley Cut

One of the most consequential alterations to the hydrodynamics and geomorphology of NLM was the creation and expansion of the Netley Cut. Constructed in 1913 by the Canadian federal government, the Netley Cut is an artificial channel linking the Red River to Netley Lake at the

most southeastern extent of Netley Marsh (Grosshans et al., 2004). Kowal (2019) conducted a historical review of archival research and aerial imagery within NLM and determined that the Netley Cut was constructed as a 27.5 m navigation channel for harvesters to access hay fields and (potentially) to alleviate upstream Red River flooding. Grosshans (2004) noted that the primary intent of the Cut was to improve drainage of low-lying haylands during seiche events and to enable boat access for local residents harvesting cordwood and hay along the shores of Netley Lake. Manitoba Hydro also stated the Cut was constructed to partially drain water from Netley Lake to make hay harvesting easier (Clean Environment Commission, 2015).

Shortly after excavation, the Cut began to widen and deepen due to erosion, prompting repeated government intervention. A bridge constructed to provide access to haylands north of the channel was lost during high flows in 1916, underscoring the instability of the channel and the difficulty of maintaining fixed infrastructure across it. Dredging and structural control measures, including construction of a sheet-pile dam and replacement bridge works, were undertaken intermittently between 1919 and the mid-1920s in an effort to limit erosion and regulate flow. Despite these efforts, channel enlargement continued, with the Cut exceeding 24 m in width and approximately 5 m in depth by the mid-1920s (Goldsborough, 2015; Grosshans et al., 2004).

The Cut was officially sealed off in 1925 by the new sheet-pile dam and would remain closed for 43 years (Kowal, 2019). During this period the marsh was hydrologically isolated from direct river flow, aside from small breaches during extreme events (e.g. the flood of 1950). A review of Kowal's aerial imagery during the period in which the Cut was closed shows the hemi-marsh environment of southeast Netley Lake fully inundated beyond 1929. This could be circumstantial, however, based on the time and date of aerial imagery with respect to water

surface elevation on Netley Lake. A combination of unusually high Lake Winnipeg water levels in the late 1960s and a flood in 1970 caused the failure of the old sheet-pile dam, reconnecting the Red River to Netley Lake in 1970. Henceforth, the Netley Cut remained permanently open and began enlarging at a rate of approximately 13.5 m per year (Kowal, 2019). The channel has widened dramatically from its original dredged size and has been estimated by several authors as being upwards of 400 m wide, with the widest cited width being 457.7 m in 2015 (Goldsborough, 2015; Grosshans et al., 2004; Kowal, 2019; Watchorn, 2015).

2.3.1 Flow Split

The enlargement of the Netley Cut has fundamentally changed water flow patterns in Netley Lake. A substantial portion of Red River discharge is now diverted through Netley Cut into Netley Lake, rather than flowing down the Red River directly to Lake Winnipeg. Unpublished field measurements based on ADCP discharge estimates between 2009-2011 indicate that on average one third of the Red River's flow enters the marsh via Netley Cut (Grosshans et al., 2012; Kowal, 2019). This diversion represents the largest hydrologic connection to Netley Lake, whereby water from the Red River can freely spread through NLM before reaching Lake Winnipeg. The enhanced connectivity means increased flows and velocities within parts of the marsh and enhanced hydraulic linkage between the river and wetland. Hydrodynamic modeling studies support these observations: when the cut is open, some flow is siphoned off, which slightly lowers the stage of the river upstream and reduces the velocity in the downstream main channel, whereas simulated closure of the cut causes marginal higher upstream water levels and slightly faster currents in the Red River (Haresign, 2012). Furthermore, flow distribution through the Netley Cut is not constant, varying with hydrological and seasonal conditions. During spring flood periods or high Red River discharge events, a greater volume of water is driven into NLM

and impacts the flow split between the Red River and Netley Cut. Conversely, under low-flow or winter ice-covered conditions, the split of water may be reduced, though flows through the cut have been verified by under-ice field measurements to persist year-round (Haresign, 2012). As previously touched upon, water movement between the marsh and Lake Winnipeg is also influenced by wind-driven lake level fluctuations. These wind and seiche events drive bidirectional exchanges through marsh inlets, including the Netley Cut, with decreasing flows out of the marsh during falling lake levels and vice-versa during rising lake levels (Erik Nielsen & Conley, 1994). Overall, however, the net hydrodynamic effect of the Netley Cut is a consistent routing of a significant share of the Red River's water and sediment load into Netley Lake.

2.4 Seiching in Lakes and Coastal Environments

Seiches are standing wave oscillations in enclosed or semi-enclosed water bodies that cause rhythmic rises and falls in water level. They typically form when sustained winds or sudden atmospheric pressure changes push water toward one end of a lake or basin; when the forcing stops or slackens, the displaced water sloshes back and forth, oscillating around an equilibrium until dissipated by friction (Einarsson & Lowe, 1968). Wind forcing is the primary driver of Lake Winnipeg's seiche activity. The lake's considerable length (~436 km), shallow depth, and strong prevailing winds mean that even moderate storms can push a large volume of water from one end to the other. When a strong northerly wind blows down Lake Winnipeg, it drives a wind setup that elevates water levels in the south basin and depresses them in the north basin. When the wind relaxes or shifts the water begins oscillating as a seiche. These oscillations can persist from hours to days, often creating distinct patterns known as modes, each defined by areas of minimal water-level fluctuation called nodes. Nodes act as pivot points or stationary lines in the lake, around which water levels rise and fall during oscillations, with the fundamental mode

having the fewest nodes and longest oscillation period, while higher-frequency modes contain multiple nodes determined by basin geometry and depth (Hamblin, 1976). In large lakes, the effect of seiches on coastal wetlands is analogous to tidal influences in estuaries, providing periodic fluctuations in water levels that regularly inundate and expose shoreline habitats. These daily water-level variations shape wetland ecosystems by influencing plant zonation, nutrient exchange, and sediment dynamics, which ultimately enhance biological diversity and productivity in coastal wetland communities (Trebitz, 2006). Unlike true tides, seiches are meteorologically forced and can be irregular, but they still produce periodic inundation and exposure of the shoreline.

The practical importance of seiches in lacustrine and coastal environments is well documented. They contribute to water exchange, mixing, and ecosystem connectivity in coastal areas while also posing hazards. For instance, storm and wind-induced seiches can lead to unexpected flooding of low-lying shores and wetlands (Farhadzadeh, 2017).

2.4.1 Impacts on Lake Winnipeg

Lake Winnipeg is notorious for its pronounced seiches and wind-driven surges. It is a large but relatively shallow lake with two distinct basins (North and South) connected by a narrow channel. This geography influences its oscillation modes. Einarsson and Lowe (1968) examined water level records (1961–1964) from six Lake Winnipeg stations and identified frequent seiches, noting that the north and south basins oscillate somewhat independently due to the constricting effect of the narrows and interceding islands. In the south basin, two dominant seiche periods of approximately 1.7 hours and 5.1 hours were observed, corresponding to a shorter transverse seiche (east-west) and longer longitudinal seiche (north-south), respectively. Interestingly, the shorter-period seiche could reach an amplitude of up to ~0.45 m in initial

oscillations, while the 5 h seiche typically had smaller initial amplitude (though rising to greater amplitudes over time) These oscillations in the south basin tend to dampen on the order of 10–12 cycles, but even a single cycle could cause the water level at the shoreline to rise or fall by several tens of centimeters in a few hours. In contrast, the north basin has different seiche nodes due to being deeper and larger than the south. Einarsson and Lowe observed prevalent oscillations with periods around 3.5–4.5 h in the North Basin along with a longer-period seiche of about 13 h.

In a constricted, two-basin system like Lake Winnipeg, the Narrows always introduce some degree of hydraulic separation between the North and South basins. In other words, the basins are never perfectly coupled: the constriction attenuates and phase shifts the oscillation as it propagates through the Narrows, so the response in the two basins is not identical. This can be described as partial decoupling. Full decoupling, in contrast, would require a true node at the Narrows so that a standing wave in one basin produces essentially no oscillatory signal on the other side. The partial decoupling of the basins means that some seiches experience varying amplitudes but consistent sign with a node at the Narrows, while other oscillations encompass the entire lake. This behavior is consistent with general theory for multi-armed lakes: such lakes can exhibit both full-lake seiche modes engaging both basins and partially decoupled modes where oscillation are constrained to one basin if a node develops at a junction (Brenner & Laval, 2018).

Hamblin (1976) applied numerical hydrodynamic models to Lake Winnipeg's open-water season. He found the lake's fundamental seiche period to be ~39 hours (extraordinarily long) and considered it to be "a maximum for any inland water body". This ~39 h mode likely corresponds to a full-lake oscillation. Hamblin also detected at least four higher modes with periods down to

~7.5 h for the fifth mode. These higher modes presumably include the ~13 h northern and ~5 h southern oscillations noted by Einarsson, among others. His modeling indicated that frictional damping has a noticeable influence on Lake Winnipeg's seiches, which may explain why the observed oscillations in the shallow south basin die out faster. Importantly, Hamblin's work highlighted the spatial variability of seiche effects: the largest water level fluctuations occur in the south basin.

Correspondingly, the impacts of Lake Winnipeg's seiche regime on shoreline processes and hydrodynamics are profound. Veldman (1969) noted that because the lake is so shallow and responsive, storm-driven seiches enable waves to attack the shore at elevations far above normal lake level. In Lake Winnipeg, the worst shoreline erosion tends to occur during these episodic seiche events, rather than as gradual year-round recession (Veldman, 1969). The rapid water level oscillations allow storm waves to penetrate inland, overtopping beaches and sand bars. This leads to shoreline inundation, sediment mobilization, and erosion of banks and wetlands that would otherwise be beyond the reach of wave action. Hydrodynamically, the seiches drive strong oscillatory currents through the Narrows and along the shorelines, continually mixing the lake's waters. The frequent high amplitude seiches effectively flush shallow embayments and wetlands, influencing water chemistry and ecological conditions. Analogous seiche-driven water level fluctuations in the Great Lakes have been shown to play a role similar to tides in structuring coastal wetland ecosystems (Trebitz, 2006), and Lake Winnipeg's seiches likely serve a comparable ecological function.

2.4.2 Impacts on Wetlands

In large freshwater lakes, seiches function much like tidal pulses, periodically inundating and exposing wetland areas. Research on the Laurentian Great Lakes has drawn parallels between

seiche influences and wetland health (Bedford, 1992; Burton, 1984; Grabas & Rokitnicki-Wojcik, 2015). One key effect is the regular hydrologic fluctuation that seiches provide. Even when not extreme, these water level changes maintain dynamic wetland conditions. A broad analysis of Great Lakes water level records found that virtually all coastal sites experience some seiche-driven fluctuation activity at all times (Mortimer, 1987). Typical day-to-day water level ranges caused by combined seiche and long-period oscillations are on the order of a few centimeters to a few tens of centimeters. For example, the average daily water level range is about 4 cm in Lake Ontario and exceeds 20 cm in Lake Erie, with the largest short-term swings generally observed at the ends of the lakes (Trebitz, 2006). At the high end, hourly-scale seiches of 10–30 cm are common in the Great Lakes (O. Anderson et al., 2023). These fluctuations are modest compared to ocean tides, but they occur in lakes that otherwise have very little tidal variation.

The hydrological fluctuation from seiches benefits wetland environments in several ways. It promotes mixing of water and nutrients, prevents stagnation, and can transport organic material and organisms in and out of marshes. Periodic inundation from seiches allows fish and aquatic invertebrates to access peripheral wetland areas and then retreat, providing tidal feeding cycles in water bodies (Keough et al., 1999). Additionally, the wetting and drying cycles influence soil moisture and nutrient availability in the wetland substrate. During a seiche-induced high water event, previously dry portions of the marsh plain may be submerged, mobilizing nutrients and sediments. As the water recedes during the low phase, oxygen is reintroduced to soils and certain areas dry out (Mariotti, 2016; Walters et al., 2014). This alternation can enhance biogeochemical processes and habitat complexity. A recent modeling study by Harrow-Lyle et al. (2023) demonstrated that when Lake Ontario coastal marshes are inundated by seiche events, there is

significant sediment resuspension and exchange of nutrients between the wetland and lake. In their analysis of three Lake Ontario marshes, seiche events were found to stir up bottom sediments in the wetlands, leading to increased phosphorus loading from the marshes into the open lake. Seiches can also alter water quality and nutrient dynamics, potentially exporting nutrients that fuel algal blooms in Lake Ontario, but also delivering lake nutrients into wetlands when water flows in reverse.

Perhaps the most critical impact of seiching is on wetland vegetation and habitat structure. Coastal wetland plant communities in the Great Lakes and other large lakes have evolved under a regime of water level fluctuations of varying frequency and amplitude that are characterized by intermittent drought and flooding conditions (Keough et al., 1999). Many studies emphasize that a diversity of water level conditions (from short-term seiches to seasonal and multi-year lake level swings) is essential for maintaining species diversity and ecological function (O. Anderson et al., 2023; Wilcox & Nichols, 2008). Wilcox & Nichols (2008) note that the richness and habitat value of Great Lakes wetland plant communities depend on water-level fluctuations of varying frequency and amplitude and provide quantitative evidence that such fluctuations drive vegetative change in these wetlands. Alternating high and low water periods prevent any one plant type from completely dominating: high water events can drown or set back upland plants, while low water periods expose mudflats and allow colonization by opportunistic species (Keddy & Reznicek, 1986; Maynard & Wilcox, 1997).

Short-term seiches contribute to this regime by causing temporary flooding and drying. While a single seiche is too brief to destroy emergent vegetation, the cumulative effect of frequent minor inundation can favor certain water-tolerant species and limit others. For example, research in Lake Huron's coastal marshes documented rapid plant community responses to water level

changes. Gathman et al. (2005) observed that an episode of elevated water in the mid-1990s did not immediately shift the physical location of plant zones, but it did alter species presence and abundance within zones over a short time span. In their 3-year study, a wet meadow zone that had been recently flooded saw declines in certain emergent plant densities (e.g., sedges and cattails) after a year of sustained high water, and only partial recovery when water levels receded the following year. They concluded that periodic flooding and drying are *"*critical to maintaining a diverse array of plant species in the wet meadow zones*"* of coastal marshes (Gathman et al., 2005, p. 160). Consistent with this, wetlands experiencing dynamic water level regimes support distinct and more diverse plant assemblages than those in artificially stabilized water levels (O. Anderson et al., 2023). Where water levels have been controlled and fluctuations dampened (for instance, parts of Lake Ontario historically regulated for navigation), wetlands often become monocultures or lose their interspersion of habitat types (Grabas & Rokitnicki-Wojcik, 2015; Keddy & Reznicek, 1986).

On the other hand, Anderson et al. (2023) noted that extreme seiche events or oscillations superimposed on already high lake levels can further stress wetland systems. If water levels rise too high or stay inundated for too long, important vegetation like sedges, rushes, and wet meadow species can drown, leading to loss of wetland area. They noted that wetlands can adapt to gradual changes by migrating upslope, but rapid or extreme rises led to losses in wetland extent when the change outpaced the vegetation's ability to adjust. In the context of Lake Winnipeg or similar large lakes, a large seiche occurring during an already high-water period could exacerbate flooding of marshes and potentially uproot vegetation or erode soil.

2.5 Marsh Restoration

Marshes are highly productive ecosystems, delivering critical ecological services such as biodiversity support, water quality improvement, carbon sequestration, and storm protection (Billah et al., 2022; Bertolini & da Mosto, 2021). Despite their substantial environmental and economic value, marshes have experienced significant degradation globally over the past century, driven primarily by anthropogenic impacts including land reclamation, sediment starvation, eutrophication from nutrient loading, and accelerated sea-level rise (Berkowitz et al., 2017). These pressures have been particularly severe in regions like the northern Gulf of Mexico, where Louisiana alone lost approximately 1.2 million acres of marshland to open water between 1932 and 2010 (Billah et al., 2022). Additional stressors, including subsidence, increasing storm frequency and intensity, and human-driven hydrological alterations, further accelerate marsh erosion and degradation.

Marsh restoration efforts have become critical components of coastal management agendas worldwide. Common restoration strategies include sediment augmentation (Materne et al., 2007; Taylor & Foret, 2015), hydrological reconnection or tidal restoration (Mariotti, 2016; Mitsch & Wang, 2000), targeted vegetation restoration (Materne et al., 2007; Mitsch & Wang, 2000), and management of barrier beach-marsh dynamics (Walters et al., 2014; Ganju, 2019). Historically, restoration approaches evolved from localized measures, such as simple vegetation planting, to integrated ecosystem-level interventions combining multiple abiotic and biotic components (Berkowitz et al., 2017; Bertolini & da Mosto, 2021). These modern approaches focus not only on restoring physical habitat area but also on promoting ecological function, sediment dynamics, resilience to climate change, and long-term stability of marsh ecosystems (Ganju, 2019; Walters et al., 2014). Restoration outcomes are typically evaluated using multiple indicators, including

sediment accretion rates, vegetation recovery, and improvements in ecosystem functions such as faunal usage and water quality (Billah et al., 2022; Mitsch & Wang, 2000). The following section outlines the primary restoration method applied in the Netley-Libau Marsh Restoration Project in 2021, focusing on the use of sediment augmentation to support marsh rehabilitation.

2.5.1 Sediment Augmentation

Sediment augmentation is often the foundation of marsh restoration, given that many degraded marshes have lost elevation or substrate volume. One widely used technique is the beneficial use of dredged material to raise marsh bed elevations. Dredged sediments from navigation channels or nearby waterways are repurposed and deposited onto marsh surfaces or shallow open-water areas that were historically hemi-marsh habitats. This practice has been employed for decades; early examples date back to the 1970s–1980s when confined disposal of dredge spoil was explored for creating marsh habitat (Berkowitz et al., 2017). Modern projects refine this approach through methods like thin-layer placement, where a slurry of dredged sediment is sprayed or spread in a thin lift (often <30 cm) across the marsh. The goal is to incrementally increase elevation without completely smothering existing vegetation or altering the marsh's natural functionality, as various plant species will have greater uptake success under specific depths (Materne et al., 2007; Wilber, 1993). Nester & Rees (1988) formally defined thin-layer placement as adding dredged sediment at a thickness that does not fundamentally change the habitat's ecological character. Empirical studies have shown the importance of controlling sediment thickness: for instance, experiments in Georgia found that adding ~23 cm of sediment allowed marsh plants to recover, whereas thicker deposits could prevent plant regrowth by burying vegetation too deeply (Reimold et al., 1978). Placing sediment in thin-layer deposits

with varying depths has differential effects on the success of emergent vegetation (Materne et al., 2007).

Numerous studies have demonstrated the effectiveness of sediment augmentation in marsh restoration (Berkowitz et al., 2017; Louisana Coastal Wetlands Conservation, 2004; Taylor & Foret, 2015). The West Bay project in coastal Louisiana uses sediment from a Mississippi River diversion to facilitate the rehabilitation of over 9,800 acres of marshland from previously open water areas over two decades (Louisana Coastal Wetlands Conservation, 2004). Similarly, in Avalon, New Jersey, dredged sediment was strategically applied in thin layers following Hurricane Sandy, leading to measurable elevation gains and rapid recolonization by vegetation (Berkowitz et al., 2017).

In addition to thin-layer placement, marsh terracing, an engineered approach increasingly used along the Gulf Coast, involves constructing segmented and elevated earthen mounds in open water areas that were once marshland. These terraces, typically built from shallow subtidal material and aligned to match or exceed the surrounding marsh elevation, reduce wave action, trap sediment, and foster natural vegetation establishment. For example, the delta management at Fort St. Philip in Plaquemines Parish, Louisiana, constructed 98 terraces to capture sediment delivered by river diversions (Prendergast, 2016). The terraces successfully reduced wave energy, encouraged sediment deposition, and accelerated marsh-building between ridge segments.

Together, these approaches highlight how sediment augmentation, whether through thin-layer placement or engineered terracing, has become a central strategy in coastal and deltaic marsh restoration. While outcomes vary depending on site conditions, elevation targets, and vegetation response, the consistent theme is that strategic reintroduction of sediment can offset subsidence,

restore habitat structure, and improve long-term marsh resilience. These findings provide context for the NLMRP, where similar methods have been piloted as a means of addressing ongoing habitat decline and hydrologic alteration.

3. Bathymetry

3.1 Introduction

Bathymetric information for NLM remains sparse, fragmented, and notably limited in published peer-reviewed literature. The primary source of bathymetric data currently available for NLM comes from Aquatic Environmental Services (AES), which conducted extensive surveys between May 2010 and August 2011 (Aquatic Environmental Services, 2011). This dataset provides detailed bed elevations and volumetric calculations for major water bodies and streams within the marsh. AES employed single-beam sonar with post-processed RTK GPS techniques to produce detailed bathymetric maps, volumetric calculations, and XYZ datasets at a 3 m resolution within the lakes and small streams that comprise the marsh. The AES report presents these products for the marsh waterbodies but does not include formal bathymetric maps of the Red River. However, a detailed review of the accompanying metadata and raw XYZ files revealed previously undocumented 1 m resolution bathymetric datasets for the Red River from upstream of Breezy Point to the Red River outlet. Within this AES dataset, coverage of the West Channel of the Red River is incomplete due to insufficient water depth at the time of survey.

The lack of comprehensive bathymetric data outside of the AES survey prompted future research to utilize historical and supplementary data that approximated bathymetric conditions in parts of NLM. Haresign (2012) highlights the insufficiency of existing bathymetric data upstream of the Netley Cut, necessitating reliance on historical cross-section surveys conducted in 1957. Although recognized as outdated, these cross-sections provided the only readily available reference data at the time. Additionally, cross-sectional bathymetry published in KGS Group's 2009 dredge assessment and limited field measurements from the Hydraulic Research

and Testing Facility (HRTF) at the University of Manitoba (2010) supplemented the AES data. Complementing the AES dataset, Manitoba Hydro conducted bathymetric surveys in 2018, focusing exclusively on the Red River from Netley Creek to the outlet of the Red River. These results were subsequently published indirectly in Becket (2020), providing recent bathymetric mapping specifically for the Red River near its entrance into the marsh. Manitoba Hydro produced rasterized images that utilized an unknown interpolation technique and provided raw XYZ points for future analysis.

Furthermore, the 2019 KGS licensing application on the NLMRP explicitly acknowledges reliance on AES's bathymetric findings. The dataset significantly informed the selection and feasibility of dredging locations for marsh rehabilitation and mudflat creation, particularly within Hardmans and Netley Lake. Decisions regarding sediment removal volume, targeted dredging areas, and optimal mudflat construction sites were informed by AES's earlier bathymetric mapping. Planned post-project monitoring emphasized comparative bathymetric surveys conducted one-year after dredging to assess sediment movement, deposition, and retention (KGS Group, 2019).

Overall, the AES 2010 survey has remained unmatched in its comprehensiveness and scope since its completion. No subsequent studies have provided comparative coverage or similar detailed resolution, rendering the AES dataset an indispensable baseline for subsequent research. All cited work since its publication has utilized the AES survey as a foundation for bathymetric mapping, analyses, and interpretation of marsh impacts.

3.2 Background

The bathymetric surveys used within this thesis were developed to characterize temporal and spatial changes in bed morphology within the lower Red River and key areas throughout the Netley-Libau Marsh. The primary objectives were to document changes in bed structure, identify erosion and deposition areas, and generate high-resolution bathymetric surfaces that could support both qualitative interpretation and quantitative analysis. Specific goals included the creation of DEMs for each individual survey period followed by comparative assessments of bed elevation changes using surface differencing and volume estimates. This approach enabled both inter- and intra-annual evaluations of morphologic change within the three key areas of bathymetric interest.

Site selection was informed by a combination of navigational importance, flow-split locations, previous datasets, and accessibility by boat. Three principal areas were identified for targeted study shown in Figure 3-1: the outlet of the Red River (location A), the dredge and deposition site developed under the NLMRP (location B), and the Netley Region (location C). These locations were selected due to their strategic role in restoration activities, sediment transport and deposition processes, dynamic hydraulic conditions, and the availability of limited but valuable historical comparison datasets. The Red River Outlet was prioritized due to ongoing shoaling and infilling that has occurred since the cessation of federal dredging in 1999. Historical profile plots referenced in KGS Group (2002), originally collected by the Canadian Coast Guard and maintained by the Canadian Hydrographic Service, provide an essential baseline for evaluating sediment movement at this location. The NLMRP site was included as the focal area of ongoing restoration work, where dredged material has been deposited to test the feasibility of sediment augmentation as a means of marsh rehabilitation. Finally, the Netley Region, including

the Netley Cut and its adjacent channels, was selected for its importance in diverting flow into the interior of Netley Lake, its contribution to sediment delivery, and its geomorphic response since the natural reopening of the Cut in 1970.

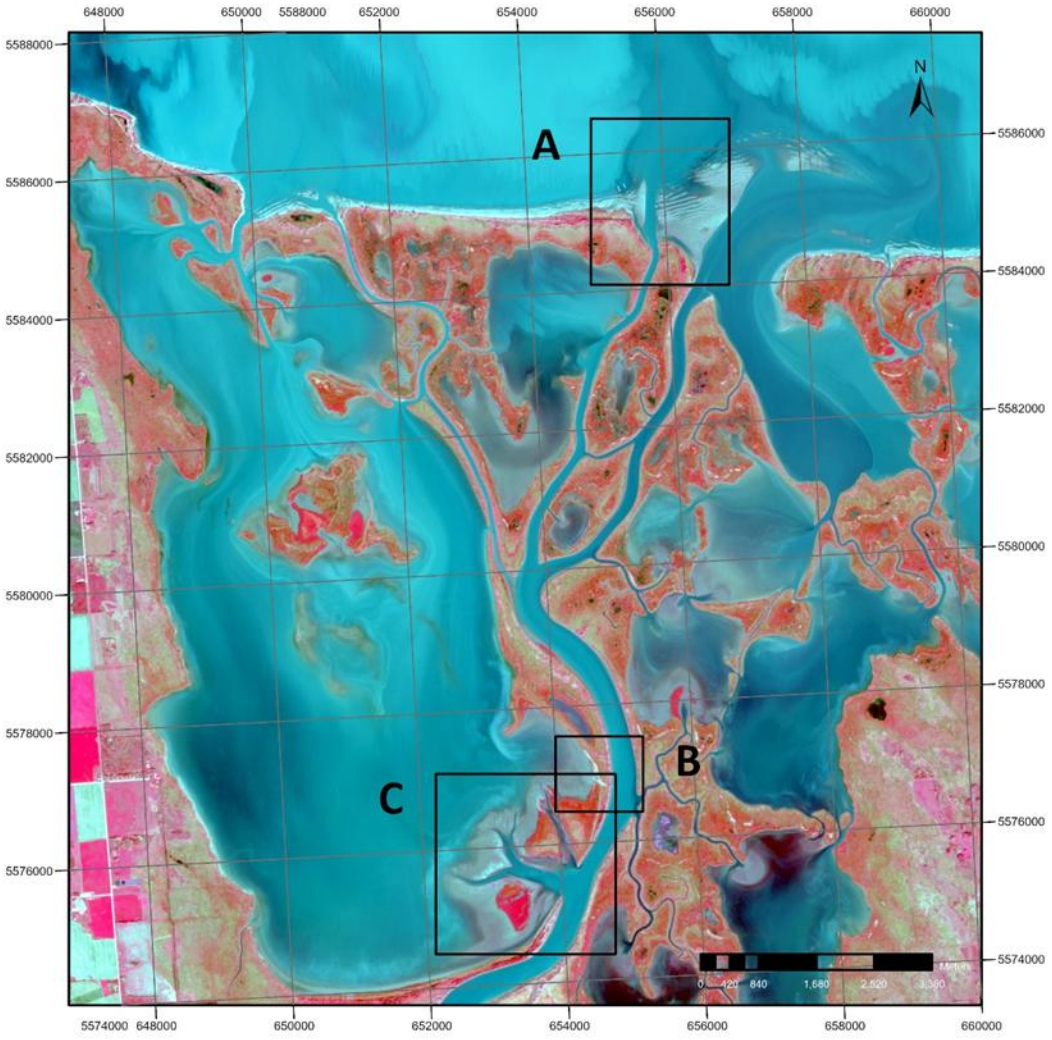

Figure 3-1 Key bathymetric survey locations within Netley-Libau Marsh

Sentinel-2 Imagery – ArcGIS Developed False Colour Infrared, September 22, 2021. 10 m Resolution: (A) Red River Outlet; (B) Netley-Libau Marsh Restoration Project; (C) Netley Cut Region.

3.2.1 Beam Systems and Swaths

Beam echo-sounder systems come in two types: single-beam echo sounders (SBES), which use a single transducer as both transmitter and receiver, and multibeam echo sounders (MBES),

which rely on separate arrays of transducers dedicated to either transmitting or receiving. MBES systems operate by forming a fan-shaped array of beams that cover an elliptical strip of the bed below a vessel's path. They employ one or several transmitting beams with hundreds or thousands of receiving beams to encapsulate a coverage area in a high degree of detail. This contrasts with SBES systems, which collect pointed depth readings directly in-line with the transducer and therefore require significantly more passes for full bed coverage or rely on interpolation techniques to inference unknown surface elevations. As a result, SBES leaves unsounded gaps between lines unless spacing is very tight, while MBES yields near-areal coverage with far higher sounding density. Practically, MBES reduces the amount of interpolation required to produce digital elevation models (DEMs), whereas SBES workflows rely heavily on interpolation to fill between measured points (Coggan et al., 2007). IHO S-44 defines survey specifications, uncertainty requirements, and the concept of full seafloor search and object detection. These objectives are typically met with MBES and rarely achievable with SBES without prohibitive line spacing and auxiliary side-scan sonars. Furthermore, the SBES swath increases with depth (approximately with range and beamwidth), and covers larger bed patches on rough or sloping terrain thus creating biased depth inferences. MBES mitigates this by distributing many narrower beams across track and by scaling swath width with depth, enabling high node occupancy at fine grids in shallow water and improved detection of small bedforms (International Hydrographic Organization, 2024; USACE, 2013). Figure 3-2 shows a water vessel mounted with both an SBES and MBES system with a single receiving and transmitting transducer below vessel and a forward mounted multi arrayed receiving and transmitting transducer below bow. θ represents the angle of an SBES system and ϕ_R represents the across-track receiving angle of an MBES system.

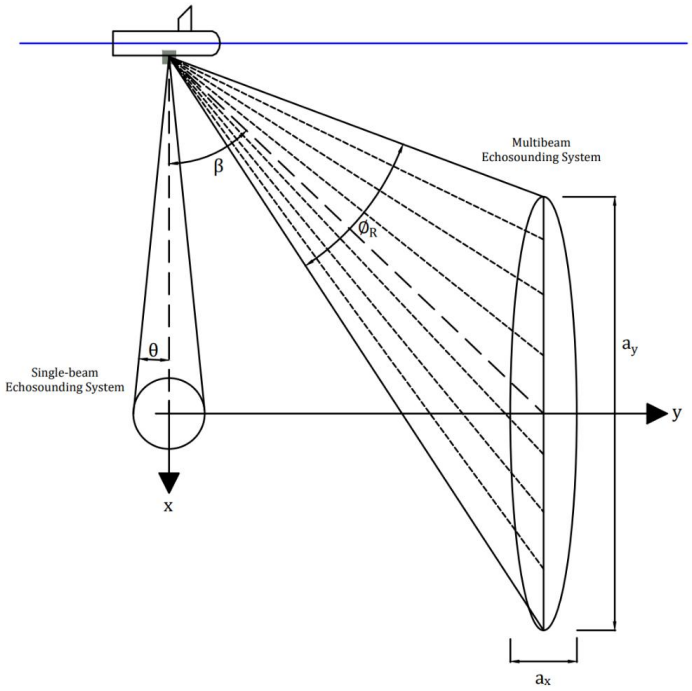

Figure 3-2 Single and multibeam echosounding systems on a water vessel.

The Sontek M9® (used within this thesis for bathymetric mapping) uses an SBES system with multiple transducers that record depth at 5 known positions. Four equidistant transducers are oriented 25° from vertical so that they point outward in different directions around the instrument, forming an X-shaped pattern for measuring flow from all sides (SonTek Inc., 2022).

In a multibeam system, depth is not measured directly. Instead, the instrument records the two-way travel time of an acoustic pulse and the angle at which each beam is transmitted relative to vertical. Depth is obtained by resolving the resulting slant range into its vertical component using basic trigonometric relationships. Thus, assuming a flat bed with zero slope and uniform beam geometry approaching a width of zero, the outermost skewed beams of the M9® (positioned at ±25° from vertical) define the extent of the sounding footprint. Under these conditions, and assuming all beams originate from a single point at the water surface, the horizontal offset (x) to each side beam at a given depth (Z) can be calculated as:

$$x = Z \cdot tan(\theta)$$

where $\theta = 25°$ is the fixed angle of the skewed beams. This value represents the lateral reach of a single beam. Since two skewed beams flank the vertical beam symmetrically, the total swath width (S_w) is twice this distance:

$$S_w \approx 2 \cdot Z \cdot \tan(25°)$$

This simplifies to a constant swath-to-depth ratio:

$$\frac{S_w}{Z} = 2 \cdot \tan(25°) \approx 0.933$$

This holds for flat-bottomed bathymetric conditions and narrow-beam configurations, such as those used in this study. It offers a useful heuristic for evaluating anticipated spatial resolution and gridded raster coverage in pre-survey planning. It also reflects the geometric constraints of small-footprint single beam systems operating in shallow water. As depth increases, the angular geometry of the skewed beams enables a progressively wider swath of sounding coverage on either side of the instruments but reduces the density of points (spatial resolution) in an equal area.

In contrast, the covered area in an MBES system can be modeled as an elliptical footprint on the seafloor (Figure 3-2). The size and orientation of this footprint are controlled by the geometry of:

- the transmitted (ϕ_t) and received (ϕ_r) acoustic beams;
- the beam angle (β);
- water depth (z); and
- local seafloor slope (ζ).

These footprints are resolved into two orthogonal components: the across-track direction (x-axis), which spans the swath perpendicular to vessel motion, and the along-track direction (y-axis), which follows the direction of travel. The across-track footprint length, a_x, defines the projection of the receiving beam on the seafloor and is influenced by the beam angle β, the seafloor slope ζ, and the angle of the receiving beam pattern, ϕ_r. It is given by:

$$a_x = \frac{2z}{\cos(\beta)\cos(\beta - \zeta)} \tan\left(\frac{\phi_r}{2}\right)$$

where z is the water depth. This equation accounts for the geometric distortion caused by oblique incidence on a sloped bottom. As either beam angle or bottom slope increases, the footprint widens, reducing spatial resolution unless line spacing or transducer density is adjusted accordingly.

Furthermore, the along-track footprint length, a_y, is governed by the transmitting beamwidth ϕ_t and the beam angle β, and is expressed as:

$$a_y = \frac{2z \cdot \tan(\phi_t/2)}{\cos(\beta)}$$

This projection is unaffected by bottom slope but varies with depth and the angle at which the beam is transmitted. Because transmitting beams are typically narrower in the along-track direction than receiving beams in the across-track direction, a_y is smaller than a_x, producing an elliptical footprint shape. Together, these tracks define the area of the seafloor covered by beam forming and influence sounding resolution and line spacing.

3.2.2 Acoustic Refraction

Acoustic depth measurements rely on the precise determination of the time required for an acoustic pulse to travel from the transducer to the bed and return. The accuracy of these

measurements is directly affected by the variability of the sound speed profile in the water column, which is determined using empirical equations that relate acoustic velocity to temperature, salinity, and pressure. Several formulations have been developed, including those by Del Grosso (1974), Mackenzie (1981), Coppens (1981), and Leroy et al. (2008). While each equation offers advantages in specific environments or depth regimes, the formulation by Chen & Millero (1977) is the most widely accepted in hydrographic and oceanographic practice due to its consistency and reliability across a broad range of conditions (National Physical Laboratory, 2000). These equations are used to construct sound speed profiles, which are essential for correcting acoustic depth measurements where beam refraction can introduce vertical error.

Furthermore, strong vertical temperature gradients can lead to changes in sound speed with depth in stratified water bodies. These gradients are typically sustained under conditions of limited vertical mixing, including low wind speeds, minimal wave activity, or stagnant flow, which allow for the development of thermal layers. When acoustic beams propagate through such stratified conditions, refraction alters the beam path, especially for oblique angles, and introduces bias into the depth measurement if not properly corrected. In contrast, under well-mixed conditions, resulting from wind-induced turbulence or convective overturning, temperature and sound speed become more uniform throughout the water column. This reduces the magnitude of refraction effects and, correspondingly, the need for detailed sound speed profiling to achieve accurate depth estimates.

3.2.3 Depth Estimation

Depth measurements derived from acoustic systems are fundamentally range calculations based on the time delay between signal transmission and return. The basic formula for estimating depth from two-way travel time is:

$$Z = \frac{C \cdot T}{2}$$

where Z is the depth, C is the speed of sound in water, and T is the round-trip travel time of the acoustic pulse. In a deep vertically stratified water column (where temperature, salinity, and pressure vary with depth) this formula becomes increasingly inaccurate when an average or assumed sound speed is applied. Stratification introduces significant vertical gradients in sound velocity, which causes the acoustic beam to bend as it travels through layers of differing density.

This bending follows Snell's Law, which governs acoustic refraction between layers:

$$\frac{\sin \theta_1}{C_1} = \frac{\sin \theta_2}{C_2}$$

where θ_1 and θ_2 are the incidence angles of the acoustic beam in two adjacent layers, and C_1 and C_2 are the corresponding sound speeds. In practical terms, this means that when a sound wave moves from a faster to a slower layer (e.g., from warm surface water into a colder thermocline), the beam angle decreases (bends toward vertical), and vice versa. This deviation alters the actual acoustic path length, introducing vertical bias into depth measurements if uncorrected.

The calculation of depth must incorporate Snell's law and the change in travel time resulting from variations in sound speed and beam angle to accurately account for this refraction effect. In a discretized water column, each layer i is assumed to have a locally constant vertical gradient of sound speed, g_i, defined as:

$$g_i = \frac{dC}{dz}$$

Snell's Law is applied not just at discrete boundaries but continuously along the beam path to resolve depth in a vertically stratified medium. This property (g_i) defines what is known as the ray parameter, or Snell's constant (κ). Showcasing that the ratio of the sine of the beam angle to the local sound speed remains constant in a stratified water column. Snell's constant is denoted as κ and expressed as:

$$\kappa = \frac{\sin\theta}{C}$$

The incremental acoustic travel time through each discrete layer i can be derived by integrating the local sound speed and beam angle relationship from Snell's Law using these definitions.

Within a given layer i, the acoustic pulse time increment Δt_i is given by:

$$\Delta t_i = \frac{1}{g_i}\int_{C_{i-1}}^{C_i} \frac{dc}{c \cdot \cos(\theta)}$$

The angle θ of the acoustic beam also changes as the sound speed changes. This change is continuous with depth within a given layer. Evaluating the above integral for a layer with constant sound-speed gradient leads to the analytical expression:

$$\Delta t_i = \frac{1}{g_i}\ln\left(\frac{C_i\left[1+\sqrt{1-(\kappa C_{i-1})^2}\right]}{C_{i-1}\left[1+\sqrt{1-(\kappa C_i)^2}\right]}\right)$$

In practice, summing the individual travel time increments across all layers provides the total two-way travel time Δ_t for the acoustic pulse to travel to the bottom and return. The true depth Z is subsequently calculated by integrating sound speed and beam angle along the travel path over half the total measured travel time:

$$Z = \int_0^{\Delta t/2} C(z) \cdot \cos[\theta(z)]\ dt$$

The sensitivity of the sound speed to environmental parameters is significant: a change of 1°C in temperature affects the speed of sound by approximately +4.5 m/s, while a 1‰ (ppt) change in salinity modifies it by roughly +1.3 m/s, and a 10 m increase in depth due to hydrostatic pressure contributes approximately +1.6 m/s (IHO, 2010). Among these, temperature is by far the most variable and influential factor in stratified environments where diel solar heating and surface exchange can lead to strong vertical thermal gradients. Salinity, while generally less variable than temperature in freshwater-dominated systems, may still exhibit depth-dependent stratification near transitional freshwater-marine boundaries or during periods of high inflow or ice melt. Pressure increases linearly with depth and becomes the dominant driver of sound speed only in deeper waters exceeding several tens of meters. Combined, these parameters govern the vertical sound speed profile, which in turn controls acoustic propagation paths through the water column. In stratified systems, abrupt shifts in temperature and salinity may lead to layered sound speed discontinuities that refract acoustic beams, shifting their paths from assumed linear trajectories and altering the measurement of returned signals. The IHO notes that such variations can introduce vertical errors on the order of several decimeters to meters depending on water depth, beam angle, and the severity of the refractive gradient. This is particularly consequential when using multi-beam or side-scan systems with oblique paths, where refraction can significantly distort bottom return angles and depths if uncorrected.

In shallow, narrow, and hydrodynamically variant systems, such as confined river channels or exposed marsh outlets, the water column is often well-mixed due to wind stress, flow, and bed friction. These conditions tend to suppress the formation of thermal or salinity stratification,

resulting in a relatively uniform vertical sound speed profile. In uniform environments, the use of an average sound speed value can be sufficient for producing bathymetric surfaces within acceptable accuracy thresholds, as the effects of beam refraction are minimized across the limited water column depth.

Surveys conducted in the Red River outlet and Netley-Libau Marsh occurred in waters less than 10 meters deep and frequently under high-flow or wind-driven conditions. Under these circumstances, vertical homogeneity was assumed to be more common, and the influence of stratification-induced refraction on depth measurements was expected to be minimal. While full sound speed profiling remains the recommended approach for all hydrographic surveys, the need for detailed correction in these environments should be evaluated in relation to prevailing field conditions, survey objectives, and required vertical tolerances. It is important to note that sound speed corrections were not applied; however, the M9® incorporated surface water temperature measurements in deriving depths.

3.3 Methodology

Bathymetric datasets were acquired using a perimeter-based, cross-weave survey strategy that emphasized adaptive field coverage rather than predefined routes. Survey extents were guided by real-time assessment of the environment, and historical bathymetric sounding paths. Figure 3-3 presents an example of a bathymetric dataset collected on July 21, 2022, at the Netley Delta, illustrating the distribution and density of raw depth soundings acquired during the survey.

While general survey areas were known prior to deployment, specific bounding polygons were not generated in advance. Instead, survey boundaries were dynamically extended in the

field to exceed the anticipated zone of interest, ensuring adequate lateral and longitudinal coverage for surface post-processing.

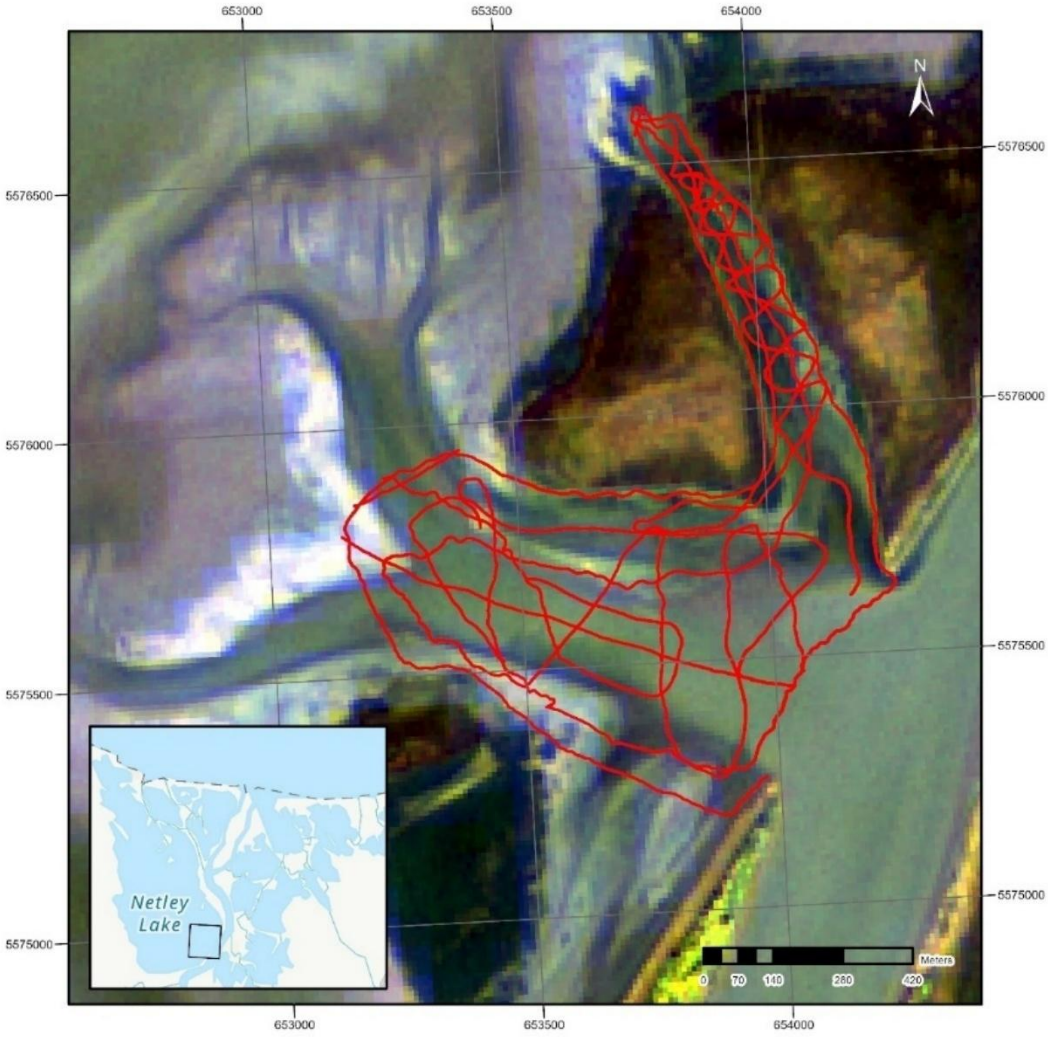

Figure 3-3 Bathymetric soundings collected on July 21, 2022, at the Netley Delta

(Sentinel-2 Imagery – Bathymetric, September 22, 2021)

Within each survey area, the cross-weave approach consisted of interlaced passes oriented along and across the flow path. Route planning and steering were adjusted on the fly, informed by visible shoreline features, field experience, and previously identified channel alignments. The cumulative result yielded dense and overlapping coverage patterns appropriate for gridded interpolation and volumetric analysis using single beam technology despite the absence of a

spacing protocol. The level of detail achieved within each zone was inherently influenced by real-time conditions including wind speed, wave action (heave), other vessel traffic, and available daylight. Survey density was also affected by the navigability of shallow or constricted areas, particularly in Netley Lake and in the vegetated margins of the marsh.

3.3.1 Equipment and Setup

Bathymetric surveys were collected using a SonTek RiverSurveyor® M9® Acoustic Doppler Current Profiler (ADCP), a multi-frequency, five-beam echosounder system configured for high-resolution bathymetry in shallow to intermediate-depth environments. The M9® integrates a 0.5 MHz vertical echosounder with two orthogonal pairs of side-looking beams operating at 1.0 MHz and 3.0 MHz, each oriented 25 degrees outward from vertical. This configuration enables simultaneous five-beam echo sounding, providing greater spatial coverage over bed geometries. The M9® supports depth measurements ranging from 0.20 to 80 meters. The system's vertical accuracy is ±1% of the measured depth, which can be improved to ±0.02% when applying a full water column sound speed correction. Vertical resolution is 0.001 meters (SonTek Inc., 2022).

Positioning and depth data were acquired using the M9® dGPS-enabled GNSS receiver in WGS84. Spatial coordinates were recorded in real time using Satellite-Based Augmentation System (SBAS) differential correction. Although the system supports RTK GPS corrections, external RTK was not employed during field deployment. Instead, depth soundings were post-processed for tide influences by vertically aligning measured values to known water surface elevations obtained at the start and end of each survey.

Figure 3-4 shows how the M9® was mounted through a rigid polyethylene SonTek HydroBoard®—a low-draft, stable tow craft designed to reduce pitch, roll, and yaw effects during surveying. The HydroBoard® features hollowed and recessed mounting locations for

deployment of both the ADCP and its Power and Communication Module (PCM), respectively. The HydroBoard® was tethered to a 20-foot outboard-powered vessel using a towline and deployed laterally at the starboard quarter to minimize wake and prop interference. A Lenovo Toughbook running SonTek HydroSurveyor Live© software was used to conduct real-time QA/QC of sounding density, bottom tracking, beam signal integrity, and survey track coverage.

Figure 3-4 Field Deployment of Sontek M9 In Netley Marsh

Prior to data collection, the systems' magnetic compass was calibrated to correct for pitch, roll, and yaw distortions introduced by local magnetic anomalies. Compass calibration was performed in the field by rotating the M9® while mounted in the HydroBoard® through two (sixty seconds each) complete 360° rotations while varying the tilt and roll to simulate expected water surface conditions. Successful calibration required achieving minimal magnetic error and

coverage over the full range of expected pitch and roll angles. This ensured robust heading accuracy during data acquisition. Heave effects during data acquisition are corrected by the M9® inertial measurement unit.

3.3.1.1 Alternative Equipment in Low Water Conditions

Alternative methods were employed to record surface elevations in specific conditions where water depth was insufficient for safe or effective deployment of the M9®. Two primary techniques were used: (1) point-based topographic measurements using a Trimble SP60® in a combined base–rover configuration with Trimble® RTX, and (2) aerial photogrammetry using a DJI Phantom 4 Pro Unmanned Aerial Vehicle (UAV).

The SP60 rover operates as an integrated base and rover system via cellular telemetry, allowing surveys to be conducted without reliance on a physical benchmark. However, when topographic points were required during the study period, the SP60 was additionally tied into a local datum point using a metal pin to ensure consistency with the project control framework. The unit was used to collect positional data for water surface reference points, survey control targets, and exposed surface features with very shallow elevations (less than 0.5 metres). At shallow locations, a solid object (typically a wooden member) was pressed firmly into the soil to provide a stable mounting surface, and the SP60 rover was positioned in the centre of the member to obtain the elevation. Data was recorded in the NAD83 coordinate reference frame, with real-time processing in Trimble Business Center® software to achieve horizontal and vertical accuracies less than 2 cm. Water surface elevations recorded with the rover were used to normalize bathymetric depth measurements and correct for tidal variation, and this correction procedure was applied to all bathymetric surveys conducted using the M9®.

For aerial photogrammetry, a DJI Phantom 4 Pro® UAV equipped with a 20-megapixel, 1-inch CMOS sensor was deployed. Flight paths were prepared using Pix4DCapture® software to establish automated grid missions with forward and side overlap of at least 80% and 70%, respectively, at an altitude of 35 m to achieve a consistent ground sampling distance across the survey area. To improve surface reconstruction in uneven terrain, two complete passes were flown for each survey block, oriented 90 degrees to each other—one perpendicular to shore and the other parallel to shore. The first block used a nadir (downward-facing) camera orientation and the second used a camera angle at approximately 15-20° from vertical. Pre-flight planning included verification of weather conditions, assessment of site obstructions, and test imagery to ensure adequate coverage of the survey area. Ground control points (GCPs) were used to provide accurate spatial reference and limit geometric distortion. They were evenly spaced across the site, surveyed with the SP60, and placed to cover high and low elevations in the survey area.

3.3.2 Data Collection Procedure

Bathymetric data were collected with the M9® configured for continuous multi-transducer depth acquisition and operated in conjunction with SonTek HydroSurveyor Live® software. Real-time acquisition was facilitated through a Lenovo Toughbook displaying live survey diagnostics, including beam return quality, GPS signal accuracy, and real-time mapping overlays of swath coverage and sounding density. Throughout each deployment, these outputs were closely monitored to ensure data completeness and quality. The software's live track overlay allowed visual assessment of line spacing and areas requiring further investigation. The boat path was adjusted in the field based on these observations to maintain consistent coverage, particularly in transitional areas such as channel margins, cutbanks, and submerged bars where

depth variability was high. Figure 3-5 shows the live read out available from HydroSurveyor Live© during a bathymetric survey.

Soundings were recorded at 1 Hz per beam with the M9® sampling continuously during vessel movement at a speed of approximately 4 – 7 km/h. Spatial resolution varied with depth, as the skewed beams widened in separation with increasing water column length. Even in shallow zones (1–5 meters), the beam geometry ensured that each pass provided sufficient coverage across the footprint of the swath, and in many cases, beams partially re-sampled previously captured areas when survey lines were kept close.

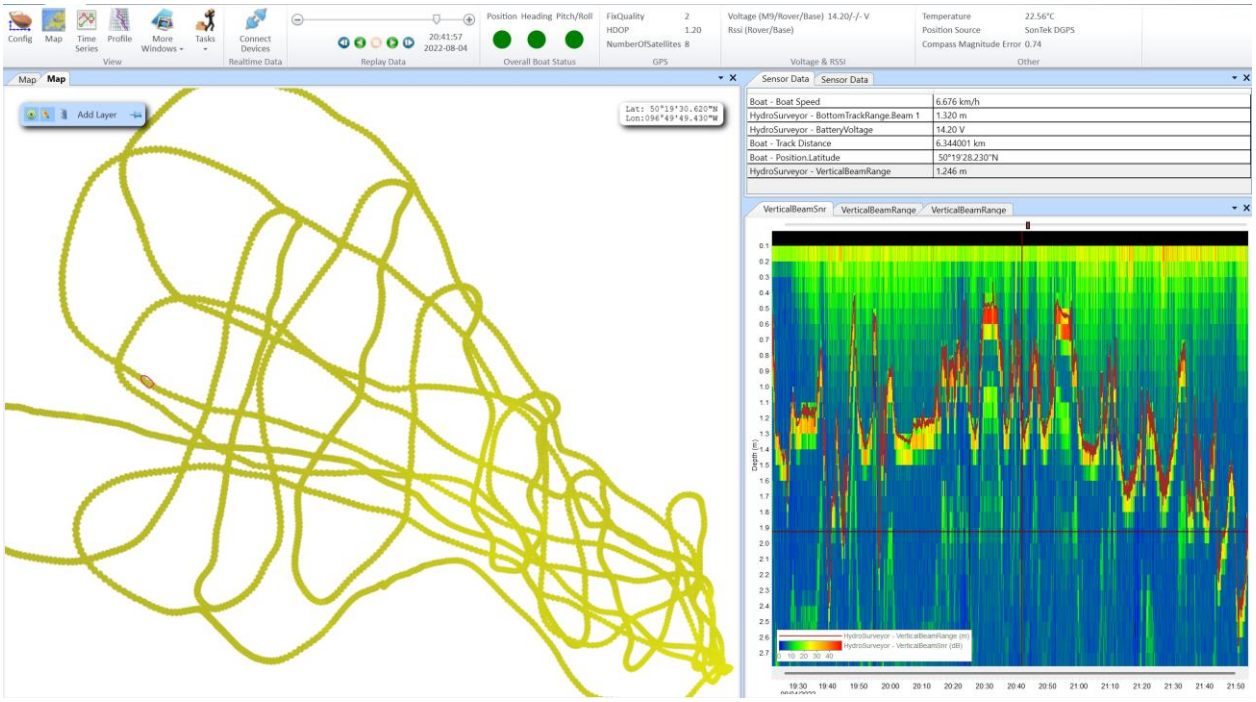

Figure 3-5 Hydro Surveyor Live© output during a bathymetric survey

Importantly, no loss of bottom track was noted during data acquisition, indicating that acoustic returns were successfully received across all beams given the range of environmental conditions. However, field conditions still influenced return quality and interpretability in subtler

ways. While water clarity has no direct effect on acoustic transmission, visual navigation near shorelines or in narrow channels was sometimes impeded by turbidity and submerged vegetation. Submerged features such as macrophyte mats, suspended debris, and natural obstructions may influence the acoustic return profile even if the system maintains bottom track.

These features often introduce anomalies in the beam returns by creating irregular or diffuse reflection surfaces above the true bed. For example, submerged vegetation may generate slightly elevated return surfaces, where the receiving beam reflects off biomass instead of penetrating to the sediment interface. Similarly, floating or suspended material may disrupt beam uniformity across the swath, resulting in returns with increased noise or reduced coherence between adjacent beams. Such effects are not always detectable with real-time diagnostics, particularly in shallow systems where vertical gradients in beam separation are small, but they become apparent during post-processing as localized irregularities in the bed surface profile. Although no large-scale debris were recorded during survey operations, surveyors remained attentive to these influences by periodically reviewing sounding profiles, comparing swath consistency across transects, and revisiting suspect areas when needed. The combination of continuous QA/QC, field-based judgment, and environmental awareness ensured that small-scale acoustic disruptions were either resolved in the field or flagged for correction during subsequent gridding and interpolation stages.

Additional factors such as wind-generated wave action and vessel-induced wake occasionally contributed to beam instability, particularly when surveying open marsh areas during long, straight transects exposed to fetch. These disturbances typically introduced slight pitch and roll to the HydroBoard®, which alter beam incidence angles and introduce low-amplitude vertical variability in returns. Nevertheless, due to the inherent stability of the towing platform and the

system's rapid sampling rate, these effects were minimal and did not compromise spatial resolution. Hydrosurveyor© software also uses real time data processing to account for the pitch, yaw, and roll of the Hydroboard® to estimate the degree of heave (vertical displacement of the ADCP relative to a uniform water level).

The data collection process provided spatially dense and continuous coverage across depths from 0.2 to 10 m under variable environmental conditions consisting of wind gusts between 0 and 40 km/h.

3.3.2.1 Positioning and Georeferencing

Accurate spatial positioning of bathymetric data was achieved through integration of horizontal and vertical georeferencing with a combination of real-time correction services and post-processing. Horizontal positioning during data acquisition was provided by the M9® dGPS unit with SBAS corrections. Soundings from the M9® were recorded in WGS84 geographic coordinates which were later projected to NAD83 UTM Z14N in ArcGIS Pro® during post-processing. While the M9® onboard GNSS was sufficient for navigation and preliminary mapping, all vertical elevations were refined using water surface elevations collected with the SP60®. Reference locations that captured the static water level were established at predetermined positions along the shoreline based on accessibility, satellite visibility, and proximity to the survey area. The SP60 operated with real-time RTX corrections using cellular telemetry, maintaining <2 cm vertical accuracy throughout all surveys. Ellipsoidal heights were transformed to orthometric elevations referenced to CGVD13 using the CGG2013a geoid model.

Water surface elevations recorded at the start and end of each survey were linearly interpolated to represent Lake Winnipeg's tidal variation and applied to all bathymetric soundings. Bed elevations were calculated by subtracting depths from the interpolated water

surface elevation. In wave-affected areas, particularly in the Red River outlet and exposed sections of Netley-Libau Marsh, water levels were determined using a seepage-based approach to approximate a wind-eliminated surface. A small depression was excavated upslope of the active wave–shore interface, allowing seepage from saturated soil to stabilize before measurement. These values were incorporated into the vertical correction process to minimize wave-induced elevation error.

All vertical positioning in this study was expressed in CGVD13. Legacy datasets and survey benchmarks were often provided in CGVD28 and required transformation to CGVD13 prior to integration. For the study area, CGVD28 sits approximately 0.42 m higher than CGVD13, with the difference derived from regional geoid separation between the two datums.

Transformations were performed using NRCan's coordinate transformation utility (GPS-H®), applying the CGVD28 HTv2.0 grid and CGG2013a geoid model with horizontal positioning provided in projected coordinates. The model interpolates the geoid separation difference, ΔN, for each coordinate location, and applies:

$$H_{2013} = H_{28} - \Delta N$$

where H_{2013} is the orthometric height in CGVD2013, H_{28} is the orthometric height in CGVD28, and ΔN for this region averages 0.42 m.

3.3.3 Data Processing and Analysis

A structured post-processing workflow was implemented using MATLAB® and ArcGIS Pro® following the acquisition and georeferencing of survey datasets described in the preceding sections. ArcGIS Pro® v. 3.4 served as the primary spatial processing environment for compiling, referencing, interpolating, and generating raster surfaces, while MATLAB® was used for

statistical analysis and to generate transects. Data exchange between platforms was handled by exporting point feature classes from ArcGIS Pro® and importing them directly into MATLAB® scripts as either shapefiles or comma separated values.

Table 3-1 summarizes all elevation-based datasets available for analysis in this thesis. The data cover nine primary survey areas (Deposition Site, Dredge Site, Netley Cut, Netley Delta, Netley Lake, Red River, Red River Outlet) collected between 2010 and 2022. For each survey entry, the table lists the acquisition date, the initial and final water surface elevations (WSE), the vertical datum, the acquisition method, and the source. HRTF acquired datasets both during the course of this thesis and in earlier work. The locations listed in Table 3-1 correspond to specific sites shown in Figure 3-1. The Deposition Area and Dredge Site refer to location B, the Netley Delta/Cut corresponds to location C, and the Red River Outlet refers to location A. The Lower Red River designation encompasses the reach of the Red River from Netley Creek to Lake Winnipeg, while Netley-Libau Marsh refers to the complete extent of the marsh. Survey entries marked with “Multiple Dates” indicate composite datasets compiled over time. Specifically, the multiple-date survey acquired by AES for NLM comprises data collected between May of 2010 and August of 2011. The multiple-date survey of the Red River conducted by Manitoba Hydro includes data collected on July 21, 28, 29, 30, and 31, and August 4, 2018.

All surveys were adjusted to a common vertical datum (CGVD13) before processing. The datasets were then used to test and select an interpolation method in ArcGIS Pro®, which was applied to produce digital elevation models for all surveys. These DEMs supported volume calculations and transect comparisons to assess changes in sediment deposition and erosion across the study areas.

Table 3-1 Areas of analysis and their respective survey metadata, 2010–2022

Location	No.	Date	Initial WSE (m)	Final WSE (m)	Datum	Method	Collected By
Deposition Site	1	2021-08-09	—	—	CGVD13	Topo	HRTF
Deposition Site	2	2021-09-10	—	—	CGVD13	Aerial	HRTF
Deposition Site	3	2022-08-04	218.252	218.227	CGVD13	Bathy	HRTF
Dredge Site	4	2021-07-29	217.209	217.120	CGVD13	Bathy	HRTF
Dredge Site	5	2021-08-17	217.023	217.087	CGVD13	Bathy	HRTF
Dredge Site	6	2021-09-15	216.767	216.826	CGVD13	Bathy	HRTF
Dredge Site	7	2022-07-14	218.121	218.014	CGVD13	Bathy	HRTF
Netley Cut	8	2014-09-15	—	—	CGVD13	Bathy	HRTF
Netley Cut	9	2020-08-20	217.670	217.685	CGVD13	Bathy	HRTF
Netley Cut	10	2021-07-08	217.021	217.0137	CGVD13	Bathy	HRTF
Netley Cut	11	2022-07-14	218.166	218.067	CGVD13	Bathy	HRTF
Netley Delta	12	2022-07-21	218.514	218.456	CGVD13	Bathy	HRTF
Netley Lake	13	2022-08-04	218.368	218.227	CGVD13	Bathy	HRTF
Netley-Libau Marsh	14	Multiple Dates	—	—	CGVD28	Bathy	AES
Lower Red River	15	Multiple Dates	—	—	CGVD13	Bathy	MH
Red River Outlet	16	2020-08-20	217.561	217.672	CGVD13	Bathy	HRTF
Red River Outlet	17	2021-07-27	217.030	217.021	CGVD13	Bathy	HRTF
Red River Outlet	18	2021-10-18	216.614	216.658	CGVD13	Bathy	HRTF

3.3.3.1 Quantifying Global Data Statistics

SBES systems, while effective for measuring bathymetric depth along discrete survey lines, inherently lack the dense spatial coverage characteristic of MBES systems. As a result, SBES datasets often contain large gaps between soundings, particularly in areas where survey line spacing exceeds the swath width. Interpolation techniques are required to estimate depths at unsampled locations to generate continuous bathymetric surfaces from these point datasets. The use of any interpolation technique has inherent assumptions that may influence both the accuracy

and reproducibility of the resulting digital elevation model. Interpolation techniques can take the form of exact or inexact, local or global, and deterministic or geostatistical (J. Li & Heap, 2008). In this study, a 1 × 1 m grid resolution was selected as the smallest practical raster cell size to balance spatial resolution with computational efficiency and load during interpolation. This grid size was applied consistently to all interpolations to ensure accurate volume estimates, irrespective of the swath width or point density.

Multiple soundings can fall inside a single 1 × 1 m cell where boat passes overlap at different acquisition times. Rasterization then collapses these soundings into one representative value. This is where differences emerge between exact deterministic methods that honour input points and inexact/geostatistical methods that smooth surfaces. Exact methods preserve measured depths, so small vertical errors or outliers show up as local spikes/pits. With sparse or uneven spacing, such as with a triangulated irregular network (TIN), interpolation techniques must span gaps with long networks that create planar facets and ridge lines that do not accurately reflect the true bed. Inexact/geostatistical methods impose smoothness that can attenuate small bedforms when gaps between survey lines are large. Studies show that interpolation error grows with distance to the nearest measurement and with slope/curvature and declines as sampling density increases. Amante & Eakins found spline outperformed inverse-distance weighted techniques on SBES-like test sets, with accuracy most sensitive to spacing and terrain heterogeneity (Amante & Eakins, 2016). TopoToRaster produced the best cross-sectional agreement overall, while deterministic methods performed worse near banks—locations where SBES sampling is most sparse and subject to slopes (Arseni et al., 2019).

To quantify the implications of using sparse soundings, spatial analysis is typically implemented that quantifies the uncertainty of a raster cell having a single value. The industry

standard is to use a Combined Uncertainty and Bathymetry Estimator (CUBE) that estimates a depth for each grid cell by combining many overlapping soundings and weighting each observation by its Total Propagated Uncertainty (TPU)—the expected error from sensor, platform, and environmental sources (e.g., attitude, refraction, tide/datum) (Calder & Mayer, 2003). With sufficient redundant MBES hits in a cell, CUBE groups consistent soundings into one or more clusters, rejects outliers that don't fit any group, and reports both the most-likely depth and an accompanying node uncertainty. Because CUBE relies on redundancy, it fits modern MBES swath workflows and hydrographic production, i.e. more overlap leads to stronger evidence that supports lower uncertainty. The CHRT variant (CUBE with Hierarchical Resolution Techniques) extends the same estimator to variable-resolution grids so dense areas can be modeled with finer cells while sparse areas remain coarser (Calder & Rice, 2011). These practices align with IHO S-44 requirements for uncertainty and seafloor search and with NOAA's Hydrographic Survey Specifications and Deliverables (HSSD), which expect swath surveys to deliver depth and per-node uncertainty products (International Hydrographic Organization, 2024; Office of Coast Survey, 2025)

SBES rarely provides the redundancy that CUBE/CHRT requires. In this study, we therefore test a CUBE-inspired proxy using two elements:

(1) global descriptive statistics (mean, median, quartiles) of mean average error (MAE) for time dependent overlapping clusters that fall within a 1×1 m cell; and
(2) spatial diagnostics (Mantel's R, Moran's I) to measure spatial dependence and clustering of differences.

Together these statistics are predicted to estimate potential error where multiple passes overlap and clarify why interpolation techniques accumulate error when sparse or uneven

sampling collapses multiple observations into a single cell. These two techniques have been proven in other studies to be a suitable method for testing the accuracy of bathymetric surveys and their interpolation techniques (Erdogan, 2009). However, unlike CUBE/CHRT, this novel SBES proxy method does not compute a probability surface per cell or TPUs. Uncertainty is inferred from spread (within-cell statistics) and from cross-time agreement rather than from a CUBE/CHRT error model; systematic errors (e.g., vertical datum shifts, instrument bias) must be controlled outside this proxy. Therefore, prior to analysis, the datasets were adjusted to match the same datum and reference system. Results are sensitive to line spacing and to the choice of interpolator (exact vs. inexact), and the spatial tests assume consistent beam geometry throughout the sampling window. Consequently, the proxy is intentionally simpler than CUBE: it prioritizes interpretability and computational speed for SBES systems while making the key assumptions (sparsity of data points, interpolator gaps between soundings, and limited redundancy) explicit.

3.3.3.1.1 Statistics in Overlapping Cells

As previously mentioned, interpolation techniques inherently collapse multiple soundings within a cell into a single representative value when producing a DEM. To analyze this issue, **s**oundings within each cell are split into groups that fall within a 1 x 1 m cell using a 1-minute return-period, where observations separated by $<$ 1 min are treated as the same group and observations separated by $\geq$ 1 min form distinct groups. The bathymetry file is pre-screened for stagnant positioning, and the flagged groupings are excluded from analysis. Cells with less than two groups are omitted from the global summaries.

Global summary statistics were computed across all overlapping grid cells to characterise systematic offsets and overall variability between bathymetric datasets. The average differences

between groups provide survey-wide descriptors at the global scale—counts of qualifying observations and overlapping cells, the global median, lower and upper quartiles, interquartile range (IQR), and global minimum/maximum. The results are used as indicators of variability, not as error. The global spread characterizes how much variability is typically present when multiple observations are reduced to a single raster node instead of diagnosing an individual cell. These statistics were only developed for datasets acquired by the HRTF, as other datasets did not have timestamp data to draw from. Figure 3-6 provides an example of overlapping survey passes where several points fall within a single cell.

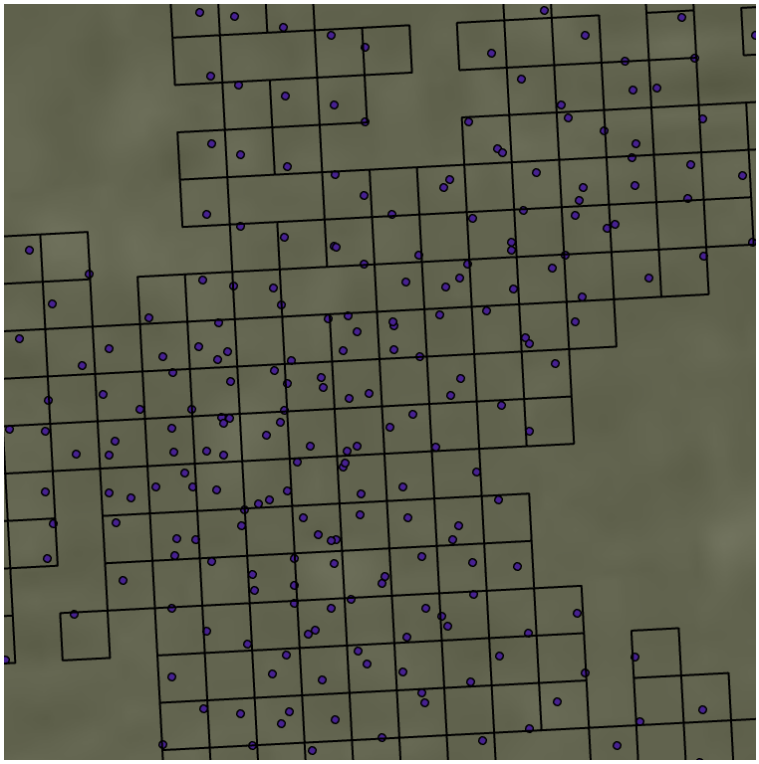

Figure 3-6 Bathymetric soundings with an overlaid 1 x 1 m grid

The mean depth is computed for every qualifying group for eligible cells containing sufficient points. Then the mean absolute difference between two observation periods z and q is calculated as:

$$\mu = \left| \frac{z_i + z_{i+1} \ldots + z_{j+n}}{n} - \frac{q_i + q_{i+1} \ldots + q_{i+m}}{m} \right|$$

The set forms a matrix of absolute mean differences across all groups within that cell if more than two groups occur in a cell. These values are interpreted strictly as relative variability because the true surface is predictive: larger absolutes indicate weaker predictability, whereas smaller absolutes indicate stronger predictability. At a global scale, the cell-level absolute mean differences are used to characterize overall model behaviour and to identify locations where interpolation is expected to collapse values within the final DEM.

3.3.3.1.2 Moran's I and Mantel's R Spatial Correlation

Global spread in absolute group-mean differences indicates how reproducible overlaps within the survey are, but it does not identify whether agreement/disagreement within these cells is spatially structured. Two complementary statistics address this at the cell level: Moran's *I* tests spatial autocorrelation among points within a cell and Mantel's *R* assesses whether the within-cell distance between soundings is associated with within-cell elevation difference. Values of *I* and *R* are then investigated across all eligible cells using Fisher's combined *p*-method to provide global evidence of (i) spatial autocorrelation and (ii) distance–difference relations for the given cell resolution (1 meter).

Moran's *I* and Mantel's *R* are computed only for cells that meet the grouping rules defined previously and contain a sufficient number of points to produce a confident p-value to estimate statistically significant cells. That is to say, a minimum point density of 5 soundings per cell with at least two soundings separated by 1 minute was used as a search criterion.

Moran's *I* and Mantel's *R* provide plain indicators of spatial structure for overlapping cells. Moran's *I* asks whether nearby points have similar depths: positive values indicate clustering of

similar values, negative values indicate neighboring highs and lows (dispersion), and values near zero indicate no clear pattern; a permutation *p*-value shows whether the pattern is stronger than expected by chance (ESRI, 2025a; Moran, 1950). Mantel's *R* correlates a matrix of Euclidean distances with a matrix of depth differences to test whether points that are farther apart tend to differ more in depth (Bakker, 2024; Crabot et al., 2019; Mantel & Valand, 1970). To report a single global indicator, per-cell p-values are investigated for *I* and *R* across all eligible cells using Fisher's method. This yields two global *p*-values that indicate whether spatial autocorrelation (Moran) and a distance–difference relation (Mantel) is widespread; it should be interpreted as a meta-test for cells that overlap within the survey.

Moran's *I*: For each eligible cell, all soundings and their coordinates are used to compute I with inverse-distance spatial weights (self-weights excluded). Significance is obtained by permutation (e.g., 999 randomizations). Outputs per cell are I and a permutation p -value. Global-level summaries report the distribution of I across cells. Below is a step-by-step description of how Moran's *I* was calculated for each survey.

Compute the Euclidean distance between every pair of points in the cell:

$$d_{ij} = \sqrt{(x_i - x_j)^2 + (y_i - y_j)^2}$$

Turn distances into proximity weights with an inverse-square decay:

$$w_{ij} = d_{ij}^{-p} \quad (i \neq j), \qquad w_{ii} = 0, \qquad p = 2$$

Normalize each row so weights are comparable across points:

$$\widetilde{w_{ij}} = \frac{w_{ij}}{\sum_{j=1}^{N} w_{ij}}$$

Compute the total weight:

$$S_0 = \sum_{i=1}^{N} \sum_{j=1}^{N} \widetilde{w_{ij}}$$

Compute the global mean depth:

$$\bar{z} = \frac{1}{N} \sum_{i=1}^{N} z_i$$

Form the weighted cross-product of centered values, which measures how similar neighboring values are:

$$\sum_{i=1}^{N} \sum_{j=1}^{N} \widetilde{w_{ij}} \ (z_i - \bar{z}) \left(z_j - \bar{z}\right)$$

Compute the unweighted sum of squares, which scales the index by the overall variability:

$$\sum_{i=1}^{N} (z_i - \bar{z})^2$$

Combine the two pieces to form Moran's I:

$$I = \frac{N}{S_0} \frac{\sum_{i=1}^{N} \sum_{j=1}^{N} \widetilde{w_{ij}} \ (z_i - \bar{z}) \left(z_j - \bar{z}\right)}{\sum_{i=1}^{N} (z_i - \bar{z})^2},$$

With normalized weights, $S_0 \approx N$, the first term is near 1. $I > 0$ indicates clustering of similar values, $I < 0$ indicates neighboring dissimilarity.

A permutation test is then applied to the observed Moran's value (I_{obs}) by holding the point coordinates and weights fixed while randomly permuting the depth value z_i. Then, recomputing

the value of Moran's *I* for each shuffle to get a set of I_p, which denotes the value of *I* at a specific permutation. After each shuffle, check to verify the number of permutations (*r*) is less than 999 and quantify $\overline{I_{\text{perm}}}$ as the mean of the permuted values. A threshold *p*-value defined as $\alpha > 0.05$ is used to test the cell for significance. The *p* value of the group of observations becomes*:*

$$p = \frac{1+b}{1+\text{r}} \quad where \quad b = \sum_{p=1}^{\text{r}} \{ |I_p - \overline{\text{I}_{\text{perm}}}| \geq |\text{I}_{\text{obs}} - \overline{\text{I}_{\text{perm}}}| \}$$

The null hypothesis here is that depths are arranged spatially at random. If the test is not significant ($p \geq \alpha$), the points are treated as spatially random; if significant ($p < \alpha$), the sign of *I* interprets the structure: positive I implies clustering of similar values (nearby points tend to have similar depths), whereas negative *I* indicates neighboring dissimilarity/dispersion (nearby points tend to be unlike).

Mantel's *R* – For the same cell, a Euclidean distance matrix among points is compared to the absolute elevation-difference matrix. The Mantel correlation (Pearson) and a permutation *p*-value are returned per cell. Below is a step-by-step description of how Mantel's *R* was calculated for each survey.

Compute the Euclidean distance between every pair of points in the cell:

$$d_{ij} = \sqrt{(x_i - x_j)^2 + (y_i - y_j)^2}$$

The absolute difference in measured depth for the same pair is represented by:

$$B_{ij} = |z_i - z_j|$$

The mean used to center distances and differences, where N is the number of observations, are:

$$\bar{D} = \frac{2}{N(N-1)} \sum_{i<j} d_{ij},$$

$$\bar{B} = \frac{2}{N(N-1)} \sum_{i<j} B_{ij}$$

Mantel's statistic *R* is the Pearson correlation between the centered pairwise distances (s_D) and centered pairwise differences (s_B). The numerator is the sum of cross-products, and the denominator is the product of the centered norms s_D and s_B, where:

$$s_D = \sqrt{\sum_{i=1}^{N-1} \sum_{j=1+1}^{N} \left(d_{ij} - \bar{D}\right)^2} \qquad s_B = \sqrt{\sum_{i=1}^{N-1} \sum_{j=1+1}^{N} \left(B_{ij} - \bar{\bar{B}}\right)^2}$$

and:

$$R = \frac{\sum_{i=1}^{N-1} \sum_{j=1+1}^{N} \left(d_{ij} - \bar{D}\right) \times \left(B_{ij} - \bar{\bar{B}}\right)}{s_D \, s_B}$$

Mantel's *R* is provided a *p*-value to determine its statistical significance following a similar process used for Moran's *I*. This is accomplished by randomly permuting the depth measurement z_i a total of *r* times until either $\alpha < 0.05$ or $r > 999$. The null hypothesis is that the distance matrix and the depth-difference matrix (computed for the same points) are unrelated—i.e. there is no association between how far apart two points are and how different their depths are. If the test is not significant ($p \geq \alpha$), there is no evidence that depth differences change with distance at the within-cell scale (meaning a flat surface in most overlapping cells); if significant ($p < \alpha$), the

sign of the Mantel correlation interprets direction: $R > 0$ indicates that larger separations tend to have larger depth differences (a distance–difference relation), while $R < 0$ suggests the opposite.

Fisher Combinations – Per-cell tests are deliberately local and often low-power (i.e. small sample size) because each cell may contain only a handful of soundings. A bathymetric survey, however, is judged on whether spatial structure is widespread, not whether any single cell has an inherent structure. Therefore, a global assessment of how the dispersion and clustering of points in multiple eligible cells provides a more adequate description of widespread survey behaviour. In bathymetry, this distinction matters as interpolation fills gaps, and its uncertainty cannot be determined inside those gaps, so isolated cell-level significance does not reflect the dataset's overall behaviour.

The per-cell permutation *p*-values are combined for a given test (Moran or Mantel) using Fisher's method in MATLAB® to summarize global behaviour (Fisher, 1932). Fisher's method addresses whether there is broad evidence of the effect across overlapping cells. Fisher is appropriate here because many cells have low to modest power individually, yet a consistent pattern of small p-values across eligible cells indicates a pervasive spatial effect. Comparisons conducted by Dewey in R© show Fisher is competitive and often powerful for detecting such distributed, weak signals (Dewey, 2025). However, in cases of both large and small *p*-values, Fisher is more sensitive to small values and therefore requires a sufficiently large amount of *p*-values to perform efficiently (> 30) (Bolboacă et al., 2011; Loughin, 2004).

A small Fisher-combined *p* for Moran indicates that clustering or dispersion of similar depths is common across overlapping cells beyond what random arrangement would produce; a small Fisher-combined *p* for Mantel indicates that distance–difference relations (larger separation ↔ larger depth differences) are common at the sampled, within-cell scale. Neither implies

conformance to hydrographic accuracy standards (that is governed by TPU), nor does either validate interpolation in unmeasured gaps; rather, these results tell us that the spatial patterns our interpolators must respect are pervasive.

3.3.3.2 Interpolation Techniques

Bathymetric surface interpolation converts discrete depth soundings into a continuous elevation model. Various interpolation methods can be used within ArcGIS Pro® to produce rasterized DEMs of the underwater terrain. Each method carries distinct assumptions and practical implications. Below, we review key interpolation techniques:

- Triangular Irregular Networks (TIN)
- TopoToRaster (TTR)
- Spline with Barriers (SwB)
- Inverse Distance Weighted (IDW)
- Ordinary Kriging (OK)

Focus is given to each interpolation techniques common uses, classification (exact vs. inexact; deterministic vs. geostatistical; local vs. global), and limitations.

3.3.3.2.1 Triangulated Irregular Network

A TIN creates a surface by connecting sample points with non-overlapping triangles. Depth values are linearly interpolated across each triangle's facet. This yields an exact, deterministic interpolation: the surface passes through each known depth and uses the measurements directly without a statistical model. TIN is generally classified as a local method because each interpolated value depends only on the three vertices of the encompassing triangle (a small subset of data). The method assumes the bathymetric surface can be approximated by facets

between neighboring soundings, an acceptable assumption when data points are dense and well-distributed (Amante & Eakins, 2016).

TIN surfaces can appear faceted and may fail to capture smooth curvature between points because of the linear nature of interpolations. It cannot generate new extreme values beyond those measured and therefore is not suited for inferring unmapped shoals or holes. In areas of high slope or complex morphology, a TIN may underrepresent peaks and depressions unless they are directly sampled. TIN models also produce sharp, angular terrain features along triangle edges, sometimes requiring post-processing to smooth the DEM.

3.3.3.2.2 TopoToRaster

TopoToRaster is a specialized interpolation method designed to create hydrologically correct DEMs in ArcGIS Pro® (ESRI, 2025c). It is based on Hutchinson's (1989) ANUDEM algorithm, which uses an iterative finite-difference approach to enforce drainage continuity (i.e. connected flow networks with minimal spurious sinks). Essentially, TopoToRaster acts like a discretized thin-plate spline with additional rules that guide the surface to follow known streams, ridges, lake shorelines, and other cartographic features. The interpolation uses a roughness penalty to smooth surfaces while allowing abrupt terrain changes; this balance ensures a surface that is flexible to model steep gradients (such as channel banks) where needed. TopoToRaster is a deterministic method and, by default, is an inexact interpolator. This technique may not exactly honor every point if doing so violates enforced drainage conditions or smoothing constraints.

TopoToRaster’s enforcement of drainage and smoothing can be a limitation in pure bathymetric contexts, since underwater terrain may contain true closed depressions or flat areas that the algorithm might otherwise interpret as errors. It is recommended that users disable drainage enforcement for bathymetric interpolation to avoid removing real depressions (ESRI,

2025). It is more computationally intensive than simpler methods, due to its iterative nature and constraints. TopoToRaster excels when integrating bathymetric data with topographic data in coastal or estuarine projects, where ensuring a continuous land–water surface and realistic flow patterns is important. It has also been noted for its high accuracy in representing complex topography. For instance, a comparative study found that an ANUDEM-generated surface, such as TopoToRaster, had significantly smaller vertical errors than those produced by simpler methods like IDW and Kriging in hilly, mountainous, and alpine terrain (Z. Li et al., 2023).

3.3.3.2.3 Spline with Barriers

Spline with Barriers (ESRI, 2025b) is an interpolation method that produces a smooth minimum-curvature surface while honoring the presence of physical barriers (such as islands, levees, or other boundaries where interpolation should not cross). It extends the thin-plate spline concept by introducing barrier polylines or polygons that partition the interpolation domain. This technique is an exact, deterministic, global interpolation: all measured depths are matched exactly, and the surface is as smooth as possible within each partitioned region. In essence, SwB adjusts the interpolation such that for any prediction location, it considers the shortest path around barriers when weighting nearby points, rather than straight-line distance through a barrier. The basic assumption is that the bathymetry in each separated area can be modeled as a continuous smooth surface unaffected by points on the other side of a barrier. It treats barrier features (e.g. a lake's shoreline or an island's outline) as discontinuities: points on one side of a barrier do not influence the other side.

SwB will produce discontinuities at the barriers themselves and suffer from oscillations within a region if there are sharp gradients. The use of a barrier as a constraint often reduces extreme oscillations by isolating complex areas. The technique is appropriate whenever the water

body is segmented by physical structures or when one needs to enforce hard boundaries in the interpolation.

3.3.3.2.4 Inverse Distance Weighted

IDW interpolation assumes that each unknown depth can be estimated as a weighted average of surrounding known depths, where the weights decrease with distance from the unknown point. This method is deterministic and usually exact: if a prediction location coincides with a sample point, IDW will return the exact measured depth. In general, IDW will not predict values outside the range of the observations. It can be implemented globally (using all points with non-zero weights) or locally (using only points within a certain radius or a fixed number of nearest neighbors).

A well-known limitation of IDW is the tendency to produce "bull's-eye" artifacts when data are sparse and underestimating depths near riverbanks (Arseni et al., 2019; ESRI, 2025d). Because IDW is an averaging method, it smooths out any unmeasured peaks or depressions: local bathymetric highs and lows only appear if the exact point was surveyed, otherwise the interpolation in those areas will be pulled toward surrounding values. Despite these issues, IDW often performs quite well when the sampling density is high relative to the variability of the terrain. Illustrating this application around shallow water islands with low variability, Pratomo et al. (2023) found that IDW achieved the lowest error (MAE and RMSE) compared to ordinary kriging and TIN.

3.3.3.2.5 Ordinary Kriging

Ordinary Kriging (OK) is a geostatistical interpolator that assumes a locally constant but unknown mean and models spatial dependence with a semi-variogram; the estimator is a weighted linear combination of nearby samples where weights reflect both distance and the

configuration of points. In ArcGIS Pro®, the workflow includes exploratory analysis, fitting a semi-variogram model (for example, spherical, exponential, Gaussian), defining a search neighborhood, and solving the kriging system to produce a prediction surface together with a prediction-error (variance) surface; barriers can be enforced to prevent interpolation across hydrologic discontinuities such as levees or shorelines (Childs, 2004; ESRI, 2025e).

Broadly, OK's performance is constrained by three elements: sensitivity to how the variogram is modeled, the need for its model assumptions to hold in practice, and the requirement for ample, spatially extensive, and correlated data. Under these conditions the empirical variogram can be unstable and difficult to fit, and alternatives such as land-use regression or trend-based models may be preferable for spatial prediction (Columbia University, 2025). Despite these issues, when spatial correlation is clear and sampling is adequate to stabilize the semi-variogram, OK performs strongly and, unlike deterministic methods, quantifies spatially explicit uncertainty that can be used directly in decision-making (ESRI, 2025e).

3.3.3.2.6 Interpolation Selection

A single interpolation method was adopted for all bathymetric analyses to ensure that mapped bed changes reflect real movement of the surface rather than artificially constructed features during modelling. Using one standard interpolation method keeps the workflow consistent and avoids comparing surfaces created by different techniques. Candidate methods were tested on a deliberately demanding dataset: the Red River Outlet survey from August 08, 2020. This reach shows strong along- and across-channel differences, large swings in depth, and a mix of tightly clustered points and wider gaps. Before testing, all soundings were placed on the same vertical datum, clipped to a fixed boundary, and outputted to the same grid size so that each method operated across an identical area and resolution.

As previously highlighted, the five techniques used in this selection were TIN, TTR, IDW, SwB, and OK. Accuracy was estimated with leave-one-out cross-validation (LOOCV) implemented in ArcGIS Pro®. In brief, a single depth point was left out, the surface was built from the remaining points, and the omitted points value was predicted where the difference between measured and predicted depth is the residual. LOOCV, and split-sample testing more generally, are widely used and considered standard for checking interpolation accuracy in bathymetric surveys. Residuals for all methods were exported and analysed in MATLAB®. Root mean squared error (RMSE) was then calculated as the main indicator of overall accuracy. To see where errors were concentrated, residuals were grouped into 50 m cells and provided a local RMSE, producing maps that highlight areas of stronger and weaker performance, such as banks, channels, and sparsely sampled sections.

The final choice of an interpolation technique should balance quantitative performance with practical realism. A decision can be structured from the lowest global RMSE with minimal bias, provided that its 50 m local RMSE maps do not show clusters of large errors in hydraulically important parts of the channel. Table 3-2 provides the RMSE of the five interpolation techniques from smallest to largest value.

Table 3-2 Comparison of interpolation methods by maximum local and global RMSE

Interpolation Technique	Max Local RMSE (m)	Global RMSE (m)
IDW	0.18	0.0241
TTR	0.28	0.0276
TIN	0.27	0.0288
OK	0.25	0.0317
SwB	0.42	0.0504

Figure 3-7 provides further evidence to select an interpolation technique by showcasing the LOOCV local RMSE in 50 x 50 m cells. In all cases, larger local RMSE cluster at the outlet where the Red River enters Lake Winnipeg and along the main navigation corridor immediately downstream. These values taper toward the margins of the interpolation extent and farther lakeward. This pattern is consistent with the bathymetry: the outlet and thalweg have steep banks and rapid depth changes, so omitting a point forces each method to predict across strong gradients, which amplifies the difference between measured and predicted depths. The thalweg represents the deepest, continuous pathway within the channel where flow is preferentially concentrated. A second hotspot appears in the northwest portion of the extent at the former breakwater location, where abrupt elevation steps and structural edges are difficult to reproduce with smooth surfaces.

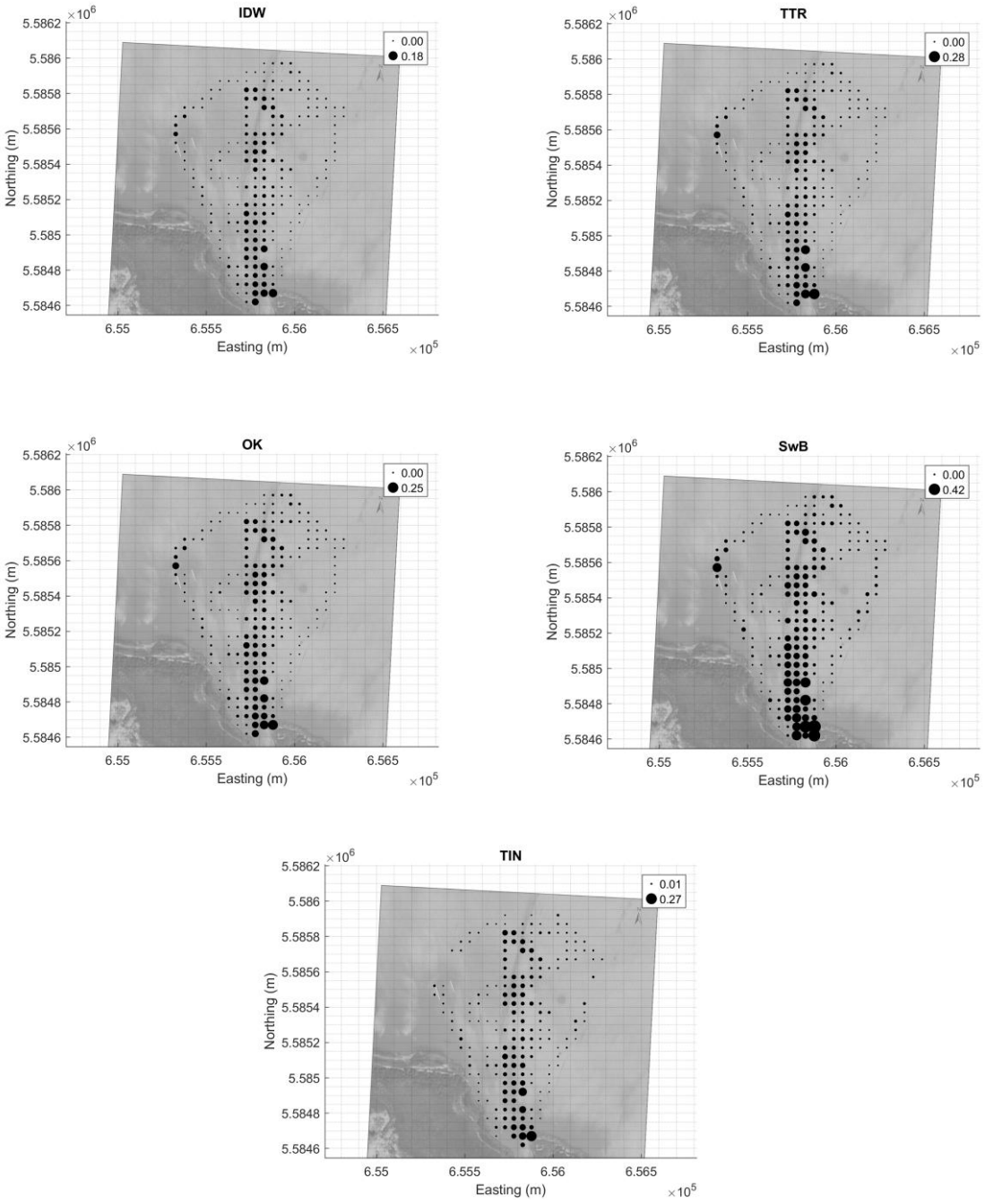

Figure 3-7 LOOCV local RMSE by interpolation method at the Red River Outlet (August 08, 2020, by HRTF)

Comparing methods, IDW shows the lowest local RMSE at 0.18 m, while SwB has the highest at 0.42 m. The remaining methods are similar, with maxima of 0.28 m for TTR, 0.25 m for OK, and 0.27 m for TIN. IDW can achieve lower residuals in LOOCV because its predictions

track nearby measurements very closely. When a single sounding is left out, several close neighbors remain, so the predicted value tends to fall near the omitted measurement, and the residual stays small. This strength is local and can come at the cost of surface continuity between transects, producing bull's eye forms and a wavy thalweg that do not match expected morphology. Methods like TTR and OK accept slightly larger pointwise residuals in exchange for more coherent features and smoother gradients, which can better represent continuous bars and underwater features. Therefore, the resulting surface should also pass a visual analysis based on site understanding, available aerial imagery, and realism of the predicted surface. For example, preferential flow paths, smooth but believable bank gradients, and an absence of bull's-eye or faceted structures. The preferred method should combine strong accuracy, an even spatial distribution of residuals, and stable behaviour under fixed settings so that surfaces remain comparable across surveys. Figure 3-8 provides the two predicted raster surfaces for the interpolation techniques with the lowest RMSE (IDW and TTR) at the Red River Outlet.

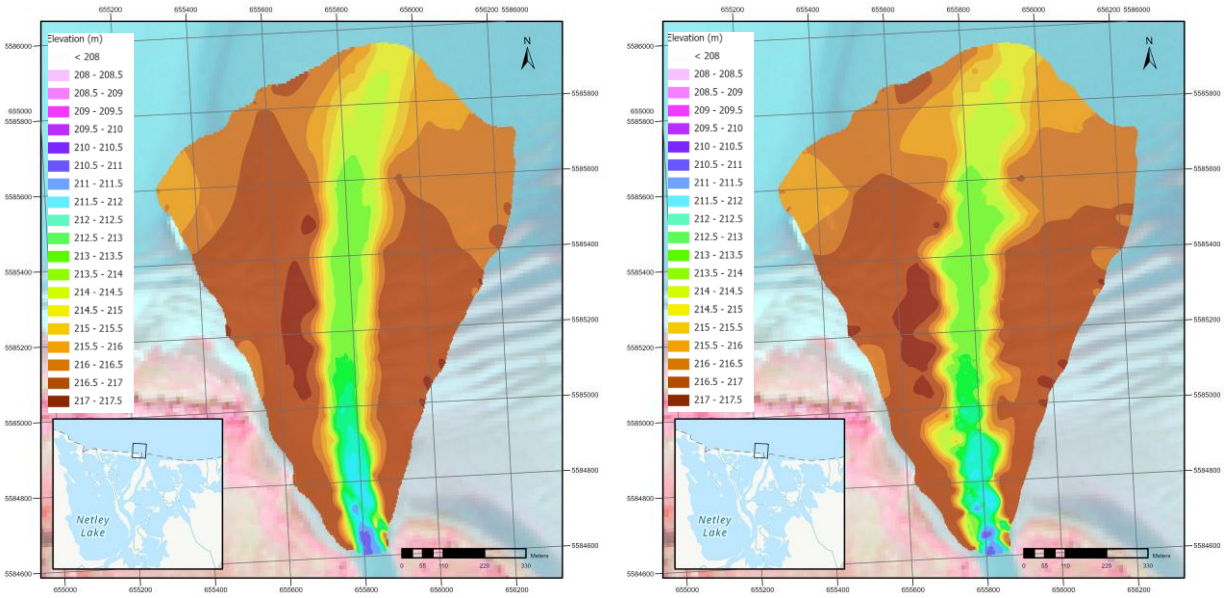

Figure 3-8 Predicted raster surfaces for TTR (left) and IDW (right) interpolation techniques at the Red River Outlet (August 08, 2020, by HRTF)

Figure 3-8 showcases the clear differences in how each method represents key geomorphic features. Along the main channel, TTR develops a coherent preferential flow path that follows the main navigation corridor, with smooth but continuous gradients into adjacent shallows. In contrast, IDW expresses a wave-like narrowing and widening along the thalweg, a pattern consistent with its tendency to pull the surface toward nearby measurements. This behaviour fragments features that are known to be continuous.

The central shoal provides a clear example. Field context indicates a single, relatively continuous bar through the mid-reach along the left bank of the main navigation corridor. In the TTR surface this bar appears as one connected feature. The IDW surface breaks into a group of nearly circular highs centered on measurement clusters, with elevations in the 217 to 217.5 m range. These “bull’s-eye” forms are typical of IDW interpolation in areas with uneven point spacing and do not reflect the expected bed form.

Differences are also evident west of the main channel near the former wharf structures. Between northing 5,585,600 m and 5,585,400 m, two lighter square footprints mark the old breakwaters. The TTR surface shows a more continuous secondary flow path that skirts these structures, which matches site history and the observed bathymetric context. The IDW surface weakens or interrupts this path, again reflecting sensitivity to local point clusters.

Taken together, the combination of low RMSE, stronger expression of the thalweg and bar continuity, and better alignment with known structural controls supports selecting TTR as the standard interpolation method for generating bathymetric surfaces in the subsequent analyses.

3.3.3.2.7 External Dataset Validation

As an additional reliability check for datasets acquired outside this thesis or by sources other than the HRTF, XYZ points were re-interpolated with TTR and compared against the supplied DEM where the original interpolation method was unknown (UNK). Figure 3-9 and Figure 3-10 illustrates this comparison for the Manitoba Hydro 2018 data at Netley Cut and at the Red River Outlet, respectively. In both areas, TTR shows lower maximum local residual RMSE relative to the measured soundings: 0.11 m versus 0.35 m at Netley Cut, and 0.16 m versus 0.53 m at the Red River Outlet. The UNK surfaces also exhibit more pronounced clustering of large RMSE near steep banks and at the channel center, whereas TTR maintains a more uniform error throughout the extent.

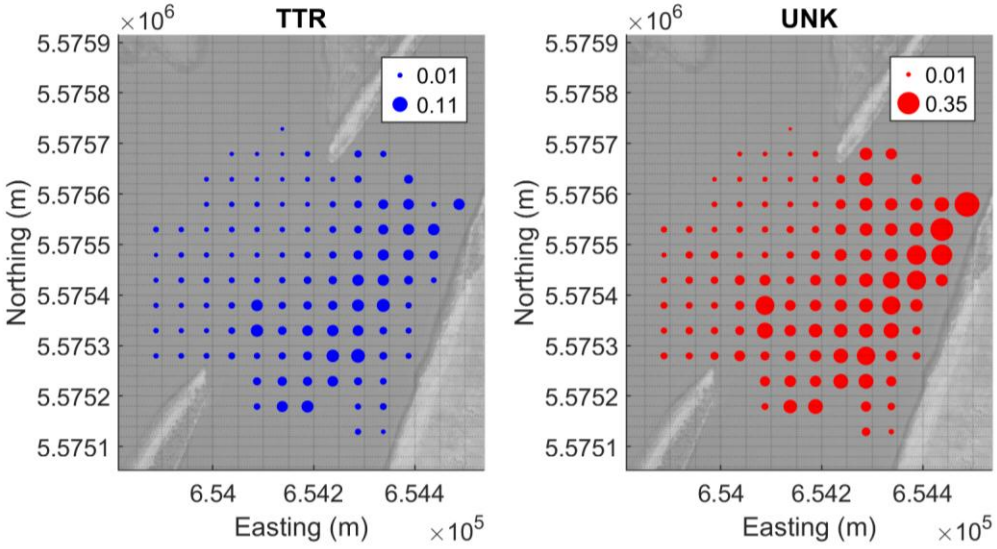

Figure 3-9 Local RMSE distribution for TTR and UNK interpolation at Netley Cut (MH, 2018)

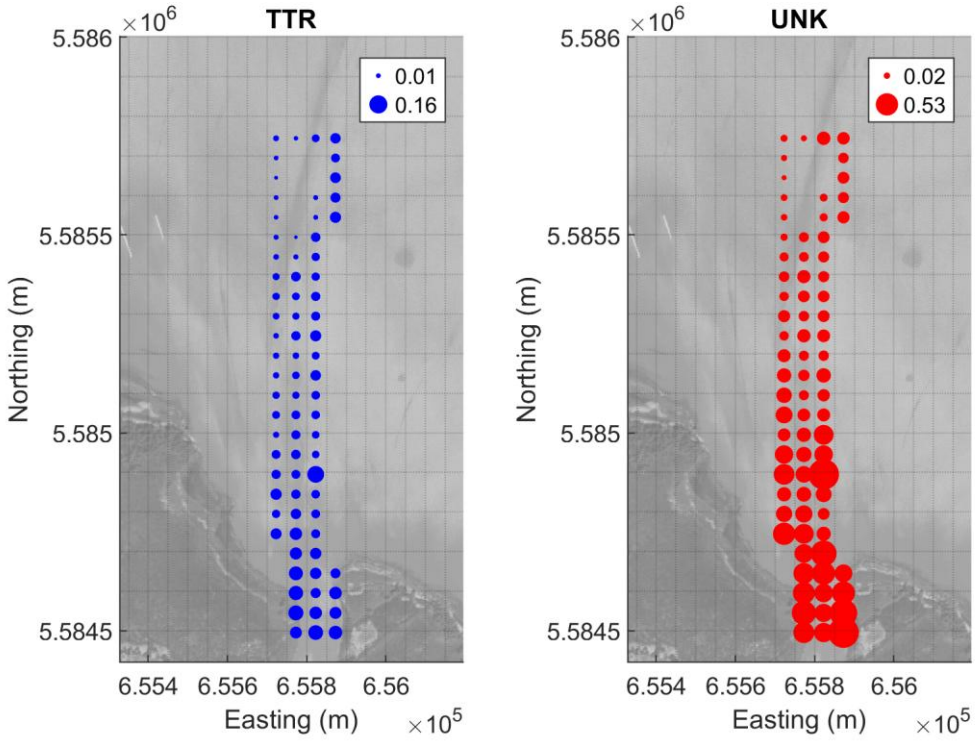

Figure 3-10 Local RMSE distribution for TTR and UNK interpolation at the Red River Outlet (MH, 2018)

An exception applies to datasets supplied by Aquatic Environmental Services. AES did not provide a DEM suitable for cell-by-cell evaluation; only finished DEM figures in PDF format and XYZ points referenced to NAD83, UTM Zone 14N. Consequently, Point to Raster (P2R) was applied directly to the XYZ data to generate working surfaces for this thesis. Because the AES PDF figures were derived from a gridded point set, the interpolation technique used to generate them could not be evaluated, and no sounding paths were provided to support a TTR-based interpolation. As a result, no quantitative comparison was possible between the provider's unknown method and TTR. Interpretations for AES data therefore rely on the P2R surfaces derived from the supplied soundings.

3.3.3.3 Estimating Volumes

Bathymetric volume estimates were derived by differencing paired DEMs for each site. Pairs were chosen within a year or between years, depending on acquisition dates, to capture both short-term and year-to-year change. The analysis footprint was the exact overlap of the two survey perimeters for most comparisons. The Netley Cut was the exception. There, a fixed polygon between the two banks at the entrance to Netley Lake was used for all comparisons to provide a consistent and hydraulically meaningful area for volume estimates.

Surface difference rasters were created in ArcGIS Pro® using the Minus raster tool with the convention '*later raster'* minus '*earlier raster'*. Under this sign convention, positive values indicate deposition and negative values indicate erosion. Volumes of deposition, erosion, and net change were then summarised from these change grids within the analysis boundaries using ArcGIS Pro® raster summarisation tools, rather than by manual multiplication of cell values by cell area. Clipping ensured that only the in-polygon portions contributed to the reported volume estimates.

3.3.3.4 Topographic and Aerial Surveys

When topographic survey data were required to supplement bathymetric datasets, they were interpolated using IDW to produce continuous surface models. These datasets were tied into NAD83, UTM-14, and CGVD13 for consistency with other survey products.

Imagery collected during aerial surveys was processed in Agisoft Metashape Professional® using a standard structure from motion workflow. Processing steps included initial camera alignment, generation of a sparse point cloud, and optimization using ground control points to refine bundle adjustment. A dense point cloud was then created, from which both a DEM and an orthomosaic were produced. Quality control procedures included review of reprojection error

statistics, visual inspection of tie point distribution, and cross-validation with GNSS-surveyed check points. Final outputs were referenced to EPSG 6657 for consistency with bathymetric and topographic datasets.

3.4 Results and Discussion

This section presents results for the main areas of bathymetric interest within Netley-Libau Marsh: the Red River Outlet, the Lower Red River Reach, the Netley-Libau Marsh Restoration Project (including the Deposition Site and the Dredge Site), the Netley Cut Delta, Netley Lake, and the Netley Cut.

An initial assessment is presented for the novel SBES proxy method used as a replacement for CUBE/CHRT-style analysis in MBES surveys. Reliability is assessed using two lines of evidence. First, accuracy is summarized by the mean absolute error of paired differences from repeat measurements. Second, spatial structure is evaluated using Moran's I to test for spatial autocorrelation and Mantel's R to examine distance–decay relationships. Statistical significance is gauged by combining individual p-values with Fisher's method. Formal geostatistical testing is not the emphasis in this section; the objective is a practical check on whether the proxy method yields interpretable results suitable for the comparisons that follow. Afterwards, the bathymetric maps and volume estimates of deposition and erosion are reported for survey pairs collected within the same year and between years, depending on acquisition dates. These results are interpreted qualitatively to identify short-term (seasonal) and long-term (multi-year) trends in sedimentation patterns.

A digital elevation model is provided for each bathymetric survey of interest. Key transects were selected in areas of interest and are referenced in the output maps to support interpretation.

All bathymetric surveys and derived rasters were produced in ArcGIS Pro® and are shown in a standard format that includes the interpolation extents, the bathymetric surface, and the DEM of surface-differences between acquisition dates for each site. This consistent presentation allows direct comparison of deposition, erosion, and net volume estimates across locations and survey periods.

3.4.1 SBES Proxy

Table 3-3 summarises spatial autocorrelation and bathymetric survey metrics for each SBES dataset processed using the proxy method described earlier. Metrics are presented by location and survey date, capturing both the surveyed area and the characteristics of the point distribution. The “Area” and “Perimeter” columns describe the physical footprint of each survey, while N indicates the number of 1 × 1 m grid cells containing at least one sounding. RI expresses the proportion of the surveyed area that required interpolation, providing an indication of how much of the surface was measured directly versus predicted. In most cases, N is substantially larger than the number of cells containing repeat measurements, which limits the ability to analyse within-cell variability.

The mean, median, and IQR columns reflect the distribution of variability calculated from paired differences in cells containing repeat soundings. Across all surveys, mean values ranges from 0.024 m to 0.109 m, while median values are consistently lower, between 0.020 m and 0.079 m. These statistics indicate that the majority of repeat measurements within the same cell differ by only a few centimetres, suggesting relatively low short-term variability where repeat soundings exist. However, M (the count of cells with more than one sounding at different times) remains a small fraction of N, meaning that only a minor proportion of the surveyed area can be used for direct repeat-sounding comparison.

Table 3-3 Summary of Spatial Autocorrelation and Bathymetric Survey Metrics by Location and Date

Location	Date	Area (m^2)	Perimeter (m)	N	RI (%)	Mean (m)	Median (m)	IQR (m)	M	Tc	SpI	SpR	p_{fI}	p_{fR}
Netley Cut	2021-07-08	268534	2899	17523	93.5	0.037	0.021	0.036	311	66	12	5	-	-
Netley Cut	2022-07-14	65472	1510	9392	85.7	0.051	0.043	0.045	333	18	1	0	-	-
Dredge Site	2021-07-29	43788	951	12807	70.8	0.056	0.041	0.050	1733	383	78	39	< 0.01	< 0.01
Dredge Site	2021-08-17	143850	2052	23123	83.9	0.044	0.031	0.046	1208	184	61	18	< 0.01	-
Dredge Site	2021-07-14	59935	1060	15026	74.9	0.059	0.046	0.062	1384	84	10	5	-	-
Red River Outlet	2020-08-20	752190	3636	22758	97	0.097	0.058	0.113	292	50	7	7	-	-
Red River Outlet	2021-07-27	160742	2848	28880	82	0.040	0.029	0.041	824	86	38	30	<0.01	< 0.01
Red River Outlet	2020-10-18	247200	3505	27908	88.7	0.073	0.042	0.064	1516	51	8	5	-	-
Netley Cut	2014-09-15	109036	1512	10821	90.1	0.109	0.079	0.110	91	0	0	0	-	-
Netley Cut	2020-08-20	223632	1955	15513	93.1	0.032	0.020	0.029	239	24	11	2	-	-
Deposition Site	2021-08-04	24145	749	5686	76.5	0.024	0.020	0.024	638	279	66	29	< 0.01	-
Netley Delta	2022-07-21	628620	4590	40652	93.5	0.051	0.038	0.054	771	86	17	7	-	-

N is the number of 1×1 m cells containing soundings. **RI** is the percent of the surveyed area requiring interpolation. **M** is the number of cells containing soundings at different times. **Tc** is the number of cells with more than five soundings per cell. **SpI** is the count of p-values less than 0.05 from Moran's test, while **SpR** is the count of p-values less than 0.05 from Mantel's test. p_{fI} is Fisher's combined p-value for Moran's test, and p_{fR} is Fisher's combined p-value for Mantel's test.

The feasibility of this approach becomes unlikely when interpreting the results of the geostatistical metrics. Tc represents the number of cells with more than five repeat soundings, forming the base for Moran's I (SpI) and Mantel's R (SpR) significance testing. Counts in these categories are generally low, and in many surveys drop to single digits. The number of cells producing statistically significant *p*-values is even smaller, often insufficient to meet the minimum of 30 observations recommended for robust Fisher's combined *p*-value testing. Where Fisher's test was applicable, combined *p*-values for Moran's I (p_m) and Mantel's R (p_{mantel}) were both < 0.01, highlighting the sensitivity of the method to a small set of significantly low results.

Overall, the metrics indicate that SBES surveys in this study generally consist of one sounding per cell for the majority of each survey extent, offering confidence that interpolation methods do not excessively collapse multiple soundings across 1 x 1 m cells. However, the scarcity of cells with sufficient measurements to reliably quantify geostatistical properties severely limits the utility of small-scale spatial autocorrelation techniques such as Moran's I and Mantel's R for. The low coverage of viable cells meeting eligibility criteria, combined with the sensitivity of Fisher's method with very sparse results, renders this approach inadequate for reliably quantifying error in SBES datasets within the present study.

Since the novel SBES proxy method did not perform as expected, an application of the spatial autocorrelation using global Moran's I was applied to all available data points in the Red River Outley survey on August 8, 2020. This method was not considered initially because it was hypothesised that SBES point distributions would already appear highly clustered due to the nature of their collection, where soundings are recorded in close succession along survey lines. Based on this, the initial step was to investigate whether individual cells within the survey showed a tendency toward greater clustering or dispersion before interpolation collapsed

multiple soundings into a single elevation value. Figure 3-11 presents the results of a subsequent global Moran's I analysis conducted on the Red River Outlet survey of August 8, 2020.

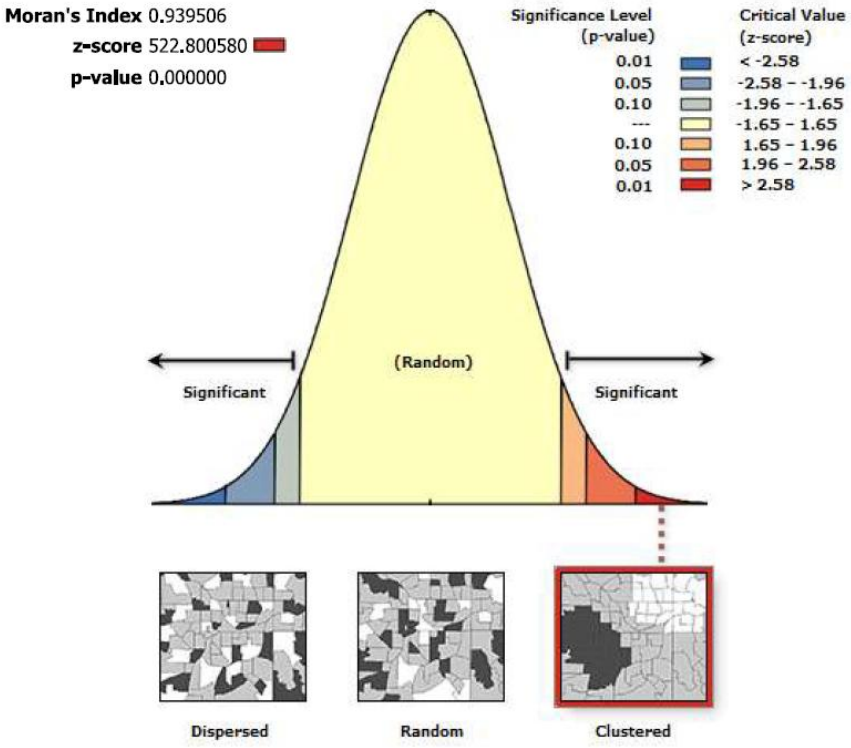

Figure 3-11 Global Moran's I results for the Red River Outlet SBES survey (August 8, 2020)

The global Moran's I analysis confirmed that the dataset is very strongly spatially clustered, returning a Moran's I = 0.940, a z-score = 522.80058, and a *p*-value < 0.01. These results indicate there is less than a 1% likelihood that the observed pattern could have occurred by random chance. This finding supports the expectation that SBES surveys, when evaluated globally, will almost invariably produce strong clustering results due to their inherent survey design, limiting the applicability of global Moran's I for distinguishing meaningful spatial error patterns in the novel SBES proxy method.

3.4.2 Netley Cut

Netley Cut was surveyed repeatedly between 2010 and 2022. Table 3-1 lists acquisition dates, instrumentation, vertical referencing, and the responsible parties for each survey. Figure 3-12 shows the interpolation footprints for all surveys over the general extent of the Netley Cut. Each dataset includes the central corridor between the left and right banks of the Cut with spatial coverage varying by year. Downstream is oriented from the south to the north of the figure, consistent with the primary flow direction from the Red River into Netley Lake and Lake Winnipeg. A fixed analysis frame was established within the Netley cut to standardise comparisons. The frame encloses the bank-to-bank section that is common to all surveys, is oriented perpendicular to the dominant flow path, and excludes peripheral areas where coverage differs among years. All volume estimates were reported for Netley Cut using this frame to control for unequal extents and to minimise edge effects from extrapolation at survey boundaries, whereas surface differencing showcased the change in elevation of the overlapping region between two interpolation extents.

The 2010 AES dataset provides the widest spatial footprint, extending across the Red River and into the Cut. A discontinuity in the input dataset occurs between the two banks within the analysis frame, where soundings do not span continuously between the Red River and the Netley Delta. The discontinuity was interpolated between the two complete datasets for the Red River and Netley Lake to obtain a working surface inside the analysis frame. Within the analysis frame for 2010, elevations are therefore unrepresented by any true elevation values and are thus interpreted with caution.

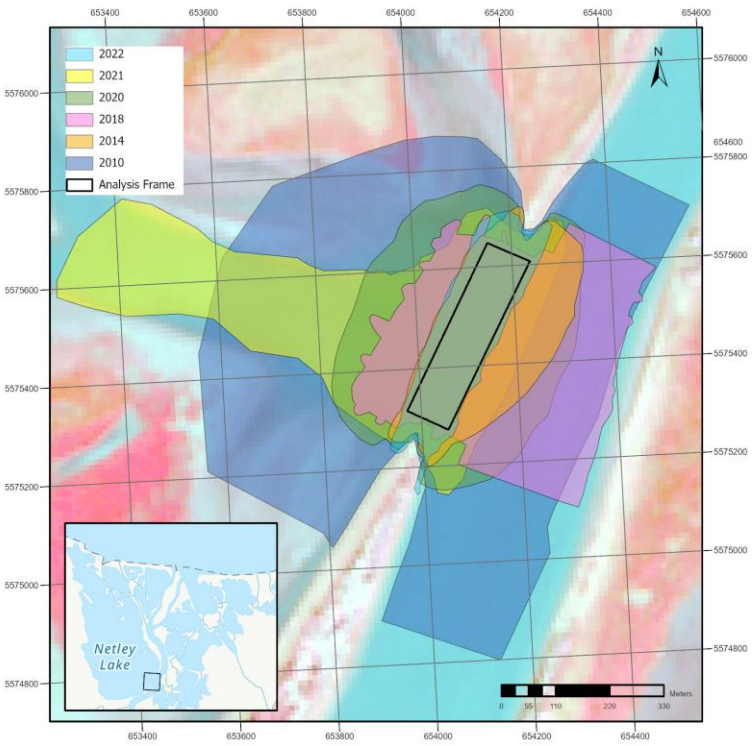

Figure 3-12 Interpolation and analysis extents for various bathymetric surveys at Netley Cut

Subsequent HRTF surveys in 2014, 2020, and 2022 utilized tightly spaced, cross-weave sounding paths focused on the Cut, yielding consistent coverage across both banks inside the analysis frame. The 2018 Manitoba Hydro dataset spans from the Red River using similar cross-weave patterns with complete left to right bank coverage through the Cut. The 2021 HRTF survey extended the interpolation window lakeward to examine changes in the main channel of the Netley Delta while still encompassing the standard analysis frame. Figure 3-13 (a) to (f) provides the completed bathymetric DEMs for each survey, enabling cross-comparison between the common analysis frame in Figure 3-12 and the full surveyed areas.

Across all six bathymetric DEMs, the mapped surfaces show strong conformity of the bed throughout Netley Cut and into the Netley Delta. Elevations drop sharply immediately downstream of the left bank, defining a persistent thalweg aligned with flow from the Red River

toward Netley Lake. The thalweg position is stable through time, with a global maximum occurring at approximately 140 m from the left bank and two local minimums occurring at approximately 200 m and 350 m. The thalweg remains similarly positioned within the Cut and has no observable inflection or lateral shift between surveys. The curvature remains low, indicating that changes are expressed primarily as small variations in width and relief rather than in alignment.

The right-bank margin (300–500 m) consistently forms a gentler shelf with a gradual slope compared to the steeper and wider left-bank margin (0–300 m). The main channel through the Cut stays aligned along the left-bank margin and continues into Netley Lake, where contours and the elongation of lower elevations indicate that flow proceeds primarily west. This persistence indicates stability within the channel, while observed surface changes in Figure 3-14 reflect minor variations in width and local bed relief rather than repositioning of any portion of the channel.

A repeatable bed high is present in all bathymetric surveys within the analysis frame approximately 150 – 200 m from the left bank. It appears as a local maximum in elevation that persists across years and interrupts the otherwise uniform cross-sectional form of the Cut. Historical accounts report efforts to close Netley Cut with a sheet-pile wall and a subsequent repair in 1924, during which a dredge boat was sunk and left in place as a partial blockade (Goldsborough & Grover, 2021). The persistence, approximate location, and expression of the local maximum are consistent with these submerged artefacts. It is therefore likely that the feature represents the combined remains of the sheet-pile wall and the sunken dredge boat.

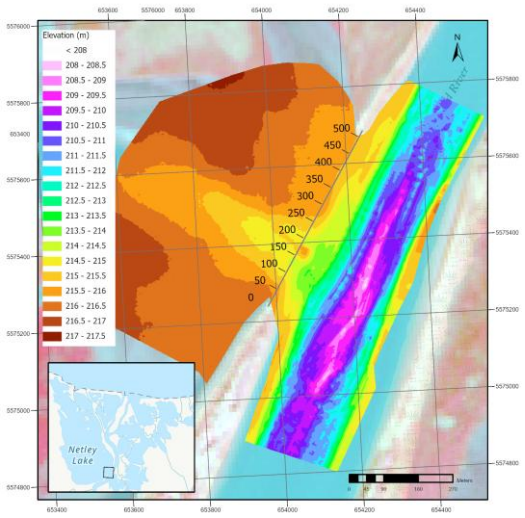

(a) AES 2010

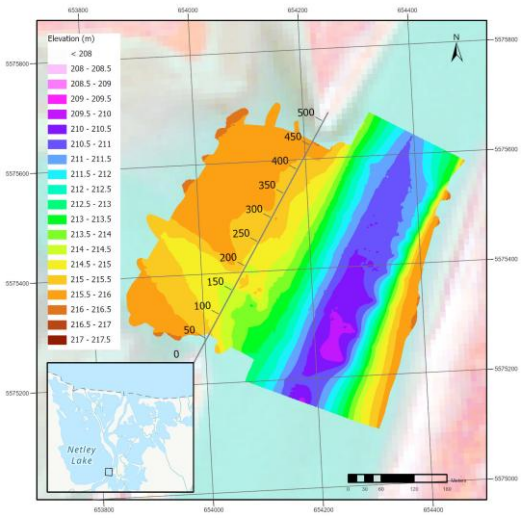

(b) MH 2018

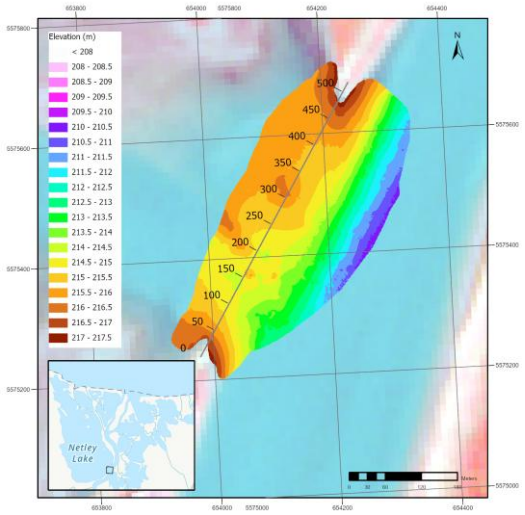

(c) HRTF 2014

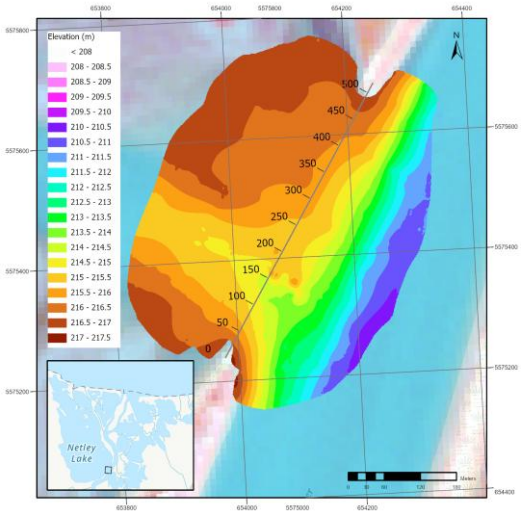

(d) HRTF 2020

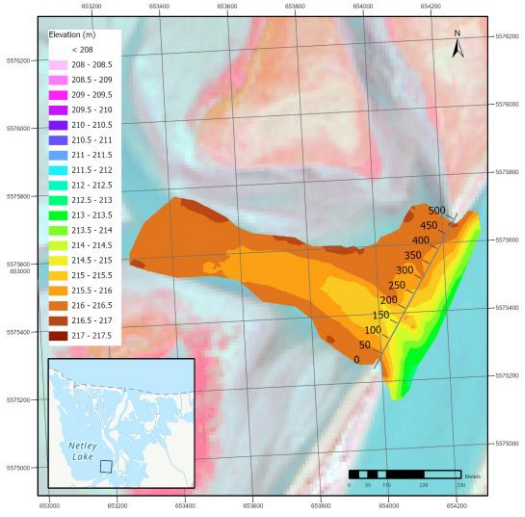

(e) HRTF 2021

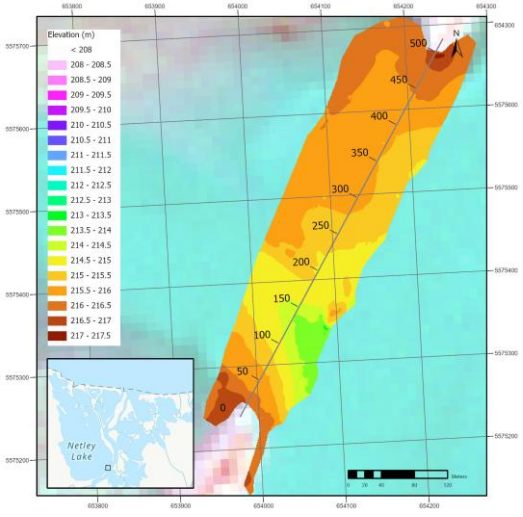

(f) HRTF 2022

Figure 3-13 Bathymetric DEMs at Netley Cut

SBES data and the interpolation methods used to create the DEMs tend to broaden small targets and can shift their apparent location between surveys. Track spacing, beam footprint, and interpolation technique contribute to a footprint that is larger than the underlying object and to a slight migration of the submerged artefacts position across DEMs.

Correspondingly, survey years that include the Red River channel show a rise in bed elevation between 2010 and 2018, highlighting infilling of the nearby portion of the Red River.

3.4.2.1 Surface Differences

Consecutive bathymetric DEMs were differenced to evaluate temporal elevation change within the overlapping interpolation extents. Figure 3-14 (a) to (e) presents these results, where the dashed grey contour denotes zero elevation change.

From 2010 to 2014 (a), the surface shows pronounced lateral banding of alternating erosion and deposition, including thin bands that extend streamwise along the Red River. Deposition is indicated within the centre of Netley Cut and along these bands. These patterns reflect interpolation effects in the AES-2010 bathymetric DEM, which combined two datasets that omitted soundings inside the Cut, and are amplified by differences in point density between soundings. In subsequent figures, where both DEMs have dense SBES coverage within the Cut, the difference surfaces are more predictable and do not display the lateral banding produced by interpolation techniques. Near the known underwater obstruction, a minimum elevation change of −1.49 m lies immediately adjacent to a maximum of approximately +1.41 m; this pair of extremes results from slight positional differences of the sunken dredge boat and former sheet-pile wall between datasets, producing an apparent shift of the artefact rather than erosion or deposition.

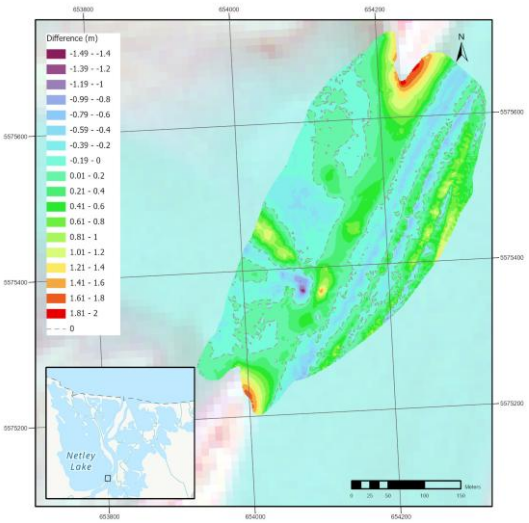

(a) 2010→2014

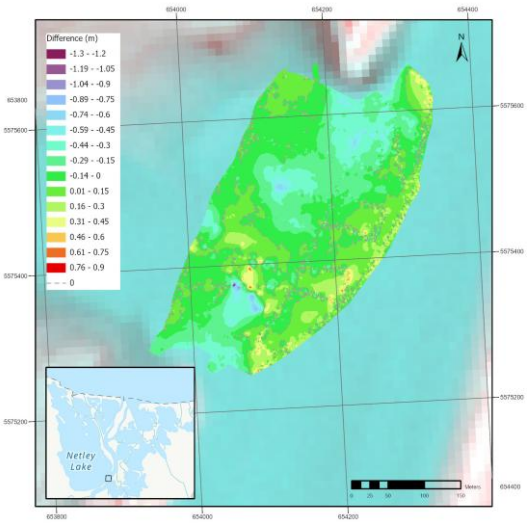

(b) 2014→2018

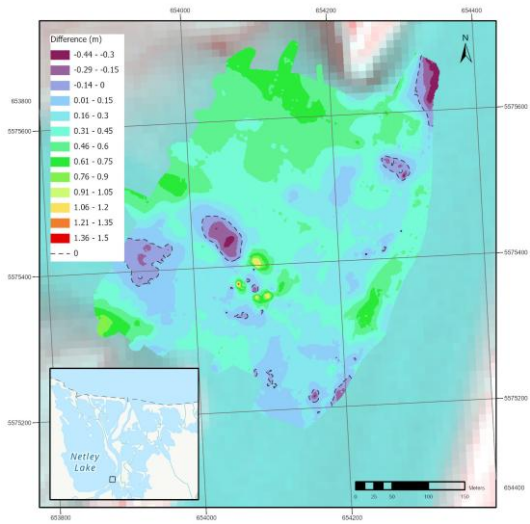

(c) 2018→2020

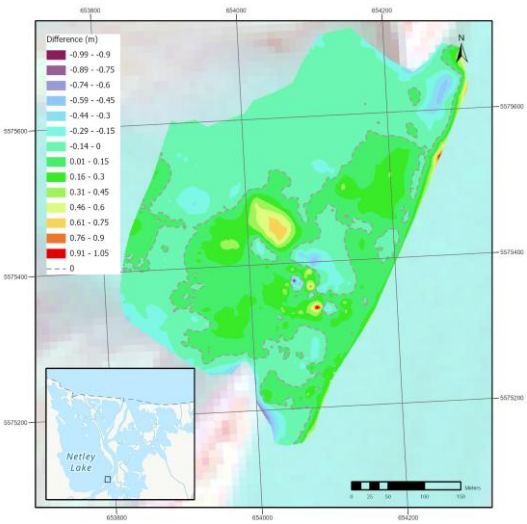

(d) 2020→2021

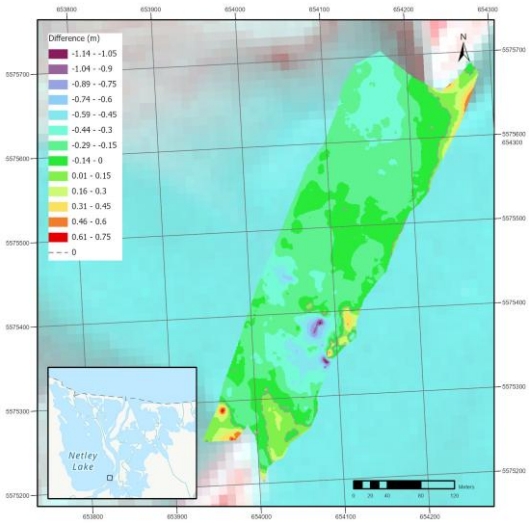

(e) 2021→2022

Figure 3-14 Surface differences between chronological acquisition dates at the Netley Cut

The 2014 to 2018 (b) comparison is more coherent and shows spatially variable change across the Cut, with deposition along the steepening right bank adjacent to the thalweg and erosion within the thalweg and across portions of the gentler right-bank margin. Between 2018 and 2020 (c) the surface is dominated by deposition with only small, isolated pockets of erosion. The 2020 to 2021 interval (d) shows deposition, including within the thalweg and along the right-bank margin. Finally, 2021 to 2022 (e) is characterised primarily by erosion across the analysis frame.

3.4.2.2 The Analysis Frame

Linking the difference maps in Figure 3-14 to the analysis frame, Table 3-4 reports net volumetric change for every survey combination, with positive values indicating deposition and negative values indicating erosion. Read chronologically across successive intervals, the Cut alternates through deposition from 2010–2014 (+1,782 m^3), erosion from 2014–2018 (−4,736 m^3), strong deposition from 2018–2020 (+12,922 m^3), modest deposition from 2020–2021 (+1,365 m^3) and pronounced erosion from 2021–2022 (−8,355 m^3). Considering the entire dataset period, the 2010–2022 comparison yields a net depositional balance of +2,978 m^3.These magnitudes align with the spatial patterns seen in Figure 3-14, where deposition increasingly dominates after 2018 before the erosion period between 2021–2022.

Table 3-4 Net volume changes between bathymetric surveys using an analysis frame at Netley Cut

Year	2010	2014	2018	2020	2021	2022
2010	(m^3)	1782	-2955	9968	11333	2978
2014			-4736	8186	9551	1196
2018				12922	14287	5932
2020					1365	-6990
2021						-8355

Table 3-5 presents the same pairwise changes as net elevation differences normalised by area (expressed as $m^3 \cdot m^{-2}$). 2010–2014 shows a small rise of +0.049 m, 2014–2018 a decline of −0.131 m, 2018–2020 a strong rise of +0.359 m, 2020–2021 a modest rise of +0.038 m, and 2021–2022 a decline of −0.232 m. Over the full record the 2010–2022 net change is +0.083 m, consistent with the +2,978 m^3 volumetric gain reported in Table 3-4. Together, the two tables quantify the same behaviour observed in the difference maps: fluctuating interval-to-interval alternation between deposition and erosion with a cumulative deposition from 2010 to 2022.

Table 3-5 Net elevation differences between bathymetric surveys using an analysis frame at Netley Cut

Year	2010	2014	2018	2020	2021	2022
2010	(m)	0.049	-0.082	0.277	0.315	0.083
2014			-0.131	0.227	0.265	0.033
2018				0.359	0.396	0.165
2020					0.038	-0.194
2021						-0.232
2022						

These elevation changes are further analysed along a single cross-section through Netley Cut. Figure 3-15 plots bed elevation against distance from the left bank and overlays all bathymetric DEMs shown in Figure 3-13. Vertical dashed lines at 12, 55, 160, 200, 370, and 500 m partition the section into three analysis windows used to compute average elevation change:

- Full-width window (12–500 m): captures the maximum bank-to-bank corridor observed between all surveys.

- Left-bank thalweg window (55–160 m): spans the deepest portion of the Cut and extends to the local bed high near 150–160 m that is consistent with the submerged sheet-pile wall and sunken dredge.
- Right-bank shelf window (200–370 m): targets the gradual, higher-elevation shelf on the right side of the channel.

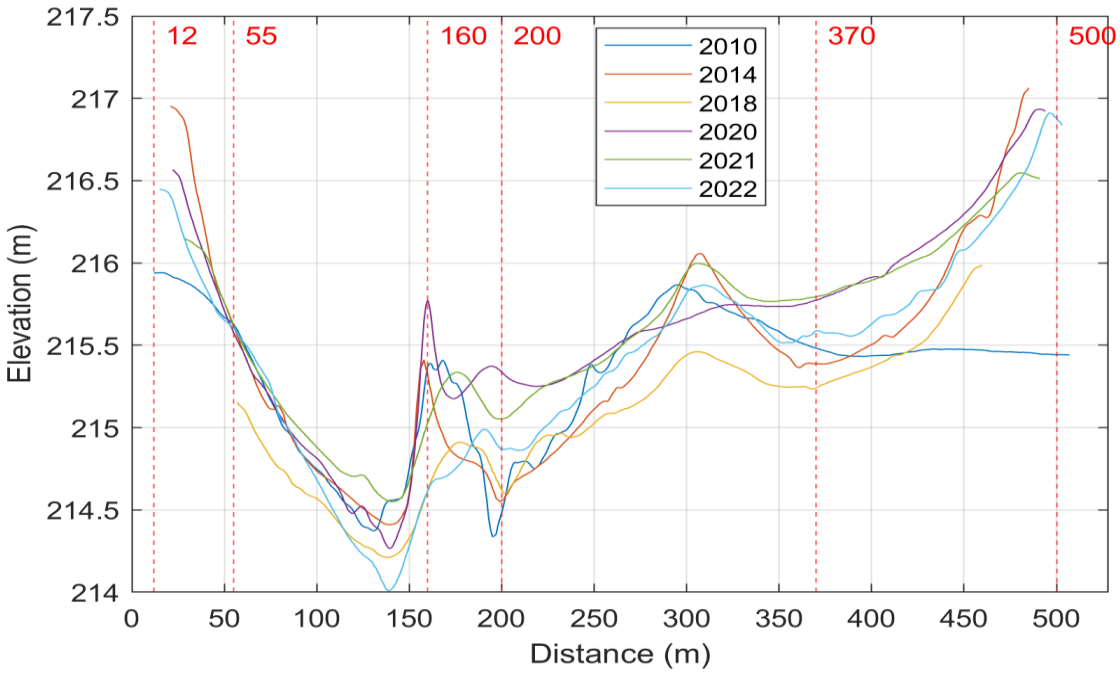

Figure 3-15 Elevation differences across distance-windows using a cross-sectional transect at Netley Cut

Across years the cross-section retains the same overall form as previously investigated qualitatively through the bathymetric DEMs. Elevations fall steeply from the left bank into the thalweg, rise through a local bed high at 150–200 m, and then climb gradually across the right-bank shelf toward 370–500 m. An exception to this trend is the AES 2010 dataset, which shows a near-horizontal segment between roughly 370 and 500 m on the right bank. This behaviour results from sparse soundings along the upper right bank where the interpolation technique

infilled from nearby lower elevations within the channel and smoothed the rise toward the bank, producing an artificially low, flat profile in this zone. Subsequent surveys with dense bank-to-bank coverage show the expected increase toward the right bank, reaffirming that the 2010 values in this segment should be treated with caution. This segment lies outside the 200–370 m right-bank analysis window, so the window-based averages reported later are not affected. Furthermore, interannual variability throughout the Cut is expressed mainly as vertical adjustment of the distance-windows rather than as shifts in position. The three windows isolate the hydraulically distinct zones of the section and provide a consistent basis for the average elevation comparisons presented in Figure 3-16.

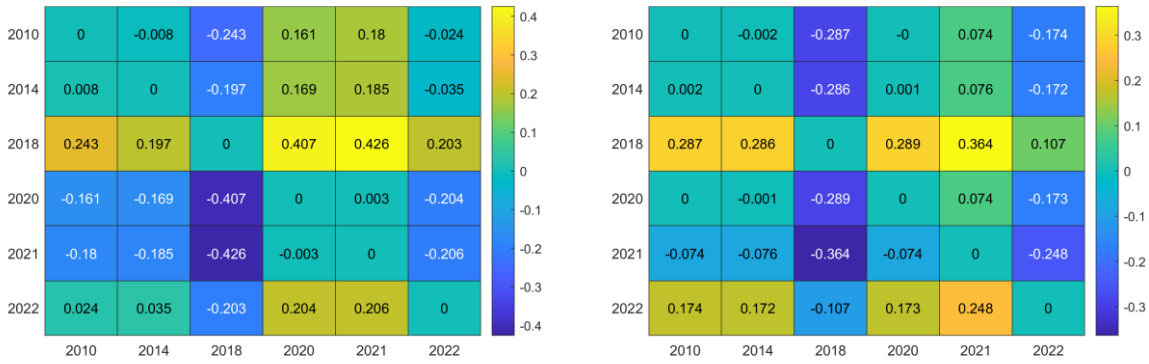

(a) 12 – 500 m

(b) 55 – 160 m

(c) 200 – 370 m

Figure 3-16 Average elevation differences across distance-windows using a cross-sectional transect at Netley Cut

The sign matrices of these heat maps confirm two behaviours. The response is uniform across the section for consecutive survey intervals. The full width, the left window, and the right window all show the same sign in 2010–2014, 2014–2018, 2018–2020, 2020–2021, and 2021–2022. These sequential years therefore represent channel-wide aggradation or degradation events that affect all windows together.

Mixed responses are common for non-consecutive multi-year comparisons. That is, survey pairs separated by one or more intervening years such as 2014 to 2022. Several of these longer, non-adjacent comparisons display opposing signs between the windows. A representative example is 2014 to 2022, which shows net aggradation for the full-width window, degradation in the left window, and aggradation in the right window. These outcomes indicate redistribution between windows over non-sequential multi-year periods rather than a uniform section-wide trend.

Year-to-year responses across the most recent sequence are particularly coherent: 2020 to 2021 shows aggradation in all windows, 2021 to 2022 shows degradation in all windows, and the two-year span 2020 to 2022 also shows consistent degradation. Despite the variability evident in non-adjacent comparisons, the persistent bank-to-bank width, the stable thalweg position, and the repeatable cross-sectional form indicate long-term stabilisation of channel geometry within the analysis frame. Therefore, the data indicate no systematic change in hydraulic conveyance within Netley Cut over the study period.

3.4.2.3 Investigating Sediment Transport against Stage and Discharge

Combined discharge and water-level records provide some hydraulic context for interpreting bed change over time. Discharge at Selkirk (05OJ005) represents the Red River inflow to the Netley–Libau system, while water surface elevation at Breezy Point (05OJ022) represents Lake

Winnipeg stage near the outlet. Together these series provide two parameters to investigate sediment deposition and erosion through Netley Cut (and subsequent areas within NLM). For 2010–2022, March–July peaks, minimums, and averages were extracted for both stations and analyses were classified using median thresholds in four states: high WSE and high discharge, high WSE and low discharge, low WSE and high discharge, and low WSE and low discharge. This framework links stage and discharge to the difference maps in Figure 3-14 and to the pairwise volume and elevation summaries in Table 3-4 and Table 3-5, allowing the observed erosion and deposition patterns to be evaluated against periods when stage and discharge would likely influence hydrodynamics within the marsh. However, it is noted that the defined median threshold is arbitrary and does not constitute a definitive value at which erosion or deposition is expected to occur, nor does it assess the period required to facilitate a certain degree of erosion or deposition. Beyond the previously defined parameters (stage and discharge), the sediment transport processes would depend on additional factors such as wind and seiching effects, sediment load present in the Red River and Lake Winnipeg, flow continuity in and out of Lake Winnipeg and NLM, and climate. All these parameters are variable by time of year and are outside the scope of this thesis to assess. Instead, the median stage and discharge are used as a baseline to infer whether stage and discharge can explain the sediment transport response between years.

Following this, Figure 3-17 displays the mean, minimum, and maximum discharge and stage for Selkirk and Breezy Point, respectively. Very high peaks are recorded in 2011 (2,250 m^3/s, 218.687 m), 2017 (1,510 m^3/s, 218.477 m), 2020 (1,500 m^3/s, 218.556 m), and 2022 (2,500 m^3/s, 218.729 m). Low periods occur in 2012 (302 m^3/s, 217.703 m) and 2021 (162 m^3/s, 217.250 m). Classifying years by median thresholds and state: high WSE and high discharge (2010, 2011,

2014, 2020, 2022), high WSE and low discharge (2016, 2017), low WSE and high discharge (2013, 2019), and low WSE and low discharge (2012, 2015, 2018, 2021).

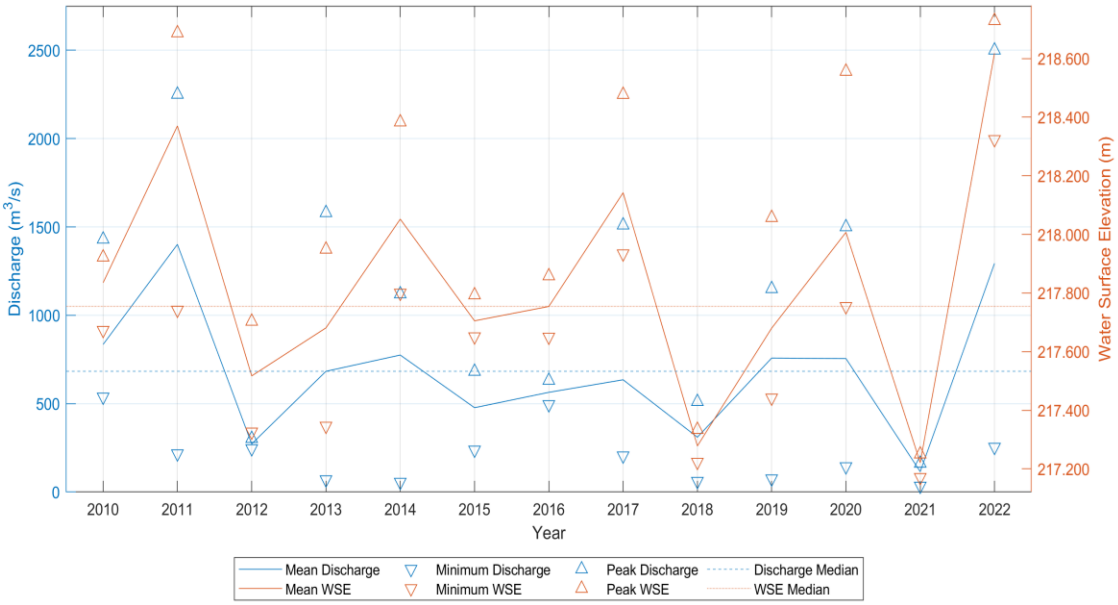

Figure 3-17 Discharge at Selkirk (05OJ005) and water surface elevation at Breezy Point (05OJ022) for March to July

2010–2014

States are high WSE and high discharge in 2010, 2011, and 2014, low WSE and low discharge in 2012, and low WSE and high discharge in 2013. The net response over the interval is deposition of +1,782 m³ with a mean bed rise of +0.049 m. If high-high years consistently produced erosion, a net lowering would be expected given their frequency in this window. Instead, the cumulative outcome is depositional, indicating no simple correlation between the median-based discharge and stage and the net volume or elevation change for this period.

2014–2018

The states are low WSE and low discharge in 2015 and 2018; and high WSE and low discharge in 2016 and 2017. The net response over the interval is erosion of −4,736 m³ with a mean lowering of −0.131 m. If low–low years consistently produced deposition, two such years would be expected to bias the period toward accumulation. Instead, the presence of two high–low years coincides with an overall erosional balance.

2018–2020

The states are low WSE and high discharge for 2019, and high WSE and high discharge for 2020. The net response over this interval is strong deposition of +12,922 m³ with a mean bed rise of +0.359 m. If the average-based state were a reliable predictor, the inclusion of a high–high year in 2020 would be expected to offset or reverse depositional that would be influenced by the mixed condition 2019. Instead, deposition dominates across the mixed sequence (low–high → high–high).

2020–2021

The states are low WSE and low discharge for 2021. The net response over this interval is modest deposition of +1,365 m³ with a mean bed rise of +0.038 m (Tables 3-3 and 3-4). This outcome is consistent with the expectation that low stage and low discharge favour quiescent infilling.

2021–2022

This interval contains the extreme high-high of 2022. The response is erosion of −8,355 m³ and a mean lowering of −0.232 m. This interval shows an erosional response coincident with a

high–high state, consistent with the tendency for very high discharge and lake stage to accompany reworking.

In summary, at the single-year scale, the relationship is clear. Years classed as low stage and low discharge correspond with net deposition, while years classed as high stage and high discharge correspond with net erosion. This pattern indicates that a combined threshold on average discharge and average water level can be a reasonable predictor of annual sediment transport response. Mixed states at the annual scale can also occur, but the low–low and high–high states show the most consistent alignment with depositional and erosional outcomes, respectively. Comparatively, the correlation disappears over multi-year windows. Aggregating years with different states blends competing tendencies, so the cumulative balance reflects the sequence and proportion of states rather than any single response. Intervals that mix high–low and low–high years do not show a relationship between the classified state and the net volume or mean elevation change. The median-based threshold therefore has diagnostic value for interpreting single-year responses, but it does not, on its own, predict multi-year outcomes with alternating conditions and competing sediment transport processes.

3.4.3 Netley Delta

Netley Delta has progressed over time into several channels that flow into Netley Lake. The delta is defined by two islands that bound three primary channels: the west (main) channel, the north channel, and the south channel. The islands function as stable cores around which sediment is reworked, guiding flow into multiple outlets and promoting a deltaic lobe that projects lakeward as shown in Figure 3-18. The resulting morphology is a broad, shallow bedform with incised flow paths that convey discharge from the Red River toward Netley Lake.

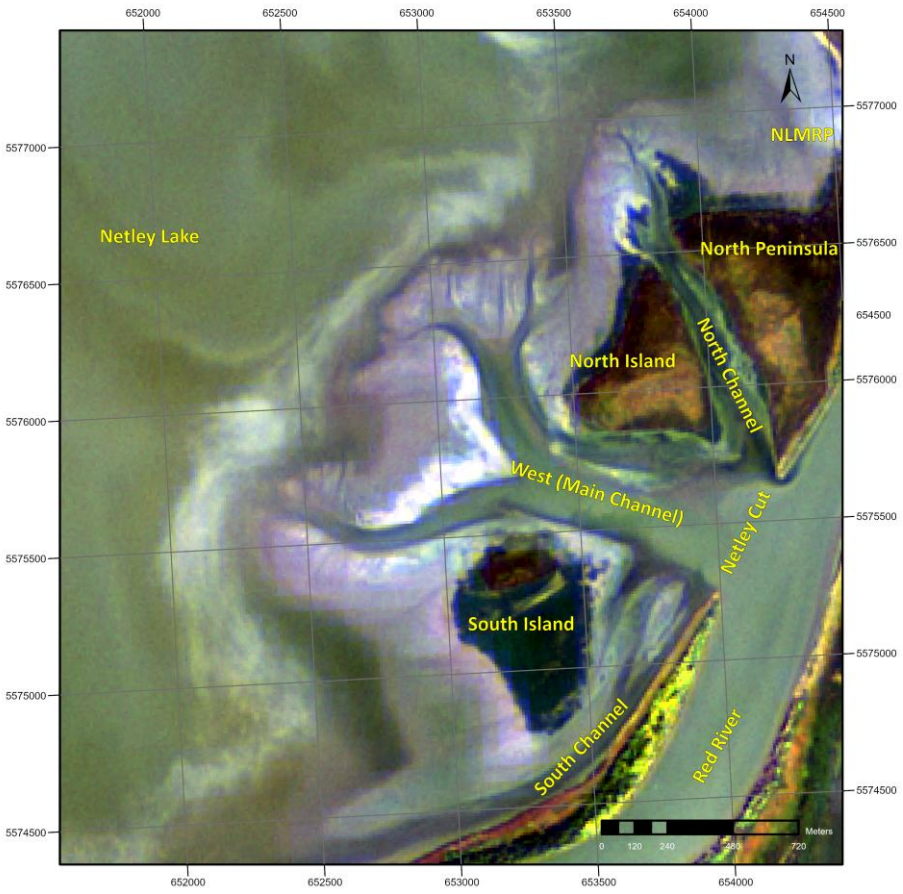

Figure 3-18 Primary channels and water features within Netley Delta

The bathymetric DEMs for the Netley Delta using the overlapping extent of the AES 2010 and HRTF 2022 surveys are shown in Figure 3-19. Two streamwise profiles are delineated on both panels for later comparison, with the west channel profile extending from Netley Lake upstream to approximately 900 m, and the north channel profile extending to approximately 1,100 m. Stationing is shown at 100 m intervals, and elevations are referenced to CGVD13. In the 2010 panel, a tightly confined west channel leads from the Netley Cut toward Netley Lake, with a minor presence of the narrow north channel bordered by the north island and peninsula. The 2022 panel covers a smaller area but displays significant deltaic growth where surveyed.

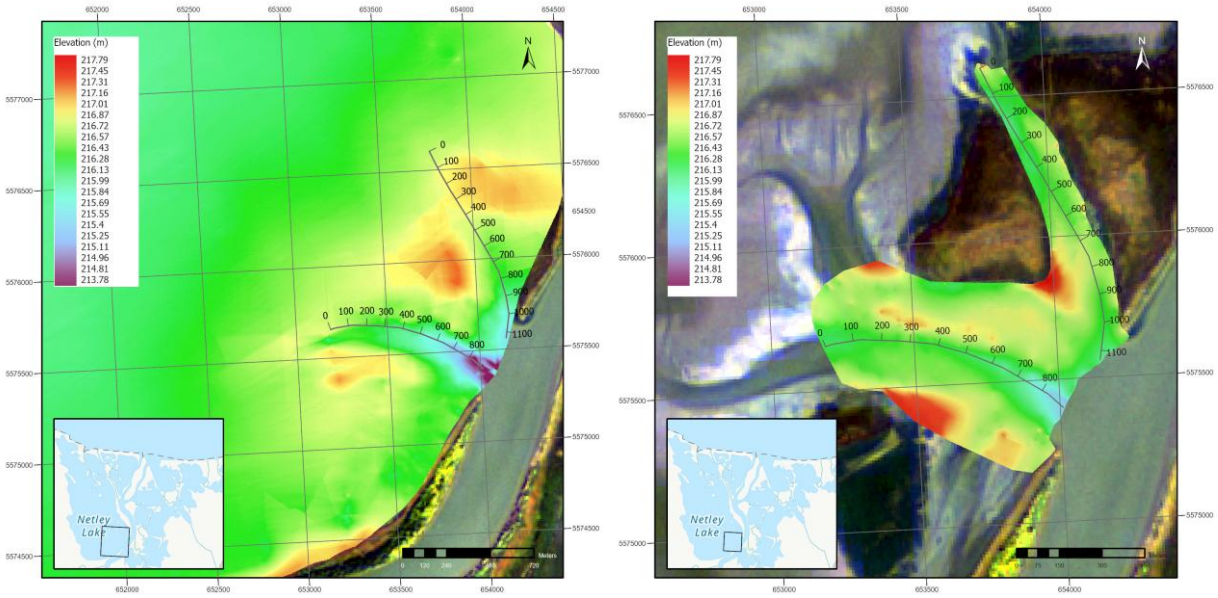

(a) AES 2010 (b) HRTF

Figure 3-19 Bathymetric DEMs at Netley Delta

The west channel remains the dominant and deepest pathway into Netley Lake. At the lake entrance it is separated by a shoal into two flow paths. The full west-channel entrance is approximately 530 m wide, with a dominant flow path of about 185 m width and a secondary, shallower path of about 70 m width. The intervening shoal ranges from 85 to 150 m in width and is approximately 700 m long. The north channel is only weakly expressed in 2010 and does not form a continuous, well-defined route toward Netley Lake, appearing instead as a shallow feature trending north from the Netley Cut. By 2022 it has developed into a clearer and hydraulically connected flow path to Netley Lake. The north channel is approximately 190 m wide at the upstream opening. An intermittent high between stations 650 m and 850 m interrupts the general deepening of this channel between 2010 and 2022.

The main similarity is the persistence of the north and south islands that bound the entrance to Netley Lake between the two panels. Within the limited near-shore coverage obtained in 2022,

sparse soundings along the island margins indicate aggraded sediment and higher elevations relative to 2010. Beyond these island extents, few features are common to both years: the 2010 surface shows only the nascent trace of a westward entrance toward Netley Lake, whereas by 2022 a distinctly organized west channel is present at the lake boundary, partitioned by a shoal, and the north-channel alignment that was incomplete in 2010 becomes established. To examine the changes described above, Figure 3-20 maps bed elevation differences between 2010 and 2022 over the same overlapping footprint and along the two streamwise profiles.

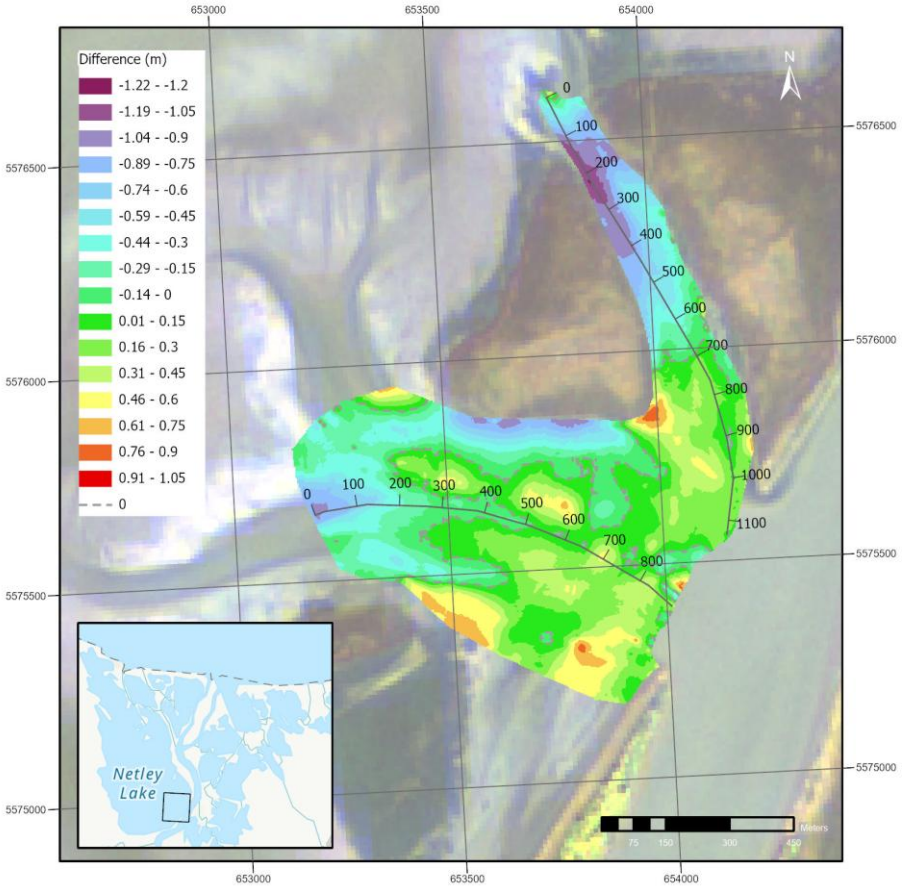

Figure 3-20 Surface differences between 2010 and 2022 at the Netley Delta

Deposition is concentrated at the entrance to mid-reach within both channels, spanning about 900–500 m along the west channel and about 1,100–700 m along the north channel. This is

followed by progressive deepening toward the lake, with erosion from 0–500 m on the west channel and from 0–700 m on the north channel. The pattern indicates a broader tendency for aggradation immediately at the entrance to the Netley Delta and within and around the Netley Cut, transitioning to bed lowering as the channels extend lakeward into Netley Lake. First, the mid-profile aggradation mapped in the delta is consistent with the analysis-frame results for the Netley Cut reported in Tables 3-3 and 3-4 for 2010–2022. Second, the spatial pattern suggests a sequence where the west and north channels widened and became better defined, depositing sediment near the entrance to the Netley Cut, while sustained flow into Netley Lake deepened the lakeward parts of both channels and carried sediment farther into the lake. To quantify the patterns mapped in Figure 3-20, Figure 3-21 and Figure 3-22 show streamwise profile elevations and elevation-difference plots sampled along the 2022 thalweg alignments for the north and west channels.

Figure 3-21 presents the north channel profile and elevation difference along the 2022 thalweg from 0 to 1,100 m. The window from 0 to 700 m has an average change of −0.727 m, indicating deepening relative to 2010, while the upstream window from 700 to 1,100 m averages +0.140 m, indicating net deposition. These values quantify the pattern noted previously: lowering of the channel closer towards Netley Lake and aggradation nearer to the Netley Cut. Both the 2010 and 2022 profiles terminate at approximately the same end elevation, ~216.67 m at 0 m, marking a consistent bed elevation that indicates the position where the north channel begins depositing material into Netley Lake.

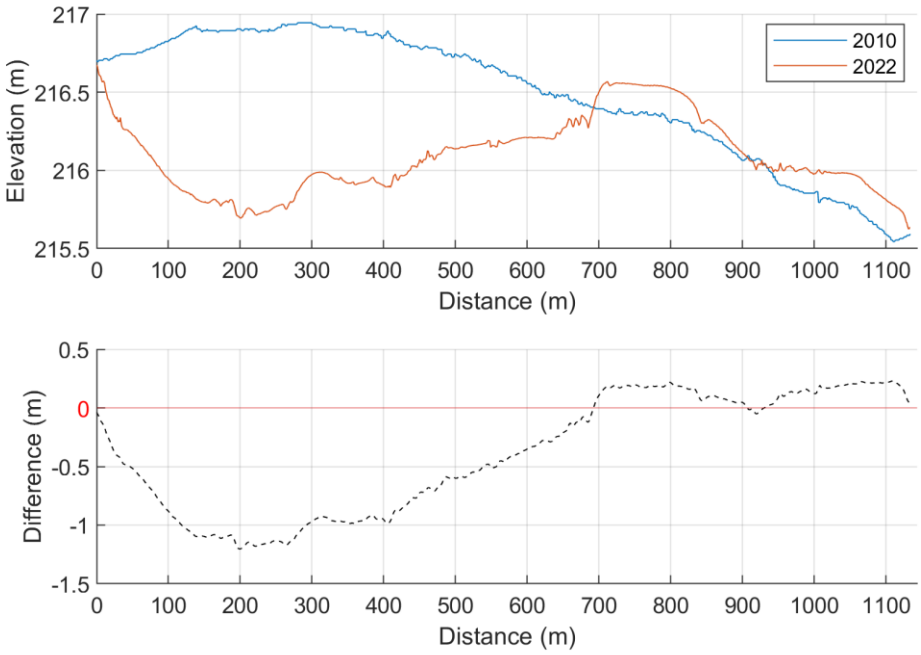

Figure 3-21 North channel profile plot and elevation difference at Netley Delta between 2010 and 2022

For the west channel (Figure 3-22), two station windows were evaluated along the 0–900 m profile. The 0–500 m window, nearest the lake, has an average elevation change of −0.354 m relative to 2010, indicating bed lowering. The 500–900 m window has an average change of +0.180 m, indicating net deposition. An oscillatory pattern is visible in the profile plot for 2022 between 200 m and 800 m. This undulation is consistent with interpolation properties from the TTR method when input soundings are unevenly distributed or locally clustered, combined with the algorithm's modified spline behavior that can misrepresent nearly flat surfaces. Better dispersion of input points generally improves results. Despite the localized interpolation oscillations, the magnitude of elevation differences between the 2010 and 2022 DEMs is sufficiently large that the profiles remain reliable for general comparison to identify zones of erosion and deposition at the reach scale. It is also noted that this issue only persisted in the west channel, despite applying the same interpolation method across the entire delta.

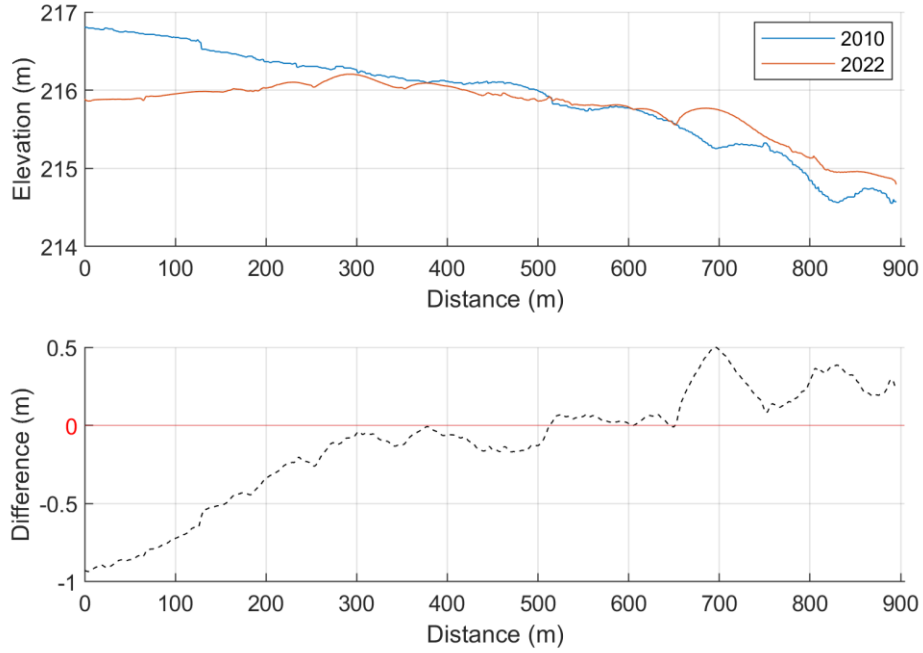

Figure 3-22 East channel profile plot and elevation difference at Netley Delta between 2010 and 2022

3.4.4 Netley Lake

The bathymetric survey in Netley Lake was conducted to support estimation of the yearly sedimentation rate from 2010 to 2022 by tracking the bed elevation along representative transects adjacent to and extending from the delta. Figure 3-23 shows Netley Lake within the southeastern portion of the Netley Delta over Sentinel-2 bathymetric imagery from September 22, 2021. Three transects are plotted with stationing in metres. Transect 1 (magenta) follows the shoreline along the emergent island complex from south to north to ~3,500 m. Transect 2 (blue) traverses just outside the delta from south to north to ~4,500 m and includes a short gap at ~2,500 m where acquisition was interrupted before resuming at a position slightly southward. Transect 3 (green) begins within Netley Lake, includes a circular segment in the central basin, and continues toward the Netley Cut to ~5,000 m, providing a lake-to-cut section across the bed.

These data were collected using the vertical beam transducer and had no post-processing interpolation applied. The three lines provide targeted sections to evaluate lakeward bed conditions across the delta front and along the approach to the Netley Cut.

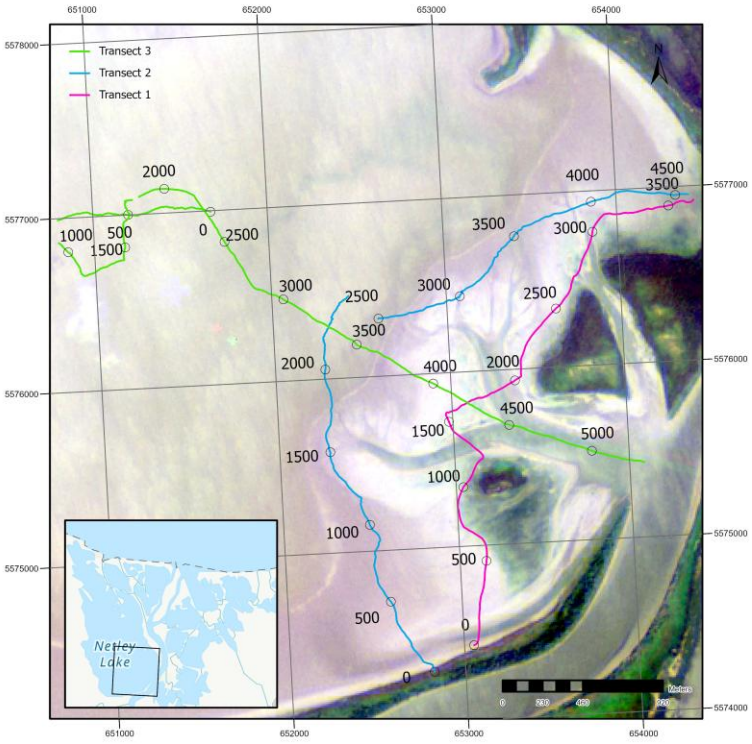

Figure 3-23 Bathymetric satellite imagery showing three main transects along the edge of Netley Delta and into Netley Lake

Along the magenta transect, six discrete channel outlets are evident, separated by two islands with relatively uniform crest elevations. These elevation differences are presented in Figure 3-24 and Table 3-6. Mean elevation change on the south island from 280–1,250 m is +0.417 m, with positive values indicating deposition from 2010 to 2022. On the north island from 2,250–2,600 m the mean change is +0.248 m. East of the north island, along the right peninsula from 3,250–3,656 m, the mean change is +0.247 m. These mean differences indicate greater deposition on the south island, roughly 1.7× the north island and the adjacent north peninsula (about 40%

lower than the south island rate). They also show the same mean change in elevation for both the north peninsula and the north island.

Table 3-6 Mean and standard deviation of surface differences between 2010 and 2022 over distance-windows within Netley Lake

Transect	Start	End	Mean	Std Dev.
Magenta	280	1250	0.417	0.083
	2250	2600	0.248	0.047
	3250	3656	0.250	0.057
Blue	280	1105	0.332	0.085
	1300	2000	0.484	0.074
Green	0	3500	0.247	0.041

Local minima along the magenta transect mark the active outlets to Netley Lake: the south channel at 216.49 m; the trifurcation within the west channel at 215.88 m, 216.24 m, and 216.28 m; and three minima within the north channel at 216.09 m, 216.73 m, and 216.69 m. Consistent with these depths, the main channel is both the widest and lowest, followed by the north channel and then the south channel. Approximate downstream widths inferred from the magenta line and taken before any trifurcations are 520 m for the west channel, 200 m for the north channel, and 150 m for the south channel.

Along the blue transect, two windows were evaluated. From 280–1,105 m the mean elevation change is +0.332 m with a standard deviation of 0.085 m. From 1,300–2,000 m the mean change is +0.484 m with a standard deviation of 0.074 m. The magnitude in the second window exceeds the deposition measured along the north island on the magenta transect (+0.248 m) and is more representative of the volume of sediment conveyed by the west channel. This window exhibits the largest net deposition among all sedimentation rates analyzed across the three transects. In terms of channel elevations, one local minimum is observed in the south channel at 216.747 m,

one in the center channel at 216.591 m, and two in the north channel at 216.846 m and 216.851 m. Relative to the magenta transect, these minima are uniformly higher: the south channel minimum is higher by 0.257 m compared with 216.49 m on the magenta line; the center channel minimum is higher by 0.351 m compared with the 216.24 m trifurcation minimum; and the north channel minima are higher by ~0.12–0.16 m compared with the 216.73–216.69 m pair, and by ~0.76 m relative to the 216.09 m low. The blue line also captured fewer local lows in the west channel, which is consistent with its alignment skirting the delta front and missing some trifurcations sampled by the shoreline-parallel magenta line. Along the blue transect, the lowest elevation occurs near the 3,000 m station, coincident with the west channel at the small deltaic outflow visible in Figure 3-23.

Along the green transect, the objective was to approximate the net deposition rate on a relatively uniform bed surface in Netley Lake. Therefore, a measurement window from 0–3,500 m was selected, which had an associated average bed elevation change of +0.247 m. Interpreted over a 12-year interval, this corresponds to an average deposition rate of approximately 2.1 cm per year. The transect also captures the emergence and lakeward advance of the central island: the global maximum along the profile shifted from station 4,321 m in 2010 to 3,968 m in 2022, a lakeward displacement of 353 m, and the peak elevation rose from 216.765 m to 217.390 m, an increase of 0.625 m. Together, these values indicate both accretion and outward growth of the middle island toward the lake interior over the survey period.

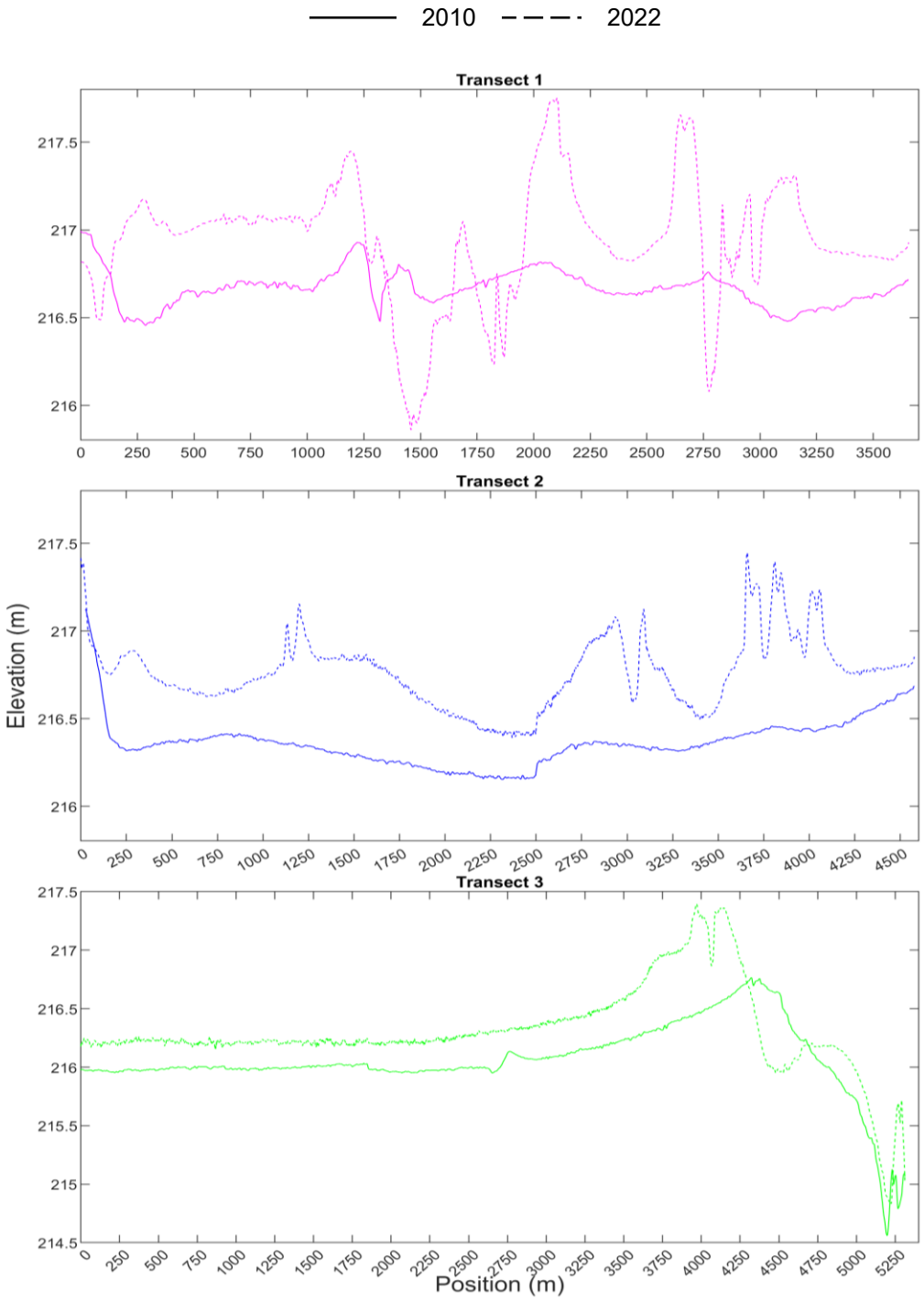

Figure 3-24 Bed elevations for three transects along the edge of Netley Delta and into Netley Lake between 2010 and 2022

3.4.5 NLMRP

The NLMRP comprised two survey areas: a dredge site on the left bank of the Red River, approximately 1,300 m downstream of the Netley Cut, and a deposition site within the interior of Netley Lake, approximately 350 m north of the north peninsula. The survey was designed to meet two objectives: (i) estimate and track the volume of material excavated from the Red River and placed within the NLMRP control extents; and (ii) quantify the retention of that placed sediment within the designated deposition area over the first year.

At the dredge site, volumes were computed from bathymetric surfaces collected before dredging, immediately after dredging, and at a one-year post-monitoring interval. At the deposition site, the sequence of methods was selected according to water levels at the time of acquisition. Prior to placement, water depths in the control area were on the order of one foot, too shallow for reliable single-beam bathymetry and sufficiently high to degrade aerial photogrammetry by surface reflectance and noise. A topographic point survey with the SP60® was therefore used for the "before" condition. The "after" condition was captured by aerial photogrammetry when complete exposure of the bed permitted delineation of the placed material. The one-year monitoring survey was completed with bathymetry when water depths were adequate, approximately 0.5–1.5 m. All datasets were referenced consistently and processed following the procedures in Section 3.3, enabling comparison of pre-, post-, and one-year states at the dredge site and analogous before-, after-, and one-year conditions at the deposition site.

3.4.5.1 Dredge Site

The interpolation extents for the three bathymetric surveys conducted at the NLMRP dredge site are shown in Figure 3-25: 2021 before dredging, 2021 after dredging, and 2022 one-year

monitoring. The before-dredging survey covers a longer reach in the streamwise direction because the exact dredging footprint was not yet fixed. In contrast, the 2021 after-dredging and 2022 monitoring surveys concentrate around the final dredge pit, producing a compact footprint centered on the active working area.

Acquisition density and track layout reflect these differing objectives. The before-dredging dataset employed wider spacing between consecutive transects, yielding more dispersed input soundings across the broader reach. The after-dredging and one-year surveys used a tighter, cross-weave pattern over the excavation area, increasing local sounding density and improving interpolation quality within the pit and immediate margins. The white light-toned linear feature extending from the left bank toward the northwest of the map marks the primary access corridor used to pipe material across the peninsula to the Netley Lake deposition site.

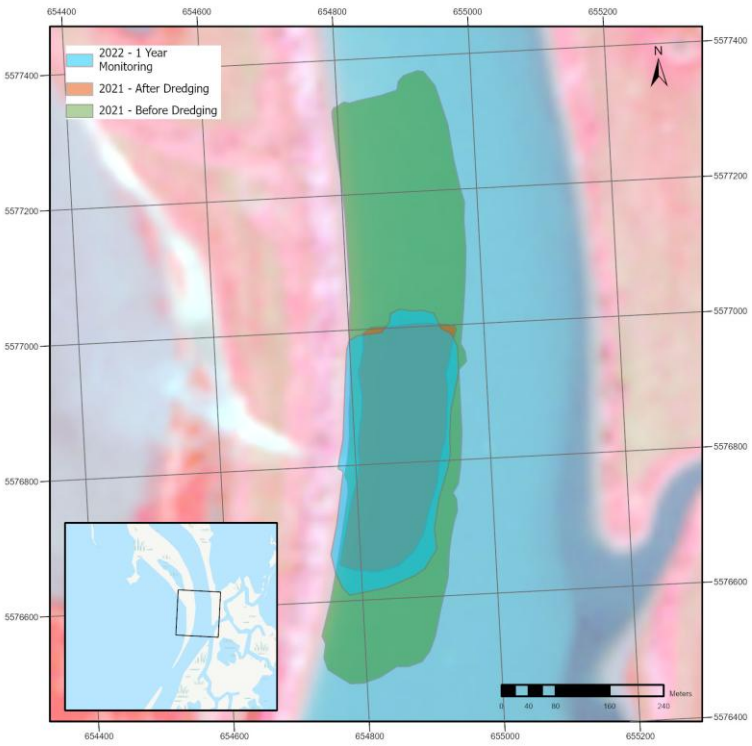

Figure 3-25 Interpolation extents for various bathymetric surveys at the NLMRP Dredge Site

Moving from survey footprints to bed conditions, Figure 3-26 presents the bathymetric DEMs for the dredge site at three stages: before dredging, immediately after dredging in 2021, and one-year monitoring in 2022. Panel (a) shows the pre-project bed with the expected main-channel form: a sloping left bank descending toward maximum depth and a relatively uniform cross-sectional cut along the bank. Four transects were established for subsequent analyses: transects 1–3 run streamwise through the survey area and transect 4 is oriented perpendicular to flow. Primary emphasis in the analysis is on transects 1 and 4.

Panel (b) delineates the excavation footprints where the dredge vessel operated. Four areas of interest are evident: a northern excavation of 3,700 m^2; a second, centrally located excavation on the southern half of the footprint of approximately 1,210 m^2; a smaller cut near the left bank on the south edge of approximately 358 m^2; and an even smaller dredged patch within the center of the survey extents of approximately 257 m^2.

Panel C (one-year monitoring, 2022) indicates substantial natural infilling of the excavated pits and a shift back toward a smoother, more uniform bed consistent with the pre-project morphology. Residual irregularities remain along the left-bank margins of the former cuts, but the interior of the footprint exhibits pronounced recovery, with bed elevations trending toward the pre-dredged surface.

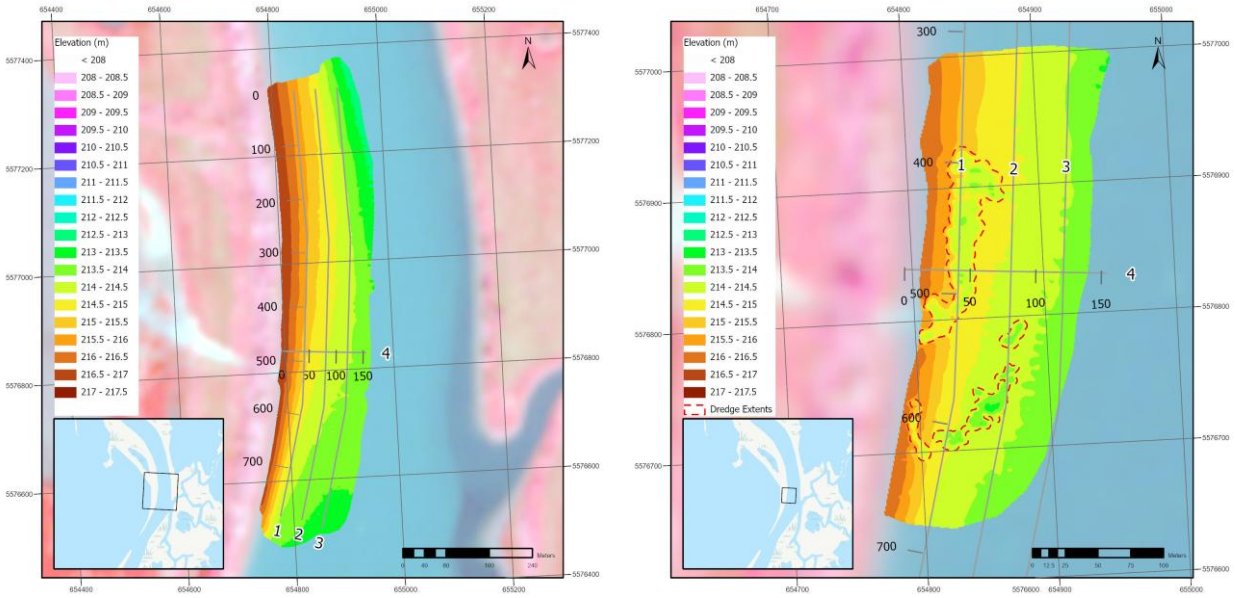

(a) Before Dredging

(b) After Dredging

(c) 1 Year Monitoring

Figure 3-26 Bathymetric DEMs and dredge extents at the NLMRP Dredge Site

Figure 3-27 illustrates surface-elevation differences between successive surveys at the NLMRP dredge site over the same analysis footprint. Panel A compares the pre-project bed to the 2021 post-dredging surface, and panel B compares the 2021 post-dredging surface to the 2022 one-year monitoring surface. Dashed outlines mark the dredge extents. From before

dredging to after dredging (panel A), large negative differences are concentrated within the four excavation areas, confirming substantial bed lowering where the vessel operated. The deepest dredge pit created during the NLMRP was estimated at 1.87 m and is shown in the south corner of the northern dredge area. Outside these pits, most of the reach exhibits small negative change on the order of 0.00–0.15 m, with isolated pockets of slight positive change. This indicates that, in addition to targeted excavation, the bed experienced minor river-wide erosion during the project period.

From after dredging to one-year monitoring (panel B), positive differences dominate within the former pits, demonstrating infilling and partial recovery toward pre-project elevations. A belt of modest erosion occurs immediately around the pit margins, while farther riverward the central channel includes additional zones of positive change. The pattern is consistent with local reworking and redistribution of nearby material into the dredged depressions, coupled with continued sediment deposition from the Red River, and indicates a tendency for the bed to return toward a smoother pre-dredge condition within one year.

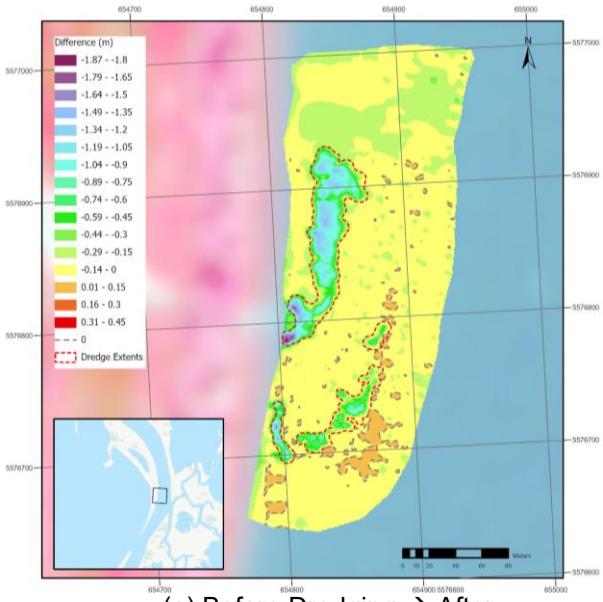

(a) Before Dredging → After

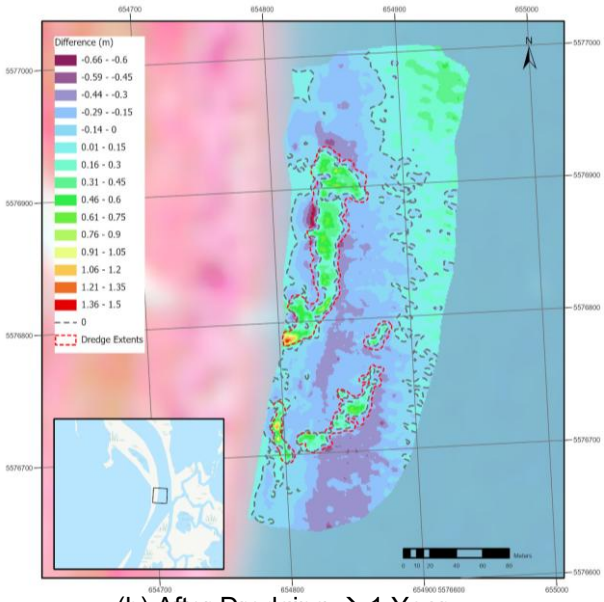

(b) After Dredging → 1 Year

Figure 3-27 Surface differences between chronological acquisition dates at the NLMRP Dredge Site

Table 3-6 and Figure 3-28 summarize these changes quantitatively. For the entire raster, net lowering was 7,740 m³ from pre- to post-dredging and 2,835 m³ from post-dredging to one-year monitoring. Within the dredge extents, the pre- to post-dredging window accounts for 3,588 m³ of the entire raster change, with an average bed lowering of 0.679 m. Over the one-year monitoring interval, the dredge extents gained about 940 m³, corresponding to an average rise of approximately 0.175 m. The reach therefore experienced net erosion across both periods, while the dredge footprints recovered part of the excavated volume during the first year. The discrepancy in the total overlapping area of the dredge extents is due to interpolation applied near the edge of the analysis frame.

Table 3-7 Volume estimate for the amount of material dredged as part of the NLMRP

Spatial scope	**Comparison window**	**Area (m^2)**	**Net volume change (m^3)**	**Average bed elevation change (m)**
Entire raster	Before to After Dredging	43631	-7,740	-0.177
Entire raster	After Dredging to 1 Year Monitoring	40673	-2,835	-0.070
Dredge extents	Before to After Dredging	5286	-3,588	-0.679
Dredge extents	After Dredging to 1 Year Monitoring	5381	+940	+0.175

Figure 3-28 plots a streamwise transect through the largest dredging zone. The post-dredging profile is the deepest. One year after dredging the bed infilled toward pre-dredging levels but remained below the previous elevation. The 2010 and 2018 profiles in this figure provide some context to the available historical datasets. However, both data exhibit discrepancies outside the narrower comparison window between 370 and 520 m. Namely, a sharp drop of about 1.0 m near

290 m in 2010, and depressions in 2018 between 100–400 m and from ~520 m to the transect end.

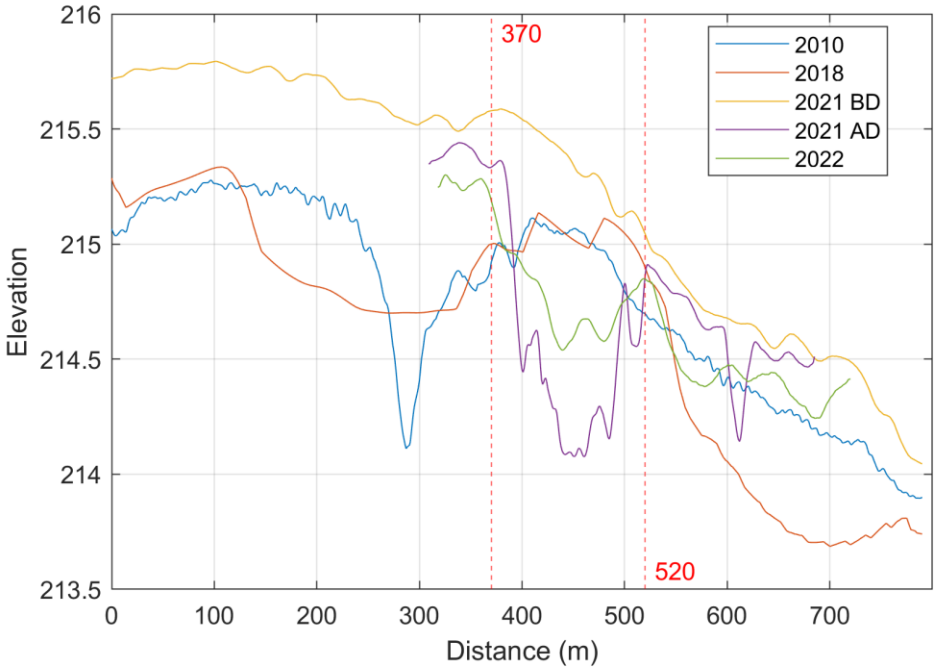

Figure 3-28 Elevation differences across distance-windows for Line ID 1 using a streamwise transect at the NLMRP Dredge Site

Inspection of 2018 survey lines indicate sparse and uneven sounding distribution on the banks of the Red River, including the absence of a continuous left-bank edge line and reliance on a single weave without a cross-edge tie, producing interpolation drawdowns where data were missing (see Figure 3-29). Over the 370–520 m window, where coverage is robust, the multi-year profiles agree and the 2022 recovery relative to 2021 post-dredging is evident.

Figure 3-29 Sounding path of the bathymetric survey conducted by Manitoba Hydro in 2018

Figure 3-30 introduces a bank-to-channel cross section across the dredge footprint to complement the streamwise results in Figure 3-28. The transect (Line ID 4) is oriented perpendicular to flow, extending from the left bank at 0 m to mid-channel at 150 m. Profiles are shown for 2010, 2018, 2021 pre-dredging, 2021 post-dredging, and one-year monitoring in 2022. Line ID 4 intersects the northern excavation and the zone of largest post-dredging change, providing a direct view of pit geometry, bank response, and the degree of recovery after one year. The pre-dredging profile in 2021 shows a smooth, parabolic slope from the left bank toward mid-channel, consistent with an undisturbed bank-to-thalweg cross section. The post-dredging profile in 2021 introduces a distinct depression within the dredge footprint and a modest overall reduction in bed elevation across the section. The depression has been largely infilled and the cross section has flattened to match adjacent bed levels by the one-year

monitoring survey in 2022. Despite this recovery, the near left-bank zone remains lower than the pre-dredging line, indicating bank-side erosion, while elevations toward mid-channel approach the pre-dredging condition. This cross-sectional behavior is consistent with the volume results, where approximately 940 m^3 of material accumulated within the dredge extents during the first year, 26% of the 3,588 m^3 excavated during the pre- to post-dredging interval.

Data quality along this transect supports interpretation across the full section. The 2018 Manitoba Hydro profile is smooth and consistent because Line ID 4 intersected a reach with a complete left-bank edge line and continuous coverage across the interpolation extent. In contrast, the 2010 profile contains localized drops that cannot be verified against survey lines, which were unavailable for review, and are therefore reported as unexplained features.

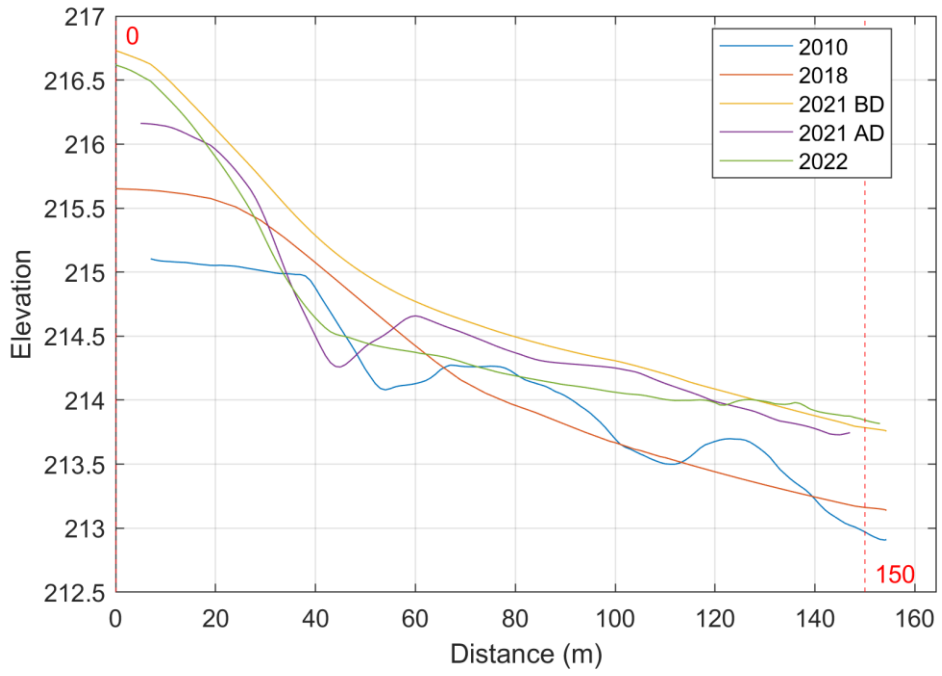

Figure 3-30 Elevation differences across distance-windows for Line ID 4 using a cross-sectional transect at the NLMRP Dredge Site

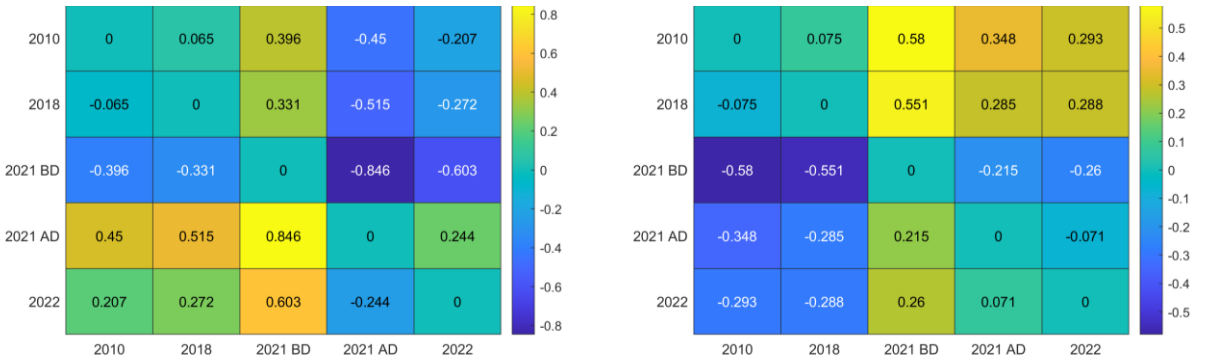

(a) Line ID 1: 370 – 520 m

(b) Line ID 4: 0 – 150 m

Figure 3-31Figure 3-31 summarizes the pairwise average elevation differences for two analysis windows: the northern dredge pit along Line ID 1 (370–520 m) and the left-bank cross section along Line ID 4 (0–150 m). In the Line ID 1 window, the largest contrast occurs between the pre- and post-dredging states, with a mean difference of about 0.85 m across the window, consistent with active excavation. The post-dredging to one-year monitoring pair shows a smaller, opposite-sign mean change of about 0.24 m, indicating partial infilling. Differences between the two pre-project datasets are small (≈0.07 m), which provides a stable baseline for interpreting project effects.

In the Line ID 4 window, which spans the left bank, the matrix indicates persistent lowering across the sequence from pre-dredging to post-dredging and into one-year monitoring. Relative to pre-dredging, the one-year profile remains lower on average by about 0.26 m, showing that bank-side erosion continued while the pit infilled. Magnitudes in Line ID 4 are smaller than those in Line ID 1, consistent with excavation and subsequent recovery being focused near mid-channel while bank adjustments recovered more gradually.

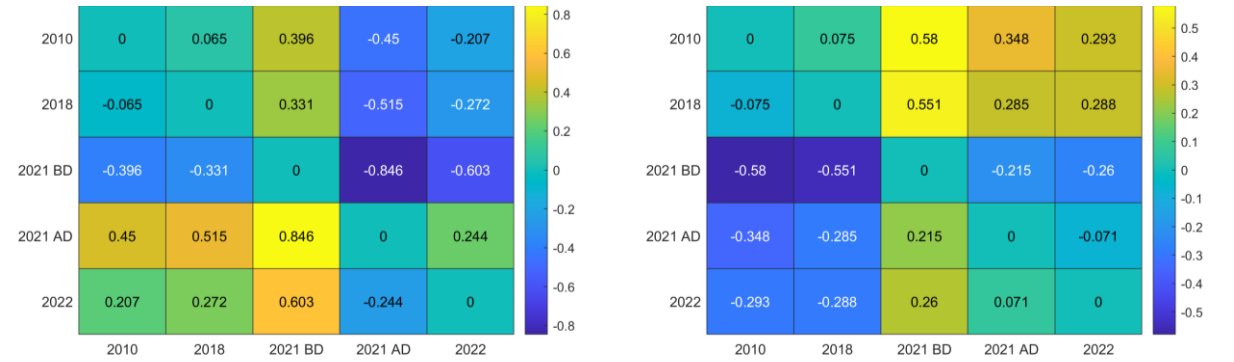

(a) Line ID 1: 370 – 520 m (b) Line ID 4: 0 – 150 m

Figure 3-31 Average elevation differences across distance-windows using a streamwise (a) and cross-sectional (b) transect at the NLMRP Dredge Site

3.4.5.2 Deposition Site

The deposition area consisted of a contained cell within Netley Lake that received dredged material pumped across the north peninsula from the Red River. Temporary containment was established with aquadams and geotubes to limit lateral spreading and to promote settling within the control boundary. Two additional, standalone geotube alignments were installed adjacent to the cell to evaluate whether wave action and local currents would trap lake-borne sediment behind or around isolated barriers. Elevation data for this site were acquired with methods tailored to lake levels at each phase: pre-placement topographic points using the SP60® when water was shallow, post-placement aerial photogrammetry when emergent surfaces were exposed, and one-year monitoring by bathymetry when water depths were deep. Because these methods differ in spatial reach, direct comparisons are restricted to the mutual overlaps, with particular caution for the post-versus-one-year pair where the intersection is smallest. Figure 3-32 delineates the deposition cell, the two standalone geotube locations, and the three survey footprints.

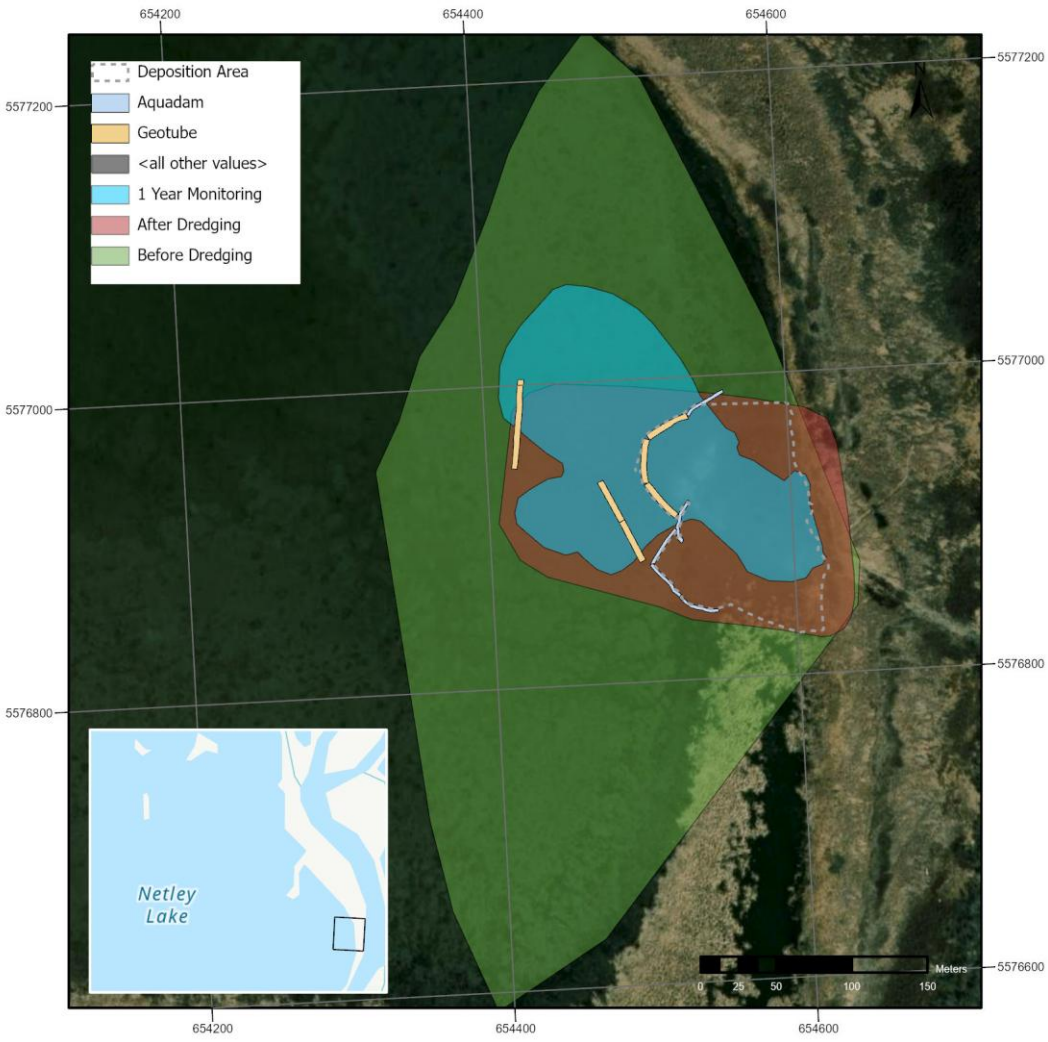

Figure 3-32 Interpolation extents for various surveys at the NLMRP Deposition Site

Figure 3-33 presents the deposition-site elevation surfaces for the three acquisition phases. Panel A shows the 2021 pre-dredging surface from sparse topographic points. Given the wide spacing and uneven distribution of points, IDW was selected instead of TTR. IDW preserves measured values and estimates intervening cells without imposing hydrologic structure, which is appropriate when points are widely spaced and breaklines are unavailable. The trade off is the familiar bull's-eye pattern seen across the interpolated surface.

Panel B shows the 2021 post-dredging terrain derived from SfM photogrammetry. This surface is the highest-resolution model in the set. Post-processing used 337 images and nine ground control points (seven inside the deposition cell and two outside) to georeference the reconstruction, yielding an average vertical error of 0.029 m. The imagery achieved a ground sampling distance of 8 mm per pixel. By contrast, the DEM used for cross-dataset comparisons is gridded at a 1 m cell size. The 8 mm value describes the native image resolution that constrains how finely the surface can be resolved during reconstruction, whereas the 1 m raster cell is the analysis grid to which the dense surface is aggregated for consistency with the bathymetric rasters. The final DEM was produced by removing vegetation using the Pixel Editor in ArcGIS Pro® and constraining the result to the defined deposition cell. Linear interpolation was applied across small, masked vegetation patches using surrounding bare-earth elevations. Residual streaking visible in the DEM reflects the geometry and extent of vegetated areas, which were clipped out or infilled where nearby elevation values supporting a simple surface. Similarly, owing to the very high image resolution, discrete elevated mounds are identifiable where the dredge head discharged material, appearing as small, bright patches with elevations higher than adjacent cells. Elevated zones also occur along segments of the geotubes, consistent with partial filling of those containment structures.

Panel C displays the 2022 one-year monitoring surface from bathymetric soundings. The surface indicates retention of material within the deposition area. A smooth and cohesive discharge mound with reduced peak elevations and a gentler transition to the ambient lake bed suggests redistribution and settling of the deposited material. Data acquisition was limited by water depths of roughly 0.5–1.5 m and by re-vegetation along the margins, so the overlap between the post-dredging and one-year footprints is smaller than the overlap between pre- and

post-dredging. Volume estimates and any direct differencing are therefore restricted to the mutual overlap of the post-dredging and one-year monitoring extents.

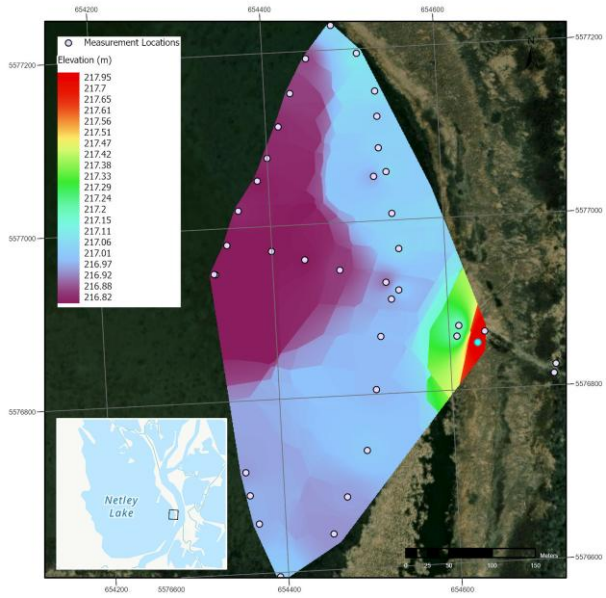

(a) Before Dredging

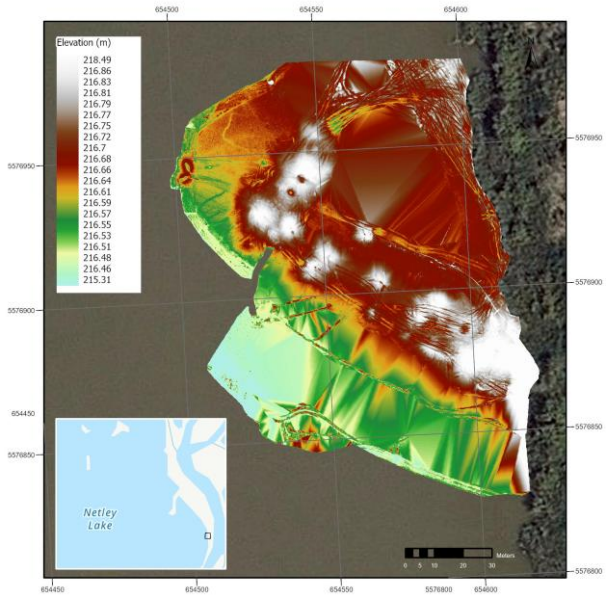

(b) After Dredging (2021)

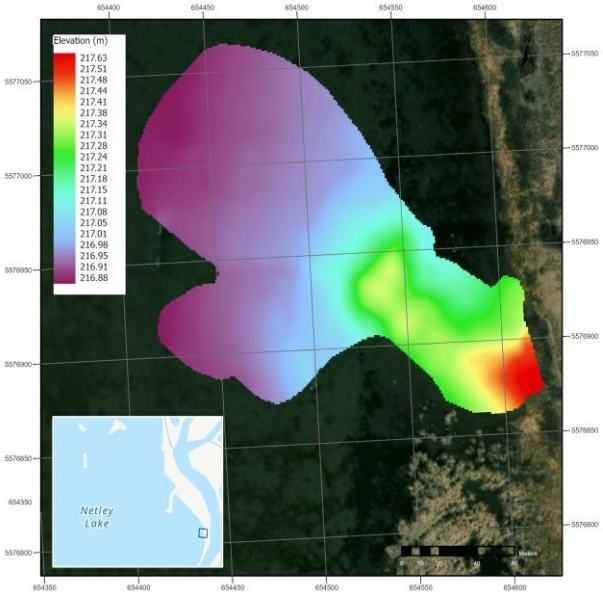

(c) 1 Year Monitoring

Figure 3-33 DEMs and dredge extents at the NLMRP Dredge Site

Surface differences at the deposition site are summarized in Table 3-8 and Figure 3-34 for three acquisition pairs. For the multi-year comparison from 2010 to the 2021 pre-dredging survey, the net change is a deposition of 25,484 m^3 over 114,030 m^2, yielding an average rise of 0.223 m. Interpreted over the interval, this corresponds to a mean accumulation rate of about 2.2 cm per year. This rate is consistent with the transect-based estimate from Figure 3-22, which indicated approximately 2.1 cm per year, indicating that the central-lake accumulation rate toward the Netley Cut is similar to the rate measured on the east side of Netley Lake near the north peninsula.

Table 3-8 Volume estimates for material deposited within the NLMRP extents

Spatial scope	**Comparison window**	**Area (m^2)**	**Net volume change (m^3)**	**Average bed elevation change (m)**
Entire raster	2010 to Before Dredging	114030	25484	0.223
Deposition Area	Before Dredging to After Dredging	13718	2416	0.176
Deposition Area	After Dredging to 1 Year Monitoring	40673	-2835	-0.070

From pre- to post-dredging (Panel b), deposition is concentrated at the discharge locations of the dredge head, forming discrete mounds within the containment cell and down-gradient toward the interior. One large erosion patch appears in the southeast corner of the footprint but was excluded from the volume calculation. That patch reflects linear interpolation across a vegetated zone that linked higher elevations near the discharge area to lower elevations along a vehicle track at the edge of the footprint. With that artifact removed, the deposited volume for this period is 2,416 m^3 over 13,718 m^2, for an average rise of 0.176 m.

From post-dredging to one-year monitoring (Panel c), the surface shows a mix of deposition and erosion consistent with natural redistribution. The strongest erosion occurs on the mounded deposits with redistribution most prominent along the east and south parts of the footprint, consistent with the largest fetch from northwest and west winds. The net change over the mapped overlap is a loss of 2,835 m^3 across 40,673 m^2, for an average loss of 0.070 m. Comparison of mean bed levels indicates that approximately 60% of the average elevation gained during the post-dredging phase was retained after one year of monitoring. This pattern suggests that a portion of the placed sediment was transported beyond the one-year survey extent and that reworking by waves and currents redistributed material within and around the deposition area. However, part of the observed decrease in bed elevation may also reflect consolidation of the dredge-deposited material and underlying sediments, which cannot be separated from erosional loss with the available dataset.

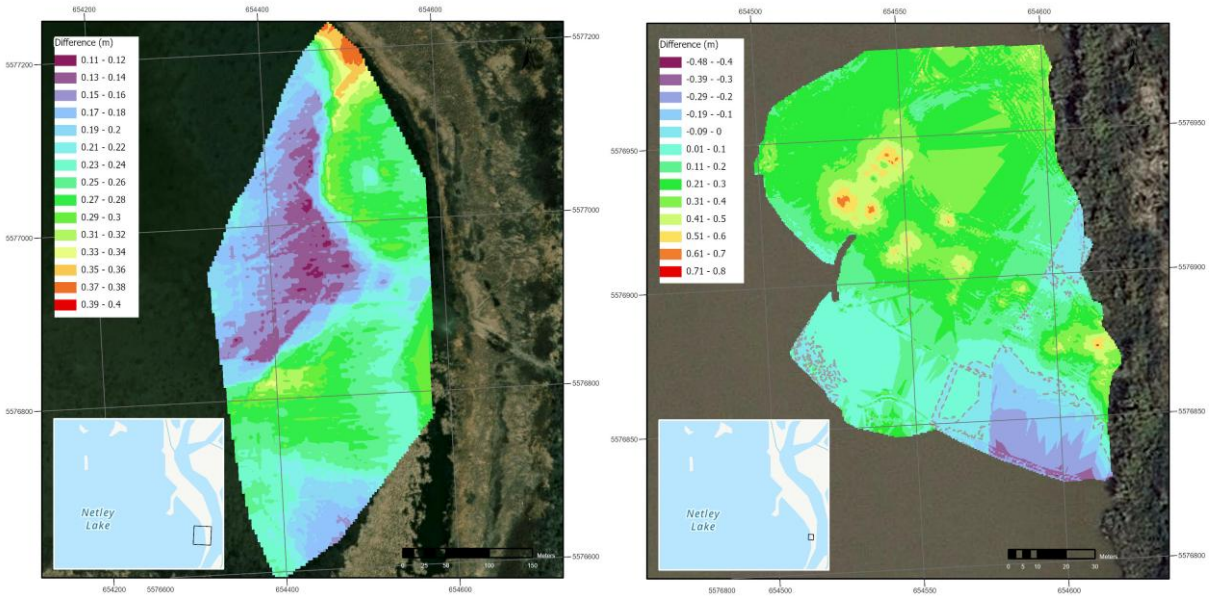

(a) 2010 → Before (b) Before Dredging → After

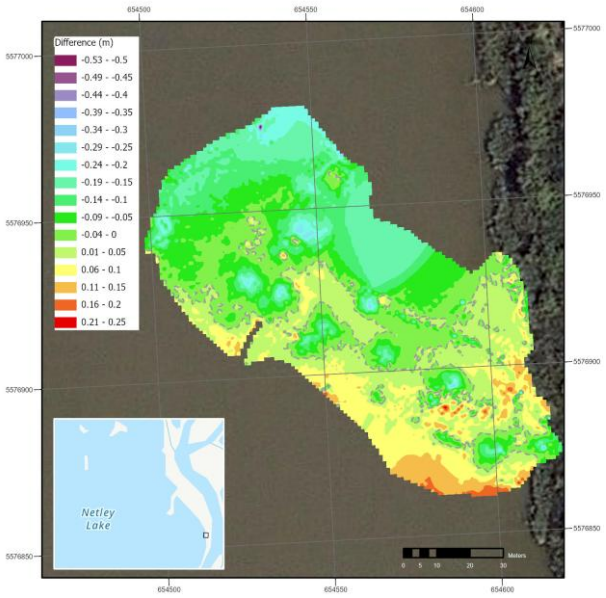

(c) After Dredging → 1 Year

Figure 3-34 Surface differences between chronological acquisition dates at the NLMRP Deposition Site

The differences between pre- and post-dredging surveys presented in Table 3-7 and Table 3-8 (respectively) indicate that approximately 3,588 m³ of material were extracted from the dredge area, while an estimated 2,416 m³ were deposited within the designated deposition area. On this basis, the retention rate of the deposition cell is approximately 67%, suggesting that about one

third of the dredged material was not contained within the cell. These volumetric estimates implicitly attribute all elevation change to erosion and deposition; however, part of the apparent loss may also reflect consolidation of the newly placed sediment and underlying layers, which cannot be distinguished from a true erosion of material with the available survey data.

The performance of the geotubes and aquadams as containment structures appears to have been partially effective in retaining sediment. The open configuration of the deposition cell, with unconfined northern and southern boundaries, likely contributed to the reduced retention rate by permitting both suspended and bedload material to migrate out of the deposition zone. While the structures were effective at limiting lateral dispersion and provided some capacity for sediment storage, the incomplete enclosure restricted their overall ability to function as a fully contained cell.

3.4.6 Red River

The lower Red River reach considered here extends from the lake outlet upstream to below Netley Creek and includes the main and east channels that deliver flow toward Lake Winnipeg. Bathymetry is examined to quantify changes in elevation along each channels' centerline and to provide context for conveyance into the Netley Cut. Available datasets consist of two historical surveys, completed by AES in 2010 and by Manitoba Hydro in 2018. No additional river bathymetry was collected for this thesis. Comparisons therefore rely on these two years, interpreted with regard to the interpolation procedures used to build each surface and the density and geometry of the underlying vessel track lines described in Section 3.3.

Figure 3-35, shows the 2018 Manitoba Hydro DEM with stationing at 1,000 m intervals from downstream at Lake Winnipeg toward Breezy Point. The main channel is stationed from 0 m, and the east channel is stationed from 1,097 m so both alignments intersect at the trifurcation at

6,300 m. The river is widest and deepest in the upstream portion of the reach (11,000 to 13,200 m) immediately adjacent to the Netley Cut and narrows downstream of the trifurcation along both the main and east channels. The main channel outlet passes through the previous navigation through the former breakwater and wharf along the west side of the outlet. The west channel is not discussed because it has historically not been surveyed; bed elevations are very shallow and unsuitable for traditional vessel-based bathymetry.

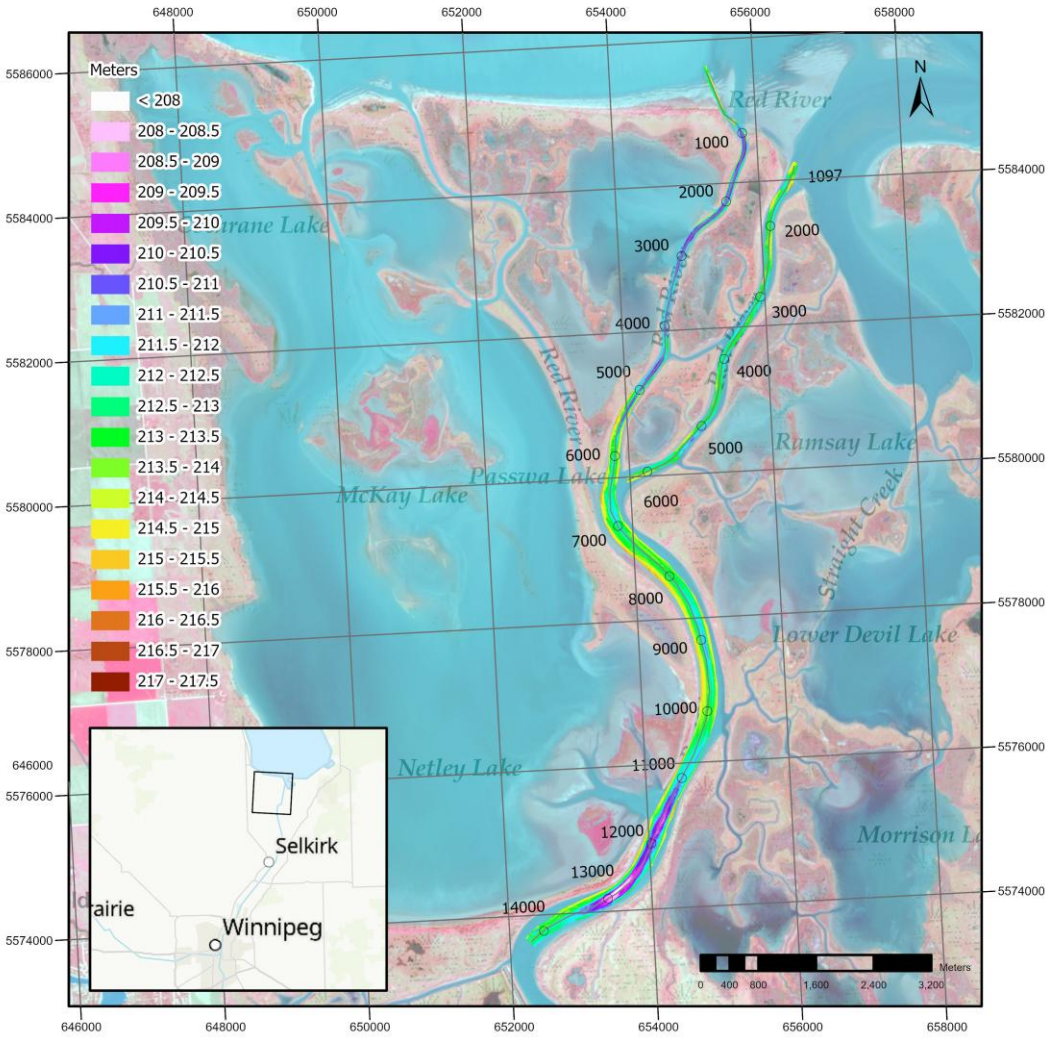

Figure 3-35 Bathymetric DEM of the Lower Red River from downstream of Breezy Point to the Red River Outlet – MH 2018

Figure 3-36 plots streamwise bed elevations for the Red River main and east channels from the AES 2010 and Manitoba Hydro 2018 datasets. The two profiles are broadly consistent in profile form, with repeated pools and intervening bars at similar stationing. Between 2010 and 2018 the main channel generally shows bed aggradation, while the east channel shows signs of scour. This pattern suggests some degree of redistribution of flow between the two routes.

Local minima delineate the deepest parts of the reach downstream of the bifurcation, while intervening high points act as hydraulic controls under subcritical conditions. The main channel from 0 to 6,300 m exhibits minima of 211.900 m, 210.921 m, 209.926 m, 210.057 m, and 209.581 m before rising toward the lake, whereas the east channel shows corresponding minima of 212.256 m, 211.802 m, 211.599 m, and 211.576 m, followed by an increase in elevation near the outlet. These values indicate that, in terms of local depth, the main channel generally remains the deeper pathway and the predominant flow path, with the east channel comparatively higher but exhibiting increased scour from 1,530 to 3,100 m. However, the pronounced deposition near the main channel outlet (0–990 m) raises the bed and creates an effective control that can limit conveyance in this reach, encouraging a greater proportion of flow to be routed into the east channel and thereby enhancing erosion there. An alternative interpretation is that increased scour and conveyance in the east channel reduce discharge and velocities in the main channel, promoting deposition at its outlet. Given the available data, the direction of causality cannot be conclusively resolved, although the outlet deposition acting as a primary control on flow redistribution is considered the more plausible mechanism.

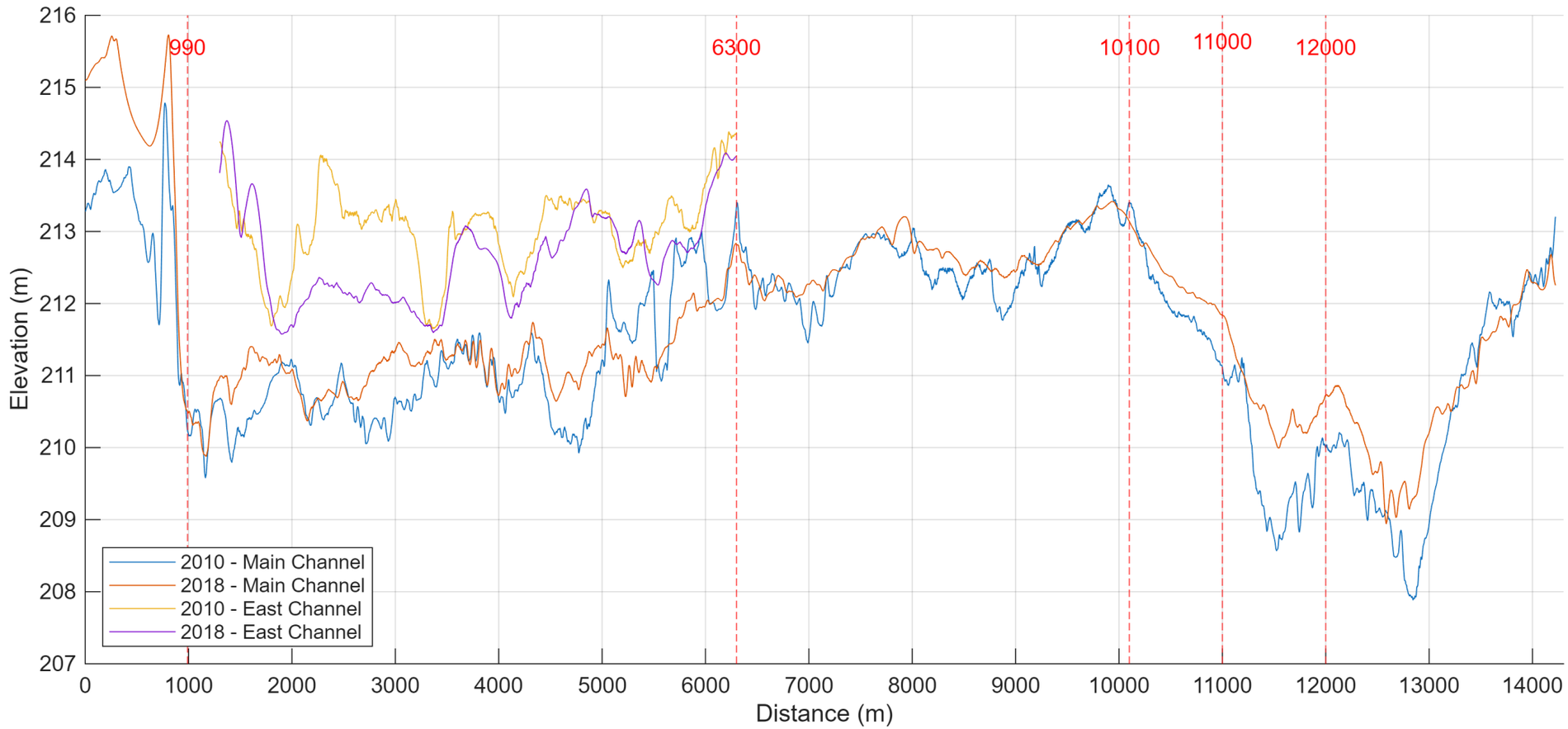

Figure 3-36 Streamwise profile plot of the Red River Main and East channels from AES 2010 and MH 2018

Figure 3-37 corresponds to the averaging windows identified in Figure 3-36 and isolates the east channel. The profile indicates predominant scour from 1,530 to 6,300 m, with the difference curve strongly negative over this reach. Short oscillations near the channel mouth in the 2018 profile, centred around 1,000–1,500 m, are consistent with gaps and geometry of the 2018 vessel track lines and should be interpreted cautiously. Despite these artefacts, both years show a comparable local minimum near 1,500 m with elevations of 211.584 m (2018) and 211.698 m (2010). At approximately 1,200 m the trough in the 2018 oscillation is near the 2010 bed level, after which both profiles rise and follow a similar trend of depositing sediment at the mouth of the east channel. Of specific interest are two averaging windows: 1,530–3,100 m and the full reach, excluding the short oscillatory section near the mouth, 1,530–6,300 m. Both indicate sustained scour, with the 1,530–3,100 m window showing the largest mean lowering of −0.744 m, compared with −0.440 m over 1,530–6,300 m. The greater scour in the 1,530–3,100 m reach is consistent with a tributary connection at Cross River between the main and east channels near 4,000 m. If Cross River captured more flow and incised during 2010–2018, the junction would have delivered increased discharge into the east channel. The added conveyance would concentrate flow through the downstream segment of the east channel toward Lake Winnipeg.

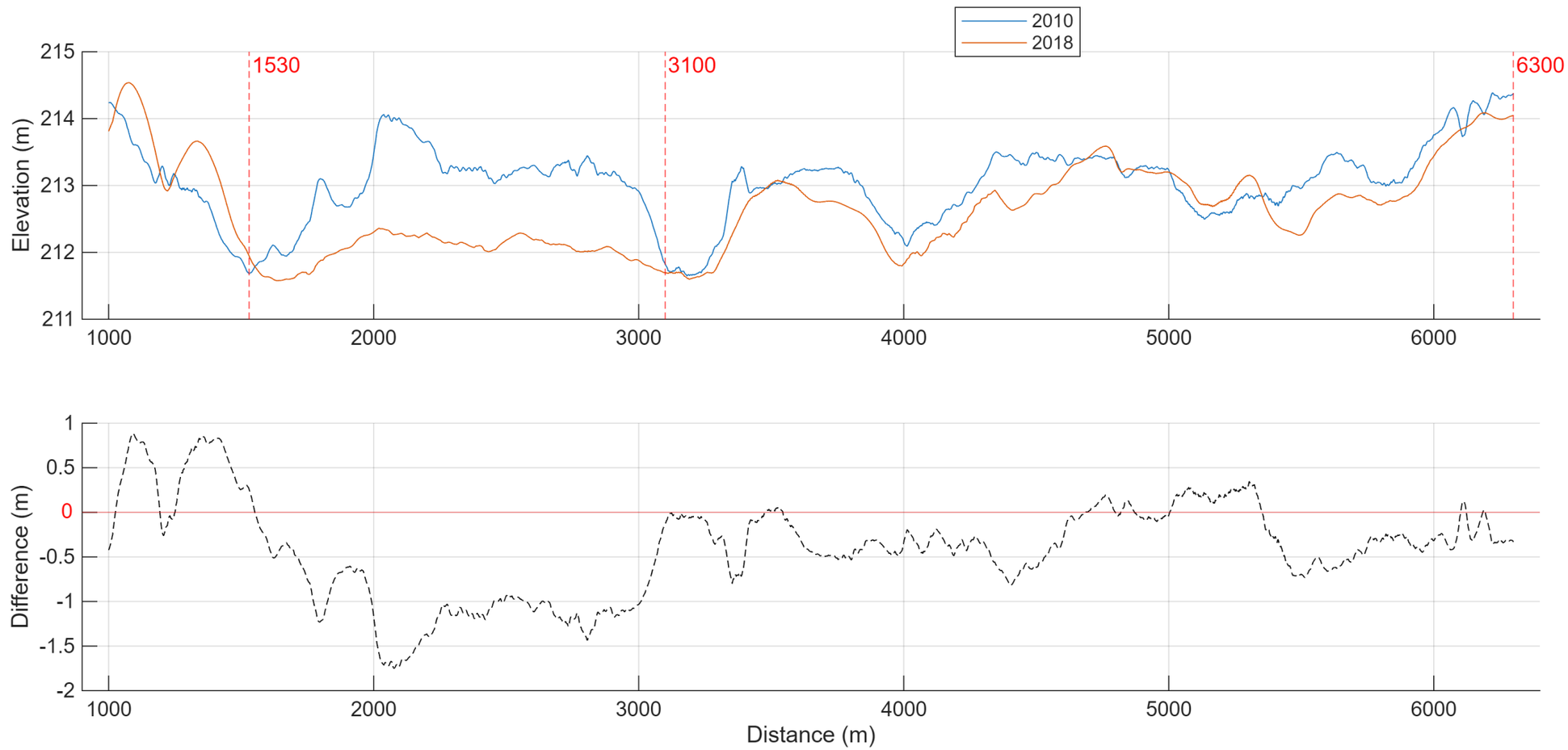

Figure 3-37 Streamwise profile plot of the Red River East channel from AES 2010 and MH 2018

Figure 3-38 partitions the main channel into five distance windows that track change along the centerline profile. The downstream reach from 990 to 6,300 m represents the segment between Lake Winnipeg and the trifurcation. The next window from 6,300 to 10,100 m spans the trifurcation to the NLMRP dredge site. Three additional windows bracket the Netley Cut: 10,100–11,000 m immediately downstream of the Cut, 11,000–12,000 m adjacent to the Cut at the outlet, and 12,000–14,200 m upstream toward Breezy Point.

The 990–6,300 m reach shows a net rise in average bed level of 0.144 m between 2010 and 2018, but the profile is not uniform. From 990 to 5,000 m deposition dominates, while 5,000–6,300 m exhibits pronounced erosion. This pattern indicates local reworking near the trifurcation where the two channels separate. From 6,300 to 10,100 m there is strong agreement between the 2010 and 2018 profiles with a smaller average rise of 0.133 m, implying comparatively stable bed conditions along this mid-reach relative to the other windows.

Change intensifies in the three windows surrounding the Netley Cut. The immediate downstream segment from 10,100 to 11,000 m shows an average increase of 0.484 m. The outlet reach adjacent to the cut from 11,000 to 12,000 m has the largest increase at 0.884 m, and the upstream segment toward Breezy Point from 12,000 to 14,200 m rises by 0.367 m. Together these values indicate substantial thickening of the bed adjacent to and flanking the cut over 2010–2018. The concentration of deposition near the outlet aligns with the delta and Cut responses described earlier, where aggradation within Netley Cut was documented in 3.4.2.

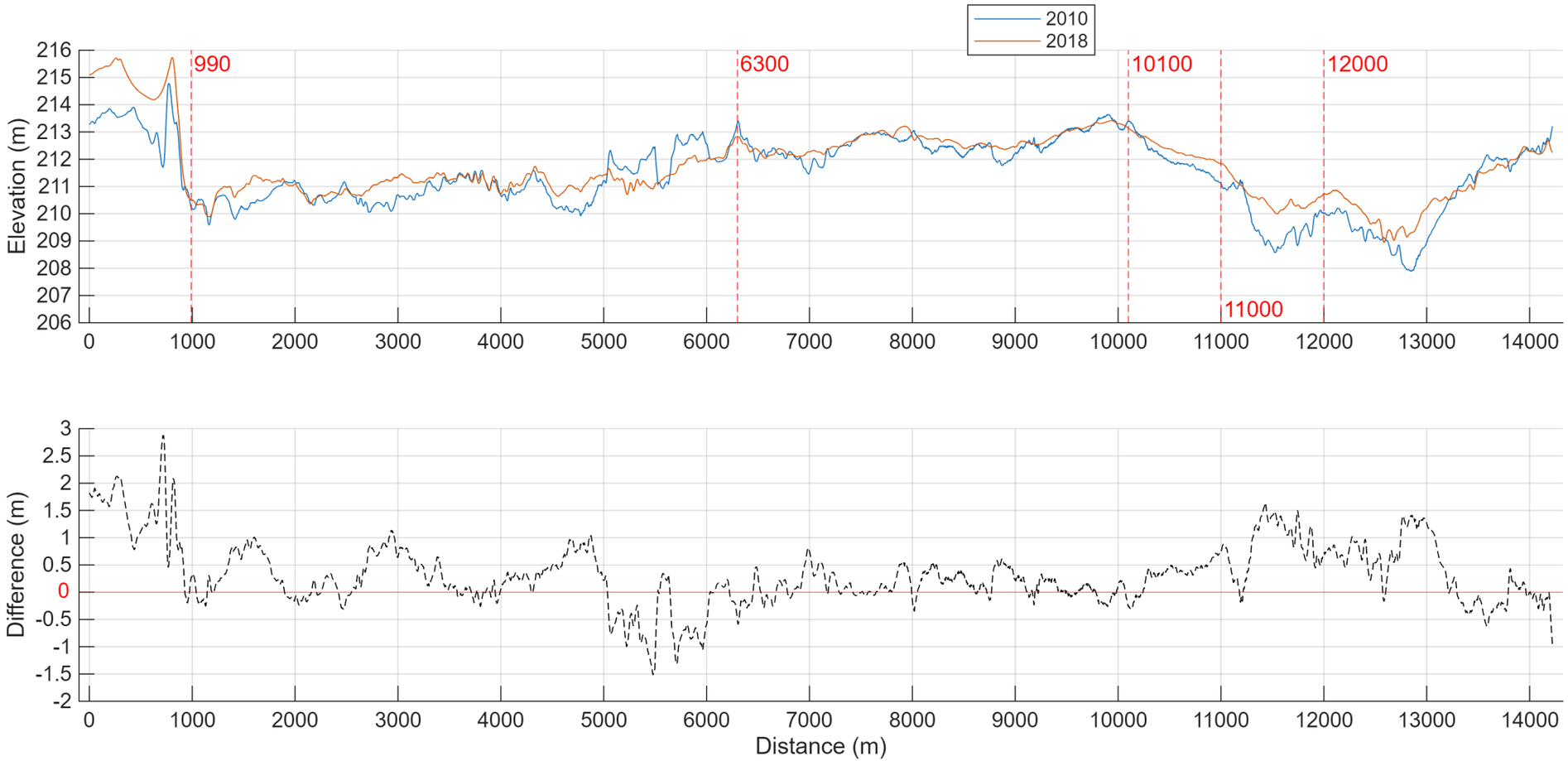

Figure 3-38 Streamwise profile plot of the Red River Main channel from AES 2010 and MH 2018

3.4.7 Red River Outlet

Figure 3-39 summarizes the spatial coverage of six bathymetric DEMs at the Red River outlet along the main channel. The 2010 and 2014 surveys concentrate on the former navigation corridor between the paired breakwaters, capturing the approach channel and the interior of the breakwater corridor. The 2018 Manitoba Hydro survey shifts coverage lakeward and east into the present navigation corridor that exits to Lake Winnipeg; only sparse soundings were collected within the corridor between the breakwaters, and there is no continuous data between the breakwaters and the river mouth. The 2020 survey provides the most expansive footprint, encompassing the mouth, the main navigation corridor, and adjacent shallow shoals. The July and October 2021 surveys focus on the active navigation corridor and immediate approach, offering dense coverage along that path with limited lateral reach.

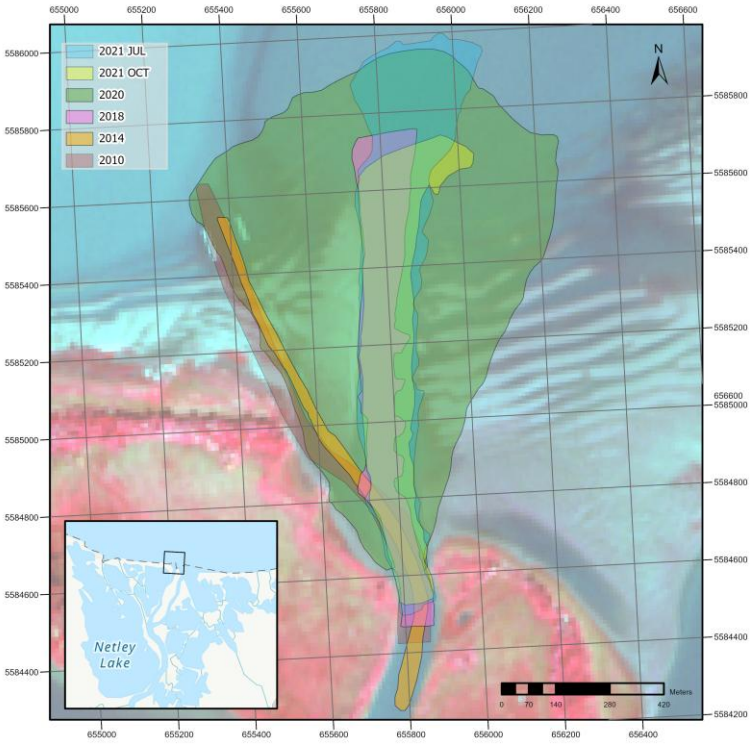

Figure 3-39 Interpolation extents for various bathymetric surveys at the Red River Outlet

Figure 3-40 compiles six bathymetric DEMs at the Red River outlet. The 2010 and 2014 panels, focused on the corridor between the breakwaters, show progressive narrowing and nearly full shoaling within the former navigation path. The 2018, 2020, 2021, and 2022 DEMs concentrate on the central outlet corridor and indicate that the breakwater corridor is now substantially infilled. Across these later surveys, discharge follows the main corridor, depths are greatest at the outlet near the shoreline, and bed levels increase lakeward where river-borne sediment is deposited. The six cross-section lines shown here correspond to Canadian Coast Guard transects, compiled in the La Salle Engineering Report and acquired by Public Works Canada and the Canadian Hydrographic Service (KGS, 2002).

KGS analyzed depths relative to the normal summer water level on Lake Winnipeg at 217.63 m for these six transects. The underlying vertical datum for that level is not documented, so absolute comparisons to the CGVD13 referenced DEMs in this thesis are not made. Assuming this datum was tied into the Geodetic Survey of Canada Datum (Local 1968 Adj.), and estimating that this datum is equivalent to CGVD28, a conversion to CGVD13 would likely be -0.373 m but cannot be known for a fact.

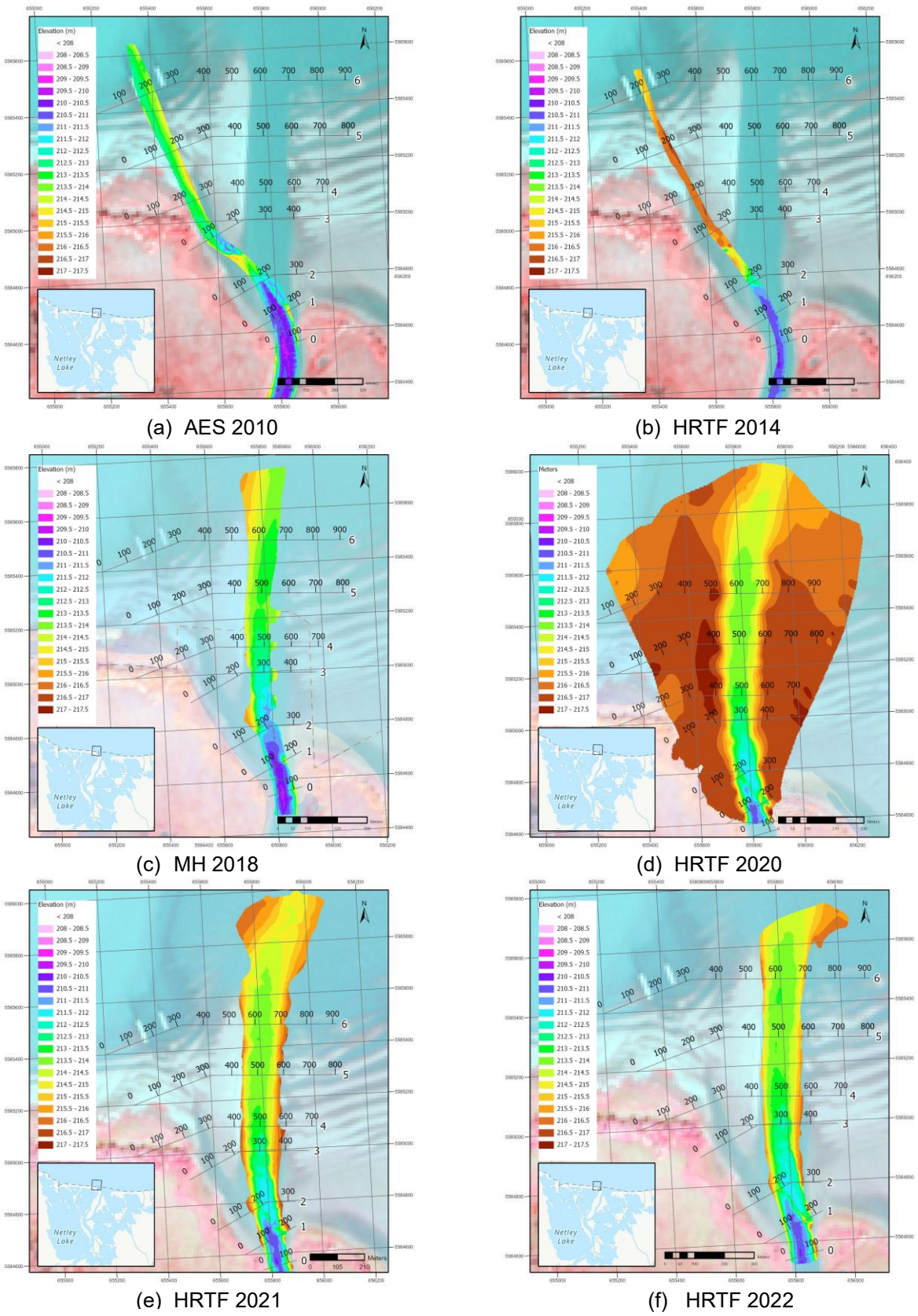

Figure 3-40 Bathymetric DEMs and dredge extents at the Red River Outlet

Figure 3-41 maps surface-elevation differences for the Red River outlet across five acquisition pairs, evaluated only over the mutual overlaps of each dataset. Panel A (2010 → 2014) shows widespread deposition within the former breakwater corridor and modest localized lowering at the mouth of the main channel, consistent with infilling of the legacy route and reworking at the lake boundary. Panel B (2014 → 2018) is constrained by limited overlap but still indicates a mixed response along the left bank of the present navigation corridor, with additional shoaling inside the breakwater corridor at the upper left. Within the active corridor, small belts of deposition alternate with erosion, reflecting channel adjustment as the deeper alignment concentrated toward the center corridor. Panel C (2018 → 2020) exhibits pockets of large positive change at the river mouth and a lakeward train of deposition along the central corridor, tapering to isolated zones of lowering near the outer footprint. Localized decreases approach about 1 m in magnitude near the distal edge. Panel D (2020 → 2021 July) is characterized by an interleaved pattern of erosion and deposition throughout the main corridor, indicating redistribution of recently placed and naturally supplied sediment across the outlet. Panel E (2021 July → 2021 October) shows a similar mixed pattern at smaller magnitudes, generally within about 0.5 m, consistent with short-interval reshaping by waves and currents during the open-water season.

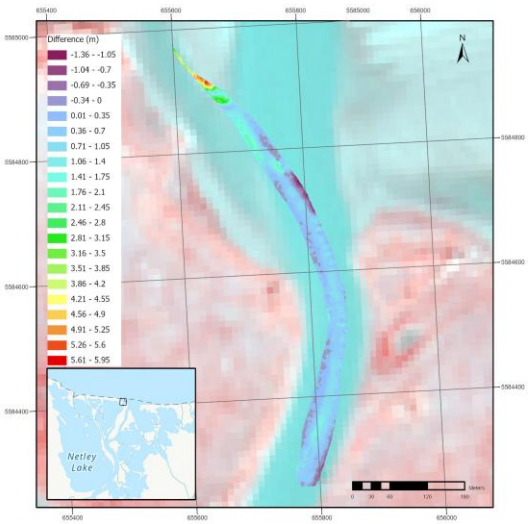

(a) AES 2010 to HRTF 2014

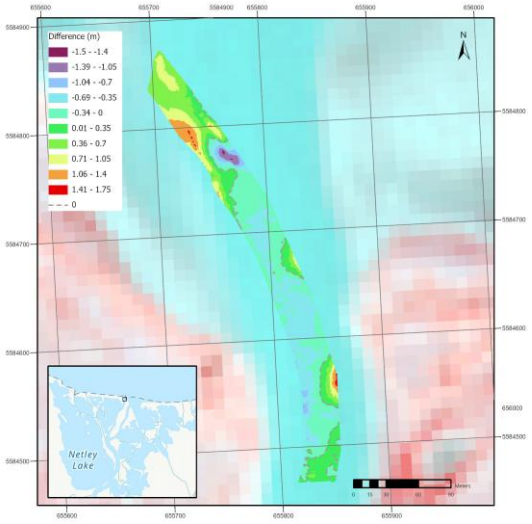

(b) HRTF 2014 to MH 2018

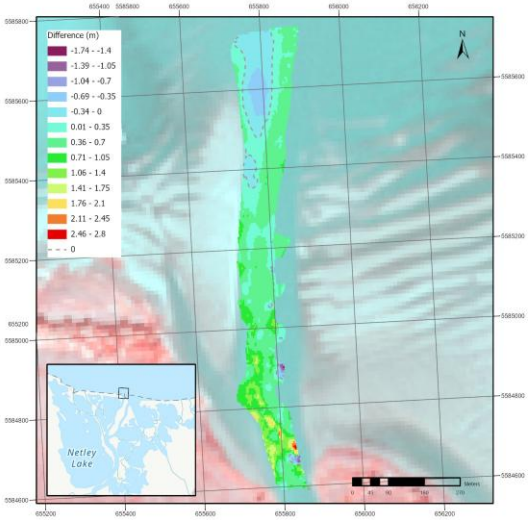

(c) MH 2018 to HRTF 2020

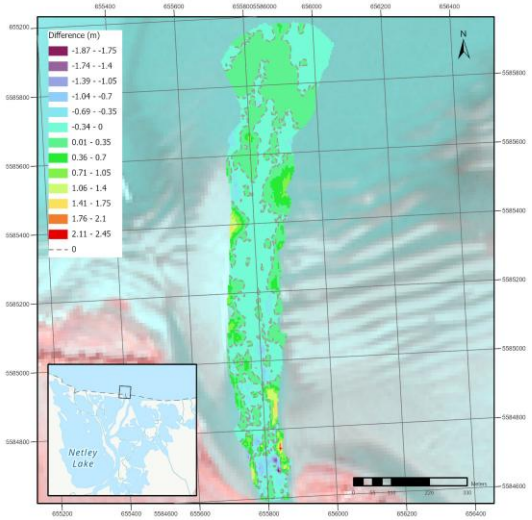

(d) HRTF 2020 to HRTF 2021 July

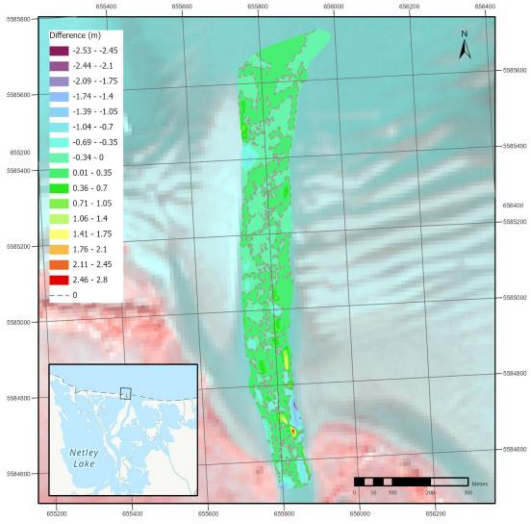

(e) HRTF 2021 July to HRTF 2021 October

Figure 3-41 Surface differences between chronological acquisition dates at the Red River Outlet

Taken together, the sequence documents continued infilling of the breakwater corridor, persistent deposition along the central navigation corridor, and short-term redistribution at the mouth between 2020 and 2021 that modulates bed levels without altering the overall outlet configuration.

Figure 3-42 presents a cross section of the outlet along Line ID 1 in Figure 3-39. Only a subset of surveys captured the full cross-sectional width; estimates from the 2020 and 2021 July datasets indicate a width of approximately 118–137 m. The section exhibits two lows separated by a narrow bar near the right bank, which diverts a portion of the flow along the right shoreline of Lake Winnipeg toward the east channel, while the primary thalweg remains toward the center-left of the outlet. Across the multi-year survey period the thalweg has risen. The minimum bed elevation increased from 210.100 m in 2010 to 210.911 m in 2022, a net rise of 0.811 m. The two 2021 surveys show near negligible differences in the minimum bed elevation.

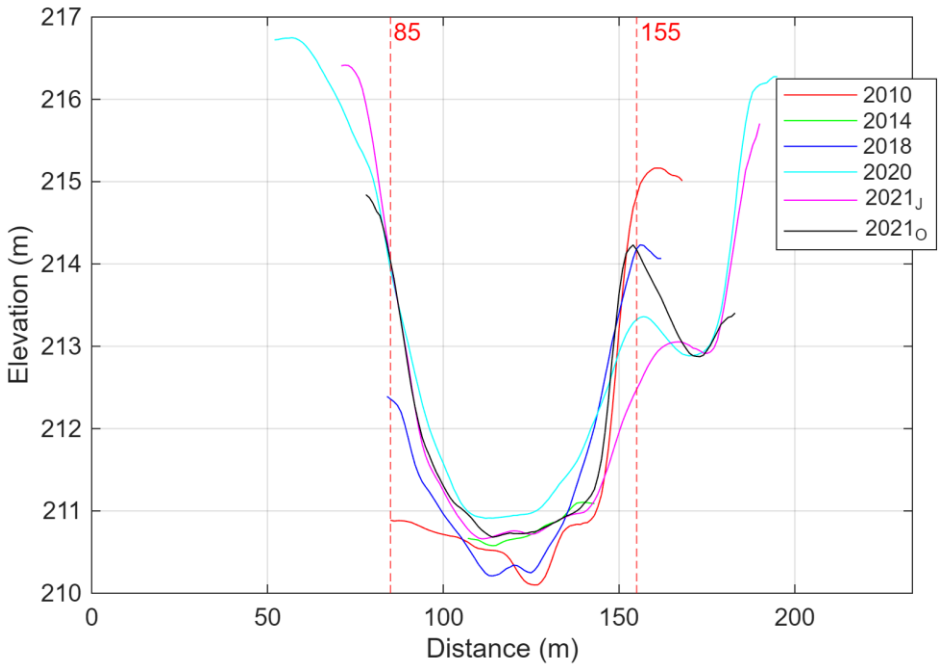

Figure 3-42 Elevation differences for Line ID 1 using a cross-sectional transect at the Red River Outlet

Figure 3-43 quantifies change within the 85–155 m window on Line ID 1. The matrix shows progressive infilling relative to 2010 with mean elevation offsets of +0.103 m (2014), +0.417 m (2018), +1.162 m (2020), +0.868 m (2021 July), and +0.947 m (2021 October). The July to October 2021 comparison indicates an additional increase of +0.077 m over roughly three months. This change is small compared with the cumulative +0.947 m increase since 2010, but if expressed as an annualised rate (0.308 m per year) it would exceed longer-term aggradation estimates for other key areas such as the Netley Delta (0.021 m per year). Given the vertical uncertainty of the differencing and the likelihood of short-term reorganisation bedforms at this site, the July to October difference is interpreted as short-term variability superimposed on the longer-term trend rather than a sustained deposition rate. The rise in the section minimum documented in Figure 3-42 from 210.100 m to 210.911 m (+0.811 m) is consistent with the window-average increase from 2010 to 2021 October of +0.947 m, confirming sustained infilling of the main navigation corridor at the outlet.

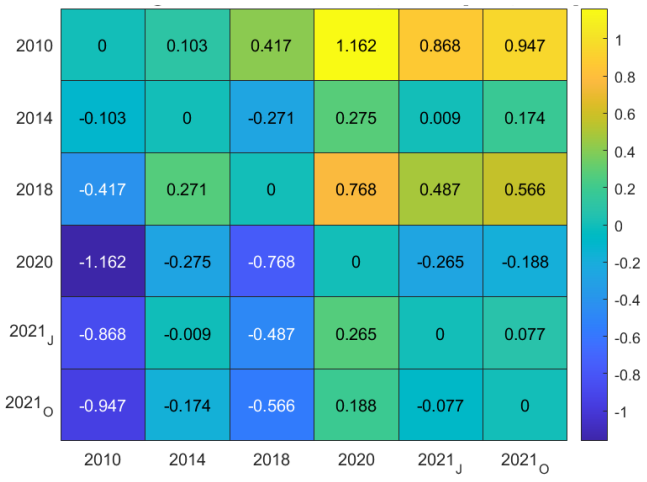

Figure 3-43 Average elevation differences across distance-windows of 85 – 155 m for Line ID 1 using a cross-sectional transect at the Red River Outlet

Line ID 3 crosses the main navigation corridor at the Red River outlet, as shown in Figure 3-40. Figure 3-43 plots bed elevation along this transect for each survey year. The short 2010 and 2014 profiles on the left side of the plot represent partial cross sections collected when surveys were focused on the previous main channel path between the breakwaters. From 2018 onward, the surveys ran the full cross section across the current navigation corridor. The cross section indicates a width of approximately 160 m within the 225–385 m window. Since 2018 the bed has risen and the thalweg has remained centered within the corridor. The minimum bed elevation increased from 211.991 m in 2018 to 212.689 m in 2020, a rise of 0.698 m, and remained elevated through 2021 with small interannual adjustments. The window-averaged differences between 225 and 385 m quantify this behavior. Relative to 2018, mean elevations are higher by 0.752 m (2020), 0.650 m (2021 July), and 0.373 m (2021 October). Relative to 2020, the section lowered slightly by 0.041 m (2021 July) and 0.233 m (2021 October), and 2021 October is 0.186 m below 2021 July. These values show sustained shoaling of the outlet corridor since 2018, coupled with short-term redistribution between 2020 and 2021.

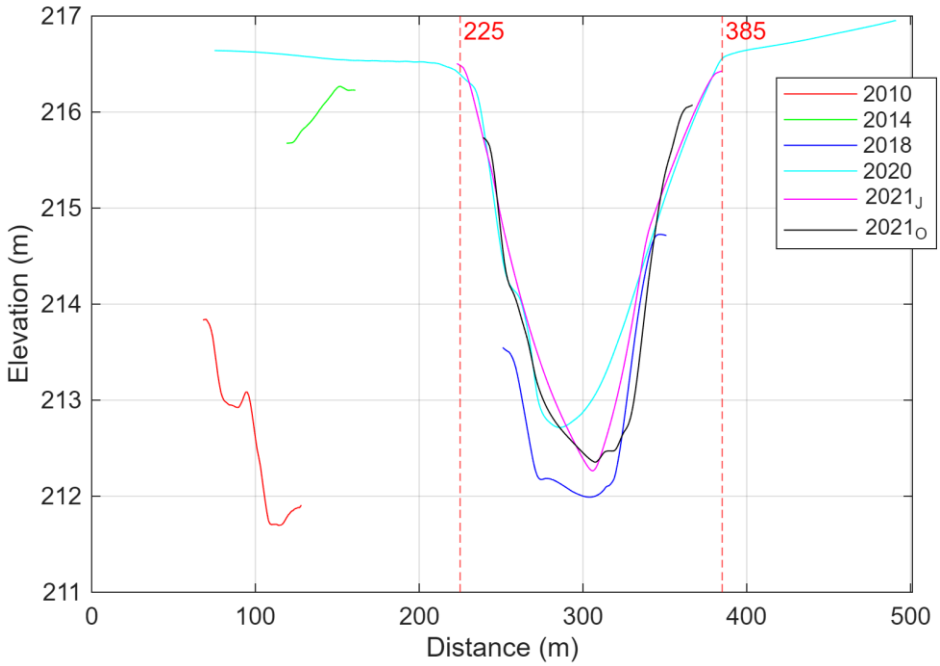

Figure 3-44 Elevation differences across distance-windows for Line ID 3 using a cross-sectional transect at the Red River Outlet

Figure 3-45 shifts to a streamwise view along the main navigation corridor using Line ID 7. Bed levels along the centerline have risen relative to 2010 and 2018, but uniformity across surveys is only evident for 2014, 2020, 2021 July, and 2021 October. The lower 2018 profile at the outlet indicates that the mouth experienced alternating episodes of erosion and deposition between 2010, 2014, and 2018, with no clear directional trend until 2020 onward, when sustained higher elevations were established along the full corridor length. A distinct underwater feature occurs about 300 m lakeward of the outlet, expressed as a local high most pronounced in the 2020 survey at 213.326 m. From 840 m moving lakeward to 0 m, the 2020 and both 2021 profiles lie above 2018, indicating net aggradation. The 2020 and both 2021 surveys shallow gradually from 600 m to 0 m, while between 0 and 840 m the 2020 and 2021 elevations alternate, reflecting short-interval redistribution without a change in corridor geometry.

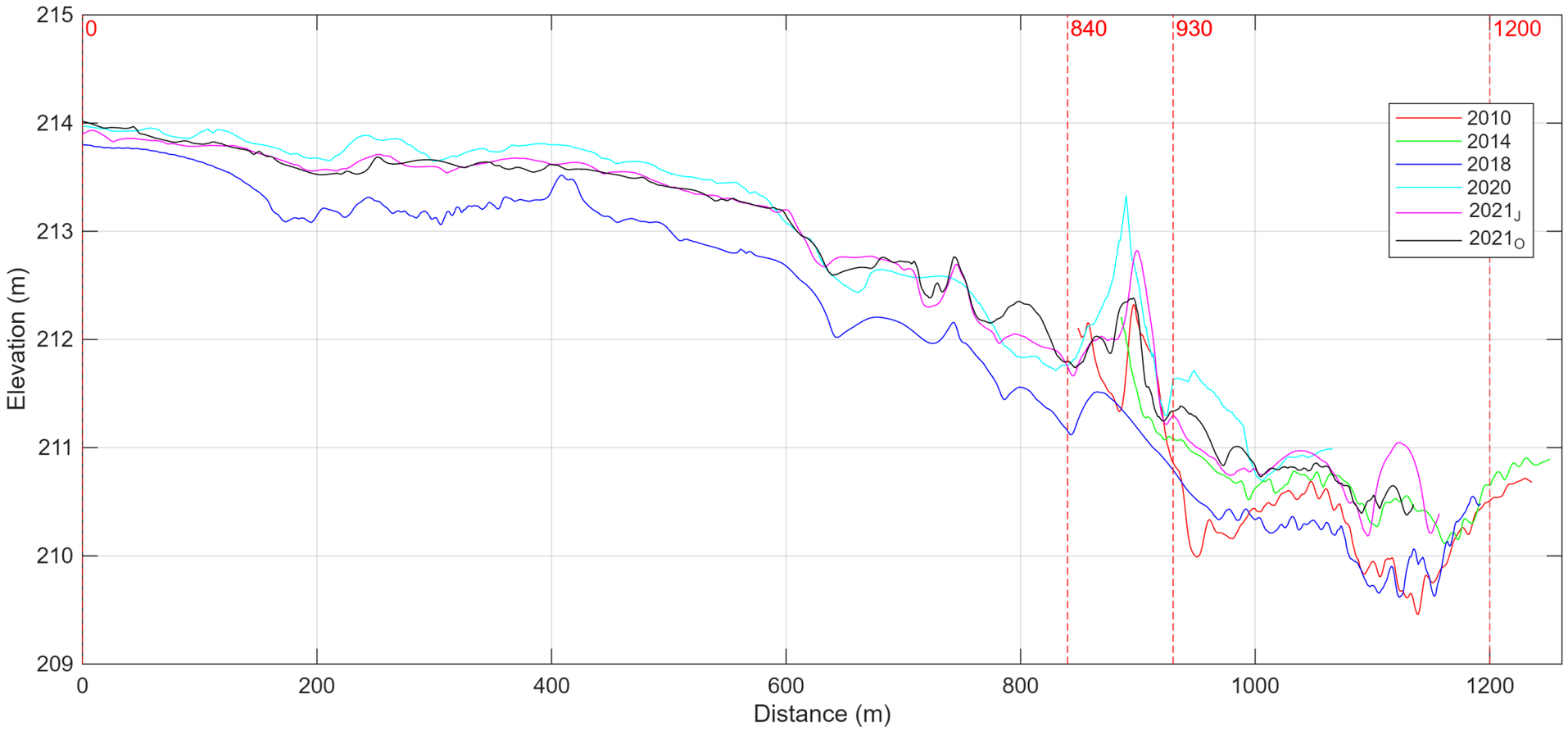

Figure 3-45 Elevation differences across distance-windows for Line ID 7 by centerline profile at the Red River Outlet

Figure 3-46 expresses the centerline changes along Line ID 7 as average differences within three windows. In the outlet reach from 930 to 1,200 m, the sequence shows persistent deposition after 2018. Relative to 2018, mean increases are +0.777 m in 2020, +0.617 m in 2021 July, and +0.604 m in 2021 October; the inter-survey change for 2021 is small at +0.012 m. The 2010 to 2018 pair shows a near-zero average change of −0.012 m, consistent with the lack of a clear trend before 2020 noted in the profiles. At the underwater feature from 840 to 930 m, the largest gain occurs between 2018 and 2020 at +0.944 m, with a modest seasonal lowering from 2021 July to 2021 October of −0.139 m. The small 2010 to 2018 offset in the 930–1,200 m window and the negative 2010 to 2018 difference at 840–930 m reflect that the 2010 survey only partly captured the feature. In the inner corridor from 0 to 840 m, deposition likewise dominates in the later years, with increases relative to 2018 of about +0.46 m (2020), +0.39 m (2021 July), and +0.41 m (2021 October), and a negligible seasonal change between the two 2021 surveys of approximately +0.014 m. Collectively, the windows confirm strong deposition from 2018 to 2020 and minor intra-annual adjustments in 2021, consistent with the cross-sectional results.

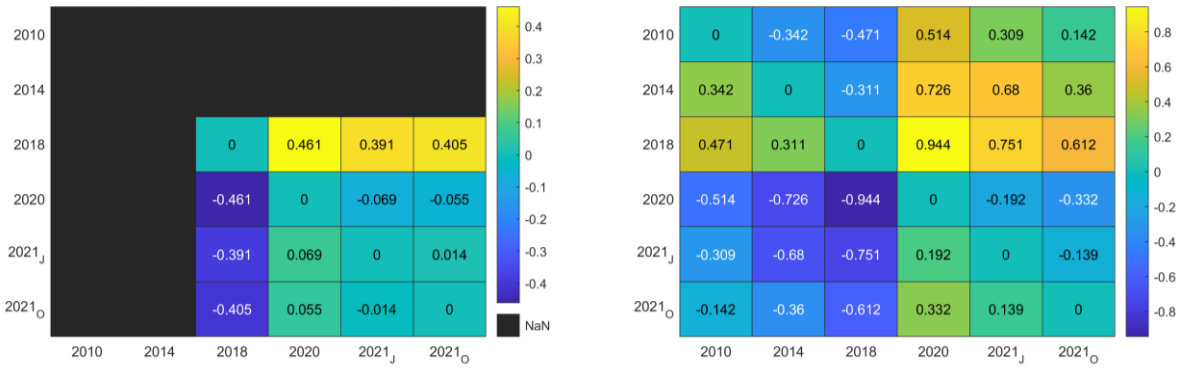

(a) Line ID 7: 0 – 840 m

(b) Line ID 7: 840 – 930 m

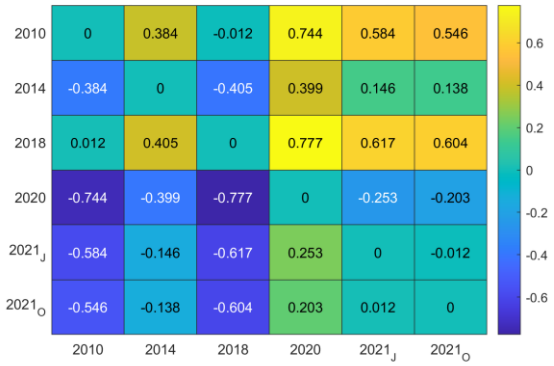

(b) Line ID 7: 930 – 1200 m

Figure 3-46 Average elevation differences across distance-windows for Line ID 7 by centerline profile at the Red River Outlet

3.5 Conclusion

The SBES proxy analysis did not provide a robust basis for quantifying spatially variable measurement error. Cells with repeat soundings were too few and unevenly distributed in space and time, which made Mantel and Moran based statistics highly sensitive to a small number of cases and unstable when combined. Global Moran's I confirmed strong spatial clustering of elevations, but this clustering primarily reflected survey track geometry rather than an interpretable error structure. As a result, the proxy approach was not adopted to derive estimate error, and uncertainty in the derived DEMs is instead addressed through instrument specifications, cross comparison with independent datasets, and the magnitude and spatial coherence of observed bed changes.

Within Netley Cut, the analysis frame shows alternating periods of erosion and deposition but only modest net change over the full record. From 2010 to 2014 the frame gained about 2,802 m^3, from 2014 to 2018 it lost about 4,736 m^3, from 2018 to 2020 it gained about 12,922 m^3, from 2020 to 2021 it gained about 1,365 m^3, and from 2021 to 2022 it lost about 8,355 m^3. The cumulative balance from 2010 to 2022 is a net depositional gain of 2,978 m^3, equivalent to an average rise of 0.083 m across the frame. Net elevation differences show the same pattern, with a strong rise of 0.359 m between 2018 and 2020 and a subsequent decline of 0.232 m between 2021 and 2022. Despite these fluctuations, the thalweg remains anchored along the left bank, the anthropogenic bed high is persistent, and there is no evidence of systematic widening or lateral migration. Classification of years by median stage and discharge shows that low stage and low discharge years (for example 2015, 2018, 2021) align with net deposition in the frame, while high stage and high discharge years (for example 2010, 2011, 2014, 2022) align with net erosion, indicating a consistent one year scale response even though the multi year trajectory is oscillatory rather than monotonic.

Netley Delta exhibits a clearer trend of deltaic growth and channel adjustment. The entrance has evolved into a bifurcated system in which the west channel remains the dominant and deepest path into Netley Lake, while the north channel transitions from a weak, discontinuous feature in 2010 to a continuous, well-defined channel in 2022. Surface-difference maps show deposition concentrated at the entrance and mid-reach of both channels and bed lowering toward the lake. Along the north channel thalweg, the 0–700 m reach deepens by about 0.727 m on average between 2010 and 2022, while the 700–1,100 m reach aggrades by about 0.140 m. Along the west channel thalweg, the 0–500 m window nearest the lake lowers by about 0.354 m and the 500–900 m window rises by about 0.180 m.

Netley Lake results demonstrate that sediment is being stored in and around the lake margins and making the lake bed shallower. Along the shoreline-of the delta, the south island and the adjacent north peninsula show mean elevation increases of 0.417 m over 280–1,250 m and 0.248 m over 2,250–2,600 m, respectively, with local minima marking the active outlets. These thalwegs occur at approximately 215.9–216.3 m in the west channel, 216.49 m in the south channel, and 216.53 m in the north channel, confirming the west channel as the deepest outlet and the north channel as a shallower but active conduit. Near offshore measurements show a mean elevation rise of 0.332 m over 280–1,105 m and 0.484 m over 1,300–2,000 m identifying a focused zone of lakeward deposition associated with the main channel outflow. The background bed level of Netley Lake, within the 0–3,500 m window, rises on average by 0.247 m between 2010 and 2022, corresponding to a deposition rate of about 2.1 cm per year. Over the same period, the apex of the middle island shifts about 353 m further into Netley Lake and its peak elevation increases by approximately 0.625 m.

The NLMRP illustrates how localized dredging and controlled deposition can support marsh restoration, albeit with debatable vegetative results relative to the degree of effort and cost. At the dredge site on the Red River, volume estimates provide net lowering of 7,740 m^3 from pre- to post-dredging, with 3,588 m^3 of that change occurring within the defined dredge footprints, corresponding to an average bed lowering of about 0.68 m. Over the subsequent year, the dredge footprints regain about 940 m^3, or roughly 26 percent of the excavated volume, as the bed rises by approximately 0.18 m, partially restoring pre-project conditions while leaving a residual lowering concentrated near the left bank. At the Netley Lake deposition site, long-term comparison between 2010 and the 2021 pre-dredge survey indicates deposition of 25,484 m^3 over 114,030 m^2, equivalent to an average rise of 0.223 m and an accumulation rate of about 2.2

cm per year, which closely matches the independent green-transect estimate. Placement of dredged material adds about 2,416 m^3 over 13,718 m^2 within the bounded cell, with a mean rise of 0.176 m. Comparison of dredged and deposited volumes suggests that on the order of two-thirds of the excavated material is retained within the deposition cell, with the remainder redistributed within the cell, exported through open boundaries, or lost to consolidation at magnitudes that are not distinguishable from erosion with the available datasets.

Along the lower Red River upstream of the outlet, the bathymetric comparisons show a shift in how flow is shared between the main and east channels, together with clear thickening of the bed around Netley Cut. The east channel has generally deepened, with the 1,530–6,300 m window lowering on average by about 0.44 m between 2010 and 2018, indicating greater conveyance capacity over several kilometres. In contrast, the main channel has shoaled over much of the same reach: between 990 and 6,300 m the bed rises on average by about 0.144 m, and immediately adjacent to Netley Cut, in the 11,000–12,000 m window, bed elevations increase by about 0.884 m. This produces a broader, shallower main channel around the Cut while the east channel develops a more continuous and deeper low.

Lastly, at the Red River Outlet, results from 2010 to 2022 show that the old corridor between the breakwaters has effectively filled in and no longer functions as an active channel, while the newer navigation corridor to the east has also become steadily shallower. Along Line ID 1, which cuts across the main corridor close to the shoreline, average bed elevations along the thalweg are higher than 2010 by 0.103 m (2014), 0.417 m (2018), 1.162 m (2020), 0.868 m (July 2021), and 0.947 m (October 2021). Over the same period, the lowest point in the section rose from 210.100 m to 210.911 m, an increase of 0.811 m. Along Line ID 3, moving further into Lake Winnipeg, the 225–385 m zone is higher than 2018 by 0.752 m (2020), 0.650 m (July

2021), and 0.373 m (October 2021), and the minimum bed elevation increased by 0.698 m between 2018 and 2020 and then stayed high in 2021. Centerline profiles along Line ID 7 show little net change between 2010 and 2018, followed by strong deposition from 2018 to 2020 and only small adjustments within 2021. Together, these results show that the active outlet corridor has been filling in since 2018, and although shorter term erosion and deposition continue to move sediment around, they do not offset the overall trend toward a shallower channel.

4. Water Levels and Discharge

The hydrodynamic setting of the lower Red River and Netley Cut, including the creation and enlargement of the Cut and its role in redistributing flow into Netley Lake, has already been outlined in Section 2.3. This section quantitatively examines the flows split between the Red River and Netley-Libau Marsh at Netley Cut and the Red River trifurcation. In addition, continuous water level measurements obtained in 2021 are investigated to determine the lag response time of water surface elevation from seiching events. The present section revisits this material only insofar as it relates directly to previous attempts to quantify discharge through Netley Cut and the Netley region.

4.1 Background

The earliest detailed assessment of discharge distribution near Netley Cut is provided by Haresign (2012). In that study, river ice freeze-up dynamics on the lower Red River were modelled using an intensive 2009 field campaign in which boat-mounted ADCP transects were collected at multiple cross-sections, including upstream of the Cut, across the Cut itself, and downstream at the lower Red River trifurcation. Haresign quantified discharges in the East and West channels of the lower Red River and in Netley Cut and then expressed the results as average proportions of total Red River flow using these ADCP transects,. Haresign indicates that, during the surveyed open-water conditions, approximately 37.1 percent of the Red River discharge was routed through Netley Cut, while 0.7, 27.4, and 28.3% flowed through the west, centre, and east channels, respectively (with a 6.5% continuity error). Although the primary focus of the work was the simulation of freeze-up processes, this analysis provides one of the only multi-section, observation-based estimates of flow distribution in the lower Red River

system and supports the conclusion that Netley Cut conveys on the order of one third of the river's discharge during typical open-water periods.

Kowal (2019) used eight ADCP-based discharge measurements from the previous dataset at Netley Cut to develop a side-weir model of flow from the Red River into the marsh, treating the Cut as a broad-crested side weir. Because these measurements were insufficient to define a local rating curve at the Cut, Kowal related the weir coefficient to reconstructed Red River discharge at Selkirk and then applied this relationship to generate a long-term April–June Netley Cut discharge series for 1915–2015. An alternative reconstruction assumed a fixed 37 % of Red River discharge entering Netley Cut, derived from the proportion reported by Haresign (2012). The side-weir model produced higher mean Netley Cut discharges than the fixed-percentage method and overestimated the limited observations by an average of about 699 m^3/s, indicating that Netley Cut discharge estimates are sensitive to model structure and calibration and that substantial uncertainty remains when extrapolating from a small set of moderately low-flow measurements.

More recent project planning documents for the Netley-Libau Marsh Restoration Pilot Project adopted similar characterisations of flow distribution. KGS (2019) prepared an Environment Act Proposal for the NLMRP that summarised hydraulic conditions in the lower Red River and used existing analyses to estimate the fraction of Red River flow entering Netley Lake via Netley Cut. Watchorn et al. (2021) employed the unpublished discharge estimates, as presented in KGS (2019), to analyze temporal changes in emergent vegetation cover in relation to increasing connectivity between the Red River and the marsh. Their analysis used discharge at upstream Red River stations as the hydrologic driver of vegetation change and did not incorporate new measurements at Netley Cut.

Nearly all quantitative statements about discharge through Netley Cut and into Netley-Libau Marsh ultimately trace back to the unpublished ADCP dataset, creating a limited empirical foundation for further assessments and greater confidence. Flow estimates through Netley Cut, Haresign's (2012) freeze-up modelling, and Kowal's (2019) side-weir reconstruction all rely on ADCP transects and bathymetry collected between 2009–2014, while KGS (2019) and Watchorn et al. (2021) reference an approximate 37–40 % flow fraction without presenting additional discharge observations at the Cut. As a result, there is no continuous discharge record at Netley Cut, and uncertainty in the flow split during low flows remains poorly investigated, despite the strong influence of Lake Winnipeg levels, wind set-up, and seiching noted earlier. Netley Cut discharge estimates are also highly sensitive to model structure and calibration: Kowal's (2019) broad-crested weir formulation produced systematically higher discharges than a constant-proportion method based on Haresign's ratio. Furthermore, both the side-weir representation and the proportional split implicitly assume predominantly unidirectional flow into the marsh, whereas Sections 2.3.1 and 2.4 highlight the likelihood of short-term bidirectional exchanges under low flow conditions. Collectively, these limitations reinforce the need identified in Section 1.2 for new measurements that provide further clarity to the Netley Cut discharge.

4.2 Methodology

The field program for this section combined mobile ADCP transects with fixed, continuous water level monitoring to characterise flow distribution within the Red River and Netley–Libau system. The overall approach comprised three linked components: (i) the deployment of instrumentation suited to shallow, low-gradient distributary channels, (ii) standardised collection

of discharge and water level data at key locations, and (iii) post-processing, verification, and synthesis of these datasets to derive flow splits and discharge.

4.2.1 Equipment and Data Collection

SonTek M9® ADCP surveys provided spatially distributed measurements of velocity structure and cross-sectional discharge at selected transects. Section *3.3.1* described the configuration of the M9® and its use for bathymetric mapping; in this section the instrument is considered in terms of its discharge measurement capabilities and its role in defining representative cross sections within the Red River and Netley Delta. Related details on the vessel platform, GNSS setup, and general field logistics are provided in earlier chapters and are not repeated here. To compliment the discrete ADCP discharge measurements, Solinst LeveLogger M5® pressure transducers were installed to obtain continuous water level records at strategic locations.

Together, the M9 and LeveLoggers provided complementary spatial and temporal resolution of the area along the lower Red River and within the Netley Delta. The ADCP transects provided discharge and velocity distributions at key locations, while the fixed LeveLogger installations recorded water levels over the monitoring period, respectively.

4.2.1.1 ADCP Measurements

ADCP's are used for direct discharge measurement by resolving the velocity field across a channel cross-section and combining it with cross-sectional geometry. During a typical survey, an instrument such as the M9® is mounted on a small vessel and towed along a transect that is approximately perpendicular to the dominant flow direction. As the platform moves, the ADCP emits acoustic pulses that measure the Doppler shift from suspended particles and converts these to depth-binned velocities. Figure 4-1 ADCP Velocity Distribution South of Netley Cut along the

Red River shows the ADCP velocity profile of a single transect south of Netley Cut along the Red River.

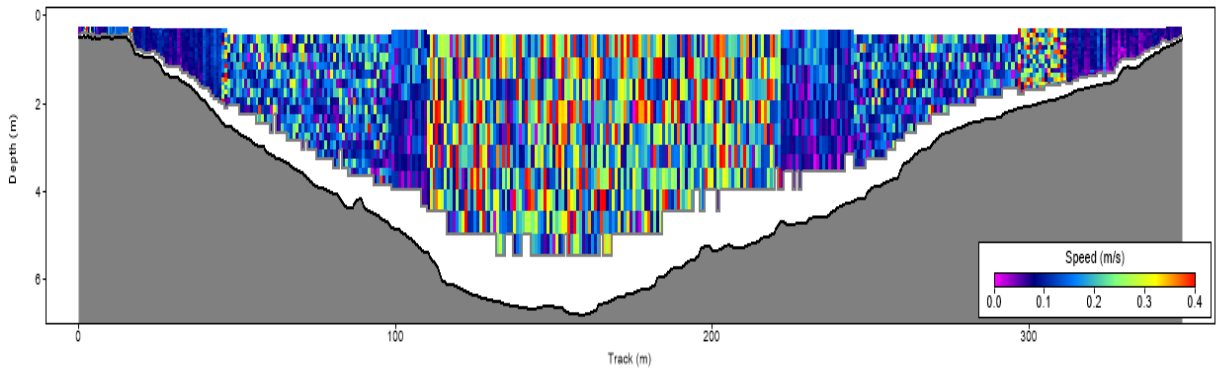

Figure 4-1 ADCP Velocity Distribution South of Netley Cut along the Red River

The software automatically subdivides the wetted cross-section into a series of narrow sub-areas, each associated with a representative velocity and area; discharge through each sub-area is calculated as the product of velocity and area, and total discharge is obtained by summing over all sub-areas. Near-surface and near-bed regions that cannot be sampled directly because of transducer submergence, blanking distance, or acoustic interference are treated as unmeasured layers. Each of these unmeasured layer's velocities are estimated by extrapolating the observed vertical velocity profile (SonTek Inc., 2022). Multiple transects are usually collected under quasi-steady conditions and averaged to produce a single discharge value. In low-velocity or two-directional flows, measurement uncertainty increases and data quality can be affected by soft or mobile beds, vegetation, or aquatic life. However, an ADCP still provides discrete, spatially resolved discharge estimates that are suitable as reference measurements for estimating discharge and deriving empirical based estimations.

Discharge measurements followed the standard moving-boat procedure but the number of transects at each site varied according to field constraints. Several repeat crossings were typically

obtained at major control sections such as Netley Cut and the Netley Delta channels, whereas at secondary locations only a single transect was sometimes completed. This approach reflected a trade-off between the recommended practice of multiple crossings at each section and the need to cover a large number of sites within limited survey windows and safe boat-operating conditions. At all sites, transects were run along preselected lines oriented approximately perpendicular to the main flow and spanning from shallow water near one bank to shallow water near the opposite bank, with boat speed kept as steady as possible to maintain uniform sampling. Where only one transect was collected, its suitability for discharge estimation was assessed by inspecting internal quality-control indicators, including consistent bed return, stable velocities along the track, and an absence of obvious disturbances such as sharp changes in boat track or abrupt velocity spikes. Single-transect measurements that met these criteria were retained as discrete discharge estimates and were treated in subsequent analyses in the same manner as averaged values from multi-transect sites.

4.2.1.2 Water Level Measurements

LeveLoggers provided continuous water-level records at fixed locations throughout the study site as shown in Figure 4-2. Each LeveLogger was mounted on a steel L-bracket and attached to the shoreline with a steel cable anchored into the ground using a length of rebar, which held the sensor in a stable position for the entire deployment period.

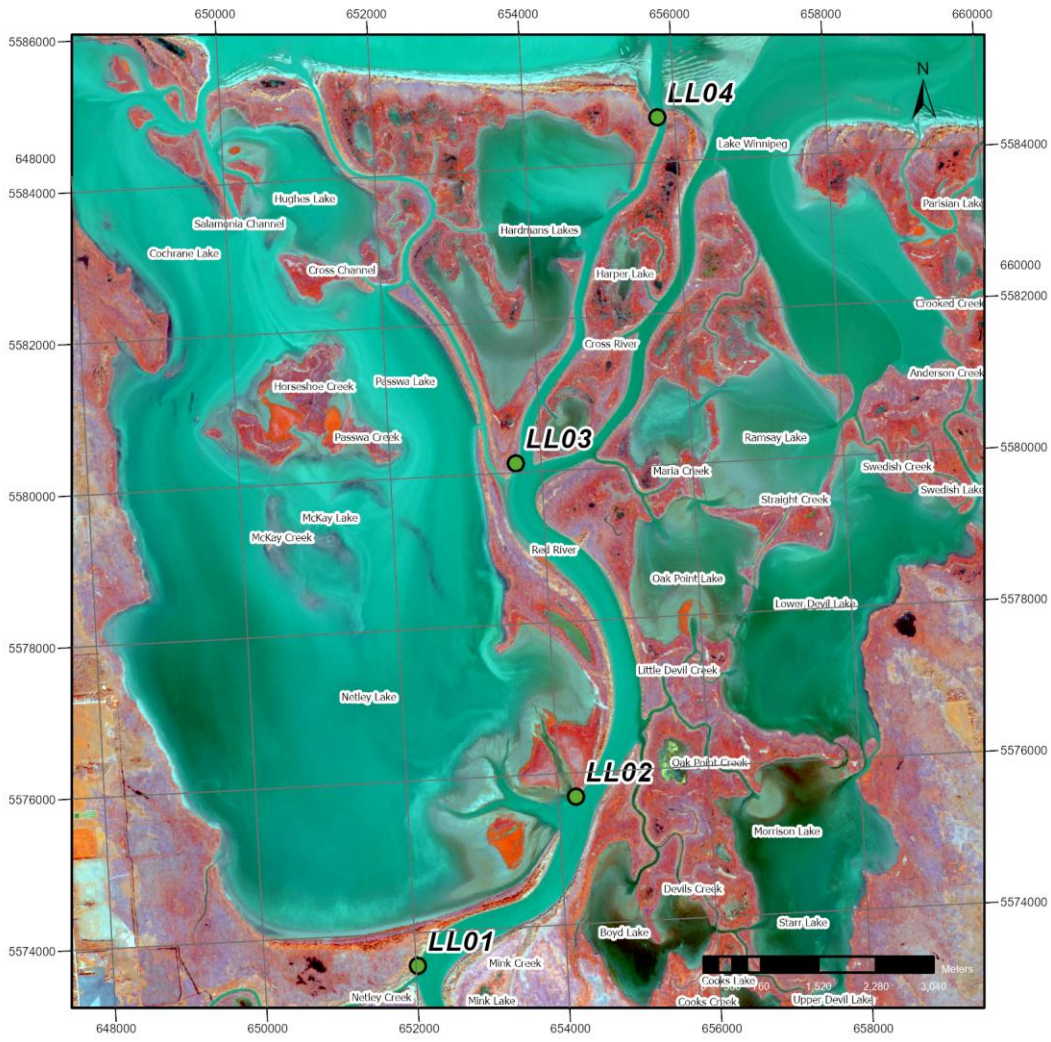

Figure 4-2 LeveLogger (LL) Deployment Locations in NLM

LeveLoggers were walked out from shore to positions that were expected to remain submerged for the full monitoring interval, so the sensors stayed continuously below the water surface. At each installation, the water surface elevation was measured with the Trimble SP60 GNSS receiver and used to reference the LeveLogger pressure readings to a known vertical datum. The LeveLoggers recorded absolute pressure and temperature at regular 5 minute intervals, while a separate Barologger in the study area recorded atmospheric pressure. Barometric compensation subtracted the Barologger record from the LeveLogger absolute pressure to obtain water pressure and then converted to water level and tied to CGVD2013.

These processed records produced continuous stage time series at each site that supported subsequent rating-curve development and discharge analyses. Table 4-1 summarises how each LeveLogger deployment was controlled over time. For each instrument, the table lists the start date, any intermediate survey date, the end date, and the elevation shifts applied at the intermediate and end checks. Where an intermediate date is shown (for example for LL02), the intermediate shift is a single vertical correction applied to the record up to that point, with the end shift applied after retrieval. Where no intermediate survey was done, those cells are left blank and only a final shift is reported. These small shifts (on the order of a few centimetres) account for minor changes in sensor position or reference over time, such as slight movement of the bracket in soft sediments, gradual loosening of the shoreline anchor, or small differences in how the water surface was surveyed at each visit. If the sensor did not move during deployment and survey error was negligible, the elevation differences between survey dates would be zero, and no shifts would be required.

Table 4-1 LeveLogger Deployment Dates and Datum Shifts

LeveLogger	Start Date	Intermediate Date	End Date	Intermediate Shift (cm)	End Shift (cm)
LL01	June 23 2021	-	Oct 18 2021	-	3.76
LL02		July 29 2021		13.55	- 0.49
LL03		-		-	8.86
LL04		-		-	0.14

4.2.2 Discharge Post-Processing and Analysis

ADCP data processing began in the field during acquisition. Each transect was checked in real-time by monitoring bottom track, depth and velocity plots, and total flow to confirm a continuous bottom return and a stable boat track across the section. Where a hydraulically closed reach could be defined (for example, where all upstream inflows and downstream outflows were

measured during the same survey), a continuity check was applied by comparing the summed inflows to the summed outflows. A degree of mismatch was expected because flow is unsteady and time dependent. However, when the time between measurements at the different cross-sections was minimised, the continuity error was expected to be relatively small, though not zero under realistic field conditions. If the continuity error was large, or if an individual transect showed errors such as loss of bottom track, abrupt changes in boat speed or heading, or discharge values that were clearly inconsistent with other cross-sections on the same visit, that transect was re-examined and, where necessary, re-measured. Where multiple transects were collected at a site, the resulting discharge estimates were compared; transects that differed markedly from the group or showed degraded quality indicators were rejected, and the final site discharge value for a given survey time was taken as the arithmetic mean of the accepted transects. The same quality checks were applied at sites where only a single transect could be obtained; if the internal quality indicators and cross-section plots did not show obvious errors, that transect was retained as the representative discharge for that visit and flagged as a single-pass measurement in subsequent analyses.

All accepted ADCP transects were exported and processed in MATLAB after field screening using a set of scripts that organised the full discharge dataset by date and by hydraulic location. The scripts first loaded all available transects, including historical measurements collected since 2009 and the surveys completed for this thesis in 2020, 2021 and 2022, and grouped them by survey date based on the file naming convention. The code used the GPS coordinates stored with each transect to plot the boat path and to extract a representative midpoint location for each date. These midpoints were then analyzed against a series of bounding polygons in geographic coordinates that represented the main areas of interest. These areas are shown in Figure 4-3

Bounding Polygons for Discharge near Netley Cut showcasing the upstream Red River, upstream Netley Cut, Netley Cut, downstream Netley Cut, Little Devil and Devil Creeks, and Figure 4-4 showcasing the west, central and east outlets of the lower Red River at the trifurcation.

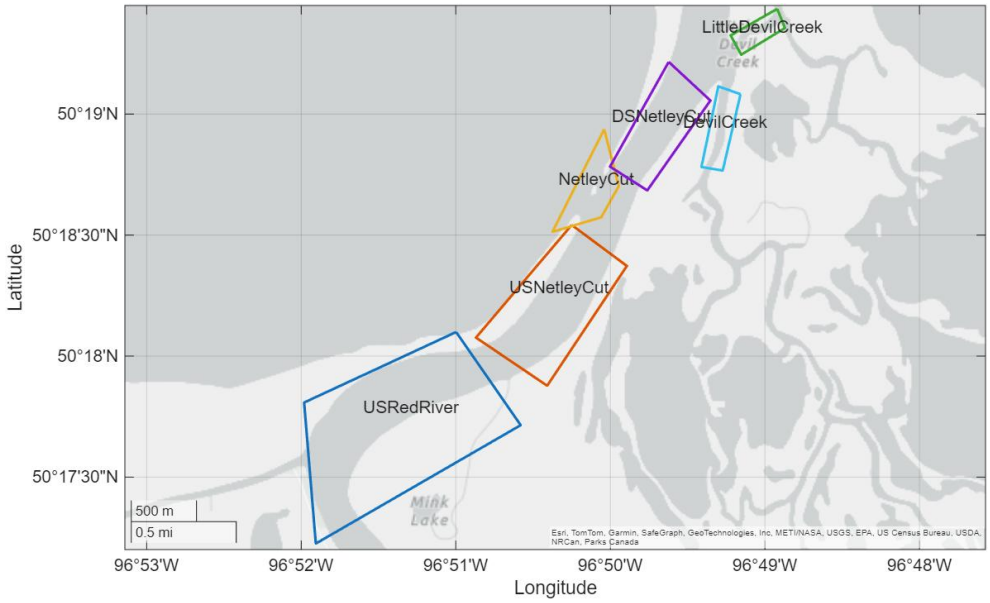

Figure 4-3 Bounding Polygons for Discharge near Netley Cut

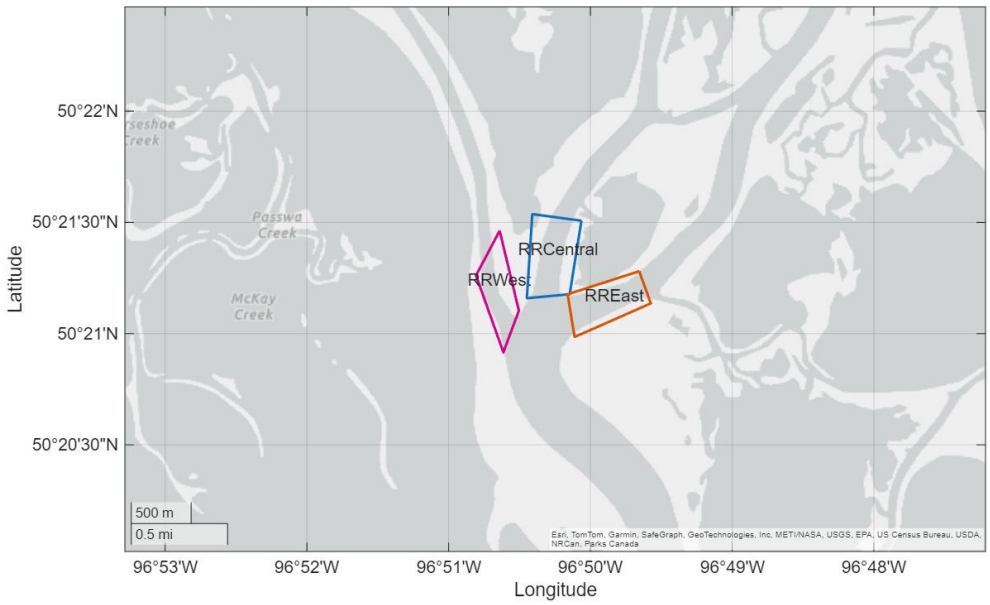

Figure 4-4 Bounding Polygons for Discharge at the Red River Trifurcation

Any transect whose midpoint fell inside a given polygon was assigned to that location, which produced a structured dataset of discharges by date and by hydraulic control section. The scripts then extracted the total discharge from each transect summary and compiled these values into date–location tables. This organisation allowed subsequent calculations of daily flow splits between the main river and distributary channels, as well as continuity checks where all inflows and outflows were measured on the same date, expressed in m^3/s and as percentages of total flow.

4.2.3 Water Level Post-Processing and Analysis

Water level post-processing used the Solinst LeveLogger software to convert raw pressure records to continuous stage time series referenced to CGVD2013. The software first applied barometric compensation by subtracting the BaroLogger atmospheric pressure record from the absolute pressure recorded at the sensor for each LeveLogger. The compensated water pressures were then converted to water depths and adjusted to elevations using the surveyed water surface elevation at the start of the deployment. Where additional water surface surveys were collected during the deployment, the differences between successive surveys were used to define simple linear corrections over time. These corrections were applied as manual linear interpolations between the known water surface elevations at the beginning and end of the deployment, or between successive survey dates, and are summarised as intermediate and end shifts in Table 4-1.

The resulting water level records were reviewed for completeness and consistency after vertical adjustments were applied,. The time series were scanned for gaps associated with erroneous or interrupted data points, and any short intervals were filled using linear interpolation over periods where water levels changed smoothly. Obvious outliers, such as isolated spikes or

drops that did not match the overall stage behaviour, were removed. The final processed records consisted of continuous five-minute water level time series for each LeveLogger, corrected for barometric pressure and referenced to CGVD2013.

4.2.3.1 Time-lag Across Netley Marsh

Stage data from multiple LeveLogger deployments were first assembled into continuous time series for each measurement location. Date and time fields in the raw records were combined into single time stamps associated with the corresponding water level and temperature observations. These records were then plotted over a common study period and within a fixed elevation range of approximately 216.3 to 217.7 m (CGVD13) to allow a consistent visual comparison of water level behaviour among locations and over time, as shown in Figure 4-5.

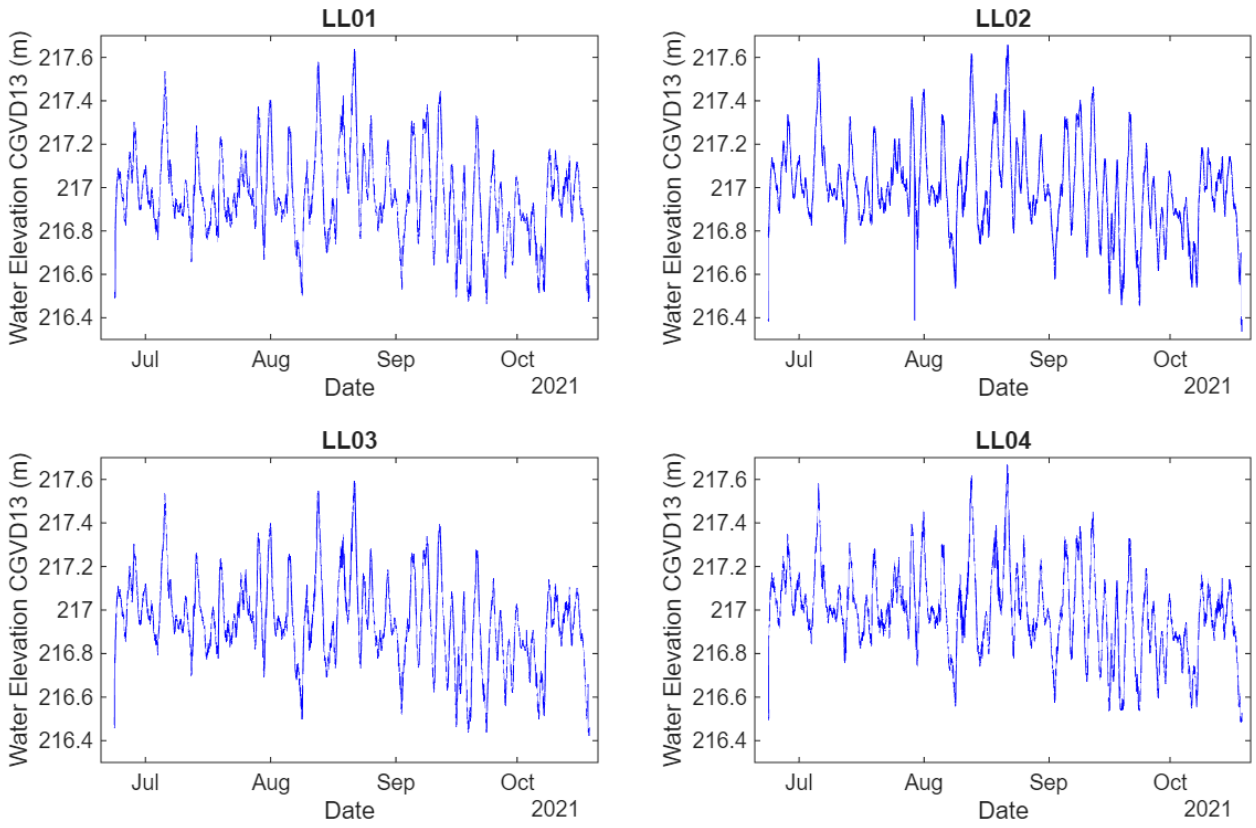

Figure 4-5 Water Surface Elevations across Netley Marsh along the Red River

Where a station was monitored in multiple deployment segments, the individual segments were concatenated and ordered chronologically to reconstruct a single continuous record.

Local maxima and minima were identified in each continuous water level record to isolate hydrodynamically meaningful events using an extremum detection procedure subject to two constraints. First, a minimum prominence threshold (how much a value “sticks out”) of 0.05 m was imposed. The minimum peak prominence of 0.05 m specifies that only crests and troughs with amplitudes of at least 5 cm relative to their local surroundings are treated as distinct hydrodynamic events. This filters out minor oscillations that may arise from measurement noise, short-period disturbances, or localised effects, and ensures that the identified extrema correspond to more substantial variations in stage that are likely to reflect system-scale processes. If this threshold were set lower, a larger number of small peaks and troughs would be detected, increasing the risk of pairing spurious events between stations and inflating the apparent variability in lag estimates. If it were set higher, some genuine but moderately sized waves could be excluded, biasing the analysis towards only the largest events.

Second, a minimum temporal separation between successive extrema, specified as eight hours, controls the effective temporal resolution of the event detection. By enforcing an eight hour separation, the procedure tends to identify at most one representative crest and one representative trough within any roughly eight hour window. This reduces the likelihood of detecting multiple peaks associated with a single broad wave or tidal-like cycle and promotes a one-event-per-wave interpretation of the resulting extrema. Shortening this separation would allow multiple extrema to be recorded within the same broader event, complicating the interpretation of propagation and increasing the number of candidate pairings. Lengthening it would reduce the number of detected events and might merge distinct but closely spaced waves

into a single representative extremum, potentially under-representing higher frequency variability.

Thirdly, a matching tolerance of two hours specifies how tightly events at different stations must align in time to be treated as the same wave. Only extrema at downstream stations that occur within three hours are considered valid matches for each reference crest or trough,. This relatively strict tolerance reduces the chance that unrelated events will be paired solely based on proximity in time, thereby improving the physical likelihood of the derived lags. However, it also means that events with longer or more diffuse propagation signatures, or where local processes introduce additional delays, may not be matched and will be excluded from the lag statistics. A larger tolerance would increase the number of matched events but at the cost of a higher risk of associating unrelated extrema. Together, the prominence threshold, minimum separation, and three hour matching tolerance define a conservative event-detection and pairing framework that prioritises robust, well-resolved waves and relatively tightly constrained propagation times between stations.

4.2.3.2 Sensitivity to Tolerance Matching, Lag Separation, and Prominence

Sensitivity of the lag time estimates to the choice of peak detection and matching parameters was explored qualitatively using a set of one-at-a-time adjustments. The minimum prominence threshold was varied from 0.01 to 0.40 m in 0.05 m increments, the minimum temporal separation between detected extrema was varied from 2 to 36 hours in 2 hour increments, and the matching tolerance between stations was varied from 1 to 24 hours in 1 hour increments. These ranges were selected to span plausible real-world values for stage variations in the marsh while ensuring that the identified extrema represented genuine water level responses rather than short-term oscillations. In particular, the parameter spacing was chosen so that local minima and

maxima would be truly representative of broader hydrodynamic behaviour, and would not systematically capture sub-daily, site-specific extremes associated primarily with surface waves or local disturbances rather than with larger-scale tidal seiching within the lake–marsh system. The remaining two variables for each parameter were held constant while the mean crest and trough lags and the number of matched events were examined across the tested range.

Propagation of these wave events between locations was evaluated by treating the upstream station (LL01) as a reference and pairing its representative extrema with corresponding events at the downstream stations (LL02, LL03, and LL04). The nearest extremum in time at a downstream station was identified for each crest and trough at the reference station. Then the time lag was computed for all matched events as the difference between the downstream and upstream event times, providing a set of positive or negative delays that describe whether and how quickly each downstream location responds to water level changes at the reference site. Mean and median lags for crests and troughs were then calculated for each station pair.

The resulting pairs of time lags were examined both numerically and graphically. For the reference station, the detected maxima and minima were overlaid on the full water level record to verify that the prominence and separation thresholds produced a physically reasonable representation of individual waves (E.g. Figure 4-6). Mean crest and trough lags between the upstream and downstream stations were then summarised in bar charts, providing a concise visual representation of typical delay times for water level signals as they propagate through the monitored reach.

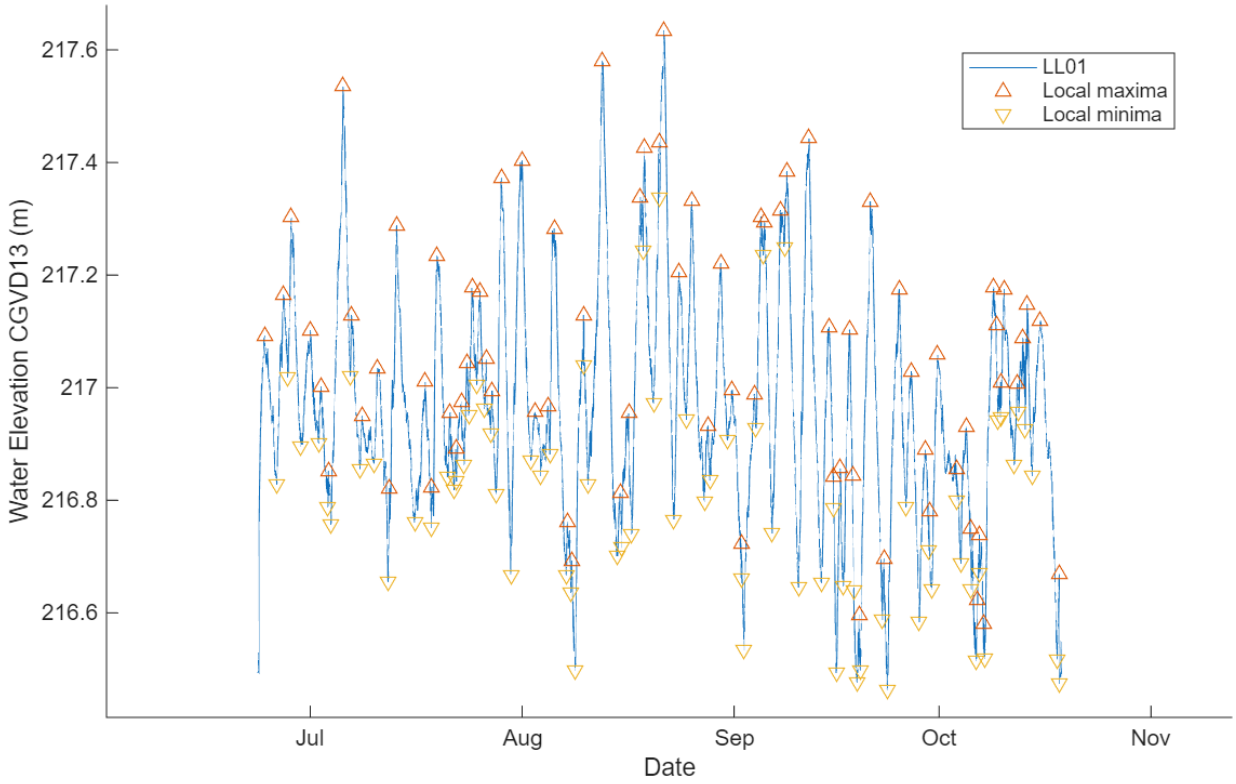

Figure 4-6 Local and Maximum Extrema for LL01

The sensitivity plots in Figure 4-7 indicated that the lag estimates were relatively insensitive to the choice of prominence threshold once the threshold exceeded approximately 0.10 m. At very low prominence values, additional small peaks and troughs were introduced, which increased the number of matched events but produced more variable lag estimates. At higher thresholds, the number of matched events decreased as only the largest excursions were retained. A threshold of 0.12 m provided a balance in which the mean lag values varied only weakly with further changes in prominence, while still retaining a sufficient number of events for each station.

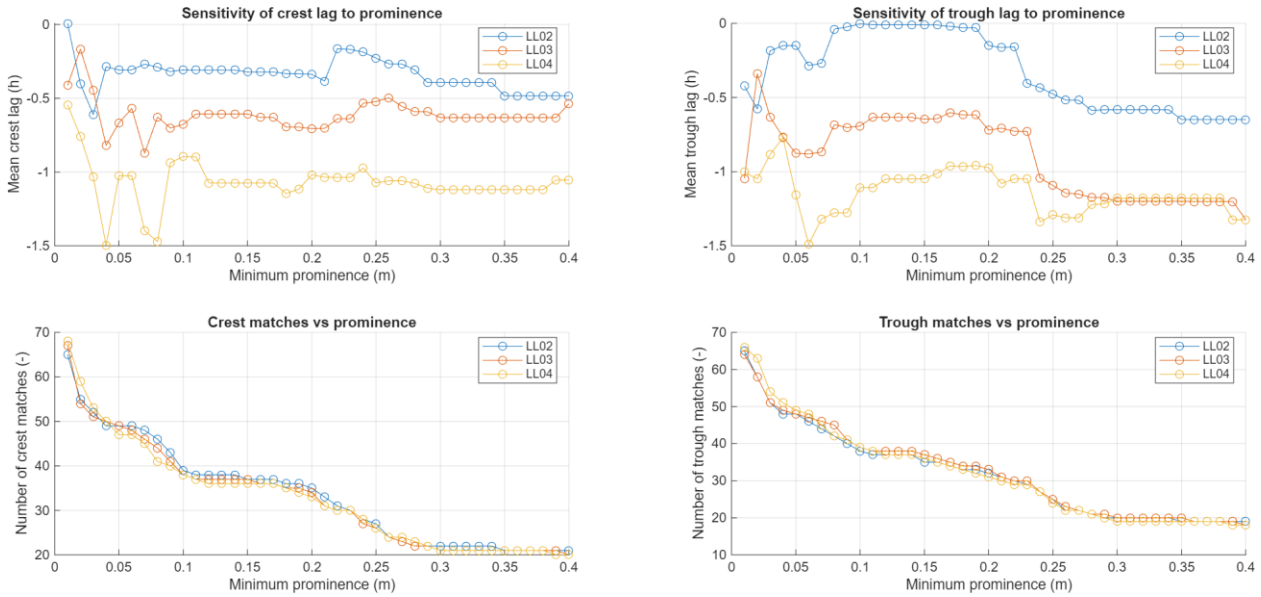

Figure 4-7 Sensitivity of Crest and Trough Lag Statistics and Event Counts to Minimum Peak Prominence (LL02–LL04 Relative to LL01)

The analysis of the temporal separation parameter showed that very short separations tended to fragment broad waves into multiple extrema influenced by local peak structure, whereas longer separations progressively filtered out these higher frequency features. A separation of 30 hours was adopted to reduce the influence of localized peak wave behaviour while still capturing the slower, larger amplitude water level variations associated with wind-driven seiching within the lake–marsh system as shown in Figure 4-8. In the sensitivity plots, this choice produced relatively stable lag estimates across the range of separation values, with a modest but acceptable decline in event counts as the separation increased.

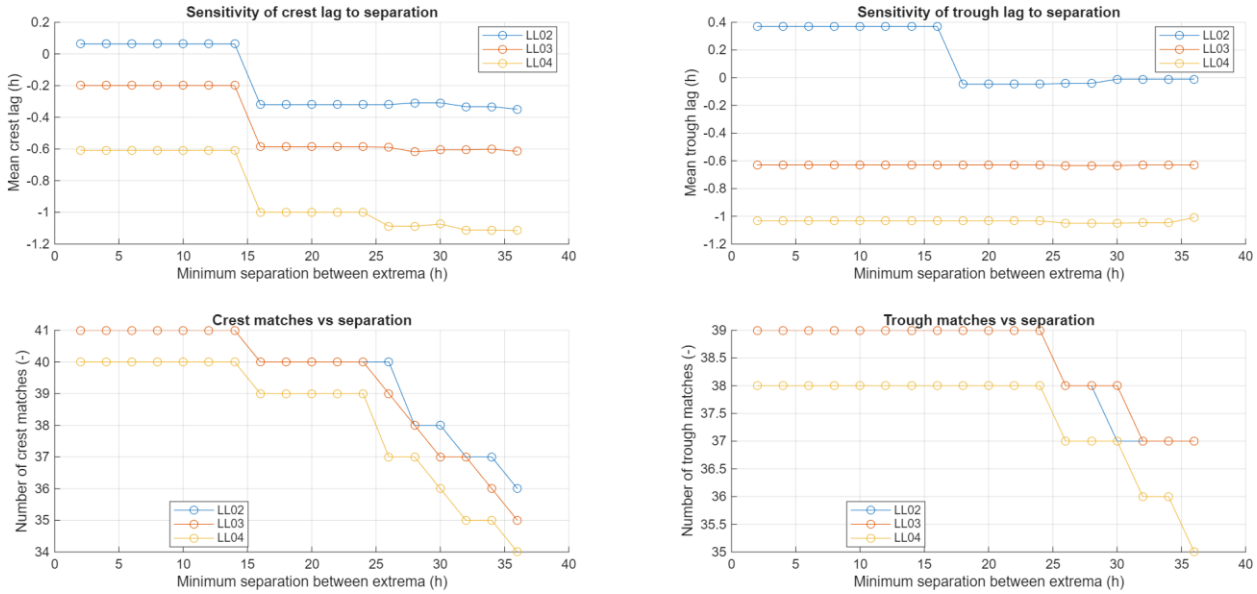

Figure 4-8 Sensitivity of Crest and Trough Lag Statistics and Event Counts to Minimum Temporal Separation (LL02–LL04 Relative to LL01)

The matching tolerance between stations controls how strictly extrema at different locations must align in time to be treated as corresponding expressions of the same wave. Only a limited number of events were matched when the tolerance was very small, and the lag statistics became noisy. Both the number of matched events and the smoothness of the mean lag curves improved as the tolerance increased, although excessively large tolerances would risk pairing unrelated extrema. A tolerance of 20 hours was therefore selected as a relatively generous window that allows subsequent peaks at different stations to be associated when they occur within a broadly similar phase of the larger-scale water level response. In the sensitivity analysis shown in Figure 4-9, the matching tolerance maintained reasonably stable lag estimates while ensuring that, for most major events, at least one matching extremum could be identified at the downstream stations.

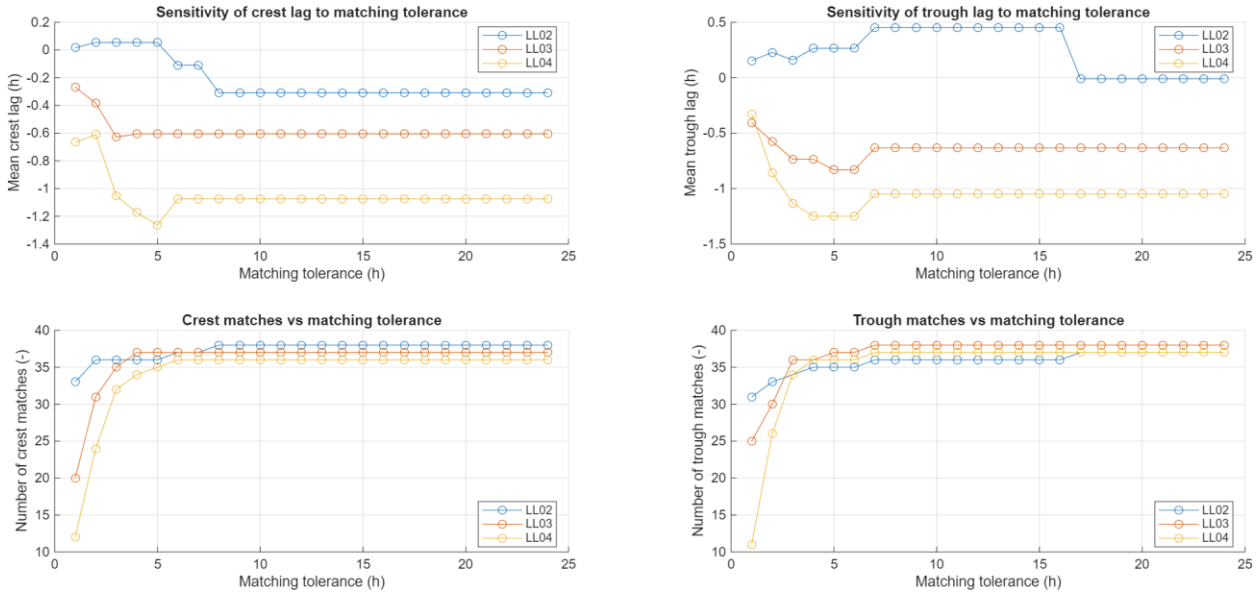

Figure 4-9 Sensitivity of Crest and Trough Lag Statistics and Event Counts to Minimum Matching Tolerance (LL02–LL04 Relative to LL01)

On this basis, the final parameter set used in the lag analysis consisted of a minimum prominence threshold of 0.12 m, a minimum temporal separation of 30 hours, and a matching tolerance of 20 hours.

4.3 Results and Discussion

Presented herein are the results from the ADCP-based discharge measurements at Netley Cut and the Red River trifurcation, followed by an analysis of water level fluctuations and time lags across Netley–Libau Marsh derived from pressure transducer records.

4.3.1 Flow Distribution

The discharge analysis is framed in terms of three connected reaches of the Red River. In Figure 4-10 the Red River reach south of Netley Cut is identified as P1 and shown in orange on accompanying figures. Netley Cut itself is identified as P2 (yellow) and represents the lateral pathway that diverts flow toward Netley Lake. The Red River reach north of Netley Cut is

identified as P3 and shown in purple. In this configuration, the standard sign convention is positive when P1 provides the principal inflow to the system, and where P2 and P3 represent the two outflow branches.

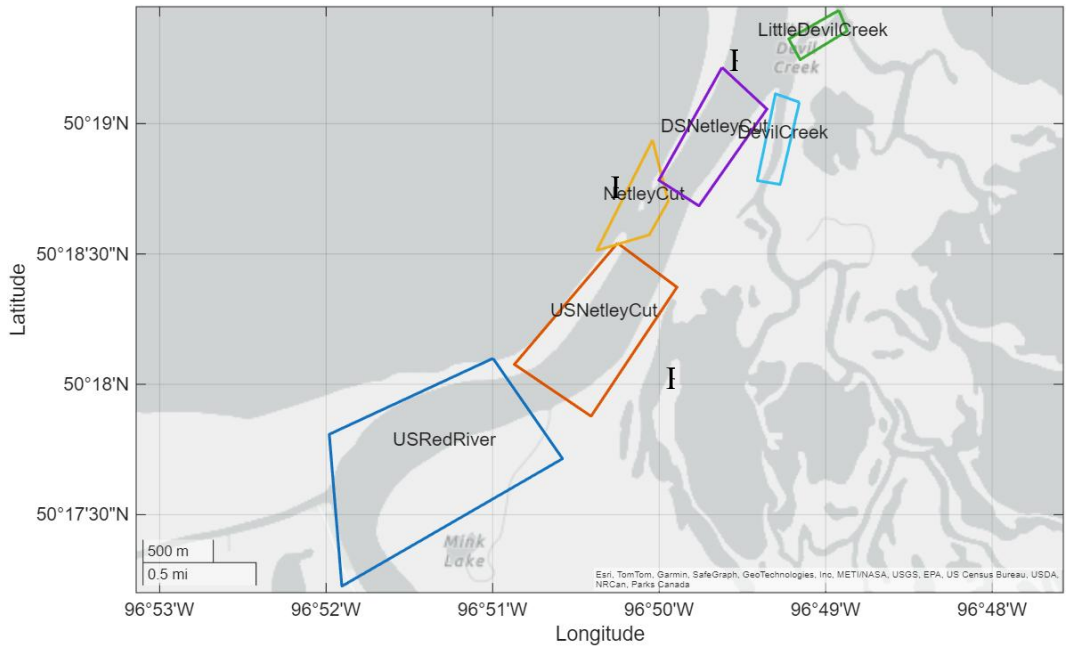

Figure 4-10 Flow Distribution at the Netley Cut

Positive discharge at P1 indicates flow from south to north along the Red River toward the Netley Cut junction. Positive discharge at P2 indicates flow from the Red River into Netley Cut and toward Netley Lake. Positive discharge at P3 indicates flow from the junction northward along the Red River toward Lake Winnipeg. Negative values indicate reversal of these directions at the respective sections.

The centre hydraulic states at Netley Cut can be interpreted in terms of the sign combinations at P1, P2, and P3 that are consistent with the observed data, namely cases where P3 remains positive:

- P1 > 0, P2 > 0, P3 > 0

  Flow is from south to north along the Red River, with part of the discharge continuing downstream through P3 and part being diverted laterally through P2 into Netley Cut. This represents the typical through-flow condition in which the Red River is the primary inflow and Netley Cut functions as an active side-spill channel toward Netley Lake.

- P1 > 0, P2 < 0, P3 > 0

  The Red River supplies inflow from the south and continues northward toward Lake Winnipeg, but P2 is negative, indicating flow from Netley Lake toward the Red River. In this case the junction receives water both from the upstream Red River and from Netley Cut, and the combined discharge exits along P3. Netley Cut behaves as an inflow branch from the marsh rather than as an outflow.

- P1 < 0, P2 > 0, P3 < 0 (inferred by continuity)

  P1 is negative, indicating that flow in the upstream Red River reach is directed away from the junction toward the south. Under these conditions, the local hydraulic gradient is reversed such that lake-driven or marsh-driven control is pushing water upstream along the Red River to at least the Netley Cut junction, rather than allowing a net lakeward conveyance through the downstream reach. Although P3 was not directly observed as negative in the available ADCP transects, P3 is treated as negative for this configuration based on continuity of the Netley Cut system: if the upstream reach (P1) is experiencing sustained flow reversal at the junction, the downstream reach adjacent to the junction must also be undergoing reversal (or near-stagnation) to satisfy a physically consistent control-volume balance

Accordingly, the sign state associated with $P1 < 0$ is interpreted as a system-scale backwater condition in which Lake Winnipeg influence propagates upstream, reversing flow in the Red River as far south as the Netley Cut. In this regime, P2 may remain positive if Netley Cut continues to convey flow toward Netley Lake, but the junction itself is governed by an upstream-directed Red River exchange, and P3 cannot be assumed to remain positive.

Because the ADCP dataset is composed of discrete transects collected under a limited set of hydraulic conditions, it does not provide direct observations of $P3 < 0$, nor does it resolve transient stagnation states ($Q \approx 0$) that may occur during reversals. These unsteady threshold conditions are therefore incorporated conceptually through the continuity assignment above.

Correspondingly, Table 4-2 summarizes all available ADCP discharge measurements collected between 2009 and 2022 at three key locations within the Red River trifurcation (see Figure 4-4) and three within the Netley Cut system as just defined. For each survey date, the table reports the instantaneous discharge at these locations providing the primary basis for describing how flow is partitioned between Netley Cut and the Red River and distributed among the three branches of the Red River trifurcation. For this study, continuity is treated independently within the Netley Cut system and within the Red River trifurcation. Discharge measured downstream of Netley Cut is not assumed to equal the total inflow to the trifurcation because additional outflows, and inflows occur between these two control volumes, including impacts from Little Devils Creek and Devils Creek.

Several entries in Table 4-2 Discharge Measurements for Netley Cut and the Red River Trifurcation, 2009–2022.are annotated to distinguish measured discharges from those inferred from the application of continuity. Values marked with a single asterisk denote cases where discharge was estimated based on continuity. In contrast, values marked with a double asterisk

correspond to survey days when ADCP transects were obtained at P1, P2 and P3. For these dates, continuity could be explicitly evaluated, and any imbalance in the system was interpreted as a continuity error arising from instrument uncertainty, incomplete lateral coverage, or changes in discharge over time while monitoring. All continuity checks implicitly assume a quasi-steady flow condition during the period of measurement, which is an approximation given that both the Red River and Netley Marsh are unsteady.

Within this dataset, P1 exhibits the largest range of discharges, from a maximum of 1,265.50 m^3/s to a minimum of -9.36 m^3/s, the latter indicating a short period of local flow reversal. P2 conveys between 539.22 m^3/s at the upper end of the observed range and -10.12 m^3/s at the lower end, again indicating that reverse flow conditions were captured during at least one survey. P3 discharge ranges from a maximum of 726.28 m^3/s to a minimum of 17.51 m^3/s, with all recorded values remaining positive and therefore directed toward the lake. The available measurements for the trifurcation branches are more limited, but they establish characteristic envelopes for each channel. In the east channel, discharges vary between 324.83 m^3/s and 53.20 m^3/s, while the centre channel carries between 433.16 m^3/s and 55.30 m^3/s over the measurement period. The west channel consistently contributes a much smaller share of the flow, with observed discharges ranging only from 8.60 m^3/s down to 1.62 m^3/s.

.

Table 4-2 Discharge Measurements for Netley Cut and the Red River Trifurcation, 2009–2022.

	Flow (m^3/s)					
Date	P1	P2	P3	West Channel	Centre Channel	East Channel
June 12 2009	540.07	232.29	307.78*	1.62	148.84	133.62
June 29 2009	1265.50	539.22*	726.28	6.94	433.16	324.83
June 30 2009	948.49	279.26*	669.23		323.44	298.51
*July 08 2009***	994.01	390.51	604.80			
July 08 2009	979.26	471.31*	507.95			
July 08 2009	986.64	390.51	605.00	7.70	268.15	230.65
July 10 2009	615.60	253.06*	362.54		97.80	190.60
July 10 2009	647.98	104.66*	543.32			
July 10 2009	631.79	178.86*	452.93			
*July 13 2009***	656.58	201.23	310.66			
*July 13 2009***	434.15	185.44	190.06	5.33	151.99	130.14
*July 31 2014***	674.14	293.90	480.51			
July 3 2019	190.26	59.22	131.03*		97.33	67.36
August 7 2020	282.37	159.87	125.44	8.60	55.30	53.20
*August 7 2020***	315.97*	136.31	179.66			
July 8 2021	-9.36	30.55	39.90*			
*July 29 2021***	140.00	-10.12	145.69			
Aug 25 2021	-0.26	17.25	17.51*			
Sept 15 2021	109.04	-5.81	114.85*			
Oct 18 2021	66.70	-2.95	69.66*			
*July 14 2022***	548.31	289.61	278.20			

Note: * identifies flow measurements at Netley Cut that were estimated on the basis of an assumed 100% continuity at that location. ** identifies flow measurements for which point measurements were obtained P1, P2, and P3, allowing estimation of continuity error in addition to the reported discharge. Positive values indicate into the system from P1 and out of the system from P2, negative values indicate a reversal of flow.

Table 4-3 further builds upon these findings by expressing the direct discharge measurements as percentage flow splits rather than absolute values. Across the observations used in Table 4-3, P2 conveys between 4.24 and 98.51 % of the discharge at P1, indicating that Netley Cut can range from a relatively minor contributor to an almost exclusive pathway. Correspondingly, P3 carries between 43.78 and 100 % of the P1 discharge, showing that at times nearly all of the flow remains in the Red River, while at other times a substantial fraction is diverted into Netley Cut. The fact that the maximum contribution of P2 reaches 98.51 % but not 100 % indicates that, within the available discrete measurements, Netley Cut has not been observed as the sole provider of flow at this junction.

A similar continuity-based approach is used to interpret the Red River trifurcation, but with an important distinction. In this case, continuity is applied to a four-part system consisting of an unmeasured transect south of the east, centre, and west channels. For each measurement where data are available at these locations, the discharges are normalised so that the south transect and the three branches represents 100 % of the flow passing through the trifurcation control volume. Within this framework, the east channel conveys between 40.90 and 66.09 % of the total discharge, the main channel between 33.91 and 59.10 %, and the west channel between only 0.57 and 7.34 %. On average, the east, centre, and west channels convey 47.59, 50.88, and 2.44 %, respectively. These ranges confirm that the east and main channels act as the primary downstream distributaries, while the west channel remains near zero. However, unlike the Netley Cut system, no survey campaign collected a complete set of simultaneous ADCP measurements at the trifurcation to verify continuity. The reported percentage splits at the trifurcation therefore rely on the assumption of local mass balance and quasi-steady conditions over the measurement

period and should be interpreted as approximate flow partitions rather than fully closed continuity checks.

Taken together, the P1, P2, and P3 percentages and the trifurcation splits reinforce that the Red River is the main hydraulic driver in this reach. When P1 is positive, flow is supplied from the south and is redistributed between P2 and P3 at Netley Cut, after which the discharge is primarily partitioned between the east and main channels downstream, with the west channel providing only a marginal periphery flow path. While brief intervals during which Netley Cut supplies effectively all local flow at the junction cannot be excluded, the available measurements indicate that some portion of the discharge is almost always routed through other pathways within the system.

.

Table 4-3 Discharge % for Netley Cut, Nearby Adjacent Distributary Channels, 2009–2022.

	Flow (%)					
Date	US Netley Cut	Netley Cut	DS Netley Cut	West Channel	Centre Channel	East Channel
June 12 2009	100.00	43.01	56.99*	0.57	52.39	47.04
June 29 2009	100.00	42.61*	57.39	0.91	56.63	42.47
June 30 2009	100.00	29.44*	70.56		52.00	48.00
*July 08 2009***	100.00	39.29	60.84			
July 08 2009	100.00	48.13*	51.87			
July 08 2009	100.00	39.58	61.32	1.52	52.94	45.54
July 10 2009	100.00	41.11*	58.89		33.91	66.09
July 10 2009	100.00	16.15*	83.85			
July 10 2009	100.00	28.31*	71.69			
*July 13 2009***	100.00	30.65	47.31			
*July 13 2009***	100.00	42.71	43.78	1.85	52.87	45.27
*July 31 2014***	100.00	43.60	71.28			
July 3 2019	100.00	31.13	68.87		59.10	40.90
*August 7 2020***	100.00	56.62	44.43	7.34	47.22	45.43
August 7 2020	100.00*	43.14	56.86			
July 8 2021	23.45	76.55	100.00*			
*July 29 2021***	96.10	6.94	100.00			
Aug 25 2021	1.49	98.51	100.00*			
Sept 15 2021	94.94	5.06	100.00*			
Oct 18 2021	95.76	4.24	100.00*			
*July 14 2022***	100.00	52.82	50.74			

Note: * identifies flow measurements at Netley Cut that were estimated on the basis of an assumed 100% continuity at that location. ** identifies flow measurements for which point measurements were obtained at all three Netley Cut cross sections, allowing estimation of continuity error in addition to the reported discharge. US = Upstream, DS = Downstream.

For the subset of observations where P1 is positive and the Netley Cut system is directed toward Lake Winnipeg, the percentage flow splits correspond to P2 discharges of 59.2 m^3/s at the lower end of the observed range, 251.65 m^3/s on average, and 539.22 m^3/s at the upper end. These values highlight that, when the hydraulic gradient is oriented from P1 toward P3 and Netley Lake, P2 diverts on average about 39.27 % of the P1 inflow, with individual events where it captures substantially more (up to 56.62 %). Previous studies reported typical diversion ratios on the order of one third, so the larger average fraction and higher peak values observed here are consistent with an increasing relative contribution of P2 over time. This interpretation aligns with the expectation that progressive widening and deepening of Netley Cut enhance its conveyance capacity, allowing a greater share of discharge to be routed into the Netley Delta, such that Netley Lake receives a larger fraction of the flow relative to the lower reach of the Red River. At the same time, the highest diversion ratios occur in only two discrete discharge measurements, both from the most recent survey campaigns, so any inference of a long-term trend toward increasing flows into Netley Lake through Netley Cut should be regarded as indicative rather than definitive.

The corresponding statistics for the percentage flow split at P2 are summarised in Table 4-4. For cases where P2 was measured directly by ADCP, Netley Cut conveyed between 30.65 and 56.62 % of the P1 inflow, with a mean of 42.25 %. For cases where P2 was estimated from continuity, the inferred flow split ranges from 16.15 to 48.13 %, with a lower mean of 34.29 %. When the measured and continuity-based values are combined, P2 ranges between 16.15 and 56.62 % of the P1 inflow, with an overall mean of 39.27 %. This combined mean is consistent with the conclusion that, under lakeward flow conditions, Netley Cut typically captures on the order of two-fifths of the Red River discharge at P1.

Table 4-4 Netley Cut flow split when P1 accounts for 100% inflow

	Flow (%)		
	Measured	Continuity	Combined
Minimum	30.65	16.15	16.15
Mean	42.25	34.29	39.27
Max	56.62	48.13	56.62

Figure 4-11 presents the series of discharge observations at Netley Cut for conditions when flow is directed from the Red River into Netley Lake. The panel shows discharges at P1, P2, and P3 in, together with the concurrent Netley Cut water surface elevation plotted as a black line. Blue symbols denote discharges obtained directly from ADCP transects, whereas red symbols indicate discharges inferred from continuity for locations where only partial measurements were available. Water levels for datasets in 2020, 2021 and 2022 were taken directly from the Netley Cut, whereas water levels for prior datasets were retrieved from Water Survey Canada at Breezy Point (05OJ022). P1 is treated as the sole inflow to the three-part system in this representation, with P2 and P3 together representing the partitioning of this inflow. For most observations, the discharge at P3 exceeds the discharge entering P2, confirming that over the survey period most of the flow contains itself to the Red River.

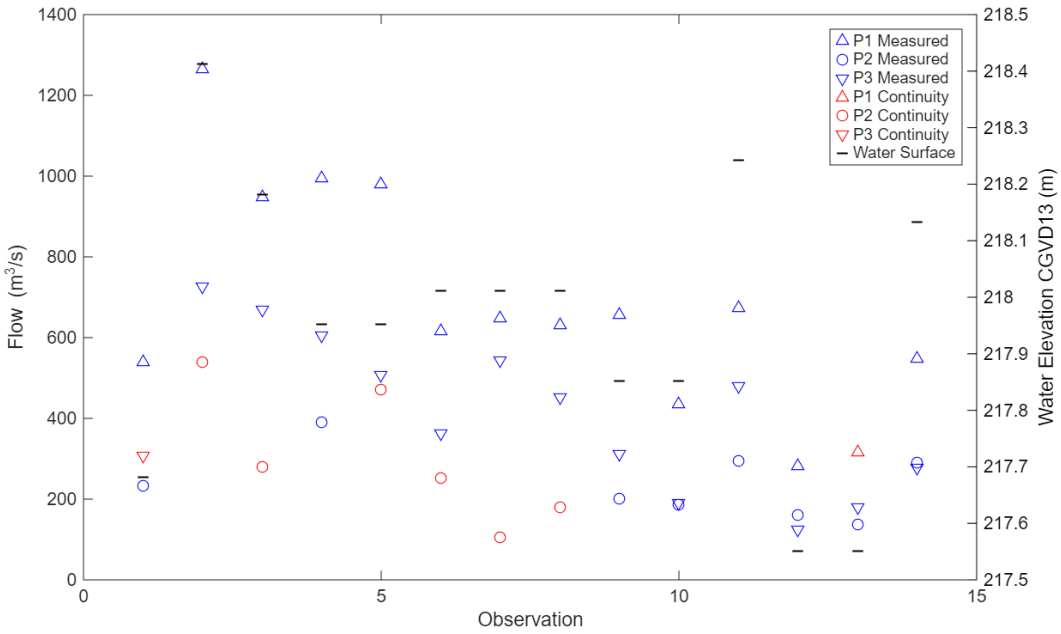

Figure 4-11 Discharge observations when P1 accounts for 100% inflow

Figure 4-12 recasts these same observations in terms of flow splits as a percentage and associated continuity error. Only cases with complete measurements at P1, P2, and P3 are included. In this figure, discharges at P2 and P3 are expressed as percentages of the inflow at P1, and the continuity error is shown as a bar chart representing the deviation from perfect mass balance for the Netley Cut control volume. The continuity errors range from approximately −22.0 % to +14.9 %, with four of the seven values lying within about ±4 %. The larger errors occur where there were longer intervals between successive transects and where hydraulic conditions changed appreciably between passes. For example, at observation 11, repeat measurements at P1 taken 23-minute apart differed by 146 m³/s, indicating that short-term variability in stage and velocity structure was significant during that period. These results illustrate that, while most surveys achieved relatively good closure, non-steady hydraulic conditions and temporal separation between transects can produce appreciable continuity errors that must be considered when interpreting the flow partitioning among P1, P2, and P3.

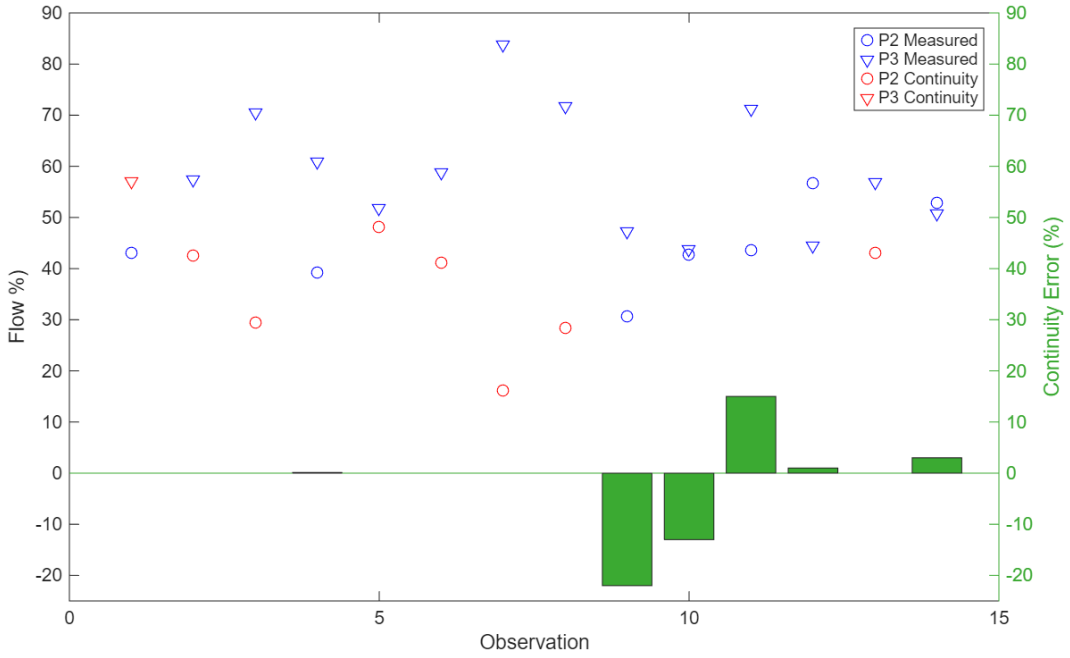

Figure 4-12 Flow split and continuity error for discharge observations when P1 accounts for 100% inflow

Figure 4-13 presents the subset of discharge observations for which P3 is treated as the sole inflow to the three-part system, that is, cases where flow is directed from north to south along the Red River. In this configuration, water enters the control volume at P3 and either continues into Netley Lake through P2 or returns toward the south along P1. The plotted points show measured and continuity-inferred discharges at P1, P2, and P3 together with the concurrent water surface elevation. Many of the P1 and P2 values lie near zero, or are slightly negative, indicating periods of flow reversal or near-stagnation in the upstream reach and in Netley Cut relative to the adopted sign convention.

These conditions arise when Red River discharges are low and lake or marsh water levels are relatively high and sustained. Under such circumstances, the hydraulic gradient between Lake Winnipeg, Netley Lake, and the lower Red River is weak or reversed, so that the usual south-to-north through-flow pattern is replaced by a configuration in which P3 dominates the inflow and

the junction behaves as a recirculation or stagnation zone. The limited but similar discharge magnitudes of P1 and P2 in Figure 4-13 indicates that exchange between P1 and P3 is constrained and that net transport toward Netley Lake through P2 is minimal under these conditions. These observations complement the earlier analysis of sign combinations at P1, P2, and P3 and confirm that, during low-flow periods with elevated water levels, Netley Cut and the adjacent reaches can shift from an actively conveying state to one characterised by weak circulation and intermittent reversals.

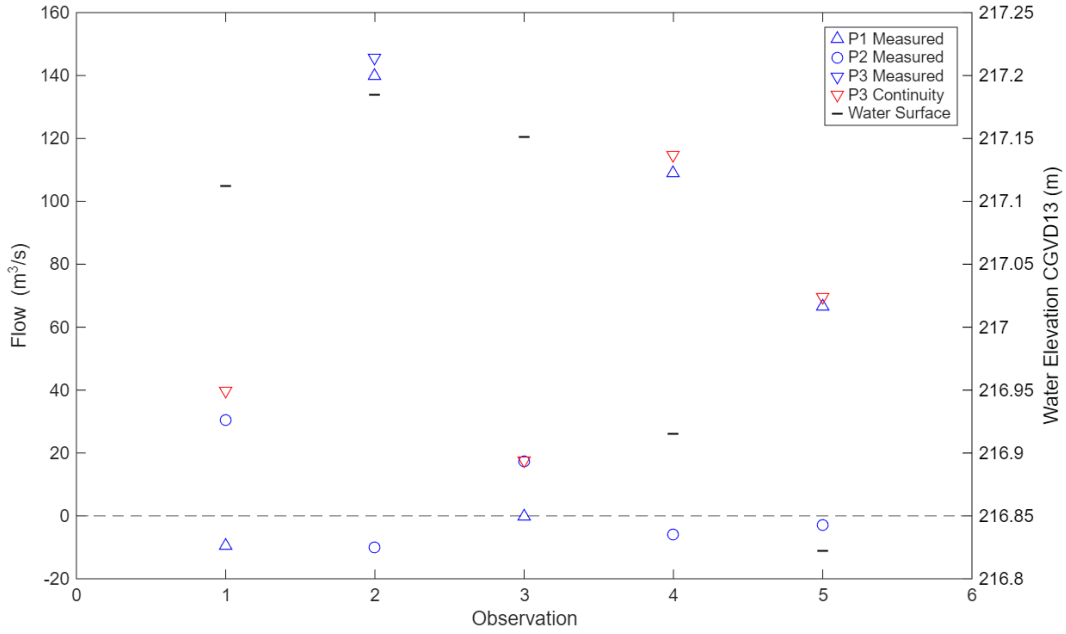

Figure 4-13 Discharge observations when P3 accounts for 100% inflow

The patterns shown in Figure 4-13 must be interpreted cautiously because only five observations are available, so the discussion herein is necessarily qualitative rather than statistically robust. Nonetheless, the data suggest that discharges at the P1, P2 and P3 exhibit similar magnitudes in pairs with the outlier showing near-zero or slightly negative flow. For total flow between 50 to 150 m^3/s, P1 and P3 are of comparable magnitude while P2 is close to zero or negative, which is consistent with flow proceeding from north to south along the Red River

with limited exchange through Netley Cut. At lower P3 discharges, below approximately 50 m^3/s, the pairing shifts: P2 and P3 become more similar, while P1 becomes stagnant or negative. This behaviour suggests that, under low-flow conditions, discharge at the junction is preferentially redirected from P3 into P2, with the upstream reach partly decoupled from the system. No clear, monotonic relationship is evident between these changes in pairing and water surface elevation, as similar stages occur in both the P1–P3 and P2–P3 pairing cases. However, the different but similar response between pairs in low-flow conditions does suggest evidence of seiching events cancelling out the discharge from the Red River at variable water levels. Overall, the observations point to the possible existence of a flow magnitude threshold at which the Netley Cut system transitions from primarily along-channel conveyance in the Red River to increased diversion into P2 from P3, but this inference remains tentative given the limited sample size.

4.3.2 Water Level Fluctuations

Water level fluctuations within Netley–Libau Marsh were evaluated using the processed LeveLogger records described in Section 4.2.3. The same constant parameter set for crest detection was applied across all stations. A minimum peak prominence of 0.12 m was used, so that only crests and troughs exceeding approximately 12 cm relative to their surrounding water levels were retained. A minimum temporal separation of 30 hours between successive extrema was imposed, limiting detection to at most one representative crest and trough over roughly a day-and-a-quarter and filtering out higher-frequency variability. Finally, a matching tolerance of 20 hours was adopted for pairing extrema between stations, so that events were considered concurrent only if they occurred within 20 hours of each other. This approach allowed the temporal shift in water level fluctuations to be analysed at the marsh scale, with particular

emphasis on seiche-driven oscillations on Lake Winnipeg and the associated response times, expressed as lag hours, from LL01 to LL02, LL03, and LL04. The objective was to characterize how rapidly water level disturbances at the lake boundary propagate through the marsh over the monitoring period from 23 June to 18 October.

The processed water surface elevation time series were examined independently for each LeveLogger to confirm that local extrema were being identified consistently across the network. Figure 4-14 presents the resulting water level records at LL01 through LL04 together with the detected local maxima and minima. Visual inspection shows that crests and troughs occur at approximately the same times at all four stations, with the orange and yellow markers displaying the crests and troughs of the water level data. Visual inspection of the extrema show that the chosen combination of prominence, temporal separation, and matching tolerance is sufficient to capture the dominant seiche-scale oscillations without over-identifying minor short-term fluctuations. Across the full record, approximately 38 local maxima and 37 local minima were identified and used in the subsequent lag analysis, providing a consistent set of events from which to quantify the response of the marsh to seiching.

Lag times were calculated relative to LL01, such that each event lag represents the time of the local extremum at a given station minus the time of the corresponding extremum at LL01 (Table 4-5). Under this convention, a negative lag indicates that the station responds earlier than LL01, while a positive lag indicates that the station responds later. If the marsh behaved as a simple, linear system, one would expect stations located farther from LL01 to exhibit progressively larger lag magnitudes, and the lag associated with local maxima and minima to be similar at a given station because both peaks and troughs reflect the same seiche-driven oscillation.

Table 4-5 Mean lag times for local water level extrema at LL02–LL04 relative to LL01

Station	Extremum	Mean lag (h)	Number of events (n)
LL02	Maxima	-0.31	38
LL02	Minima	-0.01	37
LL03	Maxima	-0.61	37
LL03	Minima	-0.63	38
LL04	Maxima	-1.07	36
LL04	Minima	-1.05	37

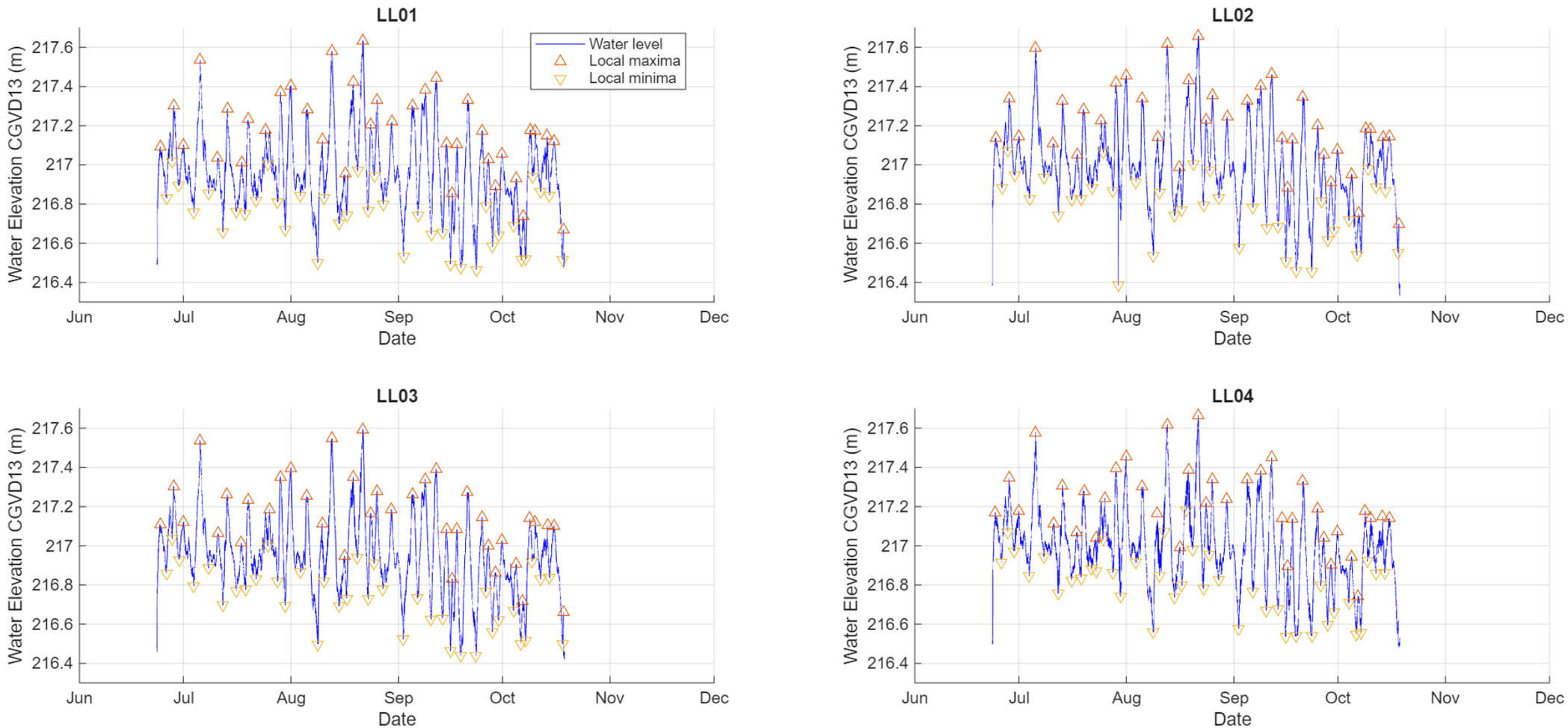

Figure 4-14 Local Water Elevation Extrema for LeveLogger Deployments in 2021

The results in Figure 4-15 are broadly consistent with these expectations. The mean lags for both maxima and minima increase in magnitude from LL02 to LL04, indicating that LL01 consistently responds last. LL02 leads LL01 by about 0.31 h for maxima and essentially coincides with LL01 for minima (−0.01 h). LL03 leads LL01 by about 0.61–0.63 h for both maxima and minima, while LL04 shows the largest offset, with mean lags of −1.07 h for maxima and −1.05 h for minima. The increase in lag magnitude from LL02 through LL04 suggests that seiche disturbances propagate through the marsh toward LL01 over a time scale on the order of one hour, and that once established, the oscillation is transmitted relatively latitudinally across the marsh.

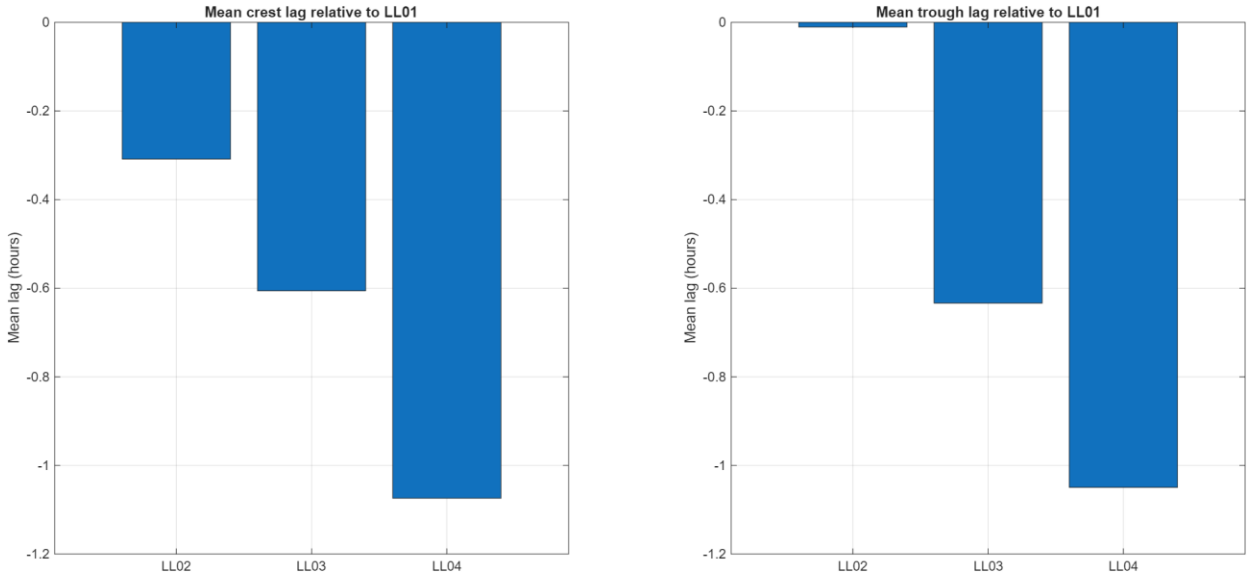

Figure 4-15 Mean crest and trough lag times at LL02–LL04 relative to LL01

The similarity between the mean lags for maxima and minima at LL03 and LL04 indicates that peaks and troughs travel through the system with comparable response times at these more distant stations. In contrast, LL02 shows a substantial difference between the mean lag for

maxima (−0.31 h) and minima (−0.01 h). One possible interpretation is that the time required to push water upstream through the marsh and establish a new high-water level at LL01 is slightly longer than the time required for the system to relax back toward its mean elevation. Under this interpretation, LL02 experiences peak water levels earlier than LL01 because the advancing high-water front has not yet fully propagated to LL01, whereas troughs at LL02 and LL01 occur nearly simultaneously once the oscillation has passed and water levels are draining back toward the mean.

4.4 Conclusion

This chapter combined discrete ADCP-based discharge measurements with continuous water level records from pressure transducers to quantify flow partitioning at Netley Cut and the Red River trifurcation, and to assess whether marsh-wide water level fluctuations and associated lag times indicate a coherent hydraulic response within Netley–Libau Marsh. Measurements collected between 2009 and 2022 were compiled using post-processed stage records from four LeveLogger sites and short continuous velocity records from two Argonaut-SW deployments. Together, these datasets quantified flow partitioning at two key hydraulic controls, characterized marsh-wide water level behaviour, and documented short-term variability in discharge and circulation.

At Netley Cut, the combined ADCP and continuity-based estimates show that the lower Red River remains the primary hydraulic driver, but that the fraction of flow diverted into Netley Lake is variable and has marginally increased relative to the estimates reported by Haresign (2012). The final combined mean flow split indicates that, when P1 provides the sole inflow, Netley Cut typically conveys 39.27 % of the concurrent discharge at P1, representing a substantial and hydraulically significant portion of the total Red River inflow. Event-scale

estimates remain clustered around this mean, and recent measurements in 2020 and 2022 include individual cases where more than 50 % of the Red River inflow is routed into the marsh, with the remaining flow conveyed downstream along P3.

Furthermore, cases where P3 supplies the sole inflow illustrate a contrasting low-flow regime in which the usual south to north through-flow pattern weakens or reverses. Elevated and persistent stages within Lake Winnipeg and Netley Lake reduce the hydraulic gradient along the lower Red River, producing near-stagnant or slightly negative discharges at P1 and P2 while P3 continues to convey modest flow. For moderate total discharges, P1 and P3 are of similar magnitude and P2 is small; at very low P3 discharges, P2 and P3 converge and P1 becomes stagnant or negative. Although based on a limited number of events, these regimes are consistent with seiche-modulated exchange, where the junction alternates between actively conveying flow and a state characterised by weak circulation and intermittent reversals.

South of Netley Cut, the trifurcation analysis indicates that mean flow splits of approximately 47.6 %, 50.9 %, and 2.4 % are routed through the east, centre, and west channels, respectively, such that the east and centre channels together carry nearly all of the Red River flow and the west channel typically conveys only a small residual. Overall, these findings indicate that the junction adjacent to Netley Cut functions as a dynamically partitioning node whose relative contributions adjust to the combination of Red River discharge and boundary water levels, and that Netley Cut represents a consistently important pathway for routing Red River water into Netley–Libau Marsh.

Continuous water level records show small stage differences, synchronous oscillations, and short time lags between monitoring sites, indicating strong hydraulic connectivity across Netley–Libau Marsh and that short-term water level variability is largely driven by seiche activity on

Lake Winnipeg. Time-lag analysis of matched maxima and minima shows that water level oscillations at interior sites typically lead those at LL01 by several tenths of an hour to just over one hour, for both peaks and troughs. This behaviour reflects spatially coherent set-up and relaxation across the marsh, with short-term storage and phase differences modulating how seiche waves move throughout the system.

5. Turbidity

Turbidity is a key water quality parameter in aquatic systems, reflecting the clarity of water and the concentration of suspended matter. Understanding turbidity in NLM is critical because the marsh's ecological role has shifted over time. Historically, NLM acted as a nutrient and sediment sink, with dense emergent vegetation trapping sediments and uptaking nutrients before water entered Lake Winnipeg. In recent decades, however, NLM's capacity to retain nutrients and sediments has declined alongside extensive loss of plant biomass (Grosshans et al., 2004). The Red River now delivers high loads of sediment and nutrients through Netley Cut into the marsh and onward to Lake Winnipeg, contributing to increased turbidity and eutrophication in both the marsh and the lake (Lake Winnipeg Stewardship Board, 2006). Turbid, sediment-laden inflows and invasive common carp (which uproot vegetation and stir up sediments) have pushed the marsh from a clear-water, vegetated state to a turbid, algae-dominated state. This degradation of water quality not only hampers marsh vegetation reestablishment (as light penetration is reduced and sediments remain suspended) but also diminishes NLM's ability to improve the water quality of Lake Winnipeg through CNP absorption (Grosshans et al., 2012).

Given these concerns, this chapter evaluates turbidity conditions in NLM under both natural (background) and project-influenced scenarios. Specifically, it examines how restoration activities under the NLMRP (notably dredging and sediment re-deposition) affected turbidity relative to natural background levels. Turbidity is also addressed in the context of environmental regulations, as it is often a regulated parameter in licenses for in-water works. The goal is to determine whether NLMRP construction activities caused any sustained increases in turbidity above natural variability, thereby informing compliance with licensing requirements and the

overall impact of the project on marsh water quality. To that end, both on-site turbidity monitoring (near the dredging and deposition operations) and continuous background monitoring (with instruments deployed in Netley Lake) were conducted and analyzed. The results are used to assess if project-induced turbidity differed from background turbidity and whether any exceedances of regulatory thresholds occurred.

5.1 Background

Turbidity is an optical property of water that indicates how clear (or murky) the water is. A highly turbid water sample appears dark, murky, or colored due to the abundance of suspended matter, allowing little to no light to pass through, whereas a non-turbid sample is clear and nearly transparent. The suspended matter that causes turbidity is often referred to as seston, which encompasses a mixture of living and non-living particles in the water. These may originate from outside the system as allochthonous inputs such as silt, clay, humus, and detritus, or from within the system as autochthonous material like phytoplankton, zooplankton, and bacteria (YSI Environmental, 2001). In general, the greater the amount of seston in the water, the higher the turbidity. It is important to note that dissolved colored substances (which contribute to the "true color" of water when particles are filtered out) are not themselves sources of turbidity, but they can affect turbidity measurements by absorbing light. Meanwhile, the apparent color of a water body (the color we observe directly) often changes with turbidity—for example, a greenish pond in summer might signal an increase in phytoplankton that both adds suspended particles and changes the water's color. The overall perceived color of water results from a combination of true and apparent color, essentially the wavelengths of light reflected back to the observer (YSI Environmental, 2001). By distinguishing between these forms of color and the sources of seston, one can better interpret turbidity readings in different environmental contexts.

Turbidity is an important parameter in water quality monitoring for several reasons. First, it serves as a convenient indicator of water clarity and suspended sediment levels, both of which are fundamental to aquatic ecosystem health. High turbidity can reduce light penetration, impairing photosynthesis in aquatic plants and algae; furthermore, suspended particles can clog fish gills, smother benthic habitats, and ultimately reduce fish resistance to disease (USEPA, 2021). Regulatory agencies frequently use turbidity as a proxy for environmental disturbance, especially when rapid assessment is needed during construction, dredging, or restoration activities (Manitoba Conservation and Climate, 2021). Correspondingly, turbidity is widely used as a surrogate measurement for suspended sediment concentration (SSC). Empirical regression models correlate turbidity readings with SSC or total suspended solids (TSS), allowing researchers and engineers to estimate sediment loads quickly in the field—a task far more efficient than laboratory-based TSS analysis. This rapid field assessment capability is why environmental projects rely heavily on turbidity monitoring to infer sediment pollution levels and ensure compliance with water quality standards.

Turbidity in natural waters is typically quantified in nephelometric turbidity units (NTU), which provide a relative measure of the intensity of light scattered at a fixed angle from a beam passed through the water column, standardized against a calibrated suspension of formazin. The Canadian Council of Ministers of the Environment (CCME) publishes guidelines for water that utilize NTU as a variable for quantifying adverse effects that may threaten aquatic life. In “clear flow” river or lake conditions these guidelines state that induced turbidity should not exceed 8 NTU above background during a 24-hour period, with a long-term average increase of no more than 2 NTU over 30 days. In more turbid or high-flow conditions, the same 8 NTU short-term limit applies when background turbidity is between 8 and 80 NTU, but when background

exceeds 80 NTU, the increase should be limited to 10% of background levels (CCME, 2002). Similar guidelines are reflected in Manitoba and British Columbia's water quality guidelines, which typically allow a 5 NTU increase over background where TSS < 25 mg/L—or no more than 10% when background is already high TSS > 250 mg/L (B.C. Ministry of Environment and Climate Change Strategy, 2021; Manitoba Water Stewardship, 2011). Thus, turbidity is typically the water quality parameter specified by environmental agencies to regulate the degree of change allowed in a water body as a result of work that may have an adverse effect on water quality.

5.1.1 Turbidimeters

A turbidimeter qualitatively measures the amount of incident light scattered by particulate matter when passing through a water sample. Light becomes scattered as it reflects off dissolved and suspended matter in the water column. The size, shape, density, and composition of a given particle will influence the degree and intensity of reflection, which affects the turbidity value. Two different types of incident light are used to address difficulties in measuring scattered light. The first type is a tungsten filament that projects light into the water column at a wavelength between 400 and 560 nm. This is referred to as broadband or polychromatic incident light as it produces white light that covers a wide wavelength. However, there can be significant interferences when using tungsten filaments due to the absorption of light by particles with matching wavelengths. LED emitting diodes were introduced as an alternative incident light source following ISO Standard 7027 to adjust for this interference. These are referred to as monochrome or near infrared (NIR) light sources and fall within the range of 760-900 nm. Due to a shorter wavelength within the NIR range, interference due to color absorption is reduced. However, the drawback to using monochromatic light sources is that there is reduced sensitivity to fine particulate matter. The wider wavelength used by polychromatic sources allows for

greater sensitivity to shorter wavelengths and thus produces a more accurate measurement of fine particles compared to monochromatic sources.

In addition to the type of light source, turbidity is dependent on the amount of scattered incident light measured by either a single or multitude of detectors aligned at specific angles to the water sample. The selected angle is based on a chosen standardized testing method that fits the environmental and physiological characteristics of the water being sampled. The common angles of measurement are 45° (backscatter), 90° (nephelometric), 135° (forward scatter), and 180° (attenuation). Recording incident light at more than one angle is referred to as multibeam detection and provides turbidity values over a larger range (Kitchener, 2019).

5.1.2 Turbidity and Nutrients in the Context of NLM

NLM historically functioned as a critical nutrient filter or "sink," with dense root systems and organic soils trapping sediments and absorbing nutrients such as carbon, nitrogen, and phosphorus from the Red River before they reached Lake Winnipeg (Wrubleski et al., 2018). This filtration capacity helped regulate water clarity and reduce nutrient loading to the lake. However, as the marsh's plant biomass and organic soils have declined, so too has its retention capacity. The construction of Netley Cut, which now channels a larger share of the Red River's flow directly into the marsh, has further transformed NLM from a sink into a conduit for nutrients and sediments. Once this sediment-laden water enters Lake Winnipeg's south basin, its velocity slows and much of the suspended material settles, adding to bottom deposits. Combined with the lake's broad, shallow surface area, this results in strong spatial variability in turbidity: the south basin, particularly near the Red River delta, is consistently more turbid, while the north basin remains comparatively clearer. Long-term monitoring between 1999 and 2007 confirms this contrast, with average turbidity values of 13–24 NTU in the south basin (and episodic peaks

above 60 NTU) compared to only 2–3 NTU in the north basin (Environment and Climate Change Canada & Manitoba Agriculture and Resource Development, 2020).

Now, with more of the Red River's flow coursing directly through Netley Cut, NLM can serve as a conduit for nutrients and sediment into Lake Winnipeg as well as a sink. The Red River drains a large, intensively developed watershed (~127, 000 km² of agricultural lands, urban areas, and industries) and carries high loads of nitrogen, phosphorus, and other pollutants. Long-term monitoring shows Red River nutrient concentrations have risen markedly. Between 1978 and 1999 alone, Red River total nitrogen (TN) increased ~29% and total phosphorus (TP) ~58% due to agricultural runoff, manure, and urban effluents in the watershed (Grosshans et al., 2004). TN and TP loading to the Red River continued to increase from 1997 to 2016 and the total yield of phosphorus and nitrogen were estimated to highly likely increase across this two decade period (Yates et al., 2022). Today the Red River is the dominant nutrient source to hypertrophic Lake Winnipeg, contributing about 69% of the lake's annual phosphorus load while providing only ~16% of total inflow. Its flow-weighted mean TP concentration (~0.418 mg/L) is an order of magnitude higher than that of the Winnipeg River, reflecting the heavy nutrient enrichment of the Red River basin (Environment and Climate Change Canada & Manitoba Agriculture and Resource Development, 2020). As the highly nutrient-rich water is thrust into NLM, eutrophication concerns within the marsh itself become exacerbated. Excessive phytoplankton and filamentous algae growth within marshes can further impair aquatic plants by inhibiting photosynthesis ('shading' of the water column) and depleting oxygen when the algae decompose (Khan & Ansari, 2005).

Turbidity is a closely related concern. The marsh's waters have shifted from a clear-vegetated state to a turbid-algal dominated state (Grosshans et al., 2004). The Red River's sediment load,

especially during floods, turns much of NLM highly turbid. Satellite imagery analysis corroborates that the south basin of Lake Winnipeg near the marsh is consistently more turbid than the clearer north basin, due in large part to sediment-laden inflows from the Red River delta (Environment and Climate Change Canada & Manitoba Agriculture and Resource Development, 2020; McCullough et al., 2001). Invasive common carp have been noted to further degrade water clarity through their benthic feeding habits, uprooting vegetation and resuspending sediment. This activity continuously disrupts plant regrowth and maintains a turbid state within the marsh ecosystem (Grosshans et al., 2004).

Research shows that the decline of emergent vegetation in NLM has likely exacerbated water quality issues. Aquatic plants and wetlands can act as a natural buffer, uptaking nutrients and trapping sediments. The extensive loss of a productive hemi-marsh environment, as evidenced by an increase in 41% of open water area and a 41% loss of emergent and wet meadowed vegetation between 1979 to 2001 (Kowal, 2019), has substantially diminished the marsh's ability to uptake nutrients biologically and stabilize sediments. The aforementioned factors (invasive carp, eutrophication, loss of vegetation, etc.) contribute to a positive feedback loop, wherein high turbidity from suspended sediment and algal blooms hinder plant reestablishment, and the lack of vegetation perpetuates poor water clarity and conditions favoring algae. On a larger scale, the degradation of NLM's water quality has implications for Lake Winnipeg. The marsh no longer sequesters as much phosphorus or sediment as it once did, so more of the Red River's nutrient load ends up in the lake, contributing to Lake Winnipeg's chronic algae blooms and ecosystem imbalances (Wrubleski et al., 2018). This loss of function has partly motivated recent marsh restoration discussions (Clean Environment Commission, 2015; KGS, 2019).

In summary, background turbidity in Netley-Libau Marsh is naturally high due to the Red River's influence and historical changes, but it is also a regulated concern. Environmental agencies often specify turbidity as a parameter to control during in-water construction, because it serves as a convenient surrogate for SSC in the field. Thus, understanding both the natural variability of turbidity in NLM and the potential elevation of turbidity by restoration activities assists in distinguishing project-related effects from background conditions, guiding adaptive management during construction, and demonstrating compliance with licensing thresholds. The following sections outline the licensing requirements that governed turbidity monitoring for the NLMRP, and the methodology used to measure turbidity on-site and in the marsh's background.

5.2 Licensing Requirements

Turbidity monitoring for the NLMRP was carried out in accordance with environmental licensing conditions set by federal and provincial authorities. Specifically, the project's authorizations from the Department of Fisheries and Oceans (DFO; Path No. 19-HCAA-00536) and from Manitoba Conservation and Climate (Environment Act License No. 3350) stipulated several water quality monitoring requirements related to turbidity (Manitoba Conservation and Climate, 2021). The latter license designated four key locations for water sampling (with concurrent drone imagery) to track turbidity during dredging and sediment deposition operations:

a) at the dredging site, within 5 m downstream of the dredge head;
b) inside the enclosed deposition area (within the containment berms);
c) in Netley Lake immediately adjacent to the deposition area (just outside the containment); and
d) in Netley Lake at least 100 m away from the deposition area (further into the lake background).

These locations (a–d) were chosen to gauge how far and to what degree turbidity from the dredging and deposition might spread beyond the work site: from directly at the dredge, to inside the containment, to near-field and far-field lake locations. The licenses further required adaptive management if turbidity rose too high. In particular, if the TSS concentration at the near-field background site (location c) exceeded that at the far-field site (location d) by more than 25 mg/L on two consecutive days, then additional containment measures would need to be implemented. (This threshold is effectively a measure of project-related turbidity increase beyond natural background. In practice, turbidity in NTU was measured and then an approximate conversion to TSS could be made using an established relationship.) An equation provided in the license for estimating TSS from turbidity was:

$$\text{TSS} = 1.0397 \times \text{Turbidity}$$

This conversion was stipulated as a guideline to relate turbidity readings to TSS levels, though it carries uncertainty without site-specific calibration. Notably, this simple linear factor assumes a consistent turbidity-to-SSC relationship; in reality, the accuracy of such an estimate can be limited by differences in sediment particle characteristics and requires field verification for precision.

5.3 Methodology

The following methodology details the instrument selection, field techniques at the dredge site, and background measurements in Netley Lake as they relate to turbidity monitoring. Turbidity was measured using a handheld turbidimeter, a fixed in situ multiparameter sonde, and supporting aerial imagery to capture both localized effects near the construction works and broader patterns at the lake scale. The equipment and its operating principles are introduced first,

followed by a description of how measurement locations were chosen at the dredge site, how compliance and reference conditions were defined, and how sampling routines were adjusted in response to low water levels, preferential flow paths, and practical constraints at the dredge head. The methodology then outlines how background turbidity and event-scale responses were monitored in Netley Lake and how these records were used to interpret and contextualize the short-term observations collected around the dredging operation.

5.3.1 Measurement Equipment

Turbidity characterization relied on a combination of point-based sensors and visual observations. A handheld turbidimeter (Hach DR900®) was used for discrete spot measurements at specific locations during construction activities, while a multiparameter sonde (Hydrolab® DS5X) provided continuous in-situ turbidity recordings suitable for tracking background conditions and lake-scale responses. In parallel, an unmanned aerial vehicle (DJI Phantom 4 Pro® or DJI Mavic Mini®) was periodically deployed to capture coincident aerial imagery of surface conditions. These images offered a view of sediment plumes and turbidity patterns and were used to interpret the spatial context of the point measurements.

5.3.1.1 Hach DR900

Turbidity was measured with a Hach DR900® for discrete spot checks during construction activities configured to an absorptometric turbidity program (HACH, 2013). In this method the instrument measures the attenuation of a collimated light beam as it passes through a filled cuvette. The reading is reported in Formazin Attenuation Units (FAU), calibrated against primary formazin standards, with an analytical range of 21–1000 FAU. Because absorptometric systems detect transmitted rather than scattered light, their response decreases as turbidity increases, and results are expressed in FAU rather than NTU (C. W. Anderson, 2005). The

DR900® itself is an LED-sourced colorimeter that operates at fixed visible wavelengths of 420, 520, 560, and 610 nm and reads sealed glass or plastic cells. Turbidity is measured at 520 nm.

Practical implications for sampling are straightforward and were conducted in the field as follows: Clean the exterior of the cuvette, fill the cuvette carefully to avoid bubbles and fingerprints, mix gently to limit particle settling, wipe the exterior, and read immediately. As with any spectrophotometric or colorimetric turbidity method, colored dissolved substances and path-length effects can bias readings; therefore, FAU measurements should be documented as such and not substituted for nephelometric results in compliance determinations (C. W. Anderson, 2005; HACH, 2013)

5.3.1.2 Hydrolab DS5X Sonde

Continuous background turbidity in Netley Lake was measured with a Hydrolab® DS5X multiparameter sonde. This sensor follows ISO 7027 nephelometry, which uses an infrared LED near 880 nm and a detector positioned at 90 degrees to the incident beam to minimize color interference (HACH, 2006). The sensor is specified for 0–3000 NTU with ±1% accuracy up to 100 NTU, ±3% to 400 NTU, and ±5% to 3000 NTU, and 0.1 NTU resolution up to 400 NTU. The instrument supports unattended logging with configurable intervals and includes deployment features such as a wiper, flow-cell options, and warm-up settings to ensure stable readings and reduced fouling during long deployments (HACH, 2010).

5.3.1.3 Note Respecting NTU and FAU

Although FAU and NTU are both calibrated against the same primary standard (formazin), they arise from different optical geometries: FAU from attenuation at 0° and NTU from scattered light at 90°. Consequently, two instruments can report very different absolute numbers for the same suspension even when calibrated correctly. USGS guidance explicitly treats

spectrophotometric and absorptometric measurements as a distinct method that should be reported in FAU and not interchanged with nephelometric NTU (C. W. Anderson, 2005). Comparative studies corroborate this non-equivalence: cross-instrument tests have documented up to five-fold differences in turbidity for a given suspended sediment concentration, while still producing strong, instrument-specific turbidity–SSC regressions when each instrument is used consistently (Rymszewicz et al., 2017). In other words, cross-calculation or one-time conversions between FAU and NTU are not recommended; results should be interpreted within each instrument's trend domain and analytical purpose.

Accordingly, this study applied two complementary data streams to different objectives. For on-site compliance and plume interpretation, the DR900 provided immediate FAU readings at locations co-located with UAV imagery. These measurements characterized short-term changes and spatial patterns in surface plumes, and because absorptometric methods respond to both scattering and absorption, they were sensitive to highly colored, dense plumes typical of active works. DR900 data were therefore used for relative comparisons over time and space using a consistent method and instrument configuration. To establish background conditions and capture event-scale responses, the DS5X logged NTU continuously in Netley Lake, a nephelometric approach that supports subsequent analyses such as event response and future development of SSC surrogates if site-specific regressions are available. Integration of the two data sets emphasizes synchronization of trends rather than numeric equivalence because FAU and NTU are not interchangeable. Co-occurring peaks, rises, and returns to baseline were compared qualitatively and, where beneficial, with qualitatively correlations on normalized departures from baseline. This preserved each instrument's integrity and avoided the inaccurate interpretations that would result from direct unit-to-unit (NTU-to-FAU) comparisons.

5.3.2 Measurement Techniques On-Site

Turbidity measurements to meet the licensing standard were initially recorded at the proposed locations a) through d) for the first three days of dredging. A modification to the measurement technique that maintained the licensing standard while accounting for dynamic site conditions was developed across the following six days and thereafter finalized for the remainder of the monitoring period. Table 5-1 identifies whether dredging, drone imagery, or turbidity readings occurred while monitors were on site, what the method of sampling was, and any accompanying reasons for activities not occurring. The methods used to acquire turbidity readings were either:

- Licensing: Turbidity readings were analyzed at the locations proposed in the license
- Testing: Turbidity readings were analyzed at the locations proposed in the license along with additional readings to test the viability of collecting samples in different locations.
- Comprehensive: Turbidity readings were analyzed at the locations proposed in the license along with a set of 35 additional readings in finalized locations.

Table 5-1 Daily account of dredging, UAV imagery, and turbidity readings during the NLMRP with accompanying water sampling method and reasoning for an activity not occurring.

Date	Dredging	UAV Imagery	Turbidity	Method	Reasoning
20-Aug-21	Yes	Yes	Yes	Licensing	—
21-Aug-21	No	Yes	No	—	I
22-Aug-21	Yes	No	Yes	Licensing	I
23-Aug-21	Yes	Yes	Yes	Testing	—
24-Aug-21	Yes	No	Yes	Testing	I
25-Aug-21	Yes	Yes	Yes	Testing	—
26-Aug-21	Yes	Yes	Yes	Testing	—
27-Aug-21	Yes	No	Yes	Licensing	II
28-Aug-21	Yes	Yes	Yes	Testing	—
29-Aug-21	No	No	No	—	IV
30-Aug-21	Yes	No	Yes	Licensing	—
31-Aug-21	Yes	Yes	Yes	Comprehensive	—
01-Sep-21	Yes	Yes	No	—	III
02-Sep-21	Yes	No	No	—	I, III
03-Sep-21	Yes	Yes	Yes	Comprehensive	—
04-Sep-21	Yes	No	Yes	Licensing	—
05-Sep-21	No	No	No	—	IV
06-Sep-21	No	No	No	—	IV
07-Sep-21	Yes	Yes	Yes	Comprehensive	—
08-Sep-21	Yes	Yes	Yes	Comprehensive	—
09-Sep-21	Yes	Yes	Yes	Comprehensive	—
10-Sep-21	Yes	Yes	No	—	III
11-Sep-21	Yes	Yes	Yes	Comprehensive	
12-Sep-21	Yes	Yes	Yes	Licensing	—
13-Sep-21	Yes	Yes	No	—	III
14-Sep-21	Yes	Yes	Yes	***Change in Procedure***	
I – High winds or rain	II – Lack of equipment	III – Low water	IV – No activities on site		

September the 14th, the final day of dredging operations, tactics changed from pumping dredged slurry into the deposition area to filling geotubes outside of the secondary containment barrier.

In summary, six days of monitoring followed the minimum licensing standard, five days consisted of testing a new comprehensive method of measuring turbidity, and six days employed the comprehensive method. Dredging activity did not occur on four days throughout the

construction period with an additional four days having no turbidity values due to low water levels. The comprehensive measurement technique consisted of recording turbidity values at 35 locations immediately outside and away from the primary containment barrier as shown in Figure 5-1. These locations were recorded on a handheld Garmin® GPS which allowed for consistent and reproducible data acquisition. The distance from primary containment to the furthest monitoring location within Netley Lake was 273 meters. This layout and distancing allowed for better representation of background conditions in Netley Lake and an understanding of how sediment plumes settle and disperse from the dredge pipe outlet. Recording in fixed locations meant that water quality samples were not at the discretion of the monitor. The comprehensive measurement technique did not include daily sampling within the containment barrier or at five meters downstream of the dredge head because turbidity values recorded during the five trial days consistently exceeded 1000 NTU under all operating and environmental conditions. At these locations the concentration of suspended material was so extreme that it produced complete optical opacity, preventing light penetration through the water column.

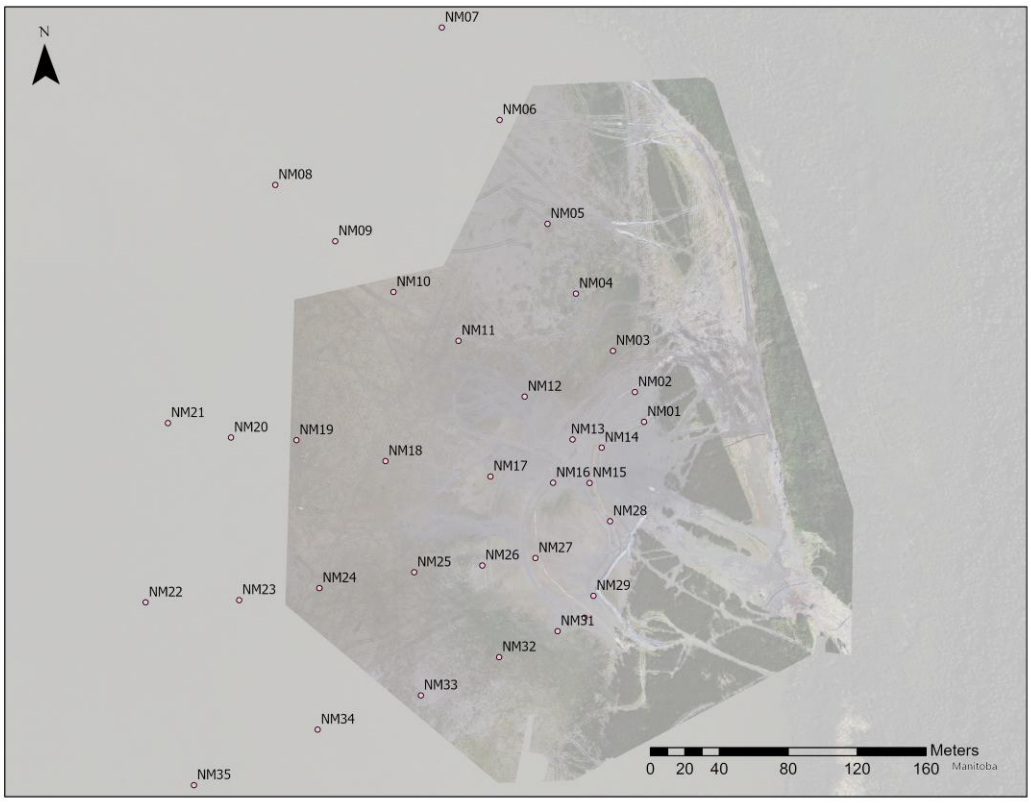

Figure 5-1 Comprehensive turbidity measurement locations for the NLMRP

As illustrated in Figure 5-2, water samples collected simultaneously inside and outside the containment zone highlight this contrast. Four representative samples are shown: three obtained immediately outside the containment barrier and one from within the barrier. The progression from left to right demonstrates the rapid increase in SSC as proximity to the dredge outlet increased. While samples collected outside the containment exhibited varying levels of cloudiness, the sample taken inside the containment zone (furthest right) appears entirely black, underscoring the inability for transmitted light to pass through the column.

Figure 5-2 Representative turbidity samples collected inside and outside the containment barrier

The absence of measurable variation above 1000 NTU in the near-field locations surrounding the dredge head rendered continued monitoring impractical and redundant. Focusing measurements beyond the barrier therefore provided more meaningful data on sediment dispersion and background conditions in Netley Lake. By capturing gradients at increasing distances away from the dredge outlet, the comprehensive approach offered insight into plume attenuation, spatial variability, and compliance relative to licensing standards, while the in-barrier conditions remained consistently beyond regulatory thresholds and beyond the resolution of the adopted instrumentation.

The change in sampling method was developed because the proposed licensing method proved to be insufficient to capture the extent, concentration, or shape of sediment plumes due to low water levels in Netley Lake, and preferential flow paths from the dredge pipe outlet.

5.3.2.1 Impact of Low Waters

Across the 26 days of construction there were four days when water levels dropped below the minimum bed elevation required to collect accurate water quality samples. The impact on water quality sampling for any respective day depended on the minimum bed elevation and the location of the dredge pipe outlet. Figure 5-3 shows the change in bed elevation throughout the deposition area before construction began. Elevations are based off single point positions taken in undisturbed soil. Once construction began, these elevations increased due to sediment deposition. If water levels were lower than those shown in Figure 5-3 and the dredge pipe outlet was situated higher than the water surface elevation, then the expelled slurry would not mix with any lake water, yielding a turbidity reading beyond the detection range of the DR900®.

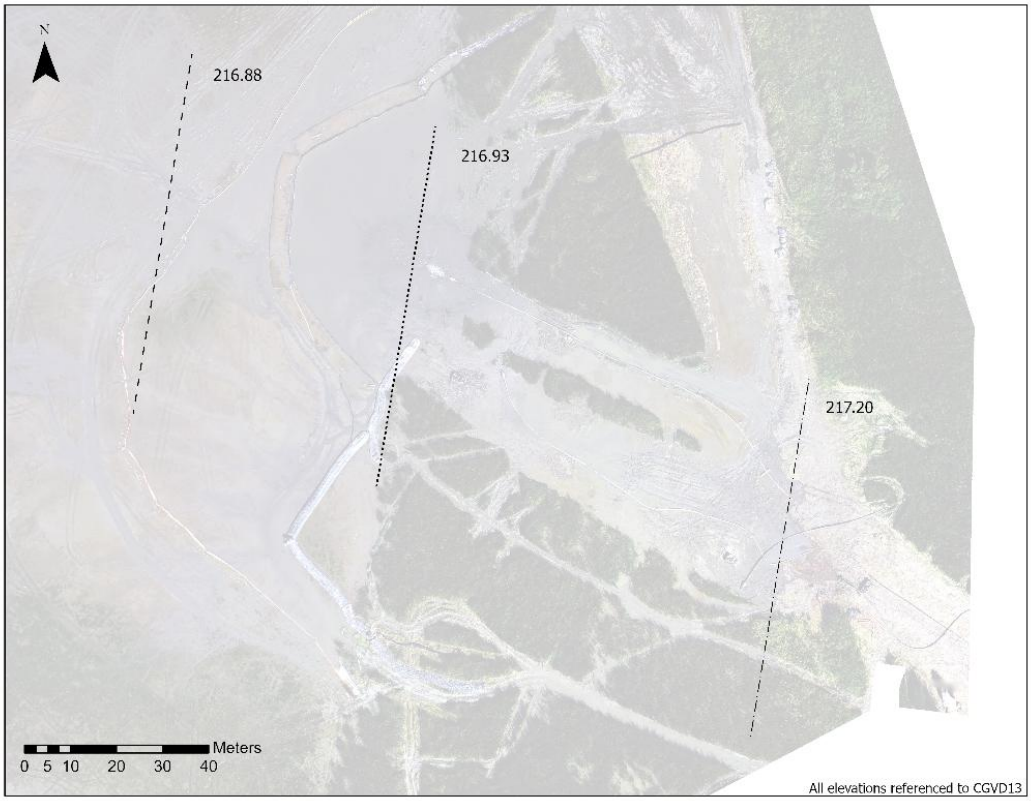

Figure 5-3 UAV imagery of deposition area showing minimum bed elevations and approximate locations

Figure 5-4 shows the variation in water surface elevation across time with a dashed, dotted, and dash-dot line representing minimum bed elevations at the secondary containment, second deposition, and first deposition locations before construction, respectively. The process of sediment deposition and the filling of primary containment units made it more difficult for water to mix with the dredged slurry because the increase in bed elevation prevented water from entering the deposition area. By the end of dredging activities, the minimum bed elevation at the primary containment barrier was between 217.10 and 217.30 meters. This is further evidence explaining why turbidity samples taken within the primary containment area were consistently greater than 1000 NTU.

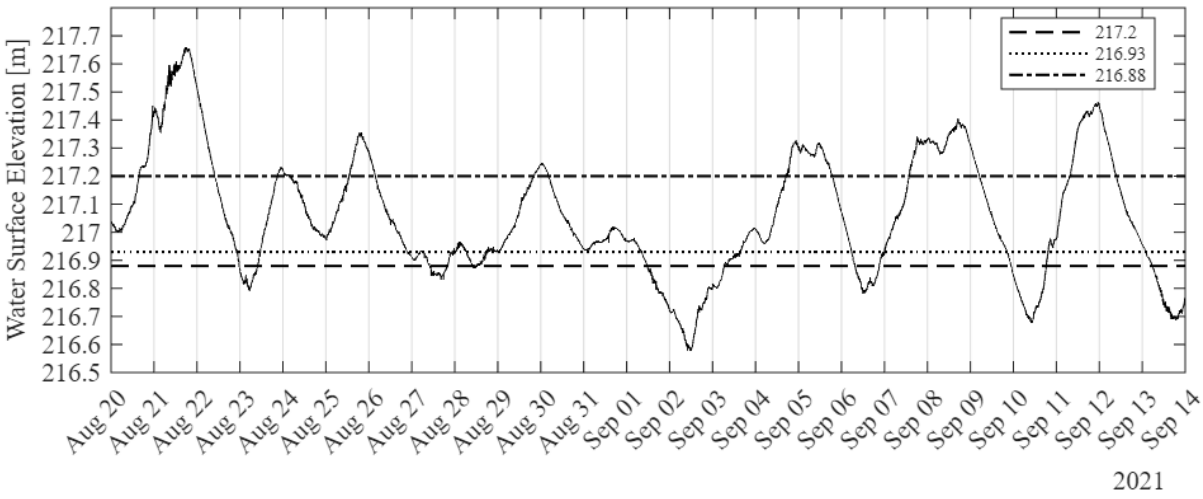

Figure 5-4 Water surface elevation recorded during deployment at the Netley Cut with minimum elevations of the deposition site

5.3.2.2 Development of Preferential Flow Paths

When water levels dropped below the minimum bed elevation at the dredge pipe outlet the outgoing slurry would create a deltaic formation before encountering water from Netley Lake (see Figure 5-5). Preferential flow paths were created between or along the primary and secondary containment barriers, which made sampling at the licensing locations b) through d) problematic. The dynamic hourly variation in water level meant that a single sampling point inside, outside, and 100 meters beyond the primary containment barrier would misrepresent sediment conditions, and therefore turbidity readings, on site. For example, water quality samples taken at locations 1, 2, 3, 4, and 5 in Figure 5-5 would yield turbidity values that could differ between 100 and 1000 NTU from each other. These sampling locations would poorly represent the dispersion and settling of sediment inside and outside of the containment barriers.

Samples taken at locations 1, 2 and 3 would yield three vastly different results for reporting at the licensing location b) “within the enclosed deposition area”.

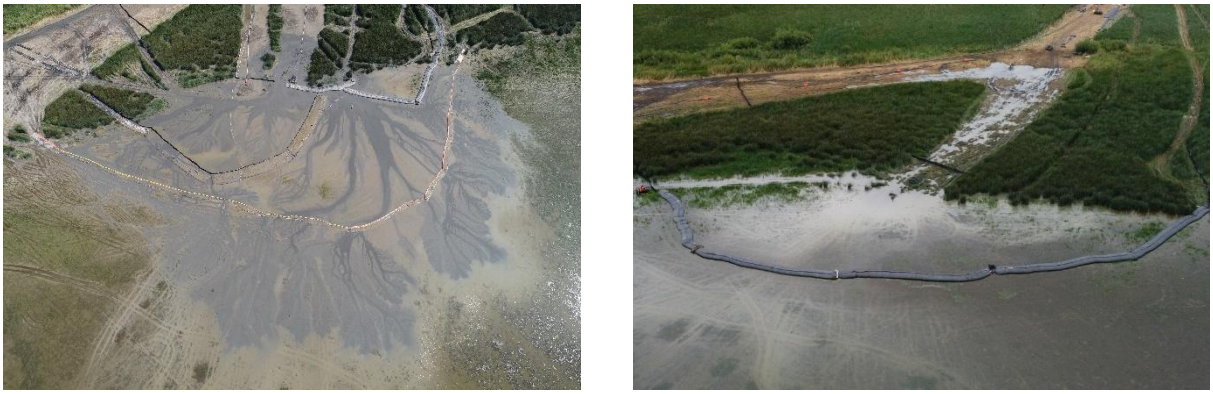

Figure 5-5 - Deltaic formation in deposition area (left) and example monitoring locations in deposition area (right)

5.3.2.3 Difficulties at the Dredge Head

Measuring 5 meters downstream of the dredge head at licensing location a) was challenging, yielded repetitive results and, if recorded improperly, could be misleading. The location was challenging due to the difficulty in acquiring a field measurement that laid in the centre of the sediment plume downstream of the dredge head. Flying a UAV simultaneously while retrieving water quality samples was not possible, nor was it beneficial to fly the UAV before collecting water samples because the location of the dredge head would change when monitors were on the water. Figure 5-6 shows the contrast between the sediment concentration of the dredge plume and background of the Red River. Monitors had to rely on visual acuity on the water which was highly difficult despite the clear delineation between the sediment plume and background river conditions shown in UAV photos. Turbidity values were recorded above the range of the HACH DR900 (NTU > 1000) during the rare occasions when samples were retrieved within the centre of the sediment plume and within 5 meters downstream of the dredge head.

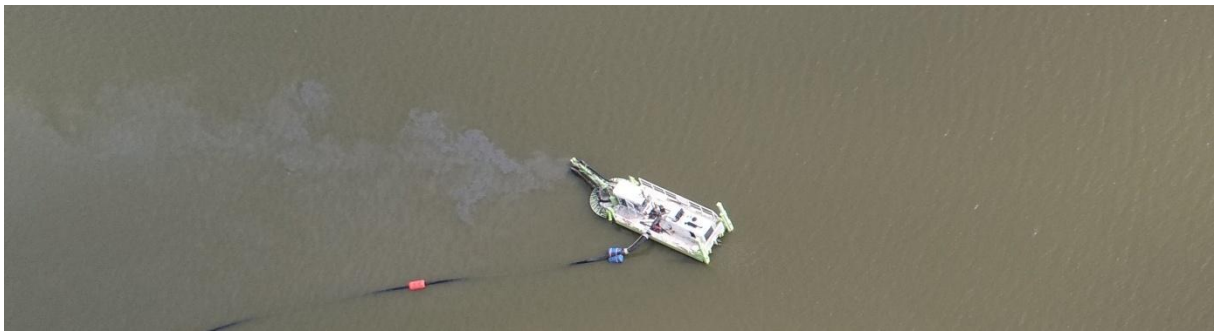

Figure 5-6 Sediment plume downstream of an Amphibex unit during dredge operations

5.3.3 Measurement Techniques in Netley Lake

While on-site measurements captured turbidity during work hours near the restoration project site, the Hydrolab® deployments (locations A, B, C in Figure 5-7) continuously tracked background turbidity in Netley Lake, far from the dredging influence. These were placed well beyond any turbidity containment, at distances such that they only measured natural variations (e.g. due to wind, biota, or water fluctuations). Locations A, B, and C were chosen to represent distinct background conditions in Netley Lake while remaining outside any potential influence of the construction area. Selection criteria included distance from the dredging and containment cells, exposure to prevailing winds and fetch, accessibility for installation and retrieval, sufficient depth throughout anticipated lake level fluctuations to keep sensors submerged, minimal boat traffic, and substrates that could hold a rigid post. One site was positioned closest to the deposition area yet still beyond any containment to detect near-field background variability. A second site was placed cross-lake along the dominant wind vector to capture wind-driven resuspension events. A third site was placed farther afield to characterize far-field background conditions. This layout established a gradient across the open-water portion of Netley Lake, allowed detection of spatial coherence in turbidity events, and reduced the risk that a single localized effect would be misinterpreted as system-wide behavior.

Operating three loggers in parallel provided several advantages. Spatial replication enabled comparison of event timing and magnitude across the lake, which improved attribution of turbidity spikes to wind, water level, or biotic activity rather than to construction. Redundancy improved data reliability by allowing outlier detection and instrument health checks through cross-comparison. The three-station array also supported simple propagation and lag analyses, for example, whether a setup event produced a simultaneous turbidity rise at all stations or a progressive response along the fetch. Finally, overlapping records mitigated data loss risk if one unit stopped early due to battery depletion or fouling.

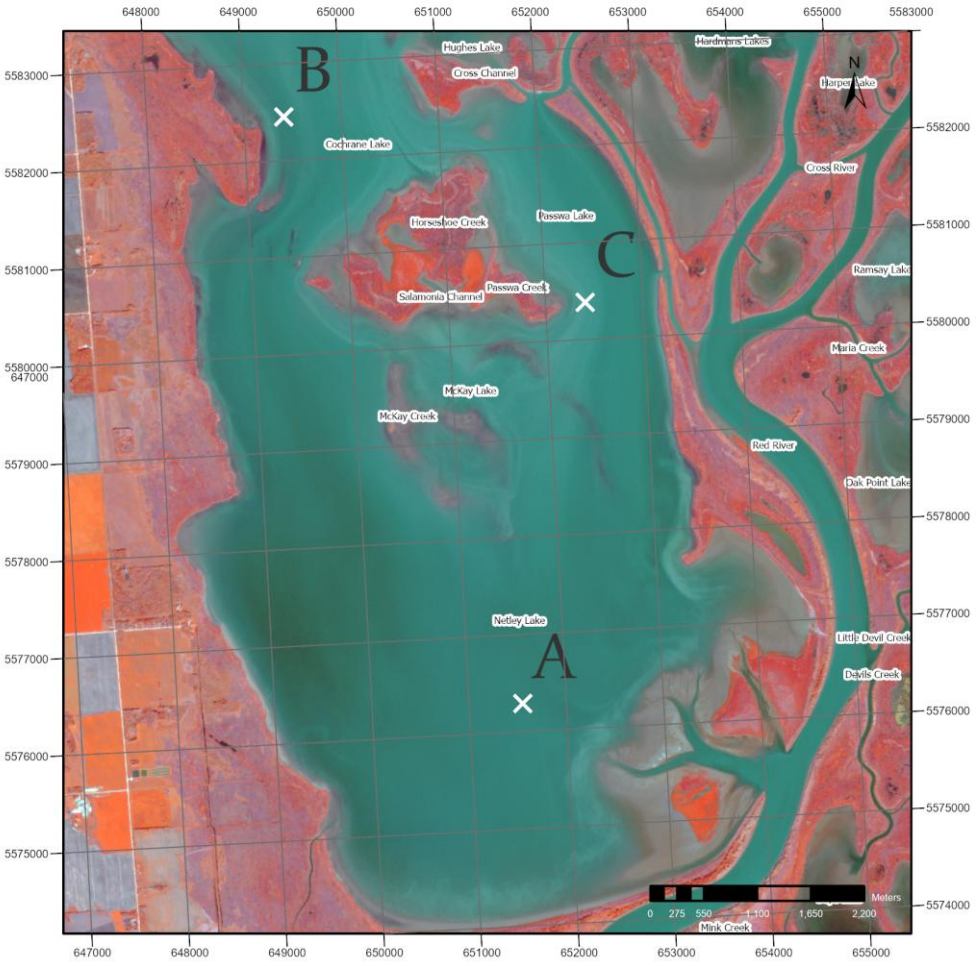

Figure 5-7 Hydrolab® deployment locations in Netley Lake

Each Hydrolab DS5X® was mounted on a galvanized steel u-channel post driven into the lakebed to refusal using a manual post driver (Figure 5-8). The post was oriented vertical and embedded sufficiently to prevent rotation or subsidence under wave loading. The sonde was secured to the post using stainless steel clamps on a rigid bracket so that the optical window sat approximately 0.30 m below the mean water surface at the time of installation. This depth minimized air exposure during short-term water level drops and reduced near-surface wave noise, while remaining shallow enough to represent the mixed layer. Before deployment, sensors were inspected, and the turbidity meter was calibrated with formazin standards that bracketed expected conditions. Time was synchronized across all units. After deployment on September 1, 2021, logging commenced the same day once installations were complete. Retrieval followed the reverse sequence.

Figure 5-8 Hydrolab® installation in Netley Lake

The Hydrolabs® were calibrated and set to analyze turbidity every 30 minutes starting at 00:00 on September 1st, 2021. Hydrolab® A, B, and C began recording turbidity values shortly after installation at 14:30, 13:30 and 12:00 on September 1st, 2021, respectively. Each Hydrolab® recorded information for approximately one month until the built-in batteries were drained.

Location A stopped on October 3rd at 2:30, B on September 30th at 5:30, and C on September 23rd at 21:00. The data from these units provides a baseline of natural turbidity fluctuations in the marsh's open water during the period of construction. Each unit's dataset was time-stamped, allowing comparison with natural conditions and with any overlapping period when dredging was ongoing, to see if construction had any detectable effect at those distances.

Records were screened for sensor out-of-water conditions, for example, flat near-zero values coincident with low lake levels, and for readings above the reliable upper range. Short spikes associated with wiper passes or air entrainment were flagged. For visualization, a short moving average was applied without altering the archived raw data. Throughout analysis, NTU results from the Hydrolabs were not converted to FAU values from the handheld DR900. Comparisons between instrument types focused on coincident trends, such as the timing of rises and returns to baseline, rather than on numeric equivalence.

5.4 Results and Discussion

This section is broken apart into two components: on-site turbidity monitoring and continuous turbidity monitoring. The result of this section clearly delineates the contrast between background turbidity in Netley Lake and turbidity levels impacted by construction activities.

5.4.1 On-site Turbidity Monitoring

As indicated in Table 5-1, either a licensing, testing, or comprehensive method for recording turbidity was employed on 17 of the 26 days during the construction period.

- Six days following the licensing requirements;
- Five days that tested the comprehensive method of measuring turbidity; and
- Six days of comprehensive measurements.

The six days that utilized the licensing standard offered minimal insight regarding the movement and concentration of sediment from dredging and deposition activities. One recorded measurement at each location for a given day meant that the results were heavily influenced by a monitor's discretion. Table 5-2 provides the recorded turbidity values for locations a) through d) following the standard licensing method. Locations for each of these readings were not detailed enough to be reproducible to assess the impact of dredging and deposition activities on the Red River and Netley Lake.

Table 5-2 Results of recording turbidity following the minimum licensing standards at the proposed locations a) through d)

		Turbidity (FAU)			
Date	**Method**	**a)**	**b)**	**c)**	**d)**
20-Aug-21	Licensing	>1000	21	42	54
22-Aug-21	Licensing	63.1	49.3	167	184
27-Aug-21	Licensing	27.1	60	98.4	49.3
30-Aug-21	Licensing	38.3	64.4	93.1	50.2
04-Sep-21	Licensing	37	98.8	59.2	63.7
12-Sep-21	Licensing	24	201	193	32.5

Recording single measurements at the licensing locations meant that the variation in turbidity was not accurately mapped across the dredging or deposition zones. As previously mentioned with respect to Figure 5-5, two samples collected at licensing locations a), b), or c) could yield completely different turbidity values (>100 FAU) that would change the interpretation of the data. Therefore, five days of testing new measurement locations were conducted to develop a comprehensive method that would ensure water quality samples were representative of site conditions. Each testing day, as shown in Table 5-3, utilized a different number of samples at various locations. All samples depended on the water level of Netley Lake and any preferential flow paths created by slurry leaving the pipe outlet. If water was not present in the deposition

area than the effluent sediment from the pipe outlet would be unable to settle in the time taken for the slurry to reach the primary and secondary containment barriers. Low water levels also resulted in pockets of standing water unaffected by the deposition of sediment because they resided outside of the preferential flow path.

Table 5-3 Results of recording turbidity during the five days of testing

	Turbidity (FAU)				
Location	**Aug 23**	**Aug 24**	**Aug 25**	**Aug 26**	**Aug 28**
< 5m from Dredge	>1000	>1000	>1000	>1000	>1000
Between 10 and 20m from Dredge	38	78	52	58	65
< 5m from Outlet	>1000	>1000	>1000	>1000	>1000
Within Deposition	159	97	>1000	>1000	>1000
Within Deposition	33	—	—	>1000	>1000
Outside Deposition	35	279	185	>1000	>1000
Outside Deposition	>1000	114	76	127	—
Outside Deposition	—	314	92	123	—
Outside Deposition	—	—	—	108	—
Outside Deposition	—	—	—	177	—
Outside Deposition	—	—	—	179	—
Outside Deposition	—	—	—	195	—
>100m from Deposition	109	72	81	51	74
>100m from Deposition	37	64	66	52	46
>100m from Deposition	—	—	49	49	62
>100m from Deposition	—	—	—	90	63
>100m from Deposition	—	—	—	42	41
>100m from Deposition	—	—	—	33	47
>100m from Deposition	—	—	—	58	43

As such, the results from five days of testing show a high degree of variability in turbidity between measurements taken in the same locations specified in the license. Values at licensing locations a), b), and c) showed variability on the order of 10^3 FAU. Furthermore, turbidity values located less than 5 meters from the dredge head for each day of testing were consistently over 1000 FAU. These values were typical of the highly turbid sediment plume being formed at the location of the dredge head. As the sediment plume moved downstream of the dredge head

turbidity levels quickly dropped due to settling and dispersion of fine sediments. Turbidity values at a distance between 10 and 20 meters downstream of the dredge head were found to decrease below 100 FAU. Similarly, turbidity values within the deposition area were unable to disperse because there was no water to mix with. A thick film of fine clays and silts was present atop standing water within the deposition zone when background lake levels were lower than the primary containment barriers. Turbidity measurements at locations of standing water and within the flow path of effluent slurry had consistent turbidity readings over 1000 FAU. Based on these results, turbidity values reported at the dredge head and within the deposition zone for comprehensive monitoring days were assumed to be >1000 FAU.

The comprehensive method utilized turbidity measurements along five lines radiating from the perimeter of the primary containment barrier. This was done to understand the extent that turbid effluent would settle or disperse when it mixed with water in Netley Lake. Measuring turbidity at the 35 monitoring locations shown previously in Figure 5-1 allowed for an evaluation of sediment movement in the deposition area and background site conditions (up to 273 meters from primary containment). These measurements were used to generate contour plots and rasterized images. Appendix A – Turbidity Sediment Plume presents large-scale images of each raster, generated using natural-neighbor interpolation to produce continuous surface plots of estimated turbidity. Figure 5-9 displays the artificial sediment plumes overlaid on drone imagery from September 3rd, 2021, for each date that possessed continuous turbidity measurements from Hydrolabs® in Netley Lake. The maximum average turbidity for the furthest measurement locations (NM 7/8/21/22/35) across all comprehensive testing dates was 157 FAU.

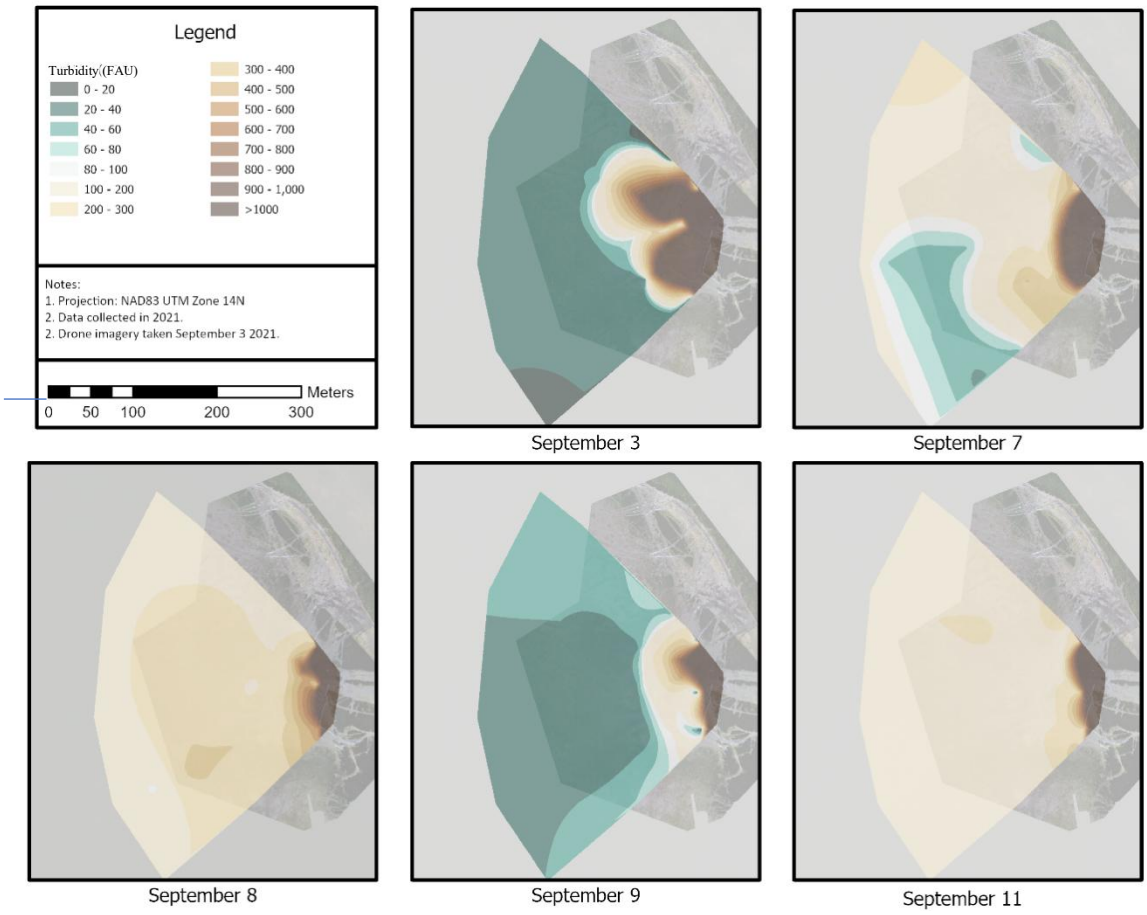

Figure 5-9 Artificial sediment plumes generated with point measurements obtained from the comprehensive testing method

The results indicate that heightened turbidity levels from the deposition zone quickly disperse in the background of Netley Lake when sediment egresses from the containment barrier. Turbid water leaving the deposition zone would dissipate within 50 to 75 meters from the containment barriers and eventually match background turbidity levels in Netley Lake. In comparison, the natural turbidity level in Netley Lake was the driving force impacting water quality at licensing location d).

5.4.2 Continuous Turbidity Monitoring

Turbidity values representing the natural conditions of Netley Lake varied drastically, from 1 to 986 NTU, during the deployment period of the three Hydrolabs®. There were several periods that went above 986 NTU but were removed from the dataset because the functional range of the Hydrolabs® was between 0 and 3000 NTU. Figure 5-10 displays a timeseries of the data recorded by each Hydrolab® throughout the entire deployment period. A moving average across two hours was applied to the graph to smooth the dataset. There are two segments in the dataset where Hydrolab® C flatlines around 2 NTU on September 16th and 19th. This likely occurred because the turbidity sensor on the Hydrolab® was not fully submersed in water. Water levels in Netley Lake on these two dates in September were below 216.7 meters.

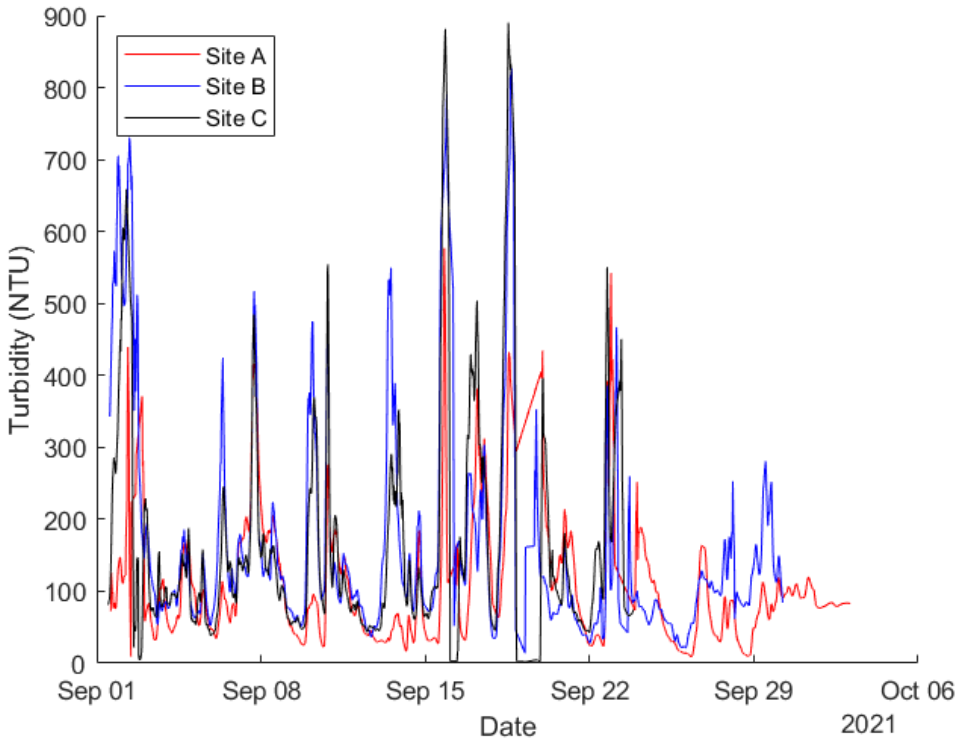

Figure 5-10 Natural turbidity levels in Netley Lake

Investigating more closely how turbidity levels change within a day is illustrated by Figure 5-11. Instantaneous turbidity values as recorded by each Hydrolab® are represented by dashed lines while solid lines represent the two-hour moving average. The dashed vertical line marks the moment on September 22 when the satellite image was captured, aligning the time series with the sediment plume conditions depicted in Figure 5-7.

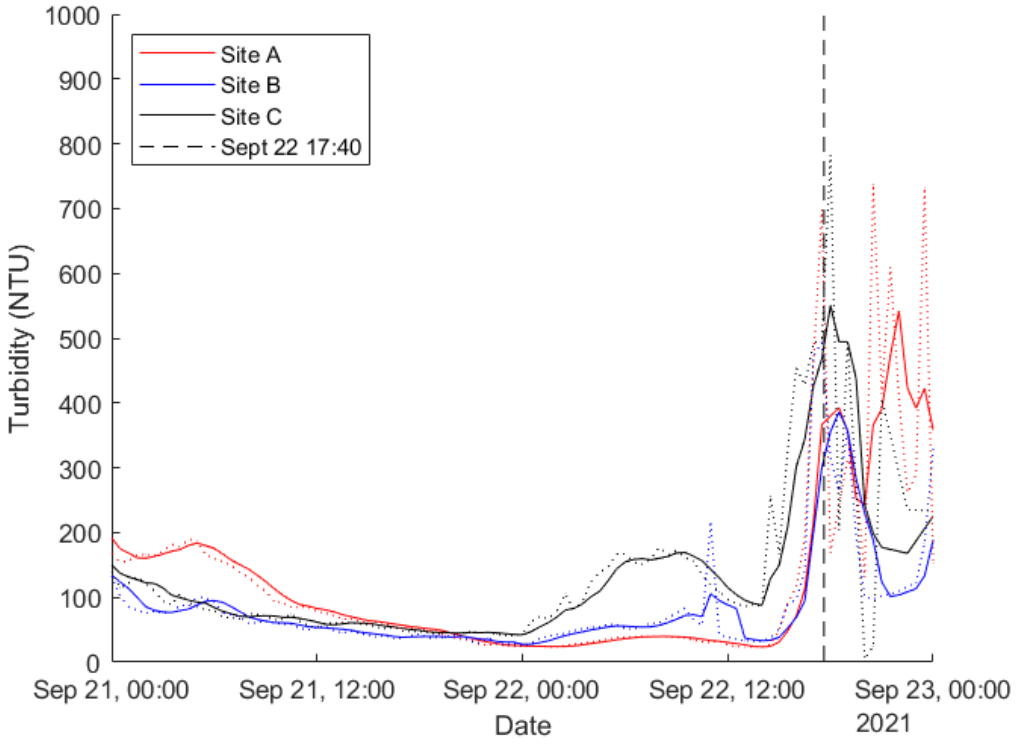

Figure 5-11 Three-day analysis of turbidity levels in Netley Lake with raw and smoothed elevations indicated by dotted and smooth lines, respectively

With each Hydrolab® being located far beyond the influence of any construction activities, the measured turbidity values represent the natural conditions of Netley Lake influenced by environmental factors such as wind, water, and biota.

5.5 Conclusion

Based on comprehensive on-site testing and continuous turbidity monitoring in Netley Lake, it can be concluded that the NLMRP construction activities (dredging and sediment deposition) had no appreciable long-term impact on turbidity levels in the marsh's open waters relative to background conditions. Any increases in turbidity due to the project were localized and temporary. Elevated turbidity was observed immediately at the dredge head and within the confined deposition area, but these high levels dissipated rapidly with distance: within tens of meters, turbidity in the surrounding marsh water returned to near-background levels. Continuous data from Hydrolab® stations showed that Netley Lake's natural turbidity varied greatly due to environmental factors, frequently reaching levels equal to or exceeding those measured near the project site. This indicates that the marsh's background turbidity signal is driven by large-scale influences (river inputs, wind/wave resuspension, etc.) rather than the localized dredging activity.

In regulatory terms, throughout the monitoring period the project remained in compliance with turbidity-related license conditions. There were no sustained instances where turbidity (or equivalent TSS) at the perimeter of the work exceeded background by the threshold requiring additional mitigation. In fact, any short-term spikes at the work site were quickly diluted by natural conditions in Netley Lake. By the time water had mixed 50–100 m away from the dredging operations, turbidity was generally indistinguishable from natural marsh turbidity.

Overall, these findings are encouraging for marsh restoration efforts: they suggest that, at least under the conditions encountered (late summer low flows and moderate winds), the dredging and sediment augmentation did not cause widespread or prolonged turbidity pollution in the marsh. The marsh's resilience and flushing capacity were sufficient to handle the

introduced sediment without significant deterioration in water clarity at a system scale. Future restoration or dredging projects in NLM should, however, remain cognizant of water level conditions—extremely low water can exacerbate local turbidity—and should plan adaptive measures accordingly (e.g., pause work during very low water or ensure adequate containment). However, under normal conditions, the data indicate that restoration dredging can be carried out without violating turbidity standards or harming the marsh's water quality. The natural turbidity dynamics of NLM dominate water clarity, and project-induced turbidity, while observable in the immediate work area, was a minor and transient addition to the marsh's background turbidity regime.

6. Summary

This thesis examined the hydrodynamics and geomorphology of Netley–Libau Marsh and the lower Red River, with emphasis on how water and sediment were routed through Netley Cut, Netley Delta, Netley Lake, and the Red River outlet to Lake Winnipeg. The work integrated repeated bathymetric surveys, discrete discharge measurements, continuous water level readings, and turbidity monitoring associated with a restoration dredging project. Collectively, these datasets established a plethora of information concerning changes in channel morphology and sedimentation rates, quantified the partitioning of Red River flow between the main river and Netley–Libau Marsh and at the Red River trifurcation, and evaluated the turbidity response of the system to localized dredging and sediment placement.

A consolidated bathymetric analysis formed the core of the thesis and showed that, over 2010–2022, Netley–Libau Marsh underwent modest but spatially structured morphological change. At Netley Cut, digital elevation models within the analysis frame around the engineered opening showed alternating erosion and deposition that nearly balanced over the 12 year record, such that net bed change generally remained within approximately ±0.2 m and the thalweg stayed fixed along the left bank, with the anthropogenic bed high persisting as a shallow sill. In Netley Delta, repeated M9 surveys demonstrated clear deltaic growth, with mean bed elevations within the main entrance channels increasing by approximately 0.2–0.3 m between 2010 and 2022, equivalent to an average aggradation rate of about 2 cm per year, and accompanied by the transition of the north entrance channel from a discontinuous depression to a continuous, well defined channel while the west entrance remained the dominant pathway into Netley Lake. Around Netley Lake, elevation change grids indicated a lakeward advance and thickening of the central delta island, with typical increases on the order of 0.25 m and local maxima approaching

0.4 m. Along the lower Red River and at the outlet, cross sectional comparisons at the navigation corridor showed that minimum bed elevations within the maintained channel rose from 211.991 m to 212.689 m between 2018 and 2020, a net shoaling of 0.698 m that was partly retained through 2021, while adjacent east channel sections deepened by several tenths of a metre and infilling between and east of the breakwaters locally exceeded 0.5 m.

Within the Netley–Libau Marsh Restoration Project dredge footprint, bathymetric differencing indicated removal of several thousand cubic metres of material and subsequent natural infilling that recovered a large fraction of this volume within one year. At the associated Netley Lake deposition cell, interannual comparisons showed that background marsh processes had already raised mean bed elevations within the cell by several tenths of a metre. Volume estimates confirmed that the total gain in stored sediment within the bounded cell was smaller than the removed dredge volume, implying that a substantial fraction of the placed material was redistributed or exported through the open boundaries, and that the deposition site functioned as an effective but leaky sink embedded within a larger, actively infilling marsh system, as highlighted by the natural sedimentation rates across Netley Lake.

Water levels and discharge discussed in this thesis combined discrete ADCP measurements with continuous pressure-transducer records. At Netley Cut, continuity-based estimates and measured discharges indicated that, under typical open-water conditions when the Red River provided the sole inflow, Netley Cut diverted on the order of 39.27 % of the concurrent Red River discharge on average, with individual events where diversion exceeded half of the inflow. South of Netley Cut, analysis of historical flow measurements at the trifurcation showed that the east and centre channels together evenly conveyed nearly all of the Red River flow—47.59 and 50.88, respectively—while the west channel carried only a small residual (<2%). Cases where

the lower Red River or Lake Winnipeg provided the dominant inflow illustrated a contrasting low-flow regime with weak through-flow and intermittent reversals that were consistent with seiche-modulated exchange. Taken together, these quantitative patterns indicate that the opening of Netley Cut, by routing a substantial fraction of Red River flow into Netley Delta and Netley Lake, had the unintended but beneficial effect of enhancing sediment delivery to the marsh and contributing to the observed long term rise in bed elevations. Furthermore, continuous water level data from multiple sites showed small inter-site stage differences, tightly synchronized oscillations, and short lag times on the order of several tenths of an hour to just over one hour. These patterns indicated strong hydraulic connectivity across Netley–Libau Marsh and explored the short-term variability in water levels by lake seiche activity.

Moreover, the turbidity component assessed the response of Netley Lake to NLMRP dredging and sediment placement using a combination of discrete Hach DR900 (FAU) measurements near the dredge and deposition sites and continuous Hydrolab DS5X (NTU) records in open water. The two instruments, based on different optical principles, were used in a complementary fashion, with FAU readings providing high-frequency, spatially targeted information at the work sites and NTU records capturing the background marsh regime. Field observations showed that dredging and deposition generated intense but highly localized turbidity plumes confined to the immediate vicinity of the dredge head and the deposition cell. Turbidity levels decayed rapidly to near-background values within tens of metres, and continuous records indicated that natural turbidity fluctuations in Netley Lake routinely reached or exceeded levels observed at the perimeter of the work area. Within the range of conditions encountered, the NLMRP therefore did not measurably alter marsh-scale turbidity beyond the natural variability associated with river inputs and wind-driven resuspension, although the results

highlighted that careful attention to water level and containment conditions remained warranted for future restoration activities.

7. Recommendations for Future Work

The multipronged nature of this thesis, combining bathymetric analysis of bedforms and sedimentation rates, discharge estimates and water level responses to seiching, and turbidity monitoring within the context of the Netley–Libau Marsh Restoration Project, highlighted several avenues where considerable further research and development could be pursued. Netley–Libau Marsh is an inherently dynamic and complex ecosystem in which river inflows, lake levels, wind forcing, and sediment transport interact in ways that are only partially captured by the present work. To name just a few high-level recommendations that build directly on gaps identified during this study and on aspects that have not yet been examined in detail:

1. *Long-term high-resolution bathymetric monitoring with MBES*

   Implement a sustained bathymetric monitoring program based on multibeam echo sounding surveys focussed on Netley Cut, Netley Delta, Netley Lake, the lower Red River trifurcation, and the outlet of the Red River Proper. Such a program should aim to resolve interannual bed changes at high spatial resolution and to quantify uncertainty explicitly, so that elevation change and volume estimates for key reaches are accompanied by reliable, spatially variable error metrics rather than relying on published instrumentation error. This is especially important when investigating intra-annual changes in bedforms or the aggradation or erosion of sediment.

2. *Integrated water level and discharge monitoring to characterise flow splits and real-time conditions*

   Continue and expand detailed monitoring programs centred on water levels and discharge at Netley Cut and the Red River trifurcation, with repeat cross sections and velocity

measurements that capture a wide range of hydrologic and lake level conditions. The existing set of raw data for these variables is still relatively small. The objective should be to develop quantitative relationships that allow real-time inference of flow splits and cross-sectional hydraulics at these sites from routinely reported environmental conditions at nearby locations such as Breezy Point, Gimli Harbour, and Selkirk.

3. *Linking turbidity variability to environmental forcing and revisiting the NLMRP*
   Quantify the variability of turbidity as a function of environmental forcing, particularly wind and seiche events, and relate these patterns to the water level seiche behaviour documented in this thesis through coordinated turbidity and stage monitoring at multiple sites. In combination with these assessments, re-survey the NLMRP dredge and deposition sites at multi-year intervals to examine consolidation and redistribution of placed sediments and to test alternative placement strategies or cell designs that may enhance vegetative colonisation, stability, and long-term habitat benefits.

8. References

Amante, C. J., & Eakins, B. W. (2016). Accuracy of interpolated bathymetry in digital elevation models. *Journal of Coastal Research*, *76*(sp1), 123–133. https://doi.org/10.2112/SI76-011

Anderson, C. W. (2005). Turbidity. In *National Field Manual for the Collection of Water-Quality Data* (2.1, Vol. 9). U.S. Geological Survey. https://pubs.usgs.gov/twri/twri9a6/twri9a67/twri9a_Section6.7_v2.1.pdf

Anderson, O., Harrison, A., Heumann, B., Godwin, C., & Uzarski, D. (2023). The influence of extreme water levels on coastal wetland extent across the Laurentian Great Lakes. *Science of the Total Environment*, *885*(February), 163755. https://doi.org/10.1016/j.scitotenv.2023.163755

Aquatic Environmental Services. (2011). *Bathymetry of Lakes in the Netley-Libau Marsh*.

Arseni, M., Voiculescu, M., Georgescu, L. P., Iticescu, C., & Rosu, A. (2019). Testing Different Interpolation Methods Based on Single Beam Echosounder River Surveying. Case Study: Siret River. *ISPRS International Journal of Geo-Information*, *8*(11), 507. https://doi.org/10.3390/ijgi8110507

B.C. Ministry of Environment and Climate Change Strategy. (2021). Ambient Water Quality Guidelines for Turbidity and Suspended and Benthic Sediments. *Water Quality Guideline Series*, *WQG*(18). https://www2.gov.bc.ca/gov/content/environment/air-land-water/water/water-quality/water-quality-

Bakker, J. D. (2024). *Applied multivariate statistics in R*. University of Washington.

Becket, M. (2020). *Investigation of the Occurrence of Ice Jams on the Lower Red River in Manitoba*.

Bedford, K. W. (1992). The Physical Effects of the Great Lakes on Tributaries and Wetlands. *Journal of Great Lakes Research*, *18*(4), 571–589. https://doi.org/10.1016/S0380-1330(92)71323-9

Berkowitz, J., VanZomeren, C., & Piercy, C. (2017). Marsh Restoration Using Thin Layer Sediment Addition: Initial Soil Evaluation. *Wetland Science & Practice*, *March*, 13–17.

Bolboacă, S. D., Jäntschi, L., Sestraş, A. F., Sestraş, R. E., & Pamfil, D. C. (2011). Pearson-fisher chi-square statistic revisited. *Information (Switzerland)*, *2*(3), 528–545. https://doi.org/10.3390/info2030528

Brenner, S. D., & Laval, B. E. (2018). Seiche modes in multi-armed lakes. *Limnology and Oceanography*, *63*(6), 2717–2726. https://doi.org/10.1002/lno.11001

Brunskill, G. J., & Graham, B. W. (1979). The offshore sediments of Lake Winnipeg. In *Fisheries and Marine Services Manuscript Report 1540*.

Burton, T. M. (1984). The Effects of Water Level Fluctuations on Great Lake Coastal Marshes. In *Coastal Wetlands* (Issue 3). Michigan State University.

Calder, B. R., & Mayer, L. A. (2003). Automatic processing of high-rate, high-density multibeam echosounder data. *Geochemistry, Geophysics, Geosystems*, *4*(6). https://doi.org/10.1029/2002GC000486

Calder, B. R., & Rice, G. (2011). Design and implementation of an extensible variable resolution bathymetric estimator. *US Hydro Conf*, 15. http://www.thsoa.org/hy11/0428P_01.pdf

CCME. (2002). Canadian Water Quality Guidelines for the Protection of Aquatic Life - Total Particulate Matter. *Canadian Environmental Quality Guidelines*, 13.

Chen, C.-T., & Millero, F. J. (1977). Speed of sound in seawater at high pressures. *The Journal of the Acoustical Society of America*, *62*(5), 1129–1135. https://doi.org/10.1121/1.381646

Childs, C. (2004). Interpolating Surfaces in ArcGIS Spatial Analyts. *ESRI Education Services*, *July-September*, 32–35. papers2://publication/uuid/7A4DAFEA-CE6C-44AE-9DC4-AE9B953BB87A

Clean Environment Commission. (2015). *Lake Winnipeg Regulation Report*. http://www.cecmanitoba.ca/doc/commission_reports/LWR_WEB.pdf

Coggan, R., Populus, J., White, J., Sheehan, K., Fitzpatrick, F., & Piel, S. (2007). Review of standards and protocols for seabed habitat mapping. In *MESH Action 2.1* (Issue February).

Columbia University. (2025). *Kriging Interpolation*. https://www.publichealth.columbia.edu/research/population-health-methods/kriging-interpolation

Coppens, A. B. (1981). Simple equations for the speed of sound in Neptunian waters. *The Journal of the Acoustical Society of America*, *69*(3), 862–863. https://doi.org/10.1121/1.385486

Crabot, J., Clappe, S., Dray, S., & Datry, T. (2019). Testing the Mantel statistic with a spatially-constrained permutation procedure. *Methods in Ecology and Evolution*, *10*(4), 532–540. https://doi.org/10.1111/2041-210X.13141

Del Grosso, V. A. (1974). New equation for the speed of sound in natural waters (with comparisons to other equations). *The Journal of the Acoustical Society of America*, *56*(4), 1084–1091. https://doi.org/10.1121/1.1903388

Dewey, M. (2025). *Comparison of methods in the metap package*.

Einarsson, E., & Lowe, A. B. (1968). Seiches & set-up on Lake Winnipeg. *Limnology and Oceanography*, *13*, 257–271.

Environment and Climate Change Canada, & Manitoba Agriculture and Resource Development. (2020). *State of Lake Winnipeg: 2nd Edition*. *45*, 77.

Erdogan, S. (2009). A comparision of interpolation methods for producing digital elevation models at the field scale. *Earth Surface Processes and Landforms*, *34*(3), 366–376. https://doi.org/10.1002/esp.1731

ESRI. (2025a). *How Spatial Autocorrelation (Global Moran's I) Works*. https://pro.arcgis.com/en/pro-app/latest/tool-reference/spatial-statistics/h-how-spatial-autocorrelation-moran-s-i-spatial-st.htm

ESRI. (2025b). *How Spline with Barriers Works*. https://pro.arcgis.com/en/pro-app/latest/tool-reference/3d-analyst/how-spline-with-barriers-works.htm

ESRI. (2025c). *How Topo to Raster Works*. https://pro.arcgis.com/en/pro-app/latest/tool-reference/3d-analyst/how-topo-to-raster-works.htm#:~:text=Topo to Raster uses this,surfaces with less input data.

ESRI. (2025d). *IDW (Geostatistical Analyst)*. https://pro.arcgis.com/en/pro-app/3.3/tool-reference/geostatistical-analyst/idw.htm

ESRI. (2025e). *Understanding Ordinary Kriging*. https://pro.arcgis.com/en/pro-app/latest/help/analysis/geostatistical-analyst/understanding-ordinary-kriging.htm

Farhadzadeh, A. (2017). A study of Lake Erie seiche and low frequency water level fluctuations in the presence of surface ice. *Ocean Engineering*, *135*(March), 117–136. https://doi.org/10.1016/j.oceaneng.2017.02.027

Fisher, R. A. (1932). Statistical Methods for Research Workers. *Oliver and Boyd, Edinburgh*.

Gathman, J. P., Albert, D. A., & Burton, T. M. (2005). Rapid Plant Community Response to a Water Level Peak in Northern Lake Huron Coastal Wetlands. *Journal of Great Lakes Research*, *31*(SUPPL. 1), 160–170. https://doi.org/10.1016/S0380-1330(05)70296-3

Goharrokhi, M. (2022). *Sedimentary processes in large , regulated river systems in the Canadian*

subarctic.

Goldsborough, G. (2015). *The Ecology of Coastal Wetlands around Lake Winnipeg and Vegetation Loss in Netley-Libau Marsh*. *January 2015*.

Goldsborough, G., & Grover, S. (2021). *Historic Sites of Manitoba: Mouth of the Red River / Netley-Libau Marsh*. Manitoba Historical Society. https://www.mhs.mb.ca/docs/sites/redriver.shtml#sources

Grabas, G. P., & Rokitnicki-Wojcik, D. (2015). Characterizing daily water-level fluctuation intensity and water quality relationships with plant communities in Lake Ontario coastal wetlands. *Journal of Great Lakes Research*, *41*(1), 136–144. https://doi.org/10.1016/j.jglr.2014.12.019

Grosshans, R. E., Venema, H. D., & Oborne, B. (2012). *Advancing Netley-Libau Marsh Restoration Efforts: Cattail biomass and nutrient survey of Netley-Libau Marsh* (Issue April). http://www.iisd.org/library/advancing-netley-libau-marsh-restoration-efforts-cattail-biomass-and-nutrient-survey-netley

Grosshans, R. E., Wrubleski, D. a, Goldsborough, L. G., Marsh, D., & Station, F. (2004). Changes in the Emergent Plant Community of Netley-Libau Marsh Between 1979 and 2001. In *Delta Marsh Field Station Occational Publication* (Vol. 4, Issue 4). University of Manitoba & Ducks Unlimited Canada.

HACH. (2006). *Hydrolab DS5X, DS5, and MS5 Water Quality Multiprobes User Manual* (Issue 003078). http://www.ott.com/download/user-manual-hydrolab-ds5x-ds5-and-ms5-water-quality-multiprobes/

HACH. (2010). *Hydrolab Series 5 Multi-parameter Sonde - Data Sheet*.

HACH. (2013). *Absorptometric Method 8237*. 1–4.

Hamblin, P. F. (1976). Seiches, Circulation, and Storm Surges of an Ice-Free Lake Winnipeg. *Journal of the Fisheries Research Board of Canada*, *33*(10), 2377–2391. https://doi.org/10.1139/f76-284

Haresign, M. A. M. (2012). *MODELLING RIVER ICE FREEZE-UP ON THE RED RIVER NEAR NETLEY CUT*.

Harrow-Lyle, T. J., Chomicki, K. M., & Kirkwood, A. E. (2023). Modelling the influence of seiche-events on phosphorous-loading dynamics in three Lake Ontario coastal wetlands. *Journal of Great Lakes Research*, *49*(2), 429–439.

https://doi.org/10.1016/j.jglr.2023.01.010

Hutchinson, M. F. (1989). A new procedure for gridding elevation and stream line data with automatic removal of spurious pits. *Journal of Hydrology*, *106*(3–4), 211–232. https://doi.org/10.1016/0022-1694(89)90073-5

International Hydrographic Organization. (2024). *S-44 International Hydrographic Organization Standards for Hydrographic Surveys* (6.2.0 (ed.); Issue 377). www.iho.int

Keddy, P. A., & Reznicek, A. A. (1986). Great Lakes Vegetation Dynamics: The Role of Fluctuating Water Levels and Buried Seeds. *Journal of Great Lakes Research*, *12*(1), 25–36. https://doi.org/10.1016/S0380-1330(86)71697-3

Keough, J., Thompson, T. A., Guntenspergen, G. R., & Wilcox, D. A. (1999). Hydrogeomorphic factors and ecosystem responses in coastal wetlands of the Great Lakes. *Wetlands*, *19*(December), 821–834.

KGS. (2002). *Engineering Aspects of No Red River Dredging*.

KGS. (2019). *Netley-Libau Marsh Restoration Pilot Project Manitoba Environment Act Proposal*.

Khan, F. A., & Ansari, A. A. (2005). Eutrophication: An Ecological Vision. *The Botanical Review*, *71*(4), 449–482.

Kitchener, B. G. B. (2019). *Reinterpreting turbidity: new methodologies for suspended-sediment research*. *August*.

Kowal, P. (2019). *A historical analysis of the changes in connectivity and plant cover in Netley-Libau Marsh, Manitoba, Canada: Distinguishing the effects of Lake Winnipeg and Red River hydrology on coastal marsh emergent macrophyte areal extent*. University of Manitoba.

Lake Winnipeg Foundation. (2014). *Netley-Libau Marsh Workshop*.

Lake Winnipeg Stewardship Board. (2006). *Reducing Nutrient Loading to Lake Winnipeg and its Watershed: Our collective responsibility and commitment to action*.

Leroy, C. C., Robinson, S. P., & Goldsmith, M. J. (2008). A new equation for the accurate calculation of sound speed in all oceans. *The Journal of the Acoustical Society of America*, *124*(5), 2774–2782. https://doi.org/10.1121/1.2988296

Li, J., & Heap, A. D. (2008). A Review of Spatial Interpolation Methods for Environmental Scientists. *Australian Geological Survey Organisation*, *GeoCat# 68*(2008/23), 154.

https://doi.org/http://www.ga.gov.au/image_cache/GA12526.pdf

Li, Z., Peng, Z., Zhang, Z., Chu, Y., Xu, C., Yao, S., García-Fernández, Á. F., Zhu, X., Yue, Y., Levers, A., Zhang, J., & Ma, J. (2023). Exploring modern bathymetry: A comprehensive review of data acquisition devices, model accuracy, and interpolation techniques for enhanced underwater mapping. *Frontiers in Marine Science*, *10*(May), 1–22. https://doi.org/10.3389/fmars.2023.1178845

Lindgren, C., & Netley Marsh Waterfowl Foundation. (2010). *Community Conservation Plan for Netley-Libau Marsh*.

Loughin, T. M. (2004). A systematic comparison of methods for combining p-values from independent tests. *Computational Statistics and Data Analysis*, *47*(3), 467–485. https://doi.org/10.1016/j.csda.2003.11.020

Louisana Coastal Wetlands Conservation. (2004). *West Bay Sediment Diversion (MR-03)*. *June*.

Mackenzie, K. V. (1981). Nine-term equation for sound speed in the oceans. *The Journal of the Acoustical Society of America*, *70*(3), 807–812. https://doi.org/10.1121/1.386920

Manitoba Conservation and Climate. (2021). *Environmental Act Licence No. 3350 - Red River Basin Commission*.

Manitoba Water Stewardship. (2011). *Manitoba Water Quality Standards, Objectives, and Guidelines*. https://www.gov.mb.ca/waterstewardship/water_quality/quality/pdf/mb_water_quality_standard_final.pdf

Mantel, N., & Valand, R. S. (1970). A Technique of Nonparametric Multivariate Analysis. *Biometrics*, *26*(3), 547. https://doi.org/10.2307/2529108

Mariotti, G. (2016). Revisiting salt marsh resilience to sea level rise: Are ponds responsible for permanent land loss? *Journal of Geophysical Research: Earth Surface*, *121*(7), 1391–1407. https://doi.org/10.1002/2016JF003900

Materne, M. D., Mendelssohn, I. A., Schrift, A., Wilson, A., & Rohwer, S. (2007). Factors Controlling the Restoration of Brown Marsh Site with Dredge Sediment Enrichment. *Louisiana Agriculture*, *50*(2), 8–12.

Maynard, L., & Wilcox, D. (1997). Coastal Wetlands. In H. H. Prince & F. M. D'Itri (Eds.), *State of the Lakes Ecosystem Conference 1996*. CRC Press. https://doi.org/10.1201/9781351070720

McCullough, G. (2014). Climate, hydrology, nutrient loading and the Netley-Libau marshes. *Netley-Libau Marsh Workshop*.

McCullough, G., Hochheim, K., & Cooley, P. (2001). *Retrospective study of suspended sediment patterns on Lake Winnipeg using NOAA AVHRR satellite imagery Klaus Hochheim*. *March*.

Michalek, M. J. (2013). Examining the progression and termination of Lake Agassiz. *Michigan State University*, 1–24. https://msu.edu/~michal76/research/407_Geomorphology_Lake Agassiz2.pdf

Final Licence to Lake Winnipeg Regulation, 1 (2021) (testimony of Minister of Conservation and Climate).

Moran, P. A. P. (1950). Notes on Continuous Stochastic Phenomena. *Biometrika*, *37*(1/2), 17. https://doi.org/10.2307/2332142

Mortimer, C. H. (1987). Fifty Years of Physical Investigations and Related Limnological Studies on Lake Erie, 1928–1977. *Journal of Great Lakes Research*, *13*(4), 407–435. https://doi.org/10.1016/S0380-1330(87)71664-5

National Physical Laboratory. (2000). *Underwater Acoustic - Technical Guides - Speed of Sound in Sea-Water*.

Nester, R. D., & Rees, S. I. (1988). *Thin-Layer Dredged Material Disposal - Fowl River, Alabama, Test Case*. *D-88-4*.

Nielsen, E. (1998). Lake Winnipeg: Coastal submergence over the last three centuries. *Journal of Paleolimnology*, *19*(3), 335–342. https://doi.org/10.1023/A:1007946402547

Nielsen, Erik, & Conley, G. (1994). *Sedimentology and Geomorphic Evolution of the South Shore of Lake Winnipeg*.

Office of Coast Survey. (2025). *HSSD - Hydrographic Survey Specifications and Deliverables*.

Pratomo, D. G., Safira, R. A. D., & Stefani, O. (2023). A Comparison of Different Gis-Based Interpolation Methods for Bathymetric Data: Case Study of Bawean Island, East Java. *Geodesy and Cartography (Vilnius)*, *49*(4), 186–194. https://doi.org/10.3846/gac.2023.18250

Prendergast, L. (2016). *2016 Annual Inspection Report: DELTA MANAGEMENT AT FORT ST. PHILLIP (BS-11)*.

Reimold, R. J., Hardisky, M. A., & Adams, P. C. (1978). *The effects of smothering a Spartina alterniflora saltmarsh with dredged material.* (Vol. 4, Issue 2).

Rymszewicz, A., O'Sullivan, J. J., Bruen, M., Turner, J. N., Lawler, D. M., Conroy, E., & Kelly-Quinn, M. (2017). Measurement differences between turbidity instruments, and their implications for suspended sediment concentration and load calculations: A sensor inter-comparison study. *Journal of Environmental Management*, *199*(May), 99–108. https://doi.org/10.1016/j.jenvman.2017.05.017

SonTek Inc. (2022). *RiverSurveyor S5/M9 System Manual Software*. *858*. https://www.xylem.com/siteassets/brand/sontek/resources/manual/rsl-manual.pdf

Taylor, A. M., & Foret, J. D. (2015). A case study on the engineering and design of the Cole's Bayou Marsh Restoration Project. *Western Dredging Association and Texas A&M University Center for Dredging Studies'*, 103–114.

Trebitz, A. S. (2006). Characterizing seiche and tide-driven daily water level fluctuations affecting coastal ecosystems of the Great Lakes. *Journal of Great Lakes Research*, *32*(1), 102–116. https://doi.org/10.3394/0380-1330(2006)32[102:CSATDW]2.0.CO;2

Tyrrell, J. B. (1896). The Genesis of Lake Agassiz. *The Journal of Geology*, *4*(7), 811–815. https://www.jstor.org/stable/30054905

USACE. (2013). *EM1110-2-1003 Hydrographic Surveying* (Issue November).

USEPA. (2021). Factsheet on water quality parameters: Turbidity. *Factsheet on Water Quality Parameters*, *2008*, 1–3.

Veldman, W. M. (1969). *Shoreline Processes on Lake Winnipeg* (Issue January). University of Manitoba.

Walters, D., Moore, L. J., Duran Vinent, O., Fagherazzi, S., & Mariotti, G. (2014). Interactions between barrier islands and backbarrier marshes affect island system response to sea level rise: Insights from a coupled model. *Journal of Geophysical Research: Earth Surface*, *119*(9), 2013–2031. https://doi.org/10.1002/2014JF003091

Watchorn, E. K. (2015). *Water and Vegetation Cover in Netley-Libau Marsh: A Time Series Analysis Based on Landsat Imagery*.

Watchorn, E. K., Goldsborough, G., Hudon, C., & Taranu, Z. E. (2021). Emergent vegetation in Netley-Libau Marsh: Temporal changes (1990–2013) in cover in relation to Lake Winnipeg level and Red River flow. *Journal of Great Lakes Research*, *47*(3), 690–702. https://doi.org/10.1016/j.jglr.2020.08.016

Wilber, P. (1993). Managing Dredged Material Via Thin-Layer Disposal in Coastal Marshes. *US*

Army Engineer Waterways Experiment Station, *Technical*(July), 699–719.

Wilcox, D. A., & Nichols, S. J. (2008). The effects of water-level fluctuations on vegetation in a Lake Huron wetland. *Wetlands*, *28*(2), 487–501. https://doi.org/10.1672/07-129.1

Wrubleski, D., Badiou, P., & Goldsborough, L. G. (2018). Coastal Wetlands of Manitoba's Great Lakes (Canada). In C. M. Finlayson, G. R. Milton, R. C. Prentice, & N. C. Davidson (Eds.), *The Wetland Book* (Issue January). Springer Netherlands. https://doi.org/10.1007/978-94-007-4001-3

Yates, A. G., Brua, R. B., Friesen, A., Reedyk, S., & Benoy, G. (2022). Nutrient and suspended solid concentrations, loads, and yields in rivers across the Lake Winnipeg Basin: A twenty year trend assessment. *Journal of Hydrology: Regional Studies*, *44*(February), 101249. https://doi.org/10.1016/j.ejrh.2022.101249

YSI Environmental. (2001). *An Overview of Turbidity, Nephelometry and an Advancement in In Situ Measurement of Turbidity*.

Appendix A – Turbidity Sediment Plume

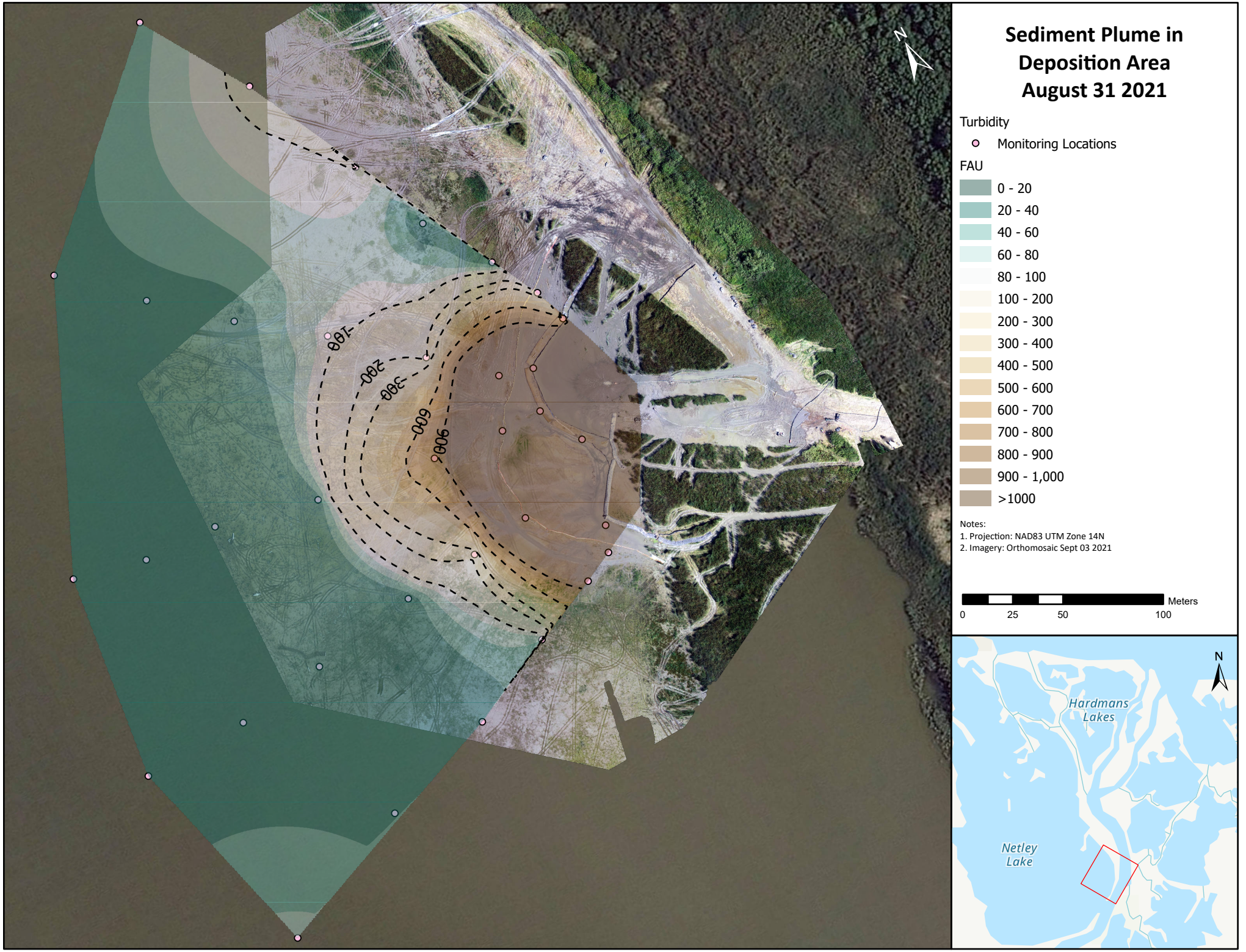
Sediment Plume in Deposition Area August 31 2021
Turbidity
Monitoring Locations
FAU
0 - 20
20 - 40
40 - 60
60 - 80
80 - 100
100 - 200
200 - 300
300 - 400
400 - 500
500 - 600
600 - 700
700 - 800
800 - 900
900 - 1,000
>1000
Notes:
1. Projection: NAD83 UTM Zone 14N
2. Imagery: Orthomosaic Sept 03 2021
Meters
0
25
50
100
N
Hardmans Lakes
Netley Lake
100
200
300
600
900

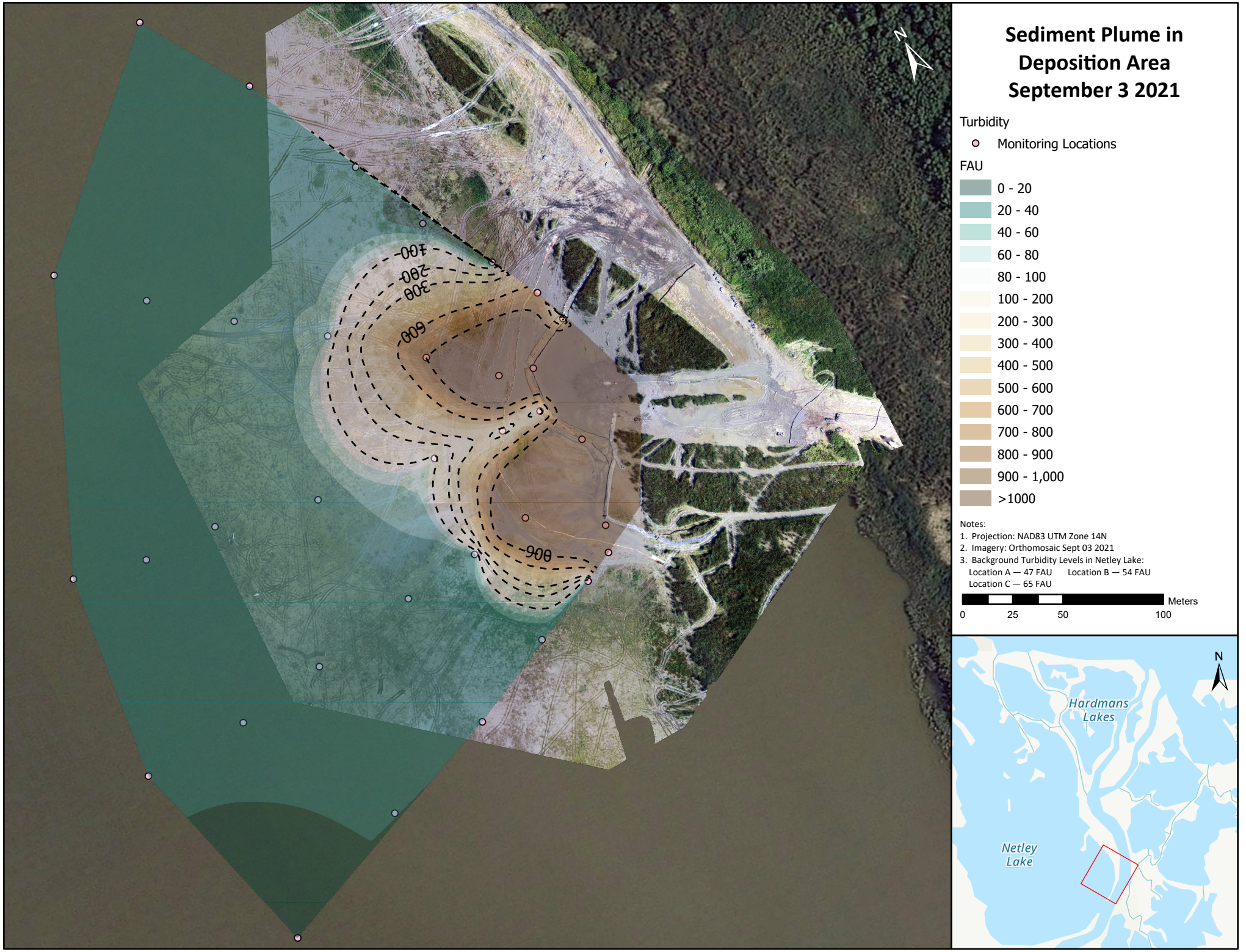
Sediment Plume in Deposition Area September 3 2021
Turbidity
Monitoring Locations
FAU
0 - 20
20 - 40
40 - 60
60 - 80
80 - 100
100 - 200
200 - 300
300 - 400
400 - 500
500 - 600
600 - 700
700 - 800
800 - 900
900 - 1,000
>1000
Notes:
1. Projection: NAD83 UTM Zone 14N
2. Imagery: Orthomosaic Sept 03 2021
3. Background Turbidity Levels in Netley Lake:
Location A — 47 FAU
Location B — 54 FAU
Location C — 65 FAU
Meters
0
25
50
100
N
Hardmans Lakes
Netley Lake
100
200
300
600
900

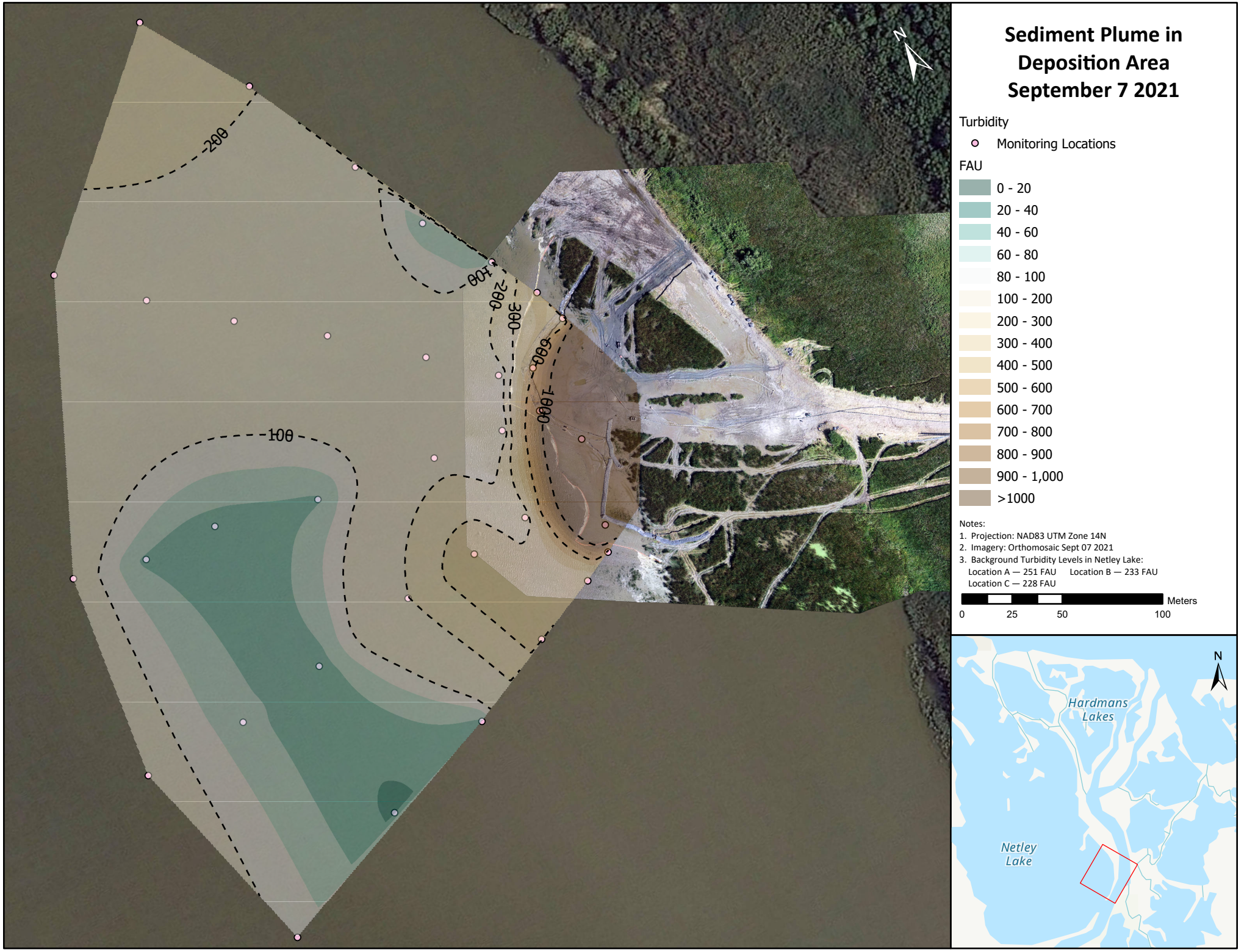
Sediment Plume in Deposition Area September 7 2021
Turbidity
Monitoring Locations
FAU
0 - 20
20 - 40
40 - 60
60 - 80
80 - 100
100 - 200
200 - 300
300 - 400
400 - 500
500 - 600
600 - 700
700 - 800
800 - 900
900 - 1,000
>1000
Notes:
1. Projection: NAD83 UTM Zone 14N
2. Imagery: Orthomosaic Sept 07 2021
3. Background Turbidity Levels in Netley Lake:
Location A — 251 FAU Location B — 233 FAU
Location C — 228 FAU
Meters
0 25 50 100
N
Hardmans Lakes
Netley Lake
100
200
300
600
1000

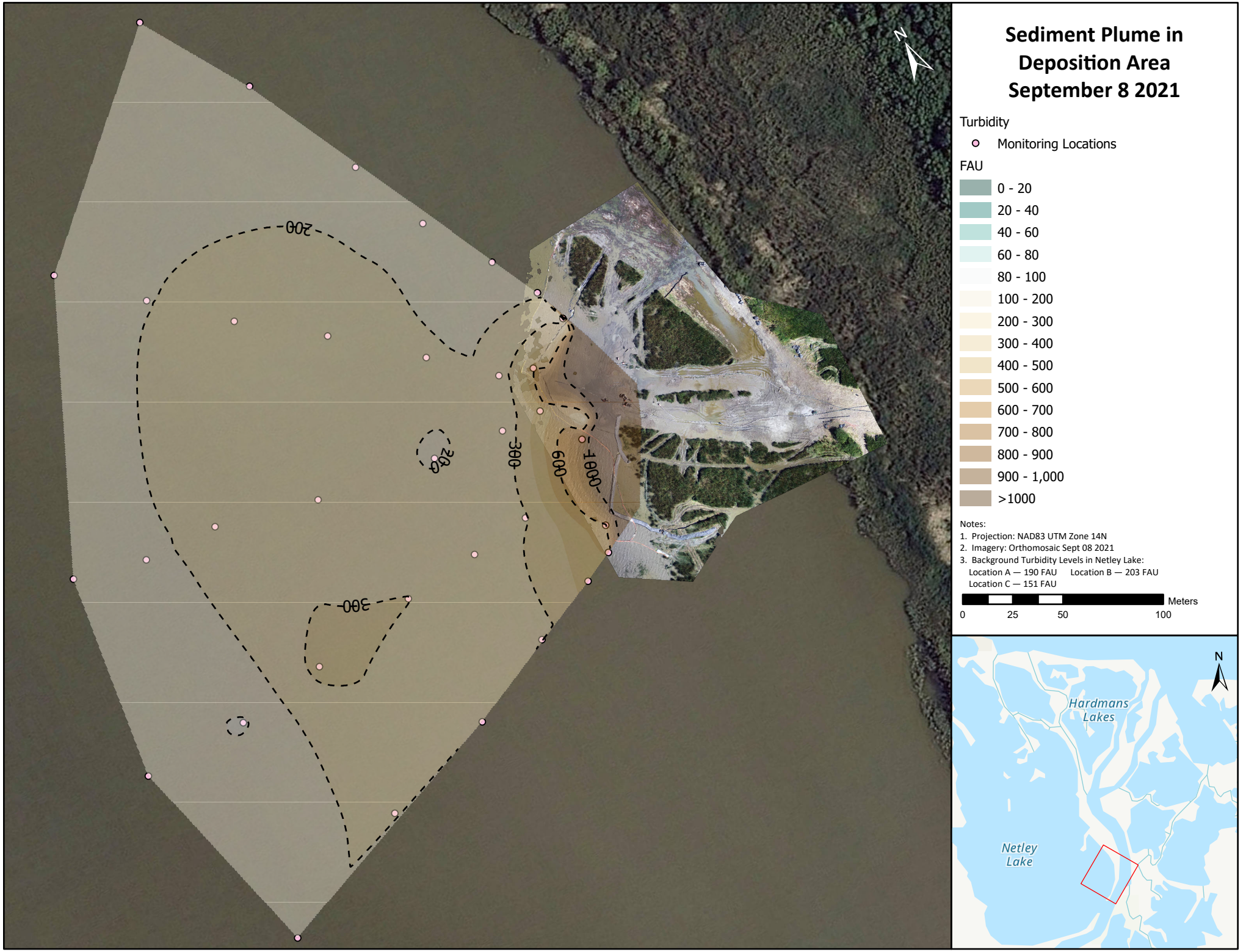
Sediment Plume in Deposition Area September 8 2021
Turbidity
Monitoring Locations
FAU
0 - 20
20 - 40
40 - 60
60 - 80
80 - 100
100 - 200
200 - 300
300 - 400
400 - 500
500 - 600
600 - 700
700 - 800
800 - 900
900 - 1,000
>1000
Notes:
1. Projection: NAD83 UTM Zone 14N
2. Imagery: Orthomosaic Sept 08 2021
3. Background Turbidity Levels in Netley Lake:
Location A — 190 FAU Location B — 203 FAU
Location C — 151 FAU
Meters
0 25 50 100
N
Hardmans Lakes
Netley Lake
200
300
600
1000

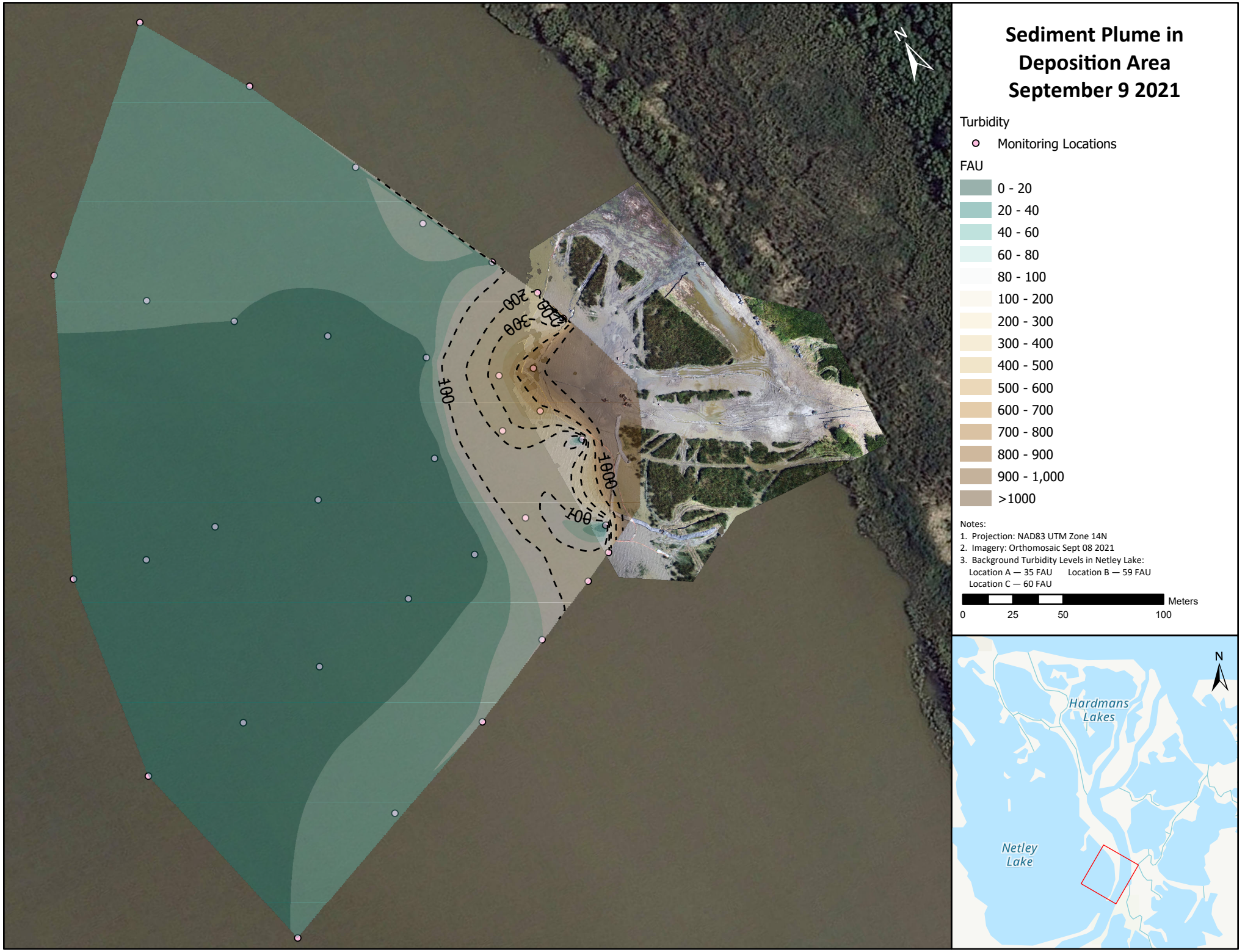
N
100
200
300
400
1000
Sediment Plume in Deposition Area September 9 2021
Turbidity
Monitoring Locations
FAU
0 - 20
20 - 40
40 - 60
60 - 80
80 - 100
100 - 200
200 - 300
300 - 400
400 - 500
500 - 600
600 - 700
700 - 800
800 - 900
900 - 1,000
>1000
Notes:
1. Projection: NAD83 UTM Zone 14N
2. Imagery: Orthomosaic Sept 08 2021
3. Background Turbidity Levels in Netley Lake:
Location A — 35 FAU Location B — 59 FAU
Location C — 60 FAU
Meters
0 25 50 100
N
Hardmans Lakes
Netley Lake

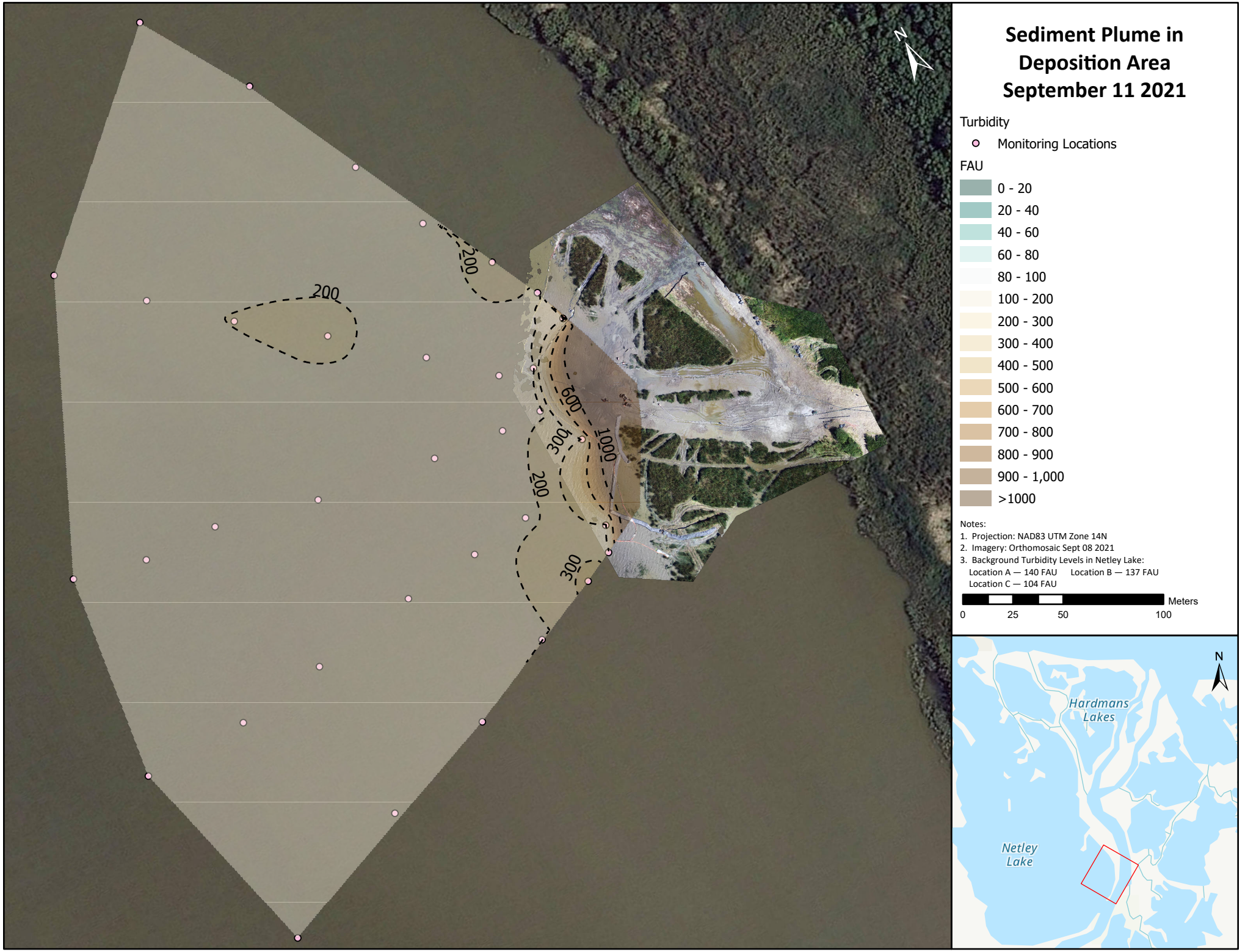
N
200
200
300
200
300
1000
600
Sediment Plume in Deposition Area September 11 2021
Turbidity
Monitoring Locations
FAU
0 - 20
20 - 40
40 - 60
60 - 80
80 - 100
100 - 200
200 - 300
300 - 400
400 - 500
500 - 600
600 - 700
700 - 800
800 - 900
900 - 1,000
>1000
Notes:
1. Projection: NAD83 UTM Zone 14N
2. Imagery: Orthomosaic Sept 08 2021
3. Background Turbidity Levels in Netley Lake:
Location A — 140 FAU Location B — 137 FAU
Location C — 104 FAU
Meters
0 25 50 100
N
Hardmans Lakes
Netley Lake